

THE UNIVERSITY OF MANITOBA

AN EXPERIMENTAL STUDY OF THE TURBULENT
KINETIC ENERGY AND VORTICITY IN A
CONICAL DIFFUSER

by

SUBHASH CHANDRA ARORA

A THESIS

SUBMITTED TO THE FACULTY OF GRADUATE STUDIES
IN PARTIAL FULFILMENT OF THE REQUIREMENTS FOR THE
DEGREE OF DOCTOR OF PHILOSOPHY

DEPARTMENT OF MECHANICAL ENGINEERING

WINNIPEG, MANITOBA
JUNE, 1978

AN EXPERIMENTAL STUDY OF THE TURBULENT
KINETIC ENERGY AND VORTICITY IN A
CONICAL DIFFUSER

BY

SUBHASH CHANDRA ARORA

A dissertation submitted to the Faculty of Graduate Studies of
the University of Manitoba in partial fulfillment of the requirements
of the degree of

DOCTOR OF PHILOSOPHY

© 1978

Permission has been granted to the LIBRARY OF THE UNIVER-
SITY OF MANITOBA to lend or sell copies of this dissertation, to
the NATIONAL LIBRARY OF CANADA to microfilm this
dissertation and to lend or sell copies of the film, and UNIVERSITY
MICROFILMS to publish an abstract of this dissertation.

The author reserves other publication rights, and neither the
dissertation nor extensive extracts from it may be printed or other-
wise reproduced without the author's written permission.



ABSTRACT

An experimental study of the turbulent kinetic energy and the isotropic vorticity balance in a conical diffuser having a total divergence angle of 8° and an area ratio of 4:1 with fully developed pipe flow at entry is described. The data for mean static pressure, mean velocity, various moments up to 4th order, and the first and second derivatives of u_1 signal are presented for pipe Reynolds number of 58000 based on the pipe average velocity and the radius.

The results show that the pressure recovery characteristic is independent of the Reynolds number. A high pressure gradient in the entry region of the diffuser produces a high mean radial velocity. This radial velocity decreases in the downstream direction with decreasing pressure gradient.

The turbulent energy balance shows that the rate of turbulent energy production reaches maximum at the edge of the wall layer extending from the wall to the point of maximum u_1' fluctuations. This layer grows with distance in the downstream direction. Within this layer, dissipation is more than production and thus a need for energy diffusion towards the wall. Results also show that the turbulence is inhomogeneous both in the radial and axial directions in the diffuser and not all the energy produced at any cross-section is dissipated there. An appreciable proportion of the energy produced is also transported in the downstream direction to meet the requirement of high dissipation there. This transport of energy is achieved by the transfer terms of which the most important is the convective diffusion due to pressure effects.

On the basis of the energy budget analysis, the claim of Okwuobi & Azad (1973) that the dissipation in diffuser is negligible and the production is mainly balanced by convective diffusion due to pressure and kinetic effects is thus refuted.

The results of the $\frac{\partial u_1}{\partial t}$ measurements show that in the core region of the diffuser the ratios of the rates of production and dissipation of the turbulent vorticity is constant, and the vorticity balance is essentially the same at all axial stations. Also the rates of dissipation and production of vorticity are constant but large compared with their difference in the region from axis to the point of maximum u_1' fluctuations. However, these rates and the ratio of dissipation to production increase significantly further towards the wall. The value of the skewness of $\frac{\partial u_1}{\partial t}$ in the constant region is comparable to that for the grid turbulence. The overall behavior of skewness of $\frac{\partial u_1}{\partial t}$ is similar to that reported for boundary layer and the pipe flow, except that the region of constant skewness of $\frac{\partial u_1}{\partial t}$ is larger in comparison to that of pipe flow.

On the basis of these results, it is claimed that the assumptions of local isotropy can also be extended to the present complex flow, and the degree of error introduced due to such an assumption in the anisotropic region near the wall is comparable to other wall bounded flows.

ACKNOWLEDGEMENTS

The author wishes to express his deep sense of gratitude to Dr. R.S. Azad, Professor, Department of Mechanical Engineering (thesis supervisor) for his guidance, help and advice during the course of this work. The encouragement and many suggestions provided by Dr. A.C. Trupp are also gratefully acknowledged.

Many hours of fruitful and stimulating conversation with the fellow graduate students were most helpful. This work was supported by the National Research Council of Canada through the research grant held by Professor R.S. Azad. The financial support provided by The University of Manitoba in the form of graduate fellowship to the author is also gratefully acknowledged.

Special thanks and appreciation are due to Vimal, who became my life companion during the course of this work, for her extreme patience, understanding and endurance of the students' life and the gruelling pace associated with the preparation of this manuscript. Thanks are also due to Mrs. P. Giardino for cheerfully typing the thesis.

Last but not the least, I would like to express my indebtedness to my parents whose unselfish sacrifices made it all possible. My father who bade farewell to us forever, during the course of this work and my mother were always a source of strength, support and encouragement. Without their inspiration, this thesis would have been impossible.

TABLE OF CONTENTS

	<u>PAGE</u>
ABSTRACT	i
ACKNOWLEDGEMENTS	iii
TABLE OF CONTENTS	iv
LIST OF TABLES	viii
LIST OF FIGURES	ix
NOMENCLATURE	xiv
1. INTRODUCTION	1
2. SURVEY OF PREVIOUS WORK	7
2.1 The Turbulent Kinetic Energy Equation	7
2.2 The Vorticity Equation	12
3. EXPERIMENTAL EQUIPMENT AND PROCEDURE	16
3.1 Wind Tunnel, Diffuser and Traversing Mechanism	16
3.2 Instrumentation	17
3.3 Data Acquisition	20
3.4 Data Processing	22
4. RESULTS OF MEAN FLOW MEASUREMENTS	25
4.1 Flow Specification	25
4.2 Mean Static Pressure	26
4.3 Mean Velocity	28
4.4 Mean Strain and Vorticity	33

	<u>PAGE</u>
5. REYNOLDS STRESS TENSOR SURVEY	36
5.1 Turbulent Intensities	37
5.2 Stress Tensor Trace	38
5.3 Correlation Coefficient	39
5.4 Tangential Stresses	39
5.5 Wall Friction Velocities	41
6. THIRD AND FOURTH ORDER MOMENTS	42
6.1 Measurement of Skewness and Flatness Factors . .	42
6.1.1 The skewness of u_1	42
6.1.2 The skewness of u_2	45
6.1.3 Flatness factors	47
6.2 Correlations of Third and Fourth Order	49
6.2.1 Triple correlations	49
6.2.2 Quadruple correlations	53
7. TURBULENT KINETIC ENERGY BUDGET	59
7.1 Energy Budget Evaluation Technique	59
7.2 Terms of Energy Equation	61
7.2.1 Production	61
7.2.2 Mean flow convection	63
7.2.3 Viscous transport	68
7.2.4 Dissipation	69
7.2.5 Convective diffusion due to kinetic effects	72

	<u>PAGE</u>
7.2.6 Convective diffusion due to pressure effects	73
7.2.7 Convective diffusion due to kinetic and pressure effects	74
7.3 Production-Dissipation Relationship in the Diffuser	75
7.4 The Turbulent Kinetic Energy Balance in the Diffuser	78
7.5 Comments on the Turbulent Energy Budget in Wall Bounded Flows	82
8. LENGTH AND TIME SCALES OF DIFFUSER FLOW	86
8.1 Distribution of Length Scales	86
8.2 Distribution of Time Scales	89
9. THE ISOTROPIC VORTICITY BALANCE	92
9.1 Skewness of $\frac{\partial u_1}{\partial t}$ (S)	92
9.2 Second Derivative of u_1 (G)	97
9.3 Vorticity Balance	99
9.4 Visual Results	101
9.5 Consequences of the Vorticity Balance.	103
10. RECAPITULATION	108
11. CONCLUDING REMARKS	112
RECOMMENDATIONS	115
REFERENCES	116

	<u>PAGE</u>
APPENDIX A - Analysis of Static Pressure Data	122
APPENDIX B - Diffuser Turbulence Data	125
APPENDIX C - Error Considerations	150
TABLES	158
FIGURES	169
VITA	256

LIST OF TABLES

<u>TABLE</u>		<u>PAGE</u>
1	Mean parameters of the flow at diffuser entry.	158
2	Diffuser radius, pressure gradient and the friction velocity at various axial stations.	159
3	Radial variation of the static pressure in the diffuser.	160 - 161
4	Atmosphere conditions for static pressure data in Table 3.	162
5	Dissipation rate in the diffuser at station 12, $\xi_2 = 0.91$	163
6	Variations in the ratio of excess production and dissipation in the diffuser.	164
7	Various constants associated with figure 79.	165
A-1	The standard error of estimation for polynomial fits of order 1 to 5 to mean static pressure data.	166
A-2	The standard error of estimation for best polynomial fit to various regions of pressure data.	167
A-3	Coefficients of 4th order polynomial fit to static pressure data for $Re = 58000$	168
B-1 to B-12	Diffuser turbulence data measured in the laboratory. . .	126 - 149

LIST OF FIGURES

<u>FIGURE</u>		<u>PAGE</u>
1	Geneology of turbulent kinetic energy balance equation.	169
2	Diffuser geometry.	170
3	Diffuser traversing mechanism.	171
4	Mean static pressure distribution.	172
5	Mean static pressure gradient in the diffuser	173
6	Mean axial velocity profiles.	174
7	Mean radial velocity profiles.	175
8	Comparison of mean axial velocity profile at station 30 to that of Okwuobi & Azad.	176
9	Comparison of mean radial velocity profiles at station 30.	177
10	Radial derivative of the mean axial velocity.	178
11	Directions of mean strain rate.	179
12	Directions of the mean principal stresses.	180
13	Distribution of relative turbulent intensities. . . .	181 - 183
14	Distribution of the turbulence intensity $\frac{u_1'}{U_b}$	184
15	Turbulent stress tensor trace in the diffuser. . . .	185
16	The correlation coefficient in the diffuser.	186
17	Distribution of the tangential stresses.	187
18	Variation of the ratio of tangential stress to the trace.	188
19	The wall friction velocities(u_{*})in the diffuser. . .	189
20	Skewness of u_1 in the diffuser.	190

<u>FIGURE</u>		<u>PAGE</u>
21	Skewness of u_2 in the diffuser.	191
22	Flatness factor of u_1 in the diffuser.	192
23	Flatness factor of u_2 in the diffuser.	193
24	Flatness factor of u_3 in the diffuser.	194
25	Radial positions where skewness of u_1 & u_2 changes sign.	195
26	Skewness of u_1 and non zero 3rd order correlations at the diffuser axis.	196
27	Flatness factors at radial positions where skewness of u_1 is zero.	197
28	Flatness factors at the diffuser axis.	198
29	Third order velocity correlations of $u_1 u_2^2$	199
30	Third order velocity correlations of $u_1 u_3^2$	200
31	Third order velocity correlations of $u_1^2 u_2$	201
32	Third order velocity correlations of $u_2 u_3^2$	202
33	Comparison of $\overline{u_2 u_3^2}$ and $\overline{u_2^3}$ at station 30.	203
34	Comparison of $\overline{u_1 u_3^2}$ and $\overline{u_1^3}$ at station 30.	204
35	Distribution of the bulk convection velocities in the diffuser.	205
36	Fourth order correlations of $u_1^2 u_2^2$	206
37	Fourth order correlation of $u_1^2 u_3^2$	207
38	Fourth order correlations of $u_2^2 u_3^2$	208
39	Fourth order correlations of $u_1^3 u_2$ and $u_1 u_2^3$	209
40	Distribution of fourth order correlations at the diffuser axis.	210
41	Turbulent kinetic energy production in the diffuser.	211

<u>FIGURE</u>	<u>PAGE</u>
42	Variation of the mean flow convection term. 212
43	Comparison of the mean flow convection term at station 30 to that of Okwuobi & Azad (1973).. . . . 213
44	Radial and axial components of mean flow convection term at station 30 evaluated from the data of Okwuobi & Azad (1972). 214
45	Mean flow convection term at station 30 obtained from figure 44. 215
46	Mean flow convection at 3 axial stations in the wall layer evaluated from the data of Okwuobi & Azad (1972). 216
47	Viscous work term in the diffuser. 217
48	Distribution of the dissipation term. 218
49	The u_1 spectra at station 30 from Okwuobi & Azad (1973). 219
50	The u_1 spectra at station 30 from Hummel (1978). 220
51	Convective diffusion due to kinetic effects in the diffuser. 221
52	Convective diffusion due to pressure effects in the diffuser. 222
53	Distribution of the convective diffusion due to kinetic and pressure effects. 223
54	Comparison of the production and dissipation terms at station 30. 224
55	Variation of the ratio of excess production to dissipation at station 30. 225
56	Turbulent kinetic energy balance in the diffuser at station 67. 226
57	Turbulent kinetic energy balance in the diffuser at station 57. 227
58	Turbulent kinetic energy balance in the diffuser at station 50. 228

<u>FIGURE</u>		<u>PAGE</u>
77	Variation of G as a function of R_λ	247
78	Ratio of the rate of dissipation and the production of vorticity.	248
79	Ratio of the dissipation and production of vorticity as a function of R_λ	249
80	Photographs of oscilloscope traces.	250
81	Maximum flatness factor of narrow band filtered u_1 signal and the intermittency factor of $\partial u_1 / \partial t$ at station 30.	251
A-1	Mean static pressure distribution for $Re = 58000$	252
C-1	Various correction factors for station 18.	253
C-2	Various correction factors for station 6.	254
C-3	A magnified view of 2 DISA single wire probes.	255

NOMENCLATURE

A,B	Inputs of the multifunction turbulent processor
$a_0 \dots a_4$	Coefficients of the polynomial
D	Pipe diameter
d	Diameter of the hot-wire
E	Output voltage from the hot-wire
E_1	One dimensional u_1^2 spectra
e_1, e_2	A.C. component of the hot-wire signals
$\dot{\epsilon}_{x_1 x_2}$	Mean rate of strain
G	Non-dimensionalized second derivative of u_1
$H_1 \dots H_4$	Correction factors for Reynolds stresses
i	Subscript; $i = 1, 2, \text{ or } 3$
j	Subscript; $j = 1, 2, \text{ or } 3$
k	constant in the hot wire response equation
k_1	one dimensional wave number
L	pipe length
L_ϵ	Characteristic length scale of the flow (equation 28)
ℓ	Sensitive length of the hot wire
M	Order of the polynomial
m	Constant in equation (8)
N	Number of data points
n	Constant in equation (8)
P	Mean static pressure or rate of turbulent energy production
p	Fluctuating component of the pressure field

P_m	Measured and normalized mean static pressure
P_c	Computed mean static pressure from the polynomial
$\frac{q^2}{q^2}$	Trace of the turbulent stress tensor; $q^2 = \overline{u_1^2} + \overline{u_2^2} + \overline{u_3^2}$
R	Pipe radius
R_d	Local radius of the diffuser
r	Radial distance from the axis
Re	Reynolds number; $Re = U_b R / \nu$
R_λ	Turbulence Reynolds number (equation 27)
R_{LE}	Characteristic Reynolds number of the flow (equation 29)
S	Skewness of $\frac{\partial u_1}{\partial t}$.
Se	Standard error of estimation
T	Kolmogoroff time scale (equation 30)
t	Time
U_1	Mean axial velocity
U_2	Mean radial velocity
U_b	Pipe bulk average velocity
u, v	A.C. signal inputs to the multifunction turbulent processor
u_i	Fluctuating velocity ($i = 1, 2, \text{ or } 3$)
$u_i u_j$	Correlation of the fluctuating velocities ($i = 1, 2, \text{ or } 3$ and $j = 1, 2, \text{ or } 3$)
u_*	Friction velocity
V	Bulk convection velocity = $\frac{\overline{u_2 q^2}}{q^2}$
y	Radial distance from the wall
y^+	Non-dimensional radial distance from the wall; $y^+ = \frac{y u_*}{\nu}$

z	Fluctuating component of an instantaneous signal
α	Angle of the mean strain rate with principal axis
α_1	A function defined as; $\alpha_1 = \frac{-7}{6\sqrt{15}} (\epsilon/\nu)^{1/2} S$
β	Angle of the principal stresses
ϵ	Turbulent energy dissipation rate per unit mass
η	Kolmogoroff length scale; $\eta = \left(\frac{\nu^3}{\epsilon} \right)^{1/4}$
λ	Taylor's microscale (dissipation length scale)
ν	Kinematic viscosity of air
ξ_1	Non-dimensional axial distance, $\xi_1 = x_1/R$
ξ_2	Non-dimensional radial distance, $\xi_2 = x_2/R$
ξ_4	Axial distance from diffuser exit towards pipe, non-dimensionalized with pipe radius R
ρ	Density of air
τ	Characteristic time scale of the flow (equation 31)
u	Kolmogoroff velocity scale; $u = (\nu\epsilon)^{1/4}$
ϕ	Angle of the inclined hot-wire
Ω_{x_3}	Mean vorticity component
ω	Fluctuating vorticity vector
ω_i	Fluctuating vorticity component ($i = 1, 2, \text{ or } 3$)
—	Overbar; denotes time average
'	Prime; denotes root mean square (r.m.s.) value

1. INTRODUCTION

Turbulence is an irregular three-dimensional, time dependent and the most complicated kind of fluid motion. The term turbulent denotes the superimposition of an irregular fluctuating motion on the main stream. This fluctuation is usually so complex in its details that it seems to be intractable to mathematical treatment, but the resulting mixing motion is very important for the course of the flow and for the equilibrium of forces. Therefore the turbulence studies may be defined as the art of understanding the Navier-Stokes equations without actually solving them. In following this path, certain theoretical principles which allow us to introduce a measure of order into the experimental material have been established.

Laboratory turbulent shear flows can usually be divided into two groups. First being free turbulent flows; i.e., the flow in jets and wakes where no restricting walls are present, and second being the wall bounded flows; i.e., flow through pipes, diffuser and along plates, etc. The wall bounded flows can further be divided in three groups on the basis of their pressure gradients: (1) negative (favourable) pressure gradient flow: pipe flow; (2) zero pressure gradient flow: flow along a flat plate and, (3) positive (adverse) pressure gradient flow: diffuser flow.

The pipe flow and the boundary layer on a solid surface, which are important in engineering and convenient to explore experimentally, have been studied vigorously by various investigators working in the field. The diffuser which is a simple, useful, fluid-mechanical element used for example in turbomachinery as a pressure recovery

device should be the next logical field of investigation. Physically, a diffuser converts mean kinetic energy into flow energy which produces positive pressure gradient in the direction of flow. This also increases the intensity of highly energetic turbulent processes near the wall, which results in high turbulence intensity in the flow field far beyond any other wall bounded flow. This high intensity of turbulence makes the diffuser research interesting and experimentally challenging, while the effect of adverse pressure gradient on the structure of turbulence is of considerable importance from the point of view of scientific knowledge. Understanding of the structure of this turbulence has been the subject of continuing turbulence research. By structure of turbulence is meant the organization of turbulence phenomenon, the source of its energy supply and the mechanism by which this energy is extracted from the mean flow, and distributed to the whole flow field and finally how it is converted to the internal (heat) energy by the action of viscosity.

The properties of the mean flow for different geometries of the diffuser have been studied by various workers and these have been summarized by Okwuobi (1972). But the experimental work on the turbulence characteristics of the flow field is generally meagre in comparison to the work for other wall bounded flows. The structure of turbulent shear flow in a diffuser was probably first investigated by Ruetenik & Corrsin (1955). They experimentally studied the turbulence properties of fully developed, plane diffuser (diverging channel) flow at a total divergence angle of 2° . Their results showed that there were large increases in turbulent energy and average

shear levels compared with those of Laufer (1951) for parallel wall channel flow. Okwuobi & Azad (1973) provided detailed measurements of the Reynolds stress tensor and also computed kinetic energy budget for one axial station in a 8° conical diffuser. The conical geometry of the diffuser was chosen as it provides a symmetric distribution of the mean and turbulent quantities about its axis. On the basis of their results, Okwuobi & Azad (1973) claimed that the dissipation of turbulent energy is generally negligible in the conical diffuser and the production of turbulent energy is mainly balanced by the kinetic and pressure diffusion in radial and axial direction. This was reported to be due to the adverse pressure gradient in the direction of the flow. No further studies have been reported about this peculiarity of the diffuser flow. Thus, further experimental studies are required to understand the physical processes involved which make the dissipation of turbulent energy negligible in the diffuser. The importance of such a study is further enhanced by the work of Hummel (1978), who measured various structure functions in the diffuser and indicated many similarities with the boundary layer flows.

Generally, the turbulent flow of real fluids is of a dissipative nature. Because of this dissipation of turbulent energy, a continuous supply of energy from some external source is necessary to maintain the turbulence. This external source is usually the mean flow. The rate of supply of kinetic energy to the turbulence is the rate at which work is done by the mean rate of strain against the Reynolds stresses in the flow as it stretches the turbulent vortex lines. The stress producing eddies are the larger ones, which are best able to

interact with the flow and extract its energy. The vortex stretching tends to make the smaller eddies lose all sense of direction, and thus become statistically isotropic. The structure of these smaller eddies is similar for all turbulent flows (Batchelor, 1947). These eddies of smallest length scales dissipate through the action of viscosity. The turbulent kinetic energy budget provides the mean balance between the production and dissipation of turbulence in the flow field. It has also been pointed out by Townsend (1956) that the turbulent energy balance should be studied first to fully understand the structure of turbulence. This is a rather natural and logical step as the energy balance is the study of the trace of Reynolds stress tensor, which is the first consequence of the turbulence. Since the apparent stresses appear in the mean momentum equations for turbulent flow and thus should first be investigated. The study of energy balance involves the long time averages of turbulent quantities which may obscure some details, but still provides significant information about the physics of flow. Knowledge of the energy balance is also important from the point of view of developing and testing mathematical models for turbulence.

Recent visual studies have further focused attention on the disturbance mechanism and the turbulence production process. Based on the visual studies, Kline et al (1967), Kim et al (1971) and Corino & Brodkey (1969) reported that the disturbance mechanism consists substantially of intrushes of fluid with high axial momentum into low momentum fluid near the wall alternating with ejections of low momentum fluid outward from the wall. Kim et al (1971), Grass (1971),

Willmarth & Lu (1972) and Wallace et al (1972) have shown that the energy production process is strongly associated with and dominated by this intermittent inrush-ejection cycle, and consequently by the large-scale turbulence, thereby confirming the earlier hypothesis. Wallace et al (1972) have pointed out that the turbulence dissipation process is also strongly related to the random and intermittent inrush-ejection cycle, because the region of the inrush and ejection events appear to correspond to the region of high local shear rates and consequently to high local dissipation of energy, which implies the presence of finer scale structure of turbulence.

The finer structure (smaller eddies) also represents the turbulence vorticity field of the flow. This vorticity is three-dimensional and the vortex stretching provides the essential maintenance mechanism. Therefore, the study of the turbulent vorticity balance is essentially an attempt to understand the finer structure of turbulence which is inevitably required for better understanding of the turbulence mechanism.

The primary objective of the experimental work presented here was to test the hypothesis put forward by Okwuobi & Azad (1973) that the dissipation is negligible in the conical diffuser. In this respect the present research work is a follow up of the work of Okwuobi & Azad (1973) which was also conducted here at The University of Manitoba.

The energy balance presented by Okwuobi & Azad was only for one axial station and thus no information is available about the nature of decreasing dissipation from the pipe flow at the diffuser

inlet to its exit. Thus it is proposed that the energy balance would be evaluated at several axial stations to study the mechanism of decreasing dissipation in detail. This would also provide a check on the results of Okwuobi & Azad. Also, since the pressure recovery is the basic physical feature of a diffuser, it would be worthwhile to estimate the relative magnitude of the pressure-velocity correlation in the turbulent field. To this end, the convective diffusion due to kinetic effects would be evaluated from the experimental data, and the pressure diffusion would be estimated by balance. At present there is complete lack of such an information in the literature available for adverse pressure gradient flows.

Most of the vorticity present in the flow field is associated with the smaller eddies which tend to be isotropic. Therefore, one of the objectives of the present study was also to gain information about the isotropic vorticity-balance through detailed measurements of the fine structure of turbulence in an adverse pressure gradient flow, thereby also investigating the applicability of isotropic assumptions to such a non-uniform flow.

The conical diffuser chosen for this study was the same as used by Okwuobi & Azad (1973), having an 8° included angle and an area ratio of 4 to 1. Sovran & Klomp (1967) have shown that such a diffuser possesses optimum pressure recovery characteristics. Also the property of axisymmetry of the conical diffuser offers the experimental advantage as it provides two similar points in the same flow situation. All tests were conducted with fully developed pipe flow at the diffuser entry.

2. SURVEY OF PREVIOUS WORK

In this chapter, material relevant to the present study is reviewed. The chapter is divided in two sections, first dealing with the turbulent kinetic energy and the second with the turbulent vorticity. Each section contains the necessary mathematical equations followed by a review of published experimental results.

2.1 The Turbulent Kinetic Energy Equation

The turbulent kinetic energy equation for the axisymmetric flow, assuming stationarity, may be written in the form (Okwuobi & Azad, 1973)*

$$I + II + III + IV + V = 0 \quad (1)$$

where the different terms have the following meaning.

Mean flow convection:

$$I = \frac{1}{2} \left[\left(\frac{u_1}{U_b} \right) \frac{\partial}{\partial \xi_1} \overline{\left(\frac{q^2}{U_b^2} \right)} + \left(\frac{u_2}{U_b} \right) \frac{\partial}{\partial \xi_2} \overline{\left(\frac{q^2}{U_b^2} \right)} \right].$$

Convective diffusion by kinetic and pressure effects:

$$II = \frac{1}{2\xi_2} \left\{ \frac{\partial}{\partial \xi_1} \left[\xi_2 \overline{\left(\frac{u_1}{U_b} \right) \left(\frac{q^2}{U_b^2} + \frac{2p}{\rho U_b^2} \right)} \right] + \frac{\partial}{\partial \xi_2} \left[\xi_2 \overline{\left(\frac{u_2}{U_b} \right) \left(\frac{q^2}{U_b^2} + \frac{2p}{\rho U_b^2} \right)} \right] \right\}.$$

*Hereafter also referred to as OA.

Production:

$$\begin{aligned} \text{III} = & \left[\left(\frac{\overline{u_1 u_2}}{U_b^2} \right) \frac{\partial}{\partial \xi_2} \left(\frac{U_1}{U_b} \right) + \left(\frac{\overline{u_1^2}}{U_b^2} - \frac{\overline{u_2^2}}{U_b^2} \right) \frac{\partial}{\partial \xi_1} \left(\frac{U_1}{U_b} \right) \right. \\ & \left. + \left(\frac{\overline{u_1 u_2}}{U_b^2} \right) \frac{\partial}{\partial \xi_1} \left(\frac{U_2}{U_b} \right) + \frac{1}{\xi_2} \left(\frac{U_2}{U_b} \right) \left(\frac{\overline{u_3^2}}{U_b^2} - \frac{\overline{u_2^2}}{U_b^2} \right) \right]. \end{aligned}$$

Viscous work:

$$\text{IV} = - \left(\frac{1}{2R_e} \left\{ \frac{1}{\xi_2} \frac{\partial}{\partial \xi_2} \left[\xi_2 \frac{\partial}{\partial \xi_2} \left(\frac{q^2}{U_b^2} \right) \right] + \frac{\partial^2}{\partial \xi_1^2} \left(\frac{q^2}{U_b^2} \right) \right\} + \frac{\nu R}{U_b^3} \frac{\partial u_i}{\partial x_j} \frac{\partial u_j}{\partial x_i} \right).$$

Dissipation:

$$\nu = \frac{R \epsilon}{U_b^3}.$$

here:

$$q^2 = u_i u_i, \quad \xi_1 = \frac{x_1}{R}, \quad \xi_2 = \frac{x_2}{R}, \quad R_e = \frac{R U_b}{\nu}$$

$$\epsilon = \nu \overline{\left(\frac{\partial u_i}{\partial x_j} + \frac{\partial u_j}{\partial x_i} \right) \frac{\partial u_i}{\partial x_j}}$$

and the normalizing quantities R and U_b are the pipe radius and the pipe bulk average velocity respectively. In the above terms the overbar indicates a time averaged quantity. The turbulent kinetic energy

budget is a conservation equation for the quantity $\frac{1}{2} \rho q^2$ and as such each term describes a rate of appearance or disappearance of turbulent kinetic energy at a point.

The terms of the energy equation can be divided into two classes: those dealing with the local creation or the dissipation of turbulent kinetic energy within the control volume and those dealing with the movement of kinetic energy into or out of the control volume. The structure of the flow both upstream and downstream of a particular point determines the behavior of the turbulent kinetic energy and therefore the normal stresses at that point. This is implicit in the energy balance equation because these quantities appear in spatial derivative terms which would require integration over the whole flow field for analytic solution.

The fundamental starting points for the development of the turbulent kinetic energy balance equation are the Navier-Stokes and the continuity equation which are respectively statements of Newton's law (a force balance) and mass conservation. Multiplication of the sum of these two equations by the total velocities yields an energy equation. By the usual processes of Reynolds decomposition and time averaging followed by subtraction of the mean energy equation, the dimensional form of the above equation is obtained. The detailed derivation of the turbulent kinetic energy equation is available in Hinze (1959) (in rectangular coordinates), Huffman (1968) (in mixed cylindrical and rectangular coordinates), Laufer (1954) in cylindrical coordinates and the details will not be repeated here. The genealogy of the turbulent kinetic energy equation is summarized diagrammatically

in figure 1. In fully developed turbulent pipe flow the energy equation becomes much simpler as both the longitudinal space derivatives and the mean radial velocity are zero. In particular, the mean flow convection term disappears entirely.

Many researchers have reported data on the turbulent kinetic energy budget for various wall bounded flow fields; i.e., Laufer (1954) in pipe flow, Ruetenik & Corrsin (1955) for slightly divergent channel flow, Klebanoff (1955) in boundary layer with zero pressure gradient, Nakagawa et al (1975) in channel flow and Hanjalić & Launder (1972 a) in an asymmetric channel flow. A general picture which emerges from these flows is that in a turbulent flow field, energy is extracted from the mean flow (production) and converted into internal energy (heat) by viscosity (dissipation). Transfer terms such as mean flow convection and convective diffusion due to kinetic and pressure effects transport energy from surplus to deficit areas, where it is dissipated. At any cross section there is always an overall energy balance between production and dissipation, which is achieved with the help of transfer terms.

Okwuobi & Azad (1973) have provided some data on the turbulent kinetic energy budget in a conical diffuser. Their results showed that the dissipation is negligible in the diffuser and the production is mainly balanced by convective diffusion term. This finding is in direct contradiction to other wall bounded flows. The diffusion term was obtained by them as a closure term in the energy equation and thus acted as the balancing term of the equation. The diffusion term simply transports the energy from one place to another and does not

dissipate it. Therefore the energy stays in the flow field and as such must show up somewhere else in the field. Okwuobi & Azad (OA) postulated that the convection of energy must be taking place in the axial and radial direction. However, the energy equations derived from the Navier-Stokes equations provide for such movement of energy. To achieve local equilibrium, OA implied that the convective diffusion is similar to that of dissipation and attributed it to the existence of adverse pressure gradient in the flow field. Such an explanation makes this flow, with adverse pressure gradient, appear entirely different from other wall bounded flows. Ruetenik & Corrsin (1955) have also measured energy budget in a fully developed, equilibrium plane diffuser flow at a total divergence angle of 2° and found that production is mainly balanced by dissipation. Since the mean pressure gradient in a conical diffuser is usually not in equilibrium, a direct comparison may not be justified. However, Sovran & Klomp (1967) stated that a diffuser with linear amplification acts as an amplifier of velocity fluctuations entering it and thus it could be expected to have some similarities to flow entering the diffuser. In the experimental setup of OA, flow at entry was fully developed pipe flow. But the energy budget presented by OA tends to imply that something very drastic happens to the flow after entering the diffuser. Since data of OA were only for one axial station, no detailed information could be gathered about this sudden change in the turbulent nature of the flow. Therefore, it would be interesting to investigate the energy balance in the whole flow field of a conical diffuser, radially and axially. This would help to check the validity of the conclusions reached by Okwuobi & Azad (1973)

and to fully understand the structure of turbulence in a conical diffuser with an adverse pressure gradient.

2.2 The Vorticity Equation

The vorticity equation derived directly from the Navier-Stokes equation by Von Karman and as reported by Batchelor & Townsend (1947) for homogeneous isotropic turbulence is:

$$3 \frac{d\omega_i^2}{dt} = 2 \overline{\omega_i \omega_j \frac{\partial u_i}{\partial x_j}} + 2 \nu \overline{\omega_i \frac{\partial^2 \omega_i}{\partial x_j^2}} \quad (2)$$

where

ω_i is the component of vorticity in the i -direction.

The first term on the right hand side is positive and represents the rate of production of vorticity; whereas the 2nd term on the right side is essentially negative and represents a rate of destruction of vorticity due to viscosity. In a flow field, when positive extension of a vortex filament occurs, the magnitude of the local vorticity increases due to the consequent lateral contraction and angular acceleration. Thus in parts of the fluid where there is a positive rate of extension of the vortex filament, the magnitude of the vorticity will be high. Taylor (1938) (referenced in Batchelor & Townsend, 1947) pointed out that this production of vorticity due to random, diffusive extension of vortex lines is a fundamental process in the mechanics of turbulence and is the reason for the very high rate of dissipation of turbulence energy.

The effect of extension of the vortex lines is to tend to make the vorticity distribution 'spotty', with small regions of high vorticity; on the other hand, the effect of viscosity is strongest in regions of high vorticity, and tends to diffuse it evenly throughout the fluid (Batchelor & Townsend, 1947). The vorticity equation (2) represents the balance between these two effects, and a simplified form of this equation which could be used for comparison with experimental data as given by Batchelor & Townsend (1947) is:

$$\frac{d\omega'^2}{dt} = \frac{7}{3\sqrt{5}} \omega'^3 S - \frac{14}{3\sqrt{5}} \omega'^3 \frac{G}{R_\lambda} \quad (3)$$

where S is the minus skewness factor of the probability distribution of $\partial u_1 / \partial x_1$ (the minus sign is introduced because the skewness is found to be negative) and is defined as:

$$S = - \frac{\overline{\left(\frac{\partial u_1}{\partial x_1}\right)^3}}{\left[\overline{\left(\frac{\partial u_1}{\partial x_1}\right)^2}\right]^{3/2}} \quad (4)$$

The contribution to $d\omega'^2/dt$ from the process of vortex extension is directly proportional to S .

The factor G/R_λ is related to the decay of vorticity due to viscosity and is defined as:

$$G = u_1'^2 \frac{\overline{\left(\frac{\partial^2 u_1}{\partial x_1^2}\right)^2}}{\left[\overline{\left(\frac{\partial u_1}{\partial x_1}\right)^2}\right]^2} \quad (5)$$

and:

$$R_\lambda = \frac{u_1' \lambda}{\nu}$$

A representative measure of the factors S , G and λ can be obtained by measuring $\left(\frac{\partial u_1}{\partial t}\right)$ and using Taylor's assumption of space-time equivalence.

Thus:

$$S = \frac{\overline{\left(\frac{\partial u_1}{\partial t}\right)^3}}{\left[\overline{\left(\frac{\partial u_1}{\partial t}\right)^2}\right]^{3/2}}$$

$$G = u_1' \frac{\overline{\left(\frac{\partial^2 u_1}{\partial t^2}\right)^2}}{\left[\overline{\left(\frac{\partial u_1}{\partial t}\right)^2}\right]^2}$$

$$\lambda^2 = \left[\frac{u_1'^2}{\overline{\left(\frac{\partial u_1}{\partial t}\right)^2}} \right] u_1'^2$$

The skewness, S , of $\frac{\partial u_1}{\partial t}$ has been measured for grid turbulence (which provides a good approximation to isotropic turbulence) and the reported values vary between 0.3 & 0.5 (Batchelor, 1947; Batchelor & Townsend, 1947; Saffman, 1963; Betchov, 1956; Panchev, 1971).

Batchelor & Townsend (1947) claimed that S was essentially constant and a value of 0.39 was suggested. Ueda & Hinze (1975) reported the values of S for boundary layer with zero pressure gradient. They found that it has a constant value of about 0.38 in the outer region

but increases near the wall reaching a maximum of approximately 0.9 at $y^+ \approx 20$ before decreasing further towards the wall. A similar distribution was also indicated by Ueda & Mizushima (1977) and Elena (1977) for pipe flow. Since S is the 3rd moment of the time derivative of u_1 , it is a good indicator of the fine structure of turbulent flow field. And the similarity in the distribution of S in shear flows to that of grid turbulence indicates that the isotropic assumptions in the small scale turbulence can be extended to these flows except near the wall. However, no such data are available for diffuser flow.

Batchelor & Townsend have also provided some information about the factor G . It was shown to vary linearly with the turbulence Reynolds number in the range 20 to 60. Values of G have not been reported for any other flow. Therefore, this study was undertaken to obtain the relative values of these parameters in a conical diffuser to assess the turbulent vorticity balance in such a flow.

3. EXPERIMENTAL EQUIPMENT AND PROCEDURE

3.1 Wind Tunnel, Diffuser and Traversing Mechanism

The experiments were conducted in a low speed open circuit wind tunnel described previously by Azad & Hummel (1971) and Okwuobi & Azad (1973). Briefly, air was blown through an 89:1 Contraction Cone and 74 diameters long steel pipe of 10.16 cm inside diameter before entering the diffuser.

The diffuser (figure 2) was machined from cast aluminum. A machined reinforcement ring which could be rotated to any angular position was adapted to the outlet end of the diffuser to support the traversing mechanism (figure 3) with a micrometer head graduated in 0.001 mm. The traversing mechanism was basically the same as used by OA with some minor changes to improve its positioning accuracy. The probes were mounted on a 2.5 cm diameter tube entering the diffuser from the downstream end. A 22 cm long taper was fitted between the end of the tube and the probe support to minimize any flow blockage effect upstream of the tube. The hot wire holder could be rotated about its axis to align the probe with the desired plane, slid in and out (in x_1 direction), and positioned in the x_2 direction by the traversing mechanism. The overall mechanical structure of the traversing mechanism was sufficiently robust to minimize probe vibration and offer ease of maneuverability. The Reynolds number of the flow was varied by changing the fan speed and observing the pressure drop across the contraction cone which was calibrated with pitot tube in terms of centre line mean velocity in the diffuser.

Okwuobi & Azad (1973) have shown that the flow in pipe upstream of the diffuser is fully developed and by using forward and reverse-facing pitot tubes, they have also shown that the flow in the diffuser does not separate.

3.2 Instrumentation

Mean static pressure along the diffuser wall was measured with a static pressure round tube having an external diameter of 1 mm. Mean velocity for hot-wire calibration was obtained using a round total pressure tube of 1 mm and 0.76 mm external and internal diameters respectively. The probe readings were recorded on a Betz projection manometer with 0.1 mm of water scale intervals. No corrections were attempted to account for turbulence.

Turbulent measurements (except that of $\frac{\partial u_1}{\partial t}$) were made with standard DISA 55P51 gold plated x-probe (1.25 mm wire length, 5 μ m wire diameter). For measurements of $\frac{\partial u_1}{\partial t}$ a special DISA 55P01 gold plated single wire probe (0.625 mm wire length, 2.5 μ m wire diameter) was used. A standard DISA 55P01 gold plated single wire probe (1.25 mm wire length, 5 μ m wire diameter) was also used to measure u_1 spectra and $\frac{\partial u_1}{\partial t}$ at one station to compare it with the results obtained with special single wire probe. The ℓ/d ratio of the wires in each case was 250. The electronic equipment included DISA 55M01 constant temperature anemometers, 55D10 linearizers, 55D35 r.m.s. meters, 55D31 digital voltmeters, Krohn-Hite 3770 filter, Tetrax 466 dual beam storage scope and a true integrating digital voltmeter. Also used were a multi-function turbulent processor TM377, a differentiator TM-TD-1 and a 5

channel multi-integrator, which were made locally and a detailed description has been given by Arora & Azad (1978).

The standard procedure recommended in the DISA technical literature for the hot-wire operation was followed to obtain the linearized turbulence signal from the single and x-wire probes. The circumferential velocity component (u_3) was obtained by rotating the x-probe on its axis by 90° from the u_1u_2 plane. The u_2u_3 component was similarly obtained by aligning the x-probe at 45° to both x_1x_2 and x_1x_3 planes. The probes were calibrated in situ on the diffuser axis at 6 cm from the diffuser exit plane. Pressure tube measurements of the centre line velocity in the diffuser at station 12 for different static pressure difference across the contraction cone formed the basis of the hot-wire calibration. The linearized outputs from the x-probe wires were matched to within 1.5% over the required operation range. The probes were calibrated for measurements at each station. The thermal stability of the electronic equipment was maintained by allowing the units to remain powered during the course of the experimental work even when the instruments were not in use.

The x-wire probe was operated at an overheat ratio of 0.8, but for the operation of special single wire probe, this ratio was reduced to 0.4. No corrections were applied to the turbulent measurements of x-wire to account for wire length effects or variation of the inclined wire response from the cosine law. The accuracy of the dissipation measurements was improved by the use of special DISA 55P01 probe, as its length and diameter were both half as compared to the standard DISA probe. However, the wire length was still larger

than the Kolmogoroff length scale $\eta = \left(\frac{\nu^3}{\epsilon}\right)^{1/4}$. Therefore, the dissipation measurements obtained from special single wire were corrected for wire length effects using Wyngaard's (1969) analysis for single wire. But no such correction was applied to the measurements of S and G, as these quantities were normalized by $\left(\frac{\partial u_1}{\partial t}\right)^2$.

To measure various moments, the linearized outputs from the x-wire were fed to the multifunction turbulent processor. At the output of which moments up to 4th order of the signals formed by adding and subtracting the input signals were available. For dissipation measurements, the linearized hot-wire signal from the special DISA 55P01 probe was fed to the TM-TD-1 time differentiator. This time differentiated signal was then fed to the two inputs of TM377. The output at B Channel of the signal processor provided the second and third powers of $\frac{\partial u_1}{\partial t}$. For the second derivative the built-in time differentiator of TM377 on Channel A was used. The hot-wire signal was filtered at 28 kHz before and after each differentiation. For this purpose, three built-in filters of TM377 and a Krohn-Hite filter was used. The differentiators used were of solid state, low noise type and were better than that of DISA 55A06. The multipliers used in TM377 were of Burr-Brown 4205-k type and provided an overall precision better than 1% for reference voltages between 0.1 and 10 volts. To improve the operation of multipliers and to decrease the measuring errors, the input signals to multipliers were amplified considerably but not enough to saturate the corresponding circuit.

In the operation of hot-wire anemometry, even small amounts of dirt depositions on the sensing element can affect its frequency

response, thereby giving erroneous results. The possibility of such an error is discussed in Appendix C along with considerations for other possible errors.

3.3 Data Acquisition

Static pressures along the diffuser wall were measured at 42 axial locations using a static pressure tube for 7 different Reynolds numbers varying from 32000 to 86000 based on pipe average velocity and pipe radius. Measurement positions were 1 cm apart near the diffuser entrance and were increased to 2 cm in the downstream direction. The radial variation of the static pressure was, however, measured for only one Reynolds number of 58000 and at 12 equidistant (6 cm) axial stations in the diffusers. These axial stations were the same as used by Okwuobi & Azad (1973).

The linearized signal from each wire of the x-probe was used as input to turbulent processor TM377. At the output, all possible combinations up to the 4th order moments of the turbulent quantities obtained by adding and subtracting the two input signals were available. The voltage output of the moments were integrated over a period of 100 seconds and then read on a digital voltmeter. All these moments were measured for 13 axial locations at 69, 67, 65, 61, 57, 50, 40, 30, 24, 18, 12, 6, and 0 cm from the diffuser exit plane (hereafter referred to as stations). These axial stations were chosen on the basis of the results of static pressure measurements. Moments were measured along the whole diffuser diameter at each axial station to confirm the existence of axisymmetry.

To measure the correlations of the two transverse velocity fluctuations ($u_2 u_3$), the x-probe was placed in the flow in such a way that its plane was parallel to the flow and at an angle of 45° to the x_2 and x_3 axes (Townsend, 1959; Wygnanski & Fiedler, 1969; Hanjalić & Launder, 1972a and Irwin, 1973). The output of the hot-wire sets are then (see Arora & Azad, 1978, for details):

$$e_1 \propto u_1 + k(u_2 + u_3)$$

$$e_2 \propto u_1 - k(u_2 + u_3)$$

subtraction of the signals gives:

$$(e_1 - e_2) \propto (u_2 + u_3).$$

The squaring of this combined signal yields:

$$\overline{(e_1 - e_2)^2} \propto \overline{u_2^2} + 2\overline{u_2 u_3} + \overline{u_3^2}$$

and the cube:

$$\overline{(e_1 - e_2)^3} \propto \overline{u_2^3} + 3\overline{u_2^2 u_3} + 3\overline{u_2 u_3^2} + \overline{u_3^3}$$

and

$$\overline{(e_1 - e_2)^4} \propto \overline{u_2^4} + 4\overline{u_2^3 u_3} + 6\overline{u_2^2 u_3^2} + 4\overline{u_2 u_3^3} + \overline{u_3^4}.$$

The results of $u_1 u_3$ correlations had shown that terms involving the odd powers of u_3 are zero (as should be the case for the axisymmetric flow),

i.e., $\overline{u_3^3}$, $\overline{u_2 u_3}$, and $\overline{u_2^2 u_3}$, etc. vanish.

Then:

$$\overline{(e_1 - e_2)^2} \propto \overline{u_2^2} + \overline{u_3^2}$$

$$\overline{(e_1 - e_2)^3} \propto \overline{u_2^3} + 3\overline{u_2 u_3^2}$$

and:

$$\overline{(e_1 - e_2)^4} \propto \overline{u_2^4} + 6\overline{u_2^2 u_3^2} + \overline{u_3^4}$$

Therefore the ratios:

$$\frac{\overline{(e_1 - e_2)^3}}{[\overline{(e_1 - e_2)^2}]^{3/2}} = \frac{\overline{u_2^3} + 3\overline{u_2 u_3^2}}{(\overline{u_2^2} + \overline{u_3^2})^{3/2}} \quad (6)$$

and

$$\frac{\overline{(e_1 - e_2)^4}}{[\overline{(e_1 - e_2)^2}]^2} = \frac{\overline{u_2^4} + 6\overline{u_2^2 u_3^2} + \overline{u_3^4}}{[\overline{u_2^2} + \overline{u_3^2}]^2} \quad (7)$$

is formed. From which, using earlier obtained data of $\overline{u_2^2}$, $\overline{u_3^2}$, $\overline{u_2^3}$, $\overline{u_2^4}$ and $\overline{u_3^4}$, the quantities $\overline{u_2 u_3^2}$ and $\overline{u_2^2 u_3^2}$ were then calculated.

3.4 Data Processing

The static pressure data obtained were normalized by total velocity head in the pipe and polynomials of degree 1 to 5 were fitted

to these data. It was found that the 4th order polynomial gave the best fit to the experimental data. Quality of fit was based on the least square error of estimation (Appendix A). Pressure derivatives were obtained by analytically differentiating these polynomials and then evaluating the same at the desired axial position. Reichert & Azad (1976) used only the 5th order polynomial for all the curve fitting analysis. They claimed that it fully represented the data though no statistical comparison was made.

Using the hot-wire data, various moments up to 4th order were normalized as follows:

$$\frac{\overline{u_i^m u_j^n}}{(\overline{u_i^2})^{m/2} (\overline{u_j^2})^{n/2}} \quad (8)$$

where m , and n vary from 0 to 4.

The normalized quantities for $i = 1$ and $j = 2 \& 3$ were hand plotted and checked for symmetry. All quantities exhibited a symmetrical nature. A smooth continuous and symmetric curve was drawn through the data points, and obvious outliers were eliminated. These faired symmetric curves were then evaluated only on one side of the diffuser axis. These non-dimensionalized data up to 3rd order were converted into proper units and were renormalized using pipe bulk average velocity and its radius for evaluation of the energy balance. The resulting data was punched in formatted form on computer cards. Simple Fortran computer programmes were written to handle the data and to generate data points at 50 to 100 equally spaced radial positions between the

centreline and the wall using Aitken's interpolation method.

Since the x-wire was operated at an overheat ratio of 0.8 which produced a temperature difference in excess of 220°C between probe wires and the surroundings. Close to the diffuser wall, due to the high thermal conductivity of aluminum, one wire nearer to the wall lost more direct heat to the diffuser wall than the other. This caused an imbalance of d.c. voltage of two wires, making the measured turbulence data unreliable. Therefore, data obtained very close to the wall, where this effect was found to exist, were not taken into consideration. If considered, these data could lead one to erroneous conclusions, which would be the result of the physical limitations of the measuring instrument rather than the physical characteristics of the flow.

Having established the axial symmetry in all the moments of u_1 , u_2 , u_3 and the correlations of u_1u_2 and u_1u_3 , it was decided to measure u_2u_3 and $\frac{\partial u_1}{\partial t}$ data only on one side of the diffuser axis.

4. RESULTS OF MEAN FLOW MEASUREMENTS

4.1 Flow Specification

Okwuobi & Azad (1973) and Hummel (1978) have reported the existence of Reynolds number similarity for turbulent quantities in a diffuser flow. Since pressure recovery is the basic feature of a diffuser, it was decided to investigate the Reynolds number similarity on the basis of the static pressure in the flow. The static pressure measurements taken for 6 Reynolds number and normalized by the total velocity head in the pipe were found to collapse onto a single curve within the experimental error, (figure 4), thus confirming the existence of Reynolds number similarity in the mean flow.

Based on this finding, a single pipe Reynolds number of 58000 was chosen for further study. Table 1 gives the mean parameters of flow for this Reynolds number at the diffuser entry. This Reynolds number was the same as used by Hummel (1978) for most of his experimental work and was close to the lower Reynolds number used by Okwuobi & Azad ($Re = 76000$). It was thought that improved experimental accuracy could be achieved with the reduced high frequency content of the lower Reynolds number turbulence. Both the high frequency signal to anemometer noise ratios and the wire length attenuation were less important for turbulence with reduced high frequency content.

In order to have a fully developed pipe flow at diffuser entry, a pipe of 74 diameters length was used upstream of the diffuser. Laufer (1954) has shown that a value of $\frac{L}{D}$ of 50 is adequate for complete flow development in a pipe. Also Sabot & Comte-Bellot (1976) have shown

that a length of 70 diameters is sufficient to ensure the renewal of turbulence in pipe for nearly the same Reynolds number as used in the present study.

4.2 Mean Static Pressure

To provide a complete picture of the pressure field in the diffuser, the axial static pressure data were analytically analyzed (Sec. 3.4, and Appendix A). It was found that the 4th order polynomial provided the best fit to the experimental data (figure 4). The analytical differentiation of the polynomial showed that a pressure gradient difference of more than an order of magnitude existed from the beginning of the diffuser to its exit (figure 5 and table 2).

The pressure in the diffuser increases continuously till it reaches atmospheric at the exit. This is why it is referred to as a pressure recovery device. The rate of recovery is maximum in the beginning of the diffuser and decreases gradually in the downstream direction. By station 30, most of the pressure has already been recovered and from here till 10 cm from the exit plane, the pressure gradient, though still positive, is more or less constant. The choice of station 30 for the energy budget measured by Okwuobi & Azad (1973) was based on geometrical reasoning, but as figure 5 indicates, it is also the beginning of the region where pressure gradient is constant and very small in magnitude. Following Okwuobi & Azad, Hummel (1978) also conducted most of his experiments at this station and found many similarities with the boundary layer results.

As the pressure in the diffuser is increasing continuously in

the flow direction, it forces the flow to adjust as it moves in the downstream direction. Therefore, it might not be inappropriate to refer to this flow as "developing diffuser flow". But it should be differentiated from the "developing pipe flow", where pressure gradient is negative and constant, and a non-turbulent core region exists. This core region is a consequence of the flow entering the pipe. In diffuser flow too, characteristics of flow at entry are retained in the core of the diffuser (Hummel, 1978). But the 'development' or the 'adjustment' of flow occurs due to pressure recovery and is independent of the Reynolds number of the range tested.

Since pressure recovery is the main feature of a diffuser, it was decided to use the pressure gradient as the parameter in selecting the axial locations for further investigation as opposed to equidistant stations chosen by Okwuobi & Azad (1973). On the basis of figure 5 of pressure gradient, the diffuser can be divided in 4 regions. The first region is where pressure gradient can approximately be described by 2 straight lines, one from entrance to station 63 and the other from 63 to about station 57; the 2nd region describes the curvilinear portion of the graph from station 57 to station 30; the 3rd region is where pressure gradient is more or less constant; i.e., station 30 to 10; and the 4th region being the exit region where the pressure gradient approaches zero. On the basis of this division and in an attempt to study all the regions, the following axial stations were chosen for detailed study:

69, 67, 65, 61, 57, 50, 40, 30, 24, 18, 12, 6, and 0

where the numbers refer to distance towards the pipe in cm from the diffuser exit. It was thought that the study of energy budget at these stations would help in the complete understanding of the mean turbulent structure in the diffuser flow. Data for stations 69 served as boundary conditions and were not used in the final data presentation. The local radius of the diffuser for these axial stations is also given in Table 2.

Because of the continuous and strong adverse pressure gradient, the flow adjustment also takes place continuously. Since there is no flow separation (Okwuobi & Azad, 1973) and the pressure gradient is varying smoothly, it is expected that flow adjustment would also be smooth. Therefore, on the basis of pressure recovery characteristics of the conical diffuser, no sudden changes in its flow structure were expected.

The mean radial static pressure in the diffuser was measured along the whole diameter of the diffuser (on both sides of the diffuser axis) to see the radial variation in the static pressure. As indicated by the data in Table 3 (Table 4 gives the relevant atmospheric conditions for data in Table 3), this radial variation was generally small. This is in agreement with the results of Okwuobi (1972) for the same diffuser, also with fully developed pipe flow at entry.

4.3 Mean Velocity

The mean axial velocities obtained from the hot-wire measurements for 12 axial stations are plotted in figure 6. As demanded by flow continuity, the change in diffuser cross-section in the axial

direction produces a reduction in mean axial velocity, this results in simultaneous rise in pressure (thus converting kinetic energy of the flow into pressure energy). The decrease in slope and magnitude of profiles, especially near the wall, is due to the retardation of the fluid layers relative to each other caused by the rising pressure in the downstream direction. Because the radial variation of the static pressure is comparatively small (Sec. 4.2, Table 3), the amount by which the axial velocity is reduced would tend to be of the same order of magnitude across the diffuser, but is modified by the shear forces. Since the flow in the diffuser does not separate, this implies that the gradient of axial velocity in radial direction at the wall never reaches zero. However, in the immediate neighborhood of the wall the curvature of the velocity profile depends only on the pressure gradient and in decelerated flows ($\frac{\partial P}{\partial x_1} > 0$), $\frac{\partial^2 U_1}{\partial x_2^2} > 0$ (Schlichting, 1968, p. 123). Since, in any case $\frac{\partial^2 U_1}{\partial x_2^2} < 0$ at a large distance from the wall, there must exist a point for which $\frac{\partial^2 U_1}{\partial x_2^2} = 0$. This is a point of inflexion of the velocity profile. Such a point was noticeable in the mean velocity profiles near the diffuser outlet, a conclusion also reported by Okwuobi & Azad (1973) and Hummel (1978).

Mean axial velocity data were normalized by pipe bulk average velocity. The normalized data were hand plotted and a smooth symmetric curve was drawn through these data points. For further analysis, data were extracted from these faired curves in the manner described previously. An analytical description of the profile development was obtained by fitting a polynomial with a best degree of fit. For axial fit, data were divided in two groups of 7 sets each, with station 40 in

both groups. Polynomials were fitted to each group separately. This was done to get better fit of polynomials to experimental data. Since the change in flow is maximum in the initial stages and is minimum near the outlet, it was thought that analysing axial data in such a manner would improve the accuracy of polynomial fit. Polynomial with lesser error of estimation was used for analytical analysis of data at station 40. Differentiation and evaluation of these polynomials provided the longitudinal velocity gradient data required for the computation of the radial component of the mean velocity. The mean radial velocity profiles (figure 7) were computed using the continuity relation:

$$\frac{U_2(r)}{U_b} = - \frac{1}{\xi_2} \int_0^{\xi_2} \frac{\partial}{\partial \xi_1} \left(r \frac{U_1}{U_b} \right) dr. \quad (9)$$

Before integration, data for the derivative of U_1 were smoothed manually. This process of fairing tended to eliminate small irregularities which appeared in the computed derivative profiles but were inconsistent with flow pattern. In figure 7, according to sign convention adopted, a positive radial velocity indicated a motion towards the diffuser wall. The radial velocity components were less than about 12% of pipe average velocity. This ratio decreases considerably towards the diffuser exit. This is consistent with the observed pressure gradient. Since it is the continuous increase in cross-sectional area which produces mean U_2 and the pressure rise, and as such must be interrelated. Therefore, it is not surprising that mean U_2 has a large magnitude in the entry region of the diffuser as compared to near the exit. After

station 65, the mean U_2 is under 6% of the pipe average velocity. Okwuobi & Azad have reported that mean U_2 is generally less than 6% of the pipe average velocity. Since their results did not include any station upstream of station 66, the two results are in agreement with each other for velocity profiles at about station 66. However, the velocity profiles further downstream tend to differ from each other considerably with the present data indicating lower magnitudes. Since the U_2 profiles were computed from the axial derivatives of U_1 profiles, it was decided to compare the axial velocity profiles at stations common to both studies. The profiles at station 30 are shown in figure 8, which indicates a good agreement between the two velocity profiles. This suggests that the U_2 profiles could only be different due to the difference in axial slopes obtained. To check this possibility, it was decided to evaluate U_2 profiles at station 30 by numerical analysis of the U_1 data. For this purpose, Okwuobi & Azad's (1972) data for 3 profiles of U_1 at station 36, 30 and 24 were analysed. This was preferred because the data upstream of station 30 in the present study was at station 40 while Okwuobi & Azad's data was available at station 36. This should not make any difference as the axial velocity profiles compare well with each other. The three axial velocity profiles were plotted and the difference in magnitude in axial direction at various radial positions between two stations 36 & 30 and 30 & 24 was taken. This difference ($U_{36} - U_{30}$ and $U_{30} - U_{24}$) was divided by their axial distance which was 6 cm in both cases. The average of these two slopes was taken to be the velocity gradient at station 30. The $\frac{\partial U_1}{\partial x_1}$ was thus obtained for $0 \leq \xi_2 \leq 1.04$. These

derivatives were plotted on a large scale and were graphically integrated. The magnitudes of U_2 were computed using the continuity equation. This profile along with that of Okwuobi & Azad (1973) and from the present study at station 30 is shown in figure 9. If we assume that the present method gives better estimate of the axial derivatives, then figure 9 implies that the polynomial fit (used in present study) underestimates the axial derivatives while the exponential fit (reported by Okwuobi et al, 1972) over estimates the same. The peak in the U_2 profile of Okwuobi & Azad (1973) occurs at slightly different radial position than indicated by other two methods. Dotted line in figure 9 is the extrapolation of the U_2 profile which was later used in checking the mean flow convection term of the energy equation.

This exercise thus indicates that the quantities evaluated using axial derivatives should be accepted with some reservations. A similar opinion was also expressed by Ramaprian and Shiva-Prasad (1976). This lack of accuracy in the axial derivatives is generally due to the following reasons:

- i The data profiles are quite far apart in the axial direction. In the present study it varies from 2 to 10 cm.
- ii Number of data points available for using analytical functions are generally small. In the present study there were 13 data sets in an axial distance of 72 cm.
- iii The data at different axial stations were taken on different days. Thus the data in axial direction contain daily variations in the wind tunnel and instrument if any, in addition to that of the normal data fluctuations.

4.4 Mean Strain and Vorticity

In an axisymmetric flow where $U_1 \gg U_2$ and $U_3 = 0$, and the downstream derivatives of mean quantities are small compared to cross-stream derivatives ($\frac{\partial}{\partial \xi_1} \ll \frac{\partial}{\partial \xi_2}$), a condition generally fulfilled by the diffuser flow, the only non-zero components of mean rate of strain and vorticity are given by:

$$\dot{\epsilon}_{x_1 x_2} = \frac{1}{2} \left[\frac{\partial U_2}{\partial x_1} + \frac{\partial U_1}{\partial x_2} \right] \quad (10)$$

$$\Omega_{x_3} = \frac{1}{2} \left[\frac{\partial U_2}{\partial x_1} - \frac{\partial U_1}{\partial x_2} \right]. \quad (11)$$

The radial description of the axial velocity profiles for this was also obtained by fitting polynomials of order 1 to 5. Generally, the 4th or 5th order polynomial resulted in the least error of estimation. These polynomials were differentiated analytically for the required derivatives. In the present case, $\frac{\partial U_2}{\partial x_1}$ is about an order of magnitude smaller than $\frac{\partial U_1}{\partial x_2}$, thus the rate of strain and the mean vorticity are approximately equal in magnitude but opposite in sign and are about half of $\frac{\partial U_1}{\partial x_2}$. Figure 10 shows the $\frac{\partial U_1}{\partial x_2}$ which in turn can be viewed as representing both mean strain and the mean vorticity.

Since the velocity and its gradient decrease in the downstream direction at any given radial position, this also causes a corresponding decrease in the mean rate of deformation and rotation of the fluid element. This is expected as the diffuser which produces a strong

adverse pressure gradient in the direction of the flow, acts as a damper for the mean quantities. As figure 10 shows, a large value of the mean velocity gradient in the radial direction that exists near the wall results in high rate of deformation and rotation of the fluid in the proximity of the wall. This feature also exists in other wall bounded flows. Also over the whole of flow field the sign of vorticity is positive. This indicates a tendency of the mean flow to turn towards the diffuser wall.

In an attempt to further specify the flow, the directions of the mean principal stresses and strain rate were also calculated using the following relationships (Corrsin, 1957);

$$\alpha \approx \frac{1}{2} \tan^{-1} \left(\frac{\frac{1}{2} \frac{\partial U_1}{\partial x_2}}{\frac{\partial U_1}{\partial x_1}} \right) \quad (12)$$

and

$$\beta = \frac{1}{2} \tan^{-1} \frac{\overline{2u_1 u_2}}{u_1^2 - u_2^2} \quad (13)$$

Due to the similarity of the curves, data for only 6 stations are presented (figure 11 and 12). At the diffuser axis, values of both α and β are zero but a short distance away ($\xi_2 \approx 0.5$) they tend to reach a constant value. Magnitudes of α in the constant region reaches almost 45° and that of β varies between 13° and 18° and tends to approach zero at the wall. This variation is similar to other wall

bounded flows but is different from that of wake flow (Corrsin, 1957). Hanjalić and Launder (1972 a) have also reported the angle α to be 45° and β to be approximately 17° for the asymmetric plane channel flow. Corrsin also suggests that if the direction of these two principal axes are different, as is the case in diffuser flow, then assumptions of simple gradient transport of momentum model in such a flow would not be successful.

5. TURBULENT STRESS TENSOR SURVEY

In order to understand the physical processes involved in an adverse pressure gradient flow, the turbulent Reynolds stress tensor for the entire diffuser was first surveyed. The turbulent stress tensor, when written in matrix form, consists of terms involving the intensities of velocity fluctuations and correlations between pairs of the fluctuating velocity components:

$$\rho \begin{vmatrix} \overline{u_1^2} & \overline{u_1 u_2} & \overline{u_1 u_3} \\ \overline{u_2 u_1} & \overline{u_2^2} & \overline{u_2 u_3} \\ \overline{u_3 u_1} & \overline{u_3 u_2} & \overline{u_3^2} \end{vmatrix} \quad (14)$$

Physically, the presence of fluctuating velocities superimposed on the mean flow introduces additional mean momentum fluxes within the fluid. By Newton's law these additional momentum fluxes appear as additional stresses within the fluid. The Reynolds stress tensor is symmetric and for axisymmetric flow the terms involving the time averaged odd powers of u_3 (i.e., $\overline{u_1 u_3}$ and $\overline{u_2 u_3}$) are equal to zero. The stress tensor therefore reduces, for the present study, to the three normal stress terms on the diagonal and the tangential $\overline{u_1 u_2}$ term. Each of the stress terms were measured with the x-wire probe using the multifunction turbulent processor TM377.

5.1 Turbulent Intensities

The distributions of the three components of r.m.s. relative turbulence intensities are shown in figure 13. At each station the u_1' component has the highest value, with $u_1'/U_1 > u_3'/U_1 > u_2'/U_1$ and the ratio of u_1'/u_2' increasing from the diffuser axis to the wall (for example, from 1.410 to 2.762 at station 30) thus indicating an increase in the degree of anisotropy in the positive radial direction. These data are in agreement with those of previously reported by Okwuobi & Azad (1973). Generally, the magnitudes of u_1' and u_3' increase in radial direction at each station, while u_2' component shows a peak near the wall. Such a distribution of intensities was also reported by Klebanoff (1955) for boundary layer flow, Laufer (1954) for fully developed pipe flow and Reutnik & Corrsin (1955) for slightly divergent channel flow.

Also in the axial direction, the magnitude of the intensities increases at each radial position except in the wall layer. Because of the expanding geometry; i.e., the wall is gradually moving away from the flow, there is always a point where intensity is lower than compared to the same upstream radial position. Thus the crossing over of the curves. This is the direct consequence of the increases region over which to attain the maximum intensity level. Since the relative magnitude of u_2' fluctuations actually decreases near the wall, this crossing over is not observed in this component.

Figure 14 shows the distribution of the turbulence intensity u_1' normalized by the pipe bulk average velocity. The peak which develops very close to the wall near the diffuser inlet ($\xi_2 \approx 1.0$)

moves towards the diffuser axis in the stream wise direction. Also the intensity level generally increases in the downstream axial direction. The peak position of $\frac{u_1'}{U_b}$ in the radial direction specifies the point of maximum turbulent production in the field. In the pipe and boundary layer, this position is found to exist at $y^+ \approx 15$. In case of conical diffuser this position shifts slightly towards the axis in the downstream direction. Thus the wall layer (from wall to the point of maximum turbulent intensity) in the diffuser expands in the direction of the flow. Also the level of turbulent activities is higher in the diffuser, which is caused by the adverse pressure gradient in the flow. Ramaprian & Shiva-Prasad (1976) have also reported that the turbulent intensities in the boundary layer are significantly enhanced by the concave curvature.

5.2 Stress Tensor Trace

Figure 15 shows the distribution of the trace of Reynolds stress tensor $q^2 = u_1'^2 + u_2'^2 + u_3'^2$, which is directly proportional to the total turbulence kinetic energy. The values of the stress tensor were computed from the normal stress measurements and were normalized by the pipe bulk average velocity. Since the total turbulence kinetic energy exhibits the same basic features common to the normal stresses the individual distributions of u_2' & u_3' are not shown here. As shown in figure 15 the total kinetic energy increases in the downstream direction. In the radial direction, the turbulent energy like that of $\frac{u_1'}{U_b}$ shows a peak which shifts slightly towards the diffuser axis, with the distance in the downstream direction. A similar variation existed

in the distribution of normalized u_1' , u_2' , u_3' data of Okwuobi & Azad. As expected, the magnitude of stress tensor trace is higher in the diffuser as compared to the pipe flow which specifies its inlet conditions.

5.3 Correlation Coefficient

The correlation coefficient $\frac{\overline{u_1 u_2}}{u_1 u_2}$ (figure 16) varies considerably in the radial direction. Due to symmetry, it has a value of zero at the diffuser axis and shows a region of constant coefficient which starts near the point of maximum kinetic energy and extends towards the wall. This is in agreement with the data of Okwuobi & Azad. This region of constant coefficient expands in the downstream direction, and appears to be closely linked to the expanding region between the diffuser wall and the point of maximum u_1' fluctuations. A region of constant correlation coefficient also exists in fully developed pipe flow (Sabot & Comte-Bellot, 1976). The maximum value of the coefficient reached in this region (approximately 0.4) is almost the same for both the flows and more or less remains constant throughout the whole diffuser.

5.4 Tangential Stresses

Figure 17 shows the distribution of tangential stresses normalized by pipe mean velocity ($\frac{u_1 u_2}{u_b}$). The nature of the distribution of tangential stresses is the same as that for the trace of Reynolds stress tensor. It also peaks at the pipe radius ($\xi_2 = 1.0$) in the

entry region of the diffuser. This peak shifts towards the diffuser axis in the downstream direction. The magnitude also increases in the downstream direction but is generally an order of magnitude smaller than the stress tensor trace. The condition of symmetry forces its value to be zero at the axis. It also tends to approach a value of zero at the diffuser wall.

For an axisymmetric flow, the Reynolds stress tensor is symmetric and the only non-vanishing terms are $\overline{q^2}$ and $\overline{u_1 u_2}$. Since these terms are the basic mean parameters of the turbulence, their ratio $\frac{\overline{u_1 u_2}}{\overline{q^2}}$ which represents the ratio of the magnitudes of correlated to the total turbulence was also calculated (figure 18) to see the effect of changing geometry on their relative magnitude. Due to similarity only 7 curves are presented. Because of the symmetric nature of $\overline{u_1 u_2}$, the value of this ratio was zero at the diffuser axis and tended to approach the same at the wall. In the central region (away from the wall and the diffuser axis), this ratio approached a constant value between 0.11 and 0.14 which is comparable to that of boundary layer (Hinze, 1959). This indicates that the diffuser flow, though developing, maintains a balance among its turbulent stress components. This would imply that the mean nature of turbulence would be similar throughout the diffuser, though the pressure gradient is changing continuously. Bradshaw et al (1967) and Hanjalić & Launder (1972 b) have attempted to relate shear stress $\overline{u_1 u_2}$ to the turbulence energy $\overline{q^2}$. Figure 18 shows a close relation between the shear stress and the turbulence stress tensor trace independent of the pressure gradient and thus, it would appear that their model could be extended to the region away from the wall in the

diffuser with an adverse pressure gradient. The present study does not give data close to the wall to justify such an extension in the wall layer.

5.5 Wall Friction Velocities

The characteristic velocity parameter u_* is important in the correlation of both mean and fluctuating velocity components near a smooth wall. The methods for accurately calculating u_* in pipe flow and constant pressure boundary layers are well established unlike the case in adverse pressure gradients. Okwuobi (1972) considered 3 methods for obtaining u_* values; namely, (i) The 'law of the wall', (ii) Ludwig & Tillman equation and, (iii) The total shear stress extrapolation to the wall, and reported that the 3rd method gives consistent results. The u_* values for the present study were obtained by the 3rd method using the relationship

$$\frac{\tau}{\rho} = \nu \frac{\partial u_1}{\partial \xi_2} - \overline{u_1 u_2} \quad (15)$$

at the wall. These values are shown in figure 19 (Table 2) along with that of Okwuobi (1972) for both of his Reynolds numbers. The agreement between the values for his lower Reynolds number and that obtained from the data of present study is good except for one point at the exit. This might be due to the extrapolation of the equation 15 to the wall in the present study, as the wall was approximately 2.5 mm away from the closest data point. For station 57 and upstream, the equation 15 could not be extrapolated to the wall. As mentioned earlier, data very close to the wall were not obtained in the present study.

6. THIRD AND FOURTH ORDER MOMENTS

6.1 Measurements of Skewness and Flatness Factors

The skewness coefficient and the flatness factor are the non-dimensional distribution of the third and fourth order moments respectively. These factors are defined as:

$$\text{Skewness} = \frac{\overline{u_i^3}}{\left[\overline{u_i^2}\right]^{3/2}}$$

and the

$$\text{Flatness factor} = \frac{\overline{u_i^4}}{\left[\overline{u_i^2}\right]^2}$$

These quantities appear as figures 20 to 24. The data shown are the skewness of u_1 and u_2 component while the flatness factors are for u_1 , u_2 and u_3 components. The skewness of u_3 was found to be approximately zero throughout, as should be the case for axisymmetric flow.

6.1.1 The skewness of u_1

The skewness of u_1 has a negative value at the diffuser axis. In the entry region of the diffuser, the skewness near the axis is constant for a short distance in the radial direction and thereafter it increases and changes sign at about the point of maximum turbulent



energy (figure 20). The radial point where skewness of u_1 changes its sign shifts slightly towards the diffuser axis in the downstream direction (figure 25), which is in agreement with the earlier noted behavior of the trace of the Reynolds stress tensor.

After reaching the zero value, the skewness continues to increase further towards the wall. Thus it has a maximum positive value near the wall, while the maximum negative value near the diffuser axis. This indicates that u_1 is highly asymmetric near the wall and the axis. At radial points where the skewness changes sign, the probability distribution of u_1 has been shown to be symmetric (Hummel, 1978), indicating a Gaussian distribution at this position. The region from the wall to this point of zero skewness is generally referred to as the wall layer, though Professor A.M. Yaglom (private communication, 1978) prefers to call it as a thick sublayer. This wall layer in the diffuser corresponds to approximately $y^+ \approx 15$ in the boundary layer where the turbulence intensity is also maximum and the skewness of u_1 is zero.

The constant region of the skewness of u_1 begins to change into a ridge near the axis in the downstream direction. This point has the maximum negative skewness in the flow field. These ridges which appeared on both sides of the diffuser axis, slowly move towards the axis with the distance in the downstream direction. These negative ridges meet each other at the axis at about station 6. Similar trend was also reported by Hummel (1978). It was further suggested by Hummel that these ridges cross over the axis after station 6. It could probably be due to the fact that in the diffuser, bursting activity

is enhanced which was also reported by Ramaprian & Shiva Prasad (1976) for a boundary layer along a concave wall. These bursts may be crossing over the axis forming the ridges on both sides of the axis.

In the axial direction, the skewness of u_1 at the diffuser axis remains constant from the beginning of the diffuser to about station 30 and from here in the downstream direction skewness increased till station 6 and after that in the axial direction it decreased again (figure 26). This observation is also similar to that reported by Hummel (1978). It is interesting to note that the skewness at the diffuser axis remains constant in the high pressure gradient region (figure 5), and increases after most of the pressure recovery has taken place. It is quite possible that this may be due to the so called 'extra memory effects' of the turbulent flow. Builtzes (1977) states that when there is a change in conditions with respect to position (non-homogeneity), as is the case in the diffuser, there will be 'extra memory effects'. Since no literature is available on the memory effects in a strong adverse pressure gradient flow as found in the present case, it is not feasible to compare present results with already published data for memory effects. And the present study was not intended to make analysis of the memory effects. However, the experiments reported in flows with negative, zero and mild adverse pressure gradients have indicated that the inner region of the boundary layer reaches an equilibrium state sooner than the outer region (Builtzes, 1977). He also reported, on the basis of the data available, that small eddies close to the wall react more quickly to changes than the bigger eddies away from the wall. It was also reported that the mean flow adjusts

first to external conditions than the turbulent flow. Thus the increase in the magnitude of skewness of u_1 after station 30 at the diffuser axis (far removed from the wall) may well be the result of high adverse pressure gradient in the entry region of the diffuser.

6.1.2 The skewness of u_2

The structure of turbulence in any wall bounded flow is to a large extent affected by the relative diffusion of momentum and turbulent kinetic energy. These diffusions are influenced to a considerable extent by the behavior of u_2 fluctuations. The expanding geometry of the diffuser in our case, results in a direct production of u_2 fluctuations in addition to their production during the transfer of energy from the u_1 motions. A similar observation was also made by Ramaprian & Shiva Prasad (1976) for boundary layer flow on a wall with concave curvature. Thus in a flow with positive pressure gradient, the magnitude of u_2 is considerably higher than other comparable flows. In view of all these, it appears that it is the effect on the u_2 fluctuations which should be studied in greater detail to arrive at a quantitative understanding of the effects of the expanding geometry of a conical diffuser. With this view in mind, all moments of u_2 upto the 4th order were measured. At present no information is available about this quantity for adverse pressure gradient flows.

The skewness of u_2 (figure 21 and Table B-1 to B-12) was zero at the diffuser axis due to symmetry. However, the magnitude of u_2 increases first with distance from axis in the radial direction with a sign corresponding to u_1 and then decreases. A change in sign of

the skewness of u_2 occurs at the same radial position as was the case for u_1 (figure 25). From the diffuser axis to this point the sign of both of these skewnesses is negative, thus indicating that these fluxes are directed away from the wall in the core region of the diffuser. After the change in sign, both fluxes have again similar signs which is now positive further towards the wall. Very close to the wall, as indicated by downstream stations, the magnitude of the u_2 skewness begins to drop. A similar trend in u_2 was also indicated by Hanjalić & Launder (1972 a). The decreasing trend of $\overline{u_2^3}$ values near the wall was not evident in the entry region of the diffuser. This was probably due to the lack of data in the wall region of the diffuser at these stations.

The overall picture of the skewness of u_2 appears more like a stretched sine wave with the curve passing through zero at the axis and again at the edge of the wall layer, which expands in the downstream direction. Hummel (1978) has shown that in the diffuser, like that in the boundary layer, sweep is more important in the wall layer and ejection more significant outside this layer. The skewness of u_2 (figure 21) is negative outside the wall layer which corresponds to ejection and it is positive in the wall layer, which indicates a movement towards the wall and thus signifies the event sweep. Thus the results of the skewness of u_2 agree with the findings of Hummel (1978).

The skewness of a turbulent velocity component can be viewed as representing the transfer of the intensity of that component by itself. Further it is normally expected that the turbulence intensity

would be transferred down the intensity gradient. Since the intensity of u_2 fluctuations reaches maximum at the point of zero u_1 skewness and decreases with distance from this point towards the axis or the wall. Thus the skewness of u_2 would be expected to change sign here. And since the u_2 intensity decreases with distance towards the wall, the skewness would be positive towards the wall. The situation is reversed from the edge of the wall layer towards the axis. The present results are consistent with such a physical reasoning.

6.1.3 Flatness factors

The flatness factor is the measure of the fourth moment of the probability density function for the corresponding parameter. While the skewness of a function is an indication of its asymmetry, the flatness factor is a measure of the extent of the skirt of its probability density. Large flatness factors imply that the probability of fluctuations quite different from mean is large; that is the normalized probability density function appears relatively wide. A signal with large amplitude, and intermittent nature produces high values of flatness factors. For the present study, the flatness factors of u_1 , u_2 and u_3 signals measured in the diffuser are given in figures 22 to 24 for 7 axial stations. Curves for other stations had a similar variation and the experimental data for all stations are included in Tables B-1 to B-12. For comparison, the flatness factor for a random signal with a Gaussian probability density function is 3.0, while sine wave has a flatness factor of 1.5.

The flatness factors for all 3 signals (u_1 , u_2 and u_3)

decrease with radial distance from axis, in the entry region of the diffuser. However, like ridges in skewness of u_1 , a bulge in the flatness factors (more prominently in u_1 and u_2) appears close to the diffuser axis after station 50 in the downstream direction. This bulge which appears on both sides of the axis (all these functions were found to be symmetric) moves towards the axis with distance in the downstream direction and forms a peak at the axis at station 6. This behavior is similar to that of the skewness of u_1 . However, this phenomenon was not well defined in the flatness factor of u_3 . In radial direction, all the 3 functions had a minimum value of the flatness factor, which occurred at the point of zero u_1 skewness. The magnitudes of the flatness factors for u_2 and u_3 at this radial position were almost 3, the Gaussian value. The magnitude of the flatness factor of u_1 was, however, less than 3 (figure 27). Thus at the edge of the wall layer, functions u_2 and u_3 were Gaussian (their skewness is zero) while u_1 was not in a true sense as its flatness factor differed from 3. After reaching the minimum value at the edge of the wall layer, the flatness factors increase again in the wall layer and attain very high values near the wall.

All three flatness factors at the diffuser axis (figure 28) had a similar trend to that of the u_1 skewness (figure 26). The flatness factor also remain essentially constant up to about station 30 and increase after that in downstream axial direction. The flatness factors decrease near the diffuser exit after reaching their maximum values. This pattern was observed for all three fluctuating velocity components. The increase in the magnitudes of the flatness factors at the diffuser

axis occurs after most of the pressure recovery has already taken place. This could again be possibly due to the 'extra memory effects' discussed in Sec. 6.1.1, as the turbulence may not be responding immediately to the strong pressure gradient in the entry region of the diffuser. However, this is merely a speculation and more work is needed to confirm the existence of such a phenomenon.

6.2 Correlations of Third and Fourth Order

In addition to the measurements of the skewness and flatness factors of u_1 , u_2 and u_3 , their various correlations of 3rd and 4th order were also measured. These included:

i) 3rd order: $\overline{u_1 u_2^2}$, $\overline{u_1 u_3^2}$, $\overline{u_1^2 u_2}$ and $\overline{u_2 u_3^2}$

ii) 4th order: $\overline{u_1^2 u_2^2}$, $\overline{u_1^2 u_3^2}$, $\overline{u_2^2 u_3^2}$, $\overline{u_1^3 u_2}$ and $\overline{u_1 u_2^3}$.

The time average correlations involving the odd powers of u_3 were found to be zero everywhere for the conical diffuser. These correlations along with the skewness and flatness factors were needed to evaluate the corrections for the non-linear hot-wire response. Magnitudes of these corrections for u_1^2 , u_2^2 , u_3^2 and $u_1 u_2$ are given in Appendix C.

6.2.1 Triple correlations

The Triple correlations for 7 axial stations are shown in figures 29 to 32. All of these moments in addition to that of the skewnesses of u_1 and u_2 appear in the diffusion term of the turbulent kinetic energy equation. The terms involving $\overline{u_2^2}$ appear as its radial

derivative and the terms containing $\overline{u_1 q^2}$ with axial derivatives. These terms contribute to the radial and axial diffusion of the undissipated turbulent kinetic energy. The radial variation of the terms $\overline{u_2 q^2}$ is generally greater than the corresponding axial variation of the quantity $\overline{u_1 q^2}$ and thus $\overline{u_2 q^2}$ contributes more to the diffusion term. However, in the entry region of the diffuser, the axial variation of the term $\overline{u_1 q^2}$ is also very significant.

Among all these triple order velocity correlations, the correlation of $\overline{u_2 u_3^2}$ shows more data scatter (figure 32). It should be expected as the correlation of u_2 & u_3 was obtained in an indirect way. To obtain this correlation, the outputs of x-wire in three different planes namely $u_1 u_2$, $u_1 u_3$ and $u_2 u_3$ were processed and data from these orientations of the x-wire were obtained on different days. Also, the aerodynamic effects of prongs are likely to be different for each setting. Further, because of the algebraic manipulations involved in calculating $\overline{u_2 u_3}$ correlation, it may contain the normal data fluctuations and errors associated with all the quantities required to obtain this correlation.

Of all the triple correlations, probably the most important are the $\overline{u_1 u_2^2}$ and $\overline{u_1^2 u_2}$. Nakagawa & Nezu (1977) have shown that using these third order moments along with the skewness of u_1 and u_2 , the probability density of the Reynolds stresses can theoretically be calculated. Forming the sum and differences of these quantities, they also obtained the conditional probability distribution of the Reynolds shear stress and thus predicted the contribution of each bursting event to the Reynolds shear stress. Their results compared well to the

experimentally obtained data and thus the importance of these triple order velocity correlations is evident. However, the present study was not intended to predict the various events of the bursting process in a conical diffuser but was rather to study the turbulent kinetic energy balance for such a flow.

A common and surprising feature of these triple velocity correlations was that the nature of their distribution was similar to the skewness of the odd power function in the correlation. Thus the nature of the $\overline{u_1 u_2^2}$ distribution was similar to that of the skewness of u_1 and of $\overline{u_1^2 u_2}$ was similar to the skewness of u_2 . A similar trend was also reported by Hanjalić & Launder (1972 a) for terms involving uneven power of u_2 for flow in an asymmetric plane channel. In the present study, this observation also applies to the distribution of $\overline{u_1 u_3^2}$ and $\overline{u_2 u_3^2}$. Thus, as expected, the correlations involving odd powers of u_3 were found to be zero as its skewness vanishes everywhere in the flow.

The magnitudes of the non-zero triple correlations (where u_2 and u_3 have even power) at the diffuser axis showed an increase in the axial direction after station 30 (figure 26). This behavior was similar to that of the skewness and flatness factors. In radial direction the change in the sign of these triple order velocity correlations, occurred approximately at the same radial position as for the skewness of u_1 and u_2 . As figures 29 to 32 indicate that this radial position where the correlations change sign shifts towards the diffuser axis in the downstream direction. This trend is also consistent with that of the skewness of u_1 and u_2 (figure 25). The curves for station 67 do

not show this position due to the lack of data in the wall layer of the entry region. But it is expected that the change in sign for this station occurs close to the wall. However this must take place before $\xi_2 = 1.05$, the wall position for this station. This implies that the radial position for the change of sign in the diffuser entry region must be moving towards the wall up to about station 57 and then moves towards the axis. This was also indicated by figure 25 which shows the radial position at each axial station where the skewness of u_1 & u_2 is zero.

In order to evaluate the diffusion term in the channel flow, Nakagawa et al (1975) assumed that:

$$\overline{u_2 u_3^2} \approx \overline{u_2^3}.$$

For the purpose of testing this assumption for the diffuser flow, the two curves were compared. Though the skewness of u_2 and the triple correlation $\frac{\overline{u_2 u_3^2}}{\overline{u_2 u_3}^2}$ are not equal, the dimensional quantities indicated good agreement (figure 33 for station 30). The small variations in these two quantities was probably due to high data scatter of $\overline{u_2 u_3^2}$. Similar agreement was also evident among data for other axial stations. Thus such an assumption may also be justified for the diffuser flow. However, in the evaluation of the energy balance, for the present study, no such assumptions had to be made as data for $\overline{u_2 u_3^2}$ for all axial stations were obtained experimentally. A similar comparison was also made between $\overline{u_1 u_3^2}$ and $\overline{u_1^3}$, but unlike $\overline{u_2^3}$ & $\overline{u_2 u_3^2}$, their magnitudes were different with $\overline{u_1 u_3^2}$ being much smaller than that of $\overline{u_1^3}$ (figure 34). However the magnitude of $\overline{u_1^3}$ was generally larger than that of

$\overline{u_2 u_3^2}$ and $\overline{u_2^3}$.

A natural way to interpret the third order velocity correlations is as a transport of the flux. This concept is embodied in the usual grouping of the triple correlations into the convective diffusion term. Thus the term $\overline{u_2 q^2}$ can be viewed as the transport of q^2 by the radial velocity fluctuations u_2 and similarly $\overline{u_1 q^2}$ as the transport of q^2 by u_1 . The quantity $\overline{u_2 q^2}$ when normalized by q^2 has been defined as Bulk Convection velocity by Townsend (1949). Thus

$$\frac{v}{U_b} = \frac{\overline{u_2 q^2}}{U_b \overline{q^2}} = \frac{\overline{u_1^2 u_2} + \overline{u_2^3} + \overline{u_2 u_3^2}}{U_b \overline{q^2}} \quad (16)$$

The distribution of this quantity (figure 35) is similar to that of quantities involved in $\overline{u_2 q^2}$. The figure 35 also shows that the direction of the bulk convection is towards the diffuser axis in the core region, and in the wall layer it is directed towards the wall. This is indicated by the negative values in the core region and the positive values in the wall layer. In our coordinate system, movement towards the wall is positive while towards the axis is indicated by the negative sign. This trend is in agreement with that of the pattern of the skewness of u_2 and also of the ejection and sweep events.

6.2.2 Quadruple correlations

All the fourth order velocity correlations of 2 function u_1 & u_2 , u_1 & u_3 and u_2 & u_3 are shown in figures 36 to 39. The arguments

about the accuracy of $\overline{u_2 u_3^2}$ also holds for $\overline{u_2^2 u_3^2}$. All these moments are shown for only 3 axial stations 61, 40 and 18 corresponding to 3 different main regions of the pressure gradient curve of figure 5. The numerical data for all the axial stations are given in Appendix B.

The fourth order velocity correlations can be divided in two groups: i) first in which both the velocity functions are even; e.g., $\overline{u_1^2 u_2^2}$, etc.; ii) second containing correlations with both functions having odd powers; e.g., $\overline{u_1^3 u_2}$, etc. Both these correlations have different characteristics.

i) Correlations with each component with even power:

These fourth order correlations can be reduced (Guitton, 1974) by noting that the instantaneous signals u_1^2 are composed of mean and fluctuating components

$$\begin{aligned} u_1^2 &= \overline{u_1^2} + z_1(t) \\ u_2^2 &= \overline{u_2^2} + z_2(t) \\ u_3^2 &= \overline{u_3^2} + z_3(t) \end{aligned} \quad (17)$$

where

$$\overline{z_1(t)} = \overline{z_2(t)} = \overline{z_3(t)} = 0$$

Taking the product of u_1^2 and u_2^2 yields

$$\overline{u_1^2 u_2^2} = \overline{u_1^2} \overline{u_2^2} + \overline{z_1 z_2} \quad (18)$$

This can be written as,

$$\frac{\overline{u_1^2 u_2^2}}{\overline{u_1^2} \overline{u_2^2}} = 1 + \frac{\overline{z_1 z_2}}{\overline{u_1^2} \overline{u_2^2}} \quad (19)$$

Gitton (1974) reports that

$$1 < \frac{\overline{u_1^2 u_2^2}}{\overline{u_1^2} \overline{u_2^2}} < 3 \quad (20)$$

A similar relationship will hold for $\overline{u_1^2 u_3^2}$ and $\overline{u_2^2 u_3^2}$. The condition for zero $\overline{z_1 z_2}$ in equation (19) corresponding to the lower limit in equation (20), is that there be no correlation between the magnitudes of u_1 and u_2 .

These fourth order correlations in the diffuser generally vary within the limits given by equation (20) and also show a minimum at the edge of the wall layer (figures 36 to 38) where the skewnesses of u_1 and u_2 changed their sign. At this radial position, the magnitude of all 3 correlations reach a value close to unity indicating that the square of the velocity fluctuations are almost independent of each other. At some stations the correlation between u_1^2 and u_3^2 generally has a value less than unity at the edge of the wall layer. This would imply a negative correlation between these quantities (Irwin, 1973). But this could also be due to the normal data fluctuations rather than indicating a definite physics. However, if this correlation is considered to be unity at this radial position, then it would imply that u_1^2 has less

correlation with u_3^2 than with u_2^2 , as the correlations between u_1^2 & u_2^2 and between u_2^2 & u_3^2 are comparable and higher than that of $u_1^2 u_3^2$. Also, the correlations of $\overline{u_1^2 u_2^2}$ and $\overline{u_2^2 u_3^2}$ show a bulge in the core region which moves closer to the diffuser axis in the downstream direction. Such a bulge was not present in the correlations of u_1^2 and u_3^2 . However, the magnitudes of all three correlations at the diffuser axis show a similar behavior as shown by the flatness factors of each fluctuating velocity component (Sec. 6.1.3). They all have an approximately constant value at the diffuser axis from entry to about station 30 and increase after that in the downstream direction and decrease again near the exit (figure 40). At the axis, however, the magnitude of the correlation $\overline{u_1^2 u_2^2}$ is the least and not of the $\overline{u_1^2 u_3^2}$. Near the wall, the magnitudes of the correlations $\overline{u_1^2 u_3^2}$ and of $\overline{u_2^2 u_3^2}$ are comparable and higher than that of $\overline{u_1^2 u_2^2}$. The magnitude of these correlations is generally lower than the flatness factors of the velocity components involved, everywhere in the field.

ii) Fourth order correlations with each component in odd power:

The measurements of 3rd order correlations had shown that each correlation followed the nature of the skewness of the function having uneven power in the correlation. However, here both functions appear in odd powers and thus we do not get a clear pattern corresponding to the skewness of any function. Rather, there is a complex combination of the both. Only other moment in which both functions have odd power is the Reynolds shear stress $\overline{u_1 u_2}$, where both have first power and thus a smooth curve results. In these two correlations of fourth order, one

function involved has first power while the second is raised to the third power. Thus a complex and wavy pattern of the correlation emerges (figure 39). These two correlations, in a way, can be interpreted as interaction between $u_1 u_2$ and u_1^2 or u_2^2 . And since u_1^2 and u_2^2 are positive and have definite value at the axis, the correlation $\overline{u_1 u_2^3}$ and $\overline{u_2^3 u_1}$ would be zero at the axis due to symmetry and will have a sign corresponding to the sign of $\overline{u_1 u_2}$. Such a pattern is indicated by the present results (figure 39). Due to the complex interaction between $u_1 u_2$ and u_1^2 or u_2^2 , the constant portion of the $\frac{\overline{u_1 u_2}}{u_1 u_2}$ curve takes a wavy pattern but close to the wall indicates a decreasing trend consistent with that of the $\frac{\overline{u_1 u_2}}{u_1 u_2}$.

Experimental results also indicate that both these correlations; i.e., $\frac{\overline{u_1^3 u_2}}{u_1^3 u_2}$ and $\frac{\overline{u_1 u_2^3}}{u_1 u_2^3}$ collapse on to each other from diffuser axis

to the edge of the wall layer and differ from each other further towards the wall. In the region of the wall layer, the correlation $\overline{u_1^3 u_2}$ had slightly lower values. The two curves differed from each other in the wall layer from station 57 in the downstream direction. This is thought to be due to the lack of data in the wall layer at the upstream stations.

Near the wall, both these correlations show a peak before decreasing in magnitude towards the wall. This peak position however shifts away from the wall in the downstream direction similar to the point where these curves start to differ from each other.

Another fourth order, tripple velocity correlation $\overline{u_1 u_2 u_3^2}$ where u_3 has even power but u_1 and u_2 both have odd powers was needed

for calculating the high intensity correction factor for $\overline{u_1 u_2}$. This was not experimentally measured but was assumed equal to $\overline{u_1 u_2^3}$

(Appendix C). This approximation was justified on the basis that

$$\overline{u_2^3} \approx \overline{u_2 u_3^2} \text{ (Sec. 6.2.1).}$$

7. TURBULENT KINETIC ENERGY BUDGET

7.1 Energy Budget Evaluation Technique

Each term in the energy balance equation except the pressure-velocity correlation part of term II, could be calculated from the experimental results. Term II which was not entirely available experimentally, was obtained as a closure term in the equation. Using the third order velocity correlation data obtained experimentally, pressure-velocity correlation was extracted from term II of the energy budget equation. The dissipation term was estimated from the root mean square measurements of the time derivative of the longitudinal velocity fluctuations, assuming small scale isotropy and Taylor's frozen turbulence hypothesis such that:

$$\epsilon = \nu \left[\frac{\partial u_i}{\partial x_j} + \frac{\partial u_j}{\partial x_i} \right] \frac{\partial u_i}{\partial x_j} = \nu \left[\frac{\partial u_i}{\partial x_j} \right]^2 = 15\nu \left[\frac{\partial u_1}{\partial x_1} \right]^2 = \frac{15\nu}{U_1^2} \left[\frac{\partial u_1}{\partial t} \right]^2 \quad (21)$$

The expediency of this method of dissipation measurement for the survey study of the energy balance was obvious because of the relative ease with which $\frac{\partial u_1}{\partial t}$ profiles could be measured.

As a preliminary experiment, a comparison of the dissipations determined from time derivative measurement was made with those evaluated from one dimensional spectra measurements using the equation:

$$\epsilon = 15\nu \int_0^{\infty} k_1^2 E_1(k_1) dk_1. \quad (22)$$

Measurements were made in the diffuser at station 12 and at $\xi_2 = 0.91$ using a regular single wire probe DISA 55P01 ($\ell = 1.25$ mm, $d = 5$ μm) operated at an overheat ratio of 0.8 and 0.5, and also with a special single wire probe DISA 55P01 ($\ell = 0.625$ mm, $d = 2.5$ μm) operated at an overheat ratio of 0.5 and 0.4. The filter cutoff frequency in both cases was 28000 Hz. The data obtained from time derivative measurements were lower by approximately 24% in case of regular probe and by 27% in case of special probe (Table 5). The difference in data obtained from the two methods must be in the electronics involved, as both methods are based on the isotropic relations. A cutoff frequency different than the Kolmogoroff frequency would also result in different values from the two methods. Values of ε obtained at different overheat ratios were comparable; i.e., ε did not appear to be dependent on the overheat ratio. Also a comparison of the ε obtained from two wires at an overheat ratio of 0.5 indicated that the values obtained from the special probe were higher than that obtained from the regular probe. The difference was of the order of 18% from $\frac{\partial u_1}{\partial t}$ data and 24% in values obtained from the spectra. This difference could possibly be due to the fact that the effective length of the special probe was half of the regular probe. For best results, the wire length should be of the order of Kolmogoroff length scale which varied from 0.06 mm to 0.14 mm in the present case. Therefore the accuracy of $\frac{\partial u_1}{\partial t}$ measurements would obviously be better in case of the special probe. Thus it was decided to use the special probe for time derivative measurements. Since the wire length of the special probe was also larger than the Kolmogoroff's length scale, the dissipation estimates obtained from

it were corrected using Wyngaard's (1969) analysis for single wire. It was thought that such a correction would improve the accuracy of dissipation measurements.

The longitudinal derivatives of the turbulence measurements appearing in the energy equation were obtained by a process similar to that used to get the longitudinal derivatives of U_1 required for the evaluation of U_2 from continuity (Sec. 4.3). Similarly the radial derivatives were obtained in the same fashion as of the mean velocity for the mean vorticity and the strain rate. Both the longitudinal and radial second order derivatives were obtained by application of the same procedures to the data for the first derivatives.

7.2 Terms of Energy Equation

7.2.1 Production

The distribution of the total turbulent kinetic energy production (figure 41) is similar to that of Reynolds stress tensor terms. It also has a peak in the radial direction at the pipe radius in the entry region of the diffuser. The peak shifts towards the diffuser axis with the distance in the downstream direction. The total production is very nearly zero at the axis and also approaches the same at the wall. As we move in the downstream direction, the region from the wall to the point of maximum u_1' fluctuation increases. Approaching of the zero value of production at the wall is very clearly demonstrated in this enlarged wall layer region (after axial station 50), as the wall layer is thick enough to allow the measurement of all parameters accurately

without the wall effect. A similar nature of the production term was also indicated by Ruetenik & Corrsin (1955) for a slightly divergent channel and Okwuobi & Azad (1973) for a conical diffuser. However, Okwuobi & Azad also show a sharp rise in production very close to the wall. In the present study, data so close to the wall were not taken into consideration. It was thought that measurements very close to the wall obtained with x-probe at an overheat ratio of 0.8 would not be reliable. Since Okwuobi & Azad also obtained their data using an x-probe operated at an overheat ratio of 0.8 and in the same diffuser as used for the present study, their wall data would also be affected by the presence of the wall. Also, such changes in production near the wall have not been observed for any other wall bounded flow.

While the production term III (equation 1) is a grouping of four terms, only the first term was significant except in the entry region where the 2nd term involving $\frac{\partial u_1}{\partial x_1}$ was also important. Generally, the other terms were approximately one to two orders of magnitude smaller. For example, at station 67, $\xi_2 = .54$, the magnitude of the first term is $.3 \times 10^{-3}$, 2nd term is $.6 \times 10^{-3}$ and the 3rd and 4th terms are $.6 \times 10^{-4}$. And at $\xi_2 = .54$, station 30, the magnitudes of each term are I = $.7 \times 10^{-3}$, II = $.86 \times 10^{-4}$, III = $.65 \times 10^{-6}$, and IV = $.54 \times 10^{-5}$. The first term of the production, which is significant throughout, contains the product of $\overline{u_1 u_2}$ and $\frac{\partial u_1}{\partial x_2}$. And since both of these quantities are zero at diffuser axis (due to symmetry), production was almost negligible at the axis. Overall, the production describes the action of Reynolds stresses to extract energy from the mean flow.

The radial velocity gradient of the mean axial velocity, $\frac{\partial U_1}{\partial x_2}$, decreases in the downstream direction, but due to the expanding geometry the cross sectional area increases towards the diffuser exit. The net result is that the total kinetic energy production increases in the downstream direction.

In general, the energy is supplied to the flow in the form of mean flow energy. The production terms indicate an increase in the turbulent kinetic energy at the expense of the mean flow energy. And the usual dynamic processes involve transfer of kinetic energy to higher wave numbers and eventual dissipation. Such a process has been confirmed for pipe flow (Lawn, 1971), channel flow (Nakagawa et al, 1975) and boundary layer (Klebanoff, 1955). These situations represent a case of negative and zero pressure gradient flow fields. In the diffuser flow, where the pressure gradient is positive and changing, the nature of production of turbulent kinetic energy is similar to pipe, boundary layer and slightly divergent channel flows. It should also be of considerable interest to study the movement of this turbulent kinetic energy and its eventual dissipation in comparison to other wall bounded flows.

7.2.2 Mean flow convection

Term I in the turbulent kinetic energy balance describes how the mean flow moves the turbulence energy in the flow field. Figure 42 shows the complete distribution of this term. In the entry region of the diffuser, magnitude of the mean flow convection at the axis is

also very small and increases towards the wall. Very close to the wall this term would decrease and approach zero at the wall. Such a trend is clearly indicated as we move downstream. Also in the downstream direction, the peak in the mean flow convection shifts towards the axis. Near the exit, this peak appears at the axis itself and towards the wall its magnitude decreases, approaching zero at the wall. Except in the entry region, the contribution of this term is almost negligible near the wall. It is worth noting that the magnitude of this term at the axis ($\xi_2 = 0$) increases considerably after most of the pressure recovery has taken place. Klebanoff (1955) has reported that in a boundary layer with zero pressure gradient the contribution of the mean flow convection is also negligible near the wall. For a slightly divergent channel, Ruetenik & Corrsin (1955) reported that the mean flow convection was generally small and constant throughout except near the wall where it decreased to zero. All these results emphasize the fact that near a solid wall, the contribution of the mean flow convection is negligible.

Results of Okwuobi & Azad do not agree with the present data for station 30, as their data show a valley at $\xi_2 = 0.96$ and a peak at $\xi_2 = 1.28$ before decreasing towards the wall. This would imply the presence of certain physical phenomenon, which was not confirmed by the present data. In an attempt to investigate this discrepancy of the two data, each term of the mean flow convection was studied. The mean flow convection term is the sum of two parts. The first part is the product of the mean axial velocity and the axial derivative of the

Reynolds stress tensor trace. The mean axial velocity U_1 is positive everywhere and since $q^2 = u_1^2 + u_2^2 + u_3^2$ increases in the downstream direction, its axial derivative is also positive, thus the first part of the term is always positive. The second part involves the product of the mean radial velocity U_2 , which is always positive in our flow, and the radial derivative of q^2 . The sum of the normal stresses (q^2) increases from the axis to the point of the maximum u_1' fluctuations in the radial direction and then decreases further towards the wall. Thus its radial derivative with respect to x_2 from the diffuser axis is positive up to the point of maximum q^2 and then becomes negative towards the wall. Also this 2nd part of the term is usually an order of magnitude smaller than the first part except in the region from the wall to the point of maximum u_1' fluctuations, where they are almost of equal order of magnitude. Thus when summed, they tend to cancel each other in the wall region and complement each other away from it.

In an attempt to obtain the nature of the curve given by Okwuobi & Azad, two parts of the mean flow convection term were subtracted rather than adding. The resultant curve is shown in figure 43, along with the data of OA. Two curves are similar in nature though different in magnitude. This shows that OA could possibly have erred in analysing their data. The energy equation involves all the radial derivatives with respect to x_2 , but OA have presented their data in terms of y/R , where y is the distance from the wall. Taking the radial derivative of q^2 with respect to y would reverse its sign as compared to its derivative with respect to x_2 . But in this case, with the

coordinate system at the wall, sign of U_2 would also change. It is quite possible that the authors inadvertently retained the positive sign of U_2 . Such an error could produce aforementioned behavior of the mean flow convection. For the difference in magnitude, attention should be drawn to the difference in mean radial velocities as discussed in Sec. 4.3.

In order to obtain the correct nature of the mean flow convection term for the data of Okwuobi & Azad (1973) and to be reasonably sure that OA had indeed erred in analysing their data, this term was evaluated from their data for station 30. The required necessary data were taken from another publication of Okwuobi & Azad (1972). The numerical method adopted for evaluating the axial derivatives of q^2 was same as used for $\frac{U_1}{U_b}$ (for U_2 profiles) from OA data discussed in Sec. 4.3. The radial derivatives of q^2 were obtained by taking the difference in the magnitude of q^2 at two radial points at $\xi_2 = \pm .02$ from the radial position where the slope was required. This difference in magnitude was divided by the radial distance ($\xi_2 = 0.04$) to obtain the required radial derivatives. The derivatives thus obtained were compared to the one obtained analytically in the present study. The radial derivatives were found to be in good agreement with each other while the axial derivatives though agreeing in trend were slightly higher for the present study. A smooth curve was drawn through these points and both terms of the mean flow convection term were evaluated at various radial positions. These terms are shown in figure 44. The mean radial velocities required for the calculation were taken from

figure 9, which were calculated by graphical integration. For this purpose the curve for U_2 was extrapolated as indicated by dotted line in figure 9.

The first term involving the axial velocity is positive everywhere while the 2nd term is negative in the wall layer. This is so, because the quantity $\overline{q^2}$ decreases towards the wall after reaching maximum at the edge of the sublayer. The mean flow convection term calculated by the addition of these terms is shown in figure 45, which also contains the curve obtained by subtracting the two terms. The term obtained by subtraction agrees in trend with that presented by OA. The difference in magnitude is most likely due to the overestimation of the mean radial velocities by OA. The true nature of the mean flow convection term indicates a negative value near the wall. The negative trend of this term was also present in the results of this study, though it was generally negligible compared to the total term. However, the underestimation of mean radial velocities in the present study would also tend to suppress the magnitude of negative part.

To be definite about this negative trend of mean flow convection term, data of Okwuobi & Azad (1972) for 2 more axial stations were analysed. The two stations chosen were 42 & 18, one upstream and one downstream of station 30. The mean radial velocities required were also taken from Okwuobi & Azad (1973) which are overestimated. For this comparison, the data for mean flow convection at station 30 were recalculated using their mean U_2 . The resulting data are shown in figure 46 for the wall region. This figure shows that the negative

magnitude of this term decreases towards the diffuser exit. The decrease in the slopes of the curve while approaching the wall for downstream axial stations tends to confirm the fact that peak of this term slowly moves towards the diffuser axis. The negative part of the term is magnified in this case because of the overestimation of mean U_2 . Thus the true nature of this term may lie somewhere between this and the one represented by the figure 42 for the present study. Therefore it may be reasonable to assume that the contribution of mean flow convection near the wall is generally small.

7.2.3 Viscous transport

Term IV of the turbulent kinetic energy balance is the viscous transport term. Only the part of the term involving the Laplacian of the turbulent kinetic energy was calculated and of these two terms only the first was significant. The second part of the Laplacian involving the 2nd order axial derivative of q^2 was at least 2 orders of magnitude smaller than the first part. The remaining part of the viscous term involving the viscosity vanishes for an isotropic flow, an assumption made in evaluating dissipation in diffuser flow.

As shown in figure 47, the viscous transport term is about 2 orders of magnitude smaller than the production. This is in agreement with the results of OA. Thus the viscous work term does not contribute significantly to the energy loss in the field. This is similar to Laufer's (1954) findings for fully developed pipe flow.

7.2.4 Dissipation

The nature and magnitude of the dissipation curves as determined from $\frac{\partial u_1}{\partial t}$ (figure 48) is similar to that of the total production.

Dissipation also has a peak at the pipe radius in the diffuser at entry but it shifts towards the wall with the flow in the downstream direction. Also like production, the total magnitude of the dissipation increases in the downstream axial direction. But unlike production, dissipation is significant in the wall layer and decreases in a thin layer next to the wall.

These results tend to contradict the findings of OA for station 30. They claimed that dissipation in general is very small compared to production and thus in the diffuser production is not balanced by dissipation. They also indicated that the dissipation is more or less constant from the axis to $\xi_2 = 0.9$ where it starts to decrease and reaches zero at $\xi_2 = 1.40$ and stays at zero further towards the wall. All wall bounded flows have a very high rate of energy dissipation near the wall, a result also confirmed by the present study for the diffuser. However, results of OA for the same diffuser do not agree with the present findings.

Since it is extremely unlikely that the differences between the pipe and diffuser flow could cause such drastic changes as claimed by OA, in the dissipation phenomenon of the fluids, the two methods used for evaluating the rate of energy dissipation were studied. For the present study ϵ was calculated, as discussed earlier, from the root mean square of the time derivative of u_1 -fluctuations. In doing

so, the condition of local isotropy and Taylor's hypothesis of frozen turbulence was assumed. The results thus obtained were corrected by using Wyngaard's length correction. OA obtained the dissipation estimates from the one-dimensional u_1 -spectra measurements using x-wire. In the process, Kolmogoroff's hypothesis of an inertial subrange is assumed to apply. The Kolmogoroff's hypothesis implies that for the spectrum of a velocity component to have an equilibrium range, rates of production, diffusion (from other layers of the flow), and transfer from other components, be small compared with the rates of dissipation and of inertial transfer through the spectrum in that range (Lawn, 1970).

A wave spectrum of $u_1'^2$ can be divided into three subranges corresponding to eddy sizes as follows (Bradshaw, 1971, p. 32; Nakagawa et al, 1975):

1. Productive subrange or energy containing range (large-scale eddy). It usually satisfies the 0 or -1 power law.
2. Inertial subrange (intermediate-scale eddy) - has a -5/3 power law.
3. Viscous subrange or dissipation range (small-scale eddy). It may be divided into two stages: one is the initial stage of a large dissipation scale at which the -3 power law is applicable and another is the final stage of a small dissipation scale at which the -7 power law is valid.

Using the spectrum data of inertial subrange, OA calculated the

rate of energy dissipation from:

$$\epsilon = [E_1(k_1) k_1^{5/3} / 0.53]^{3/2} \quad (23)$$

which also assumes the condition of local isotropy and Taylor's hypothesis. Normally in the wall bounded flows the region of inertial subrange extends to about 1 log cycle (Laufer, 1954; Monin & Yaglom, 1975, vol. II, p. 491) and the region beyond $-5/3$ slope on the higher wave number side represents the dissipation range. The u_1 spectra graph of OA (figure 49) has a very wide inertial subrange extending to about $2\frac{1}{2}$ log cycles. A surprising feature was the complete absence of the dissipation range. Also the data of u_2 spectra of OA showed a $1\frac{1}{2}$ log cycle region of the inertial subrange and again the dissipation range was absent. The u_2 -spectra normally shows no inertial subrange (Laufer, 1954). Hummel (1978) measured u_1 -spectra in the same diffuser at 6 radial positions at station 30 and all curves exhibited regions of -1 , $-5/3$, -3 , and -7 power slopes (figure 50). The absence of the dissipation range in OA data could possibly have occurred due to a x-wire having heavy dirt depositions. As discussed in Appendix C, the data obtained from a hot wire even with small dirt depositions can lead to highly erroneous results. Such a wire is not likely to respond properly to fluctuations of increasing order and thus affecting the measured spectra. The dissipation estimates from such a data could very well be in error and thus forcing a highly erroneous physical conclusion. Also Tutu & Chevre (1975) have reported that u_1 measurements from x-wire

are generally in error. Lawn (1971) and Nakagawa et al (1975) claimed that the spectral method may give the most reliable results for ϵ , but since the spectra is essentially the frequency distribution of energy, it is imperative that it be measured very accurately. And the one dimensional spectra measured with the x-probe is contaminated by cross-talk from other component (Wyngaard, 1968).

7.2.5 Convective diffusion due to kinetic effects

The convective diffusion due to kinetic effects which involves the derivatives of triple order velocity correlations was calculated from the experimental data. The axial derivatives of $\xi_2 \overline{u_1 q^2}$ and the radial derivatives of $\xi_2 \overline{u_2 q^2}$ were needed for the computation of this term. Both these quantities were normalized by the pipe radius and pipe bulk average velocity. The radial derivative was at least an order of magnitude higher than the axial derivative. The convective diffusion due to kinetic effects which is the sum of these two effects is very negligible in the entry region of the diffuser (figure 51). In the downstream direction, a valley with a negative value near the axis and a peak with a positive value at the pipe radius appears. Further towards the wall, the sign of the kinetic diffusion again becomes negative. The effect of the kinetic diffusion is to transport the energy away from the region where production is maximum to the region of the high dissipation. Also, its magnitude in the diffuser increases in the downstream direction. In the entry region, where the radial distance between the diffuser wall and the pipe radius is not large, the kinetic diffusion

does not reach a negative value in this region. This is presumed to be only due to lack of data acquisition very close to the wall. In the downstream direction, the valley and the peak tend to shift towards the diffuser axis. Near the exit, where the region between the wall and the point of maximum u_1' fluctuations is large and the data could be obtained in the wall region without any wall effects, diffusion of energy due to kinetic effects tends to reach a value of zero at the wall.

7.2.6 Convective diffusion due to pressure effects

The contribution of the convective diffusion due to pressure effects is also to transfer the turbulent kinetic energy from surplus to deficit areas. This term (figure 52) has a large magnitude in the regions where the difference in the production and dissipation is also large. And unlike other wall bounded flows, pressure diffusion in the diffuser is not negligible. Since there is a net transfer of turbulent kinetic energy out of the diffuser ($q_{out}^2 > q_{in}^2$) (figure 15), the integral of the pressure diffusion term is not equal to zero for the flow in the diffuser.

The pressure diffusion term involves the derivatives of the correlations of pressure and the velocity fluctuations in radial and axial directions. This was the only term that could not be measured experimentally and was thus obtained as a closure term in the energy balance equation 1.

At the wall since all other terms of the energy equation; i.e.,

production, dissipation, mean flow convection and kinetic diffusion all are zero, pressure diffusion would also be expected to go to zero.

Since the convective diffusion due to pressure effects is obtained as a closure term, it would also have the inherent cumulative errors of all other terms of the energy equation.

7.2.7 Convective diffusion due to kinetic and pressure effects

The term II of the energy balance equation is the sum of the kinetic and pressure diffusion. The total diffusion term also shows a valley at about the pipe radius in the entry region (figure 53) which shifts towards the axis in the downstream direction. Also the magnitude of this valley decreases towards the diffuser exit.

OA have also presented convective diffusion by kinetic and pressure effects for station 30. Their curve also has a peak but at different radial position and the magnitude at the peak is about 4 times greater than found in the present study. Very close to the wall it showed a sharp rise in its magnitude. OA obtained this curve as a closure term in the energy equation. In their case, magnitudes of the mean flow convection and of dissipation terms were very small and because of that nature, the magnitude of the convective diffusion was similar to that of the production. And as discussed earlier, the mean flow convection and the dissipation data presented by them appear to be in error, therefore the resulting convective diffusion would also be in error.

production decreases gradually to zero at the wall. The dissipation also decreased after reaching its maximum but this decrease occurs in a very thin layer near the wall. The maximum of dissipation reaches closer to the wall than production. Thus, near the wall, dissipation is much greater than production while in the region $0.25 < \xi_2 < 1.2$ production is greater than dissipation. It is from this region that the transfer terms transport energy to the high dissipation regions. On the average, the areas of two curves for this station are approximately equal with dissipation being about 8.7% less than the production. Also dissipation near the wall is much higher than at the diffuser axis, thus contradicting the claims of Okwuobi & Azad (1973).

At any cross-section, the total turbulent energy available is the sum of the energy produced there and the energy transferred to that place from other regions. The transfer terms of equation 1, involve the radial and axial derivatives of 2nd and 3rd order functions. The magnitude of the axial derivatives is very significant in the entry region of the diffuser and decreases in the downstream axial direction. The undissipated turbulent energy at any cross section is moved downstream by these transfer terms. This relationship for any cross-section can be expressed as:

$$\text{Production} + \text{inflow} = \text{Dissipation} + \text{outflow} \quad (24)$$

An estimation of the areas of production and dissipation curves indicated that the dissipation was about 27% less than the production at station 50 but was 12% more than production at station 6

(Table 6).

It is expected that the dissipation would be much less than production in the entry region of the diffuser. However, a true estimation of the magnitudes of two terms in the entry region could not be obtained as the data very close to the wall were not taken into consideration and thus the two curves could not be integrated over the whole cross-section.

This indicates that in the region of high pressure gradient, production exceeds dissipation and the extra undissipated energy is transferred in the downstream direction. But the dissipation increases gradually in the downstream direction to dissipate the energy being transferred there. A balance in the form of equation 24 is maintained. Since the turbulent kinetic energy leaving the diffuser is greater than entering it (figure 15), therefore the total production is greater than the total dissipation and the two terms would not balance each other for the whole diffuser as a control volume.

Figure 55 shows the parameter $\frac{P-\epsilon}{\epsilon}$ across the diffuser radius at station 30. Once again, the graph is presented for only one station due to qualitative similarity. The curve identifies clearly the regions with excess and deficient turbulent energy. In the region near the diffuser axis $0 < \xi_2 < 0.25$, dissipation is greater than production (indicated by the negative sign) and the same is true near the diffuser wall. And in the region $0.25 < \xi_2 < 1.2$ production is greater than the dissipation. Though the production may be maximum at about the pipe radius ($\xi_2 = 1.0$) (figure 54), the maximum positive difference between

production and dissipation (excess energy) occurs at about $\xi_2 \approx 0.7$ and maximum negative difference is seen to occur at the wall (figure 55). The curve changes its sign at $\xi_2 \approx 0.25$ and at ≈ 1.2 . Since the region between the diffuser wall and the point of maximum u_1' fluctuations increases in the downstream direction, the wall radial position where $\frac{P-\epsilon}{\epsilon}$ changes its sign also shifts. In the entry region, we do not even reach $\xi_2 = 1.2$ and since the data very close to the wall were not obtained, this radial position could not be established. But as figure 54 shows, this position would be between the wall and the point of maximum u_1' fluctuations. At the exit plane this change in sign occurred at $\xi_2 = 1.1$ instead of 1.2. This is consistent with the radial position of maximum production which also shifts away from the wall with the distance in the downstream direction.

On the basis of the production and dissipation data presented, it could be concluded that the turbulent energy dissipation is greater than the production in a small region next to the wall. This means a diffusion of energy towards the wall to satisfy the requirement of high dissipation there. These results are in agreement with Klebanoff's (1955) conclusion for the flat plate boundary layer. However, in the case of the diffuser, the region where dissipation is greater than production, grows in the downstream direction.

7.4 The Turbulent Kinetic Energy Balance in the Diffuser

Figures 56 to 62 show the turbulent kinetic energy balance in the diffuser covering the entire pressure gradient range. Because of

qualitative similarity, the energy balance curves for other measured stations are not presented. As expected, these curves show that the development of the flow due to changing pressure gradient is very smooth and as such all measured parameters should vary smoothly in radial and axial direction.

In the curves presented, sign convention adopted is the same as of OA and of Ruetnik & Corrsin (1955). Thus production is viewed as a gain to the turbulent field and dissipation as a loss. The sign of the other terms was based on the mathematical evaluation of each term. Thus physical and mathematical reasoning had to be used in grouping the different terms of the energy equation. Since the contribution of the viscous term was generally negligible throughout, it was not plotted in the energy balance curves.

Basically, the overall picture emerging from all these curves is the same; i.e., production and dissipation at any cross-section are of same order, though not necessarily equal. Thus refuting the claim of OA that the dissipation was negligible in the diffuser. Any difference in the amount of energy produced and dissipated at any point is convected and/or diffused away in axial and radial direction by the transfer terms. Also as the difference in the magnitude of production and dissipation decreases in the downstream direction, so is the net magnitude of all transfer terms. This should be expected as the transfer terms neither produce nor dissipate any energy in the flow field.

The plotted energy balance curves give the distribution of

each term as a function of radial distance from the axis. At radial points where production and dissipation are equal, the radial component of transfer terms would approach zero as there is no energy to be transferred from there. After station 50 in the axial direction, a change in the sign of convective diffusion due to pressure and kinetic effects occurs in the radial direction near the wall. This change occurs where production and dissipation are equal in magnitude and the mean flow convection is zero and stays the same up to the wall. In the entry region, the contribution of the convective diffusion is negligible at the axis but develops a peak at about $\xi_2 \approx 0.9$. In the downstream direction, its magnitude increases at the axis and its peak also shifts towards the axis. Also towards the diffuser exit, magnitude of the peak decreases, which could possibly be due to the fact that the energy is being distributed over a larger area and also the difference between production and dissipation is less here.

The mean flow convection also has a peak very near the wall in the entry region. This peak also shifts towards the axis and its magnitude decreases in the downstream direction. Also the magnitude at the axis increases and eventually the peak appears at the axis itself. However, generally the mean flow convection has a lower magnitude as compared to the convective diffusion. Therefore, it is the diffusion of the turbulent energy towards the wall which satisfies the requirement of high dissipation near the wall. In the total diffusion term, it is the pressure diffusion which governs its characteristics as opposed to kinetic diffusion. This finding is significantly different from

other wall bounded flows where the contribution of the pressure diffusion is generally negligible except close to the wall. The effect of kinetic diffusion is to transport the turbulent energy away from the region of high production. This is similar to other wall bounded flows, however its magnitude increases in the downstream direction in the diffuser.

Figure 60 also shows the energy budget data of OA for station 30. The two production curves are comparable except near the wall but similarity ends there. Their dissipation is very small and is zero at and close to the diffuser wall. Also the mean flow convection shows a valley at $\xi_2 \approx 0.9$. As discussed earlier, their data of these terms appear to be in error. The convective diffusion term of OA was not plotted as it was obtained from the erroneous results and thus would also be in error.

The similarity between the two production terms in figure 60 was also investigated. The production term at station 30 mainly involves $\overline{u_1 u_2}$ and $\frac{\partial u_1}{\partial x_2}$. Since the mean velocity is calculated from the d.c. output of the x-wire probe in both cases, it is generally not critically affected due to a drop in frequency response of a hot-wire probe with dirt depositions. The correlation of $\overline{u_1 u_2}$ is mainly due to the lower frequency components and are not affected to the same degree as are high frequency components. Also since the magnitude of $\frac{\partial u_1}{\partial x_2}$ is usually higher than $\overline{u_1 u_2}$ and thus it controls the magnitude of the production. Therefore, the agreement between the two production data should not be surprising.

7.5 Comments on the Turbulent Energy Budget in Wall Bounded Flows

Since the energy budget provides insight to the turbulence structure, a comparison of the data obtained for the diffuser is made to other wall bounded flows with different pressure gradients. Hummel (1978) has shown that the region $\xi_2 > 1.0$ in the diffuser approximately corresponds to the region $y^+ < 15$ in the pipe and boundary layer and it has been found that the turbulence energy production is maximum here. This region from the wall to the point of maximum production is referred to as the wall layer. In the diffuser, this wall layer region grows with the distance in the downstream direction.

The distribution of α and β , the angle of the principal strain and of the principal stresses is similar to that of the other wall bounded flows. It is also true for the turbulent intensities and thus indicates a similarity in the production of turbulent energy. Nakagawa et al (1975) state that the dissipation rate of turbulence is an essential quantity for dynamics of turbulence and it has been found to be true for the diffuser as well. However, the maximum of production and dissipation do not occur at the same radial position in the diffuser. Dissipation reaches maximum closer to the wall than the production, which probably is due to the growth of the wall layer in the diffuser. At station 30, for example, dissipation at the radial position where production peaks is 82% of its maximum value and is only 60% of the production. Transport terms carry this excess energy to the regions of high dissipation. Since the local inequilibrium in production and dissipation is higher in the diffuser as compared to other wall bounded

flows, the magnitude of the transport term is significantly higher. Particularly the diffusion of turbulent energy is very important in the diffuser, while it is much smaller in the pipe and boundary layer (Schubaur, 1954). It is the magnitude of this term that makes the eddy viscosity model unapplicable to such a flow (Klebanoff, 1955). The total diffusion at the point of maximum production is about 58% of the production (at station 30 of the diffuser), while it is approximately 16% in the fully developed pipe flow (Laufer, 1954). It is so because in the pipe, production and dissipation reach maximum at the same radial position, and thus no excess energy is available to be transferred to other regions. Also the axial component of transfer terms vanish in the fully developed pipe flow.

The magnitude of the diffusion term for the conical diffuser used in the present investigation is much higher than the Ruetenik & Corrsin's (1955) results for a divergent channel. However, the total divergence angle of the channel used by Ruetenik & Corrsin was only 2° , whereas it was 8° for the diffuser used in the present study. Such a diffuser produced an extremely complicated flow with a very high positive pressure gradient (figure 5). Ramaprian & Shiva-Prasad (1976) have shown that the diffusion of the turbulent kinetic energy is enhanced by the concave curvature in the wall of a plate. Schraub & Kline (1965) have reported that the positive pressure gradient increases the rate of the bursting process; i.e., ejections, sweeps and interactions. Also Nakagawa & Nezu (1977) have reported that there is a direct relationship between the turbulent diffusion and the bursting process.

Therefore, it is reasonable that diffusion of turbulent energy be very high in the conical diffuser used for the present investigation.

If the whole diffuser is considered as a control volume, then the turbulent kinetic energy leaving the control volume is higher than entering the diffuser (figure 15). An integration of the curves of $\frac{q^2}{2}$ Vs ξ_2^2 at stations 67 and 0 indicated that the mean turbulent kinetic energy U_b $[(\frac{1}{2\rho}) \int_{Ac} q^2 d \xi_2^2 / Ac]$ where Ac is the local cross sectional area) at these two stations was respectively 0.0047 and 0.0093 per unit mass. This shows that, since there is a net outflow of turbulent energy out of the control volume, the integral of transfer terms would not be zero in the diffuser. The results indicate that unlike other wall bounded flows, the integral of pressure diffusion in the diffuser was not zero. However, in other wall bounded flows, the production and dissipation of turbulent energy are equal and there is no net outflow of turbulent energy from the control volume. Whereas in the diffuser, total production exceeds total dissipation and therefore the transfer terms must exist to convect the undissipated energy out of the control volume.

The present results also show that of all the transfer terms, the pressure diffusion is the most significant. Laufer (1954) has reported that in fully developed pipe flow, the pressure diffusion is generally negligible except close to the wall where it is significant and also higher than the kinetic diffusion. Ramaprian & Shiva-Prasad (1976) have also reported the same for the flow along a flat-plate. They have also shown that a mild longitudinal concave curvature in the wall increased the contribution by both terms but the magnitude of the pressure diffusion

was still higher than the kinetic diffusion. Since the presence of strong adverse pressure gradient in the diffuser increases the significance of u_2 fluctuations (Sec. 6.1.2) this in turn, would increase the contribution of both the terms of diffusion; i.e., by kinetic effects ($\overline{u_2 q^2}$) and pressure effects ($\overline{pu_2}$) in radial direction. However, it is difficult to estimate the expected relative increase in the contribution of each term. It is though possible that the existence of adverse pressure gradient (conversion of kinetic energy into pressure energy) may contribute more to the pressure velocity correlation. This is further complicated by the presence of the derivative of $\overline{pu_1}$ correlation which vanishes for negative pressure gradient flow. Therefore, though it may be justified to neglect the effect of pressure-velocity diffusion for negative pressure gradient flows (Hanjalić & Launder, 1972 a & 1972 b), it cannot be assumed true for the case of a diffuser flow.

8. LENGTH AND TIME SCALES IN DIFFUSER FLOW

The fine structure of turbulence that is responsible for the viscous dissipation was obtained by the electronic differentiation of the single hot-wire signal u_1 and using the simplified expression for ϵ in the form of equation 21 (Sec. 7.1).

8.1 Distribution of Length Scales

The Kolmogoroff's length scale η and the dissipation length scale (Taylor's microscale) λ were obtained using the expressions:

$$\eta = \left(\frac{\nu^3}{\epsilon} \right)^{\frac{1}{4}} \quad (25)$$

and

$$\lambda^2 = 15\nu \frac{u_1'^2}{\epsilon} \quad (26)$$

The turbulence Reynolds number was calculated from:

$$R_\lambda = \frac{u_1' \lambda}{\nu} \quad (27)$$

These parameters are shown in figures 63 to 65 for 7 axial stations, as a function of the radial distance ξ_2 . The Kolmogoroff's length scale η decreases monotonically in radial direction with the distance from the diffuser axis (figure 63). A typical range of magnitude being from about 0.138 mm maximum at the diffuser axis to about 0.056 mm in the wall region at station 67. This range decreases to about 0.105 mm at the axis to about 0.073 mm near the wall at station 6. Data at

station 50 and downstream show an increase in the values of η in the wall region. Absence of this feature in upstream stations is probably due to lack of data in the wall region. The thickness of the wall layer increases in the downstream direction due to the expanding geometry and allows the measurement of required quantities without any wall effect on the sensing device. Up to station 40 in the downstream direction, values of Kolmogoroff's length scale η collapse on to a single curve between the diffuser axis and $\xi_2 = 0.9$. The length scale η decreases in this radial region further in the downstream direction. The increase in the values of η near the wall is more pronounced at stations after 40 in the direction of the flow. Also the range of η values from axis to wall decreases towards the exit from station 40. It is worth noting that in this region the pressure gradient is more or less constant and has a very small magnitude as compared to the entry region of the diffuser (figure 5). That is in the axial direction, the magnitude of η away from the wall collapses onto a single curve for high pressure gradient but decreases in the region of constant and small pressure gradient.

The dissipation length scale (Taylor's microscale) λ has a peak in the radial direction at about $\xi_2 = 0.4$, which shifts away from the axis in the downstream direction up to station 50 and remains at the same position for station 40 (figure 64). However, further in the downstream direction the peak starts to shift back towards the diffuser axis. From the peak position to the wall, the magnitude of λ decreases monotonically. Also the magnitude of λ at any radial position

increases up to station 40 in the axial direction but starts to decrease from station 30 onward and thus causes the crossing over of the curves at $\xi_2 = 1.0$, as the expanding geometry provides larger region to reach the same lower value. However, it is again worth noting that the decrease in λ like that of η occurs when most of the pressure recovery has already taken place and pressure gradient has become more or less constant. From station 40 in the downstream direction, the values of λ in the wall layer decrease linearly with increasing radial distance while upstream data show a more complex variation.

The turbulence Reynolds number R_λ also shows a peak initially appearing at about $\xi_2 = 0.75$ which shifts towards the wall up to station 40 in the downstream direction. Thereafter it starts to move towards the axis (figure 65). The values of R_λ after the peak decrease linearly towards the wall as a function of radial distance. The magnitude of R_λ generally increases in the axial direction from entry to exit, thus indicating an increase in the turbulence in the flow field.

A characteristic length scale of the flow field defined as (Lumley, 1970):

$$L_\varepsilon = \frac{q^3}{3^{3/2}\varepsilon} \quad (28)$$

was calculated and its ratio with the Kolmogoroff's length scale η (equation 25), which represents the length scale characteristic of dissipative range of wave numbers was plotted (figure 66) for 3 axial stations. These 3 stations represent the 3 distinct regions of the pressure gradient curve from entry to exit. The ratio L_ε/η has a

peak at about $\xi_2 = 0.75$ in the entry region which shifts towards the diffuser axis in the downstream direction. From the peak position towards the wall, the ratio of characteristic lengths decreases linearly. But in axial direction, the magnitude of the ratio increases in the direction of the flow. The value of the ratio except close to the wall generally varies between 100 and 750. A large value of this ratio, as found in the present study, indicates that the dissipating eddies are independent of the large energy extracting eddies which are of the order of mean flow.

A characteristic Reynolds number defined as (Lumley, 1970):

$$R_{L_\epsilon} = \frac{qL_\epsilon}{3^{1/2}\nu} = \frac{q^4}{9\nu\epsilon} \quad (29)$$

was calculated and is shown in figure 67 for the same 3 stations as was figure 66. Its distribution is similar to that of L_ϵ/η . In grid turbulence R_{L_ϵ} is usually constant (Lumley, 1970), but as figure 67 indicates it is not the case in the conical diffuser.

8.2 Distribution of Time Scales

In addition to the length scales of the flow, the time scales are also equally important in the study of the fine structure of turbulence. A time scale defined by Kolmogoroff which is indicative of the dissipative range of the wave numbers is:

$$T = (\nu/\epsilon)^{1/2}. \quad (30)$$

Figure 68 shows this parameter for the 3 axial stations. The time scale decreases towards the wall but increases again very close to the wall. This is indicated by two curves for stations towards the exit. The inverse of the time scale T represents the vorticity of the flow. And as figure 69 indicates, vorticity reaches a maximum near the wall where time scale had the smallest value. Vorticity increases in the downstream direction in the core region but the reverse is true near the wall.

The time scale (equation 30) was also investigated in relation to the characteristic time scale of the flow (τ) defined as:

$$\tau = \frac{q^2}{2\varepsilon} \quad (31)$$

and forming the ratio of 31 to 30:

$$\frac{\text{Characteristic time scale of the flow}}{\text{Characteristic dissipative time scale}} = \frac{q^2/2\varepsilon}{(v/\varepsilon)^{1/2}} = \frac{q^2}{2(\varepsilon v)^{1/2}}$$

The distribution of the ratio of these two time scale (figure 70) is similar to that of the length scales of figure 65. Also, the ratio of time scales has a similar range of variation as compared to length scales.

The time scale of the Reynolds stresses may always be expected to be of the order of the inverse of the mean strain rate, however, this is not true of the time scales of the dissipation. The ratio of two time scales in fact is of the order of $R_{LE}^{1/2}$ (Lumley, 1970), so that

the time scale $(\nu/\epsilon)^{1/2}$ may be expected to become shorter and shorter to that of the mean motion as the Reynolds number increases. Lumley (1970) also states that the influence of the strain rate on the structure of the dissipative region is proportional to the $R_{LE}^{-1/2}$. Since the characteristic Reynolds number R_{LE} (figure 67) increases in the downstream axial direction, the quantity $R_{LE}^{-1/2}$ would be expected to decrease in the same order. Such a distribution is shown in figure 71. The value of $R_{LE}^{1/2}$; i.e., the inverse of numbers given in figure 71 has been reported to vary from 6.6 to 60 in homogeneous turbulence (Lumley, 1970). An estimate of $R_{LE}^{1/2}$ from figure 71 indicates it to vary between 20 and 80.

9. THE ISOTROPIC VORTICITY BALANCE

9.1. Skewness of $\frac{\partial u_1}{\partial t}$ (S)

Measurements of S (equation 4) at 7 different axial stations are shown in figure 72. These 7 stations represent different slopes of pressure gradient curve. Curves for other 5 stations had similar distribution. As figure 72 indicates, values of S vary within a range of 0.38 to 0.5 from the diffuser axis to the point of maximum u'_1 fluctuations, which occurs approximately at the pipe radius ($\xi_2 = 1.0$). A similar range for the values of S was reported by Batchelor & Townsend (1947) in a grid generated isotropic turbulence. They suggested that S is essentially constant and has an average of 0.39. A value of 0.37 was reported by Kuo & Corrsin (1971) and it was estimated to be 0.44 by Kolmogoroff (Batchelor, 1947). Betchov (1956) reported it to vary between 0.4 and 0.5. Saffman (1963) suggested its range to be from 0.3 to 0.5. The present results up to $\xi_2 = 1.0$ compare favourably with these data for grid turbulence. In the wall layer (between the wall and the point of maximum u'_1 fluctuations), however, values of S increase with increasing radial distance towards the wall. The magnitude of S near the wall, towards the diffuser exit reaches as high as 1.0. Since the data very close to the wall were not obtained, its behavior further towards the wall for the diffuser is not known. In the entry region, values of S obtained near the wall were not as high as 1.0. This is probably due to the lack of data obtained in the wall layer in the entry region of the diffuser.

The increasing nature of S near the wall has also been reported by Ueda & Hinze (1975) in a flat plate boundary layer, Ueda & Mizushima (1977) and Elena (1977) in a fully developed pipe flow. Their results indicate that at about $y^+ = 20$, S reaches a maximum value between 0.9 and 1.0 before decreasing further towards the wall. In the region away from the wall ($y^+ > 100$), S remains constant and has a value of approximately 0.38. From $y^+ = 100$ towards the wall, it starts to increase with radial distance till it reaches its maximum value. The present results are in agreement with these previously published results in wall bounded flows, indicating that the fine structure of turbulence is similar. Thus there is a possibility that even in the diffuser, S would decrease after reaching its maximum value. However, a notable difference is that in the boundary layer and the pipe, S attains its maximum value approximately at the point where turbulence production is maximum, whereas it remains constant up to the point of maximum production in the diffuser. Hummel (1978) has compared the position of $y^+ = 15$ as the outer edge of viscous sublayer in the boundary layer to the $\xi_2 = 1.0$ in the diffuser. On the basis of data of S , such a comparison may not be valid. However, it is possible that another layer, where viscous effects are dominant as compared to the inertia terms, may be developing near the diffuser wall. The skewness of S in the diffuser may be reaching its maximum value at the edge of this layer. The point of maximum turbulent production and the edge of the viscous sublayer coincide in the pipe and boundary layer, but are being forced apart by the expanding geometry in the diffuser.

Since S represents the rate of production of vorticity by the process of vortex stretching, and because its distribution and magnitude in the diffuser except in the wall layer is similar to that for an isotropic flow, it can be argued that the assumptions of the local isotropy in the diffuser away from the wall are justified. With the same argument, it can be said that the increasing values of S near the wall indicate the increasing degree of anisotropy. The ratio of $\frac{u'_1}{u'_2}$ in the diffuser increases towards the wall (Sec. 5.1), which is also a consequence of increase in the degree of anisotropy. The lack of isotropy near the wall has been reported for all other wall bounded flows (Ueda & Hinze, 1975; Lawn, 1971). Therefore, the results obtained with isotropic assumptions near the wall would be subject to error and this fact should be borne in mind while interpreting the same. But since the magnitude of S in the diffuser reaches the same value as for the other wall bounded flows, it can be said that the degree of anisotropy would also be the same. Thus the errors introduced due to isotropic assumptions would also be of the same order, hence, the results in the diffuser can be compared to that of the pipe and boundary layer.

The high values of S near the wall indicates it to be a region of high turbulent activity. This is in agreement with the results of the visual studies of Kline and his associates and also of Brodkey and his associates that the turbulence is generally produced near the wall. Ueda & Hinze (1975) have reported that the skewness factor of $\frac{\partial u_1}{\partial t}$ is associated with the inrush of the high momentum fluid lumps into

the inner wall layer. Hummel (1978) has shown that like other wall bounded flows, the sweep phase represented by the 4th quadrant correlation of $\overline{u_1 u_2}$ is higher than the ejection phase of 2nd quadrant correlation in the wall layer. In addition to this, theoretical calculations of Nakagawa & Nezu (1977) have also shown that the ejection phase should be lower than sweep close to the wall. This would require that the values of S be large in the wall layer, as was found in the present study (figure 72). Also since S involves the measurement of $\frac{\partial u_1}{\partial t}$ which represents the finer structure of turbulence, it can be concluded that the fine structure of turbulence is similar in all wall bounded flows.

In pipe and boundary layer flows, the point of maximum u_1' fluctuations specifies the edge of sublayer. Inside the sublayer (towards the wall), sweep is more important while outside of the sublayer, ejection is more significant. A similar situation also exists in the diffuser, and on this basis the wall layer of the diffuser can be viewed as a rather thick sublayer as suggested by Professor A.M. Yaglom (private communication, 1978). The diffuser flow amplifies this region where sweep event is higher than the ejection, as compared to the pipe and boundary layer flows.

Batchelor & Townsend (1947) reported that the measurements of S in their flow were independent of the turbulence Reynolds number R_λ . The values of R_λ in their flow varied from 20 to 60. The region where S remains approximately constant (within the range .37 to .5) in the diffuser has a turbulence Reynolds number varying from 200 to 600 (figure 73), which is an order of magnitude higher than that of the

grid turbulence reported by Batchelor & Townsend (1947). In the wall layer (from wall to the point of maximum u_1' fluctuations) R_λ decreases towards the wall after reaching its maximum value but S increases with decreasing R_λ . However, the lowest value of R_λ measured near the wall is 130 which is still higher than the grid turbulence of Batchelor & Townsend (1947). Ueda & Hinze (1975) reported that in the region where S was constant, lowest value of R_λ was of the order of 100. In the present study, deviation in values of S occurred near the wall at values of R_λ for which S was constant away from the wall. This indicates that the increase in S is due to proximity of the wall and not due to decrease in R_λ . This illustrates that it is the wall that influences the level of turbulent activity and thereby the degree of anisotropy in the flow. Thus it can be concluded that the concept of isotropy can be used in a region away from the wall in a flow as complex as ours, but it may not be valid close to the wall. This was also pointed out by Frenkiel & Klebanoff (1975).

Saffman (1963) following Batchelor & Townsend (1956) suggested that the Kolmogoroff's time scale (equation 30) is related to the skewness of $\frac{\partial u_1}{\partial t}$ in the form:

$$(\nu/\epsilon)^{1/2} = \frac{7}{6\sqrt{15}} \frac{S}{\alpha_1}$$

or:

$$\alpha_1 = \frac{7}{6\sqrt{15}} \left(\frac{\epsilon}{\nu}\right)^{1/2} S = \frac{\omega_i \omega_j (\partial u_i / \partial x_j)}{\omega^2} \quad (32)$$

This function α_1 is shown in figure 74 and $(\epsilon/\nu)^{1/2}$ which represents the vorticity in the field was given in figure 69. The units of α_1 would be the same as of $(\epsilon/\nu)^{1/2}$; i.e., sec^{-1} . The behavior of α_1 follows the distribution of S in the field. The region where S was constant, α_1 is also seen to be constant and for increasing S , α_1 also increases. Thus the α_1 curve which represents the product of S and the turbulence vorticity of the field, identifies the region of nonisotropy in the flow field.

9.2 Second Derivative of u_1 (G)

Measurements of G which represent the decay of vorticity in the flow field due to viscosity are shown in figure 75. Due to similarity, data for only 7 axial stations are presented. Generally the magnitude of G increases slightly in the axial direction and near the wall in the radial direction, it also shows a rising trend after station 50. The increasing values of G in the axial direction indicate that the effect of viscosity in smoothing out turbulent fluctuations increases in the direction of flow. Since the effect of viscosity is usually felt at very small length scales, it must decrease in the downstream direction to satisfy the higher values of G . Such a decreasing trend of the Kolmogoroff length scale η was found in the flow (figure 63). Also near the wall the length scale decreases considerably, thus indicating that the effect of viscosity is also higher near the wall. The generation of the small scale fluctuations is due to the non-linear terms in the equations of motion. As the fluid moves downstream, its length scale decreases due to the presence of inertia in the flow,

thus increasing the ability of viscosity in dissipating small scale energy into heat. Such an explanation would imply that the turbulent energy is being transported in radial and axial directions. The turbulent kinetic energy budget (Sec. 7) indicated such movement of turbulent energy in the radial and axial direction.

In the vorticity equation 3, parameter G appears in the form $\frac{G}{R_\lambda}$. And since G and R_λ both increase in the downstream axial direction, their ratio (figure 76) was found to be independent of the axial position. This indicates the dependence of G on R_λ . At large Reynolds number, though the relative magnitude of viscous effects in a flow tend to become vanishingly small, however, the increased effect of non-linear inertia terms in the Navier-Stokes equation generate additional motion at scales small enough to be affected by viscosity. This ensures a balance in the flow field by keeping viscosity effects at a finite level.

In the radial direction, the ratio $\frac{G}{R_\lambda}$ is constant from the diffuser axis to $\xi_2 \approx 1.0$ and increases sharply further towards the wall. This behavior is similar to that of S (figure 72) and indicates a close relationship between the production of vorticity and its decay in the flow field. The effect of viscosity on small scale motions in dissipating the energy depends on the rate at which it is supplied with the energy by the larger-scale motion. Therefore, a close relationship between the parameters S and G should be expected.

9.3 Vorticity Balance

Using isotropic assumptions, Batchelor & Townsend (1947) simplified the vorticity equation 3 in terms of S , G , and R_λ parameters in the following form:

$$G = \frac{30}{7} + \frac{1}{2} R_\lambda S. \quad (33)$$

This relationship was shown to hold (with S as constant = 0.39) in the decay of vorticity in grid generated isotropic turbulence. To check the applicability of this equation for the flow under investigation, values of G were plotted as a function of R_λ (figure 77). The solid line represents the equation 33 with $S = 0.39$ as suggested by Batchelor & Townsend for isotropic flow. Agreement between grid turbulence data ($20 \leq R_\lambda \leq 60$) and the diffuser data ($200 \leq R_\lambda \leq 600$) excluding the wall region is excellent. Because of the interrelation between S and G , the values of G near the wall do not follow the isotropic distribution. Values of G deviating from equation 33 are those obtained in the wall layer of the diffuser. It has been known that the degree of anisotropy increases closer to the wall, this fact is further confirmed by the nature of S and G distribution in the diffuser.

Rewriting equation 33 as:

$$\frac{2G}{R_\lambda S} = 1 + \frac{60}{7 R_\lambda S}. \quad (34)$$

If S is assumed as constant and equal to 0.39, then the above equation

can be written as:

$$\frac{2G}{R_\lambda S} = 1 + \frac{22}{R_\lambda}$$

If R_λ is large enough, then the second term on the right hand side can be dropped. Thus:

$$\frac{2G}{R_\lambda S} = 1.0 \quad (35)$$

for isotropic turbulence.

This relationship was plotted and is shown in figure 78. Since S and $\frac{G}{R_\lambda}$ are both constant in the core region, equation 35 was found to be true in the diffuser. But in the wall region, the curve deviates from unity. Equation 35 implies that in the core region, magnitude of S is about twice that of $\frac{G}{R_\lambda}$. This was also evident from figures 72 and 75. However, in the wall region, plot of $\frac{2G}{R_\lambda S}$ deviates from unity and increases with distance towards the wall. Very close to the wall, it reaches a value as high as 4.0. If $\frac{2G}{R_\lambda S}$ can be considered as a ratio of decay to production of vorticity, then its magnitude equal to unity would imply that the terms of production and dissipation of vorticity approximately balance each other. Thus the increasing nature of $\frac{2G}{R_\lambda S}$ towards the wall would indicate that the effect of viscosity is greater and exceeds the effect of vortex extension in the wall region. This increase in the effect of viscosity reaches almost 400% very close to the wall. As indicated by $\frac{2G}{R_\lambda S}$ values, it is not a simple function of R_λ but is rather influenced by the proximity of the wall (figure 79).

The increased contribution of viscosity in dissipation near the wall was also indicated by the turbulent kinetic energy balance for the conical diffuser (Sec. 7).

9.4 Visual Results

Perhaps the most significant progress towards an understanding of turbulence mechanism has been achieved recently, by using direct visual studies of individual events and by sampling the turbulence upon detection of a specific event. The turbulent signal and its derivative which formed the basis of this study were observed on a storage oscilloscope and were photographed. The statistical analysis of the data had shown that though the wall region indicates a considerable degree of anisotropy, the flow away from the wall has properties of isotropic turbulence. Therefore the three signals u_1 , $\frac{\partial u_1}{\partial t}$ and $\frac{\partial^2 u_1}{\partial t^2}$ were studied visually in both the isotropic and anisotropic regions. The storage capability of the oscilloscope was an invaluable asset for this purpose.

Two sets of photographs were taken at axial station 12 and at radial positions $\xi_2 = 0.69$ and 1.71 (figure 80 a & b). Both figures have 3 photographs; in photograph (i), the upper trace is the u_1 signal and the lower trace is of $\frac{\partial u_1}{\partial t}$. In photographs (ii) and (iii) the upper trace is $\frac{\partial u_1}{\partial t}$ and the lower trace is of $\left(\frac{\partial u_1}{\partial t}\right)^3$ and $\frac{\partial^2 u_1}{\partial t^2}$ respectively.

The u_1 signal at $\xi_2 = 0.69$ is somewhat negatively skewed but the signal and its derivative both are continuous, thus indicating that its intermittency factor would be close to one. However, near the wall

u_1 signal itself is positively skewed and rather shows some intermittent movement of the fluid and its derivative shows this intermittency even more clearly. There are periods of sudden activity followed by quiet periods. Since S ; i.e., skewness of $\frac{\partial u_1}{\partial t}$ is associated with the inrush of the high momentum fluid into the inner wall layer, the $(\partial u_1 / \partial t)^3$ signal further shows that this inrush of fluid occurs in lumps and is intermittent in nature. This signal has a very small magnitude in the core region and in comparison is very significant near the wall giving high values of S in the wall region. The 2nd derivative of u_1 signal which is indicative of high frequency components decayed by viscosity, is also intermittent. Since the 2nd derivative is related to the first thus has some similarities to it. These findings tend to confirm qualitatively the results of statistical analysis. The 2nd derivative is very uniform near the axis but shows abrupt changes near the wall.

It can be inferred from these visual studies that the turbulence production generally occurs near the wall. This production process is very intermittent but organized. Since the turbulence production is mainly due to the interaction of the mean flow and the large scale eddies, it should be expected to be anisotropic. Turbulence needs time to distribute its energy and reach isotropy. Therefore it cannot be expected to reach this stage at its place of production. As this newly produced turbulence travels away from the place of its production, due to inertia it transfers its energy to small scale turbulence and thus tends to attain the state of isotropy. And since near the axis, no new turbulence is produced, the photographs taken show low level of

turbulent activity. Even near the wall, large eddies do transfer significant amount of their energy to smaller eddies because of high mean strain and shear in the field. These smaller eddies are immediately acted upon by the viscosity to dissipate their energy. The 2nd derivative of u_1 near the wall attests to that since the 2nd derivative is much more significant near the wall, it indicates that the effect of viscosity is higher here. This would confirm the statement of Klebanoff (1955) that a significant part of turbulence dies in infancy.

9.5 Consequences of the Vorticity Balance

The study of the vorticity balance in terms of the parameters S and G provides information about the process of vorticity production by vortex stretching and its dissipation due to the effect of viscosity. The results very close to the wall were not obtained, but since the wall layer, which occupies a very small region in the pipe, expands in the diffuser with the flow in downstream direction and thus allows some measurements in the wall layer without any wall effect on the sensor. Therefore, the nature of the various parameters measured downstream can be considered to be true in upstream stations as well. With this fact in mind, the results show that the ratio of the rates of production and dissipation of ω'^2 and the nature of vorticity balance is essentially the same at all axial stations. This suggests that there is a dynamical similarity at all axial stations of those aspects of the turbulence which control the vorticity balance. In radial direction the ratio of the production and dissipation of vorticity is constant from the

diffuser axis to the point of maximum u_1' fluctuations. Further towards the wall, effect of viscosity becomes larger than the vortex extension. It is in this region that the contribution of sweeps to shear stress is also larger than that of ejection event (Hummel, 1978).

The results also show that even in shear flows, there exists a region which has certain similarities to that of an isotropic flow. The presence of the wall and the ensuing complexities prohibit the extension of these isotropic ideas to the wall layer. In order to understand the limitations of isotropy in shear flows, the mechanism of turbulent energy transfer should first be investigated. Tennekes & Lumley (1970) have stated that the vorticity found in the larger eddies in a turbulent flow is of the same order as the vorticity of the mean flow, and that the respective strain rates are also comparable. Except in the entry region the axial derivative of U_2 is generally negligible in the diffuser used here and the radial derivative of U_1 (figure 10) is the main contributing factor to the mean vorticity and the mean strain. In the core region of the diffuser, the radial derivative of U_1 is small and is the same for all axial stations and varies linearly with distance. This may account for small values of S and G in this region. However, in the wall region, $\frac{\partial U_1}{\partial \xi_2}$ is very high which would help in increasing the rate of vortex stretching in producing eddies and also decreasing their scale to the level to be acted upon by viscosity. This results in high values of S and G in the wall region.

Turbulence is produced as a large scale structure and is

directly influenced by the magnitude of $\frac{\partial u_1}{\partial \xi_2}$. The energy from large scale eddies is passed on to smaller eddies through vortex stretching. The process of vortex stretching tends to make the smaller scale eddies loose all sense of direction and become statistically isotropic and also their contribution to the Reynolds stress vanishes. This fine structure has also been reported to be intermittent in nature (Batchelor & Townsend, 1949). Therefore, it may be of interest to investigate the intermittency of $\frac{\partial u_1}{\partial t}$ signal in relation to the changing role of the parameter $\frac{\partial u_1}{\partial \xi_2}$ which controls the large scale structure of the turbulence.

Following Kuo & Corrsin (1971), Hummel (1978) measured the maximum flatness factor of narrow band filtered u_1 signal and the intermittency factor of $\frac{\partial u_1}{\partial t}$ at station 30 (figure 81). His results indicate that the intermittency factor is almost constant and has a value of 1.0 in the core region where S was also constant. There after the intermittency factor decreases towards the wall. The photographs of $\frac{\partial u_1}{\partial t}$ taken from the oscilloscope (Sec. 9.4) also showed that the signal was intermittent near the wall. The maximum flatness factor is also almost constant in the core region and has a value between 22 to 25 where the intermittency factor of $\frac{\partial u_1}{\partial t}$ is 1.0. The flatness factor increases sharply in the wall region (figure 81). There is an obvious relationship between the maximum flatness factor of the narrow band filtered u_1 signal, the intermittency of $\frac{\partial u_1}{\partial t}$ and its skewness. It suggests that if the maximum FF of the narrow band filtered u_1 signal is less than about 25, then $\frac{\partial u_1}{\partial t}$ is not intermittent and skewness of $\frac{\partial u_1}{\partial t}$ is also constant.

In this region of shear flows, the isotropic assumption can be applied. With the decrease in the intermittency factor of $\frac{\partial u_1}{\partial t}$, its skewness and the FF of the narrow band filtered u_1 signal increases, indicating an increase in the level of anisotropy.

It was also found that the results of the skewness of $\frac{\partial u_1}{\partial t}$ (S) for the diffuser compare very well to that of the pipe and boundary layer. The nature and the magnitude of S in these flows is almost the same. Therefore, the degree of error introduced in the diffuser results with the assumption of isotropy would be of approximately the same order as in the pipe and boundary layer. However, in the fully developed pipe flow, S reaches a maximum at the point of maximum turbulent energy production while in the diffuser it remains almost constant up to this point. That is, in the pipe S deviates from its constant value before the point of maximum production. This indicates that the region of constant S where isotropic theory is valid is larger in the diffuser in comparison to the fully developed pipe flow.

Hummel (1978) has stated that the outer edge of the viscous sublayer ($y^+ \approx 15$) is comparable to that of $\xi_2 \approx 1.0$ in the diffuser. This appears to be valid from the point of maximum turbulent energy production. But the study of vorticity balance indicates that the maximum of S does not occur at $\xi_2 \approx 1.0$ but rather occurs very close to the wall. This indicates that the maximum of S is probably affected by the wall. It is also probable that another layer analogous to the viscous sublayer in the boundary layer is developing near the wall in the diffuser. The skewness of $\frac{\partial u_1}{\partial t}$ (S) may be reaching maximum at the

edge of this layer. This would suggest that unlike pipe and boundary layer flows, the maximum of turbulence kinetic energy and vorticity productions are being forced apart by the strong adverse pressure in the diffuser.

10. RECAPITULATION

The present experimental study was undertaken as a result of the finding of Okwuobi & Azad (1973) that the dissipation of turbulent energy in a conical diffuser is negligible and the production is generally balanced by the convective diffusion by kinetic and pressure effects. The purpose of this study was to investigate the physical phenomenon which renders the dissipation negligible in the flow. At the outset of this study, it was thought that this process of changing from the pipe flow characteristics where dissipation is significant to the diffuser characteristics where the dissipation is reported to be negligible, must be gradual. With this objective in mind, detailed measurements of all the quantities except that of the pressure velocity correlations were made in the diffuser at 13 axial stations. Since most of the turbulent energy is dissipated by the action of viscosity on smaller eddies, it was also decided to make detailed measurements of the parameters indicative of the fine scale structure. Attempts were made to minimize the experimental errors that can occur during the course of a survey type experimental study.

The results of the present analysis contradicted the earlier reported claims of Okwuobi & Azad (1973), that the dissipation was negligible in the diffuser. On the contrary, it was found that even in the diffuser, dissipation was of the same order as production. However, the production and dissipation were not necessarily equal in magnitude at all the axial stations. The results indicated that in the entry region of the diffuser, production was much higher than the dissipation. The difference in production and dissipation of turbulent energy

decreases in the downstream direction and eventually dissipation exceeds production near the diffuser exit. As a result, there was some undissipated turbulent energy in the entry region of the diffuser. This excess energy was transported downstream by the inhomogeneity in the turbulence quantities in the axial direction. The picture here is different from the fully developed pipe flow where all the energy produced at a cross-section is dissipated there. It turns out that for the case in study, an appreciable proportion of the energy produced is convected and diffused both in the radial and axial directions. The results indicated that of all the transfer terms in the flow, the pressure-velocity correlation (pu_1 and pu_2) is the most significant in the diffuser. Thus the assumption of negligible contribution of pressure diffusion for many other flows can not be justified in the case of diffuser.

Because of the expanding geometry, the wall layer in the diffuser expands considerably in the downstream axial direction. Thus the radial position where the turbulent production reaches maximum moves farther away from the wall with the distance in the downstream direction. The dissipation was generally more than production in this layer from wall to the point of maximum u_1' fluctuations. The edge of this wall layer is comparable to the edge of sublayer in pipe and boundary layer which occurs at about $y^+ \approx 15$. It was also noted that the point of maximum production of turbulence coincides with that of zero skewness and minimum of fourth order velocity correlations including the flatness factors of all 3 fluctuating velocity components. This is consistent with the pattern exhibited by pipe and boundary layer flows at the

point of maximum production.

The measurements of fine structure of turbulence, which contains most of the vorticity, indicated that in the region from diffuser axis to the edge of the wall layer, there is qualitative and quantitative similarity between the isotropic and diffuser flows. This similarity existed at all the axial stations. Thus, on this basis, the assumptions of local isotropy in the core region of the diffuser can be justified. However, in the wall layer the pattern of the fine structure differs considerably from that of the isotropic behavior. This structure in the wall layer of the diffuser is influenced by the proximity of the wall and is highly intermittent. It is also the region of high turbulence activity. This behavior is similar to that reported for pipe and boundary layer flows.

The parameter S increases in the wall layer and reaches maximum close to the wall. In pipe and boundary layer flows, it reaches maximum at the edge of sublayer where turbulence production is maximum, whereas it remains constant up to this point in the diffuser. Thus the maximum of S and of the production of turbulence do not occur at the same radial position in the diffuser. This implies that these are governed by two different physical phenomena which are being forced apart by the adverse pressure gradient in the diffuser. In this respect, diffuser flow is considerably different from the pipe and boundary layer flows.

Initially, the fully developed pipe flow entering the diffuser is in a state of dynamic equilibrium between pressure force and shear stress force. When the flow enters the diffuser, the mean axial

velocity U_1 decreases to preserve the continuity. Simultaneously, the pressure increases resulting in a change in momentum with maximum effect on the velocity profile near the wall. This changing momentum flux in the wall proximity produces a thickening wall layer and a displacing effect on the position of maximum velocity fluctuations and turbulent shear stress towards the diffuser. The retardation of the mean axial velocity increases the relative turbulence intensities. The third and fourth order moments of these velocity fluctuations indicate that the 'extra memory effects' may be present in the flow in the region far removed from the wall.

11. CONCLUDING REMARKS

An experimental study of the turbulent kinetic energy and the isotropic vorticity balance for a conical diffuser with fully developed pipe flow at entry has been presented. Quantitative data of the measurements of mean static pressure, mean velocity, turbulence intensities, correlation coefficients, skewness & flatness factors, all the 3rd & 4th order correlations of two velocity components, first & second derivative of the u_1 signal and also the skewness of $\frac{\partial u_1}{\partial t}$ signal are presented for an entry Reynolds number of 58000.

The mean static pressure distribution in the axial direction of the diffuser showed that the rate of pressure recovery is maximum in the entry region and decreases significantly towards the exit. The general feature of the radial distribution of the turbulence fluctuations is the occurrence of a peak very close to the wall near the diffuser inlet; the peak progressively shifts away from the wall with the distance in the streamwise direction. This causes the thickening of the wall layer in the diffuser in the downstream axial direction. The distribution of the turbulence intensity levels is qualitatively similar, but quantitatively much in excess of those in pipe flow.

The results of the turbulent kinetic energy budget show that the rate of turbulent energy production approximately reaches a maximum at the edge of the wall layer which extends from the wall to the point of maximum u_1' fluctuations. At the edge of this layer, the skewness of u_1 & u_2 changes sign and all the 4th order moments show a minimum at this point, which is similar to that of pipe and boundary

layer flows. Within the wall layer, dissipation is more than production and thus a need for energy diffusion towards the wall. The results also showed that not all the turbulence energy produced at any cross-section is dissipated there. In the entry region production is higher than dissipation, while near the exit dissipation is higher than the production. To maintain an overall balance between production and dissipation in the diffuser, transfer terms transport the excess energy in both radial and axial directions. It is also shown that the diffusion due to pressure velocity correlations (ρu_1 and ρu_2) is the most important parameter in transferring the excess turbulent energy to the deficient regions.

The measurements of the fine structure of turbulence revealed that the analysis of Batchelor & Townsend (1947) for isotropic turbulent vorticity balance is equally valid for the diffuser flow except in the wall layer. In the core region, where this analysis is applicable, ratio of the rates of production and dissipation of ω'^2 is constant, and the vorticity balance is essentially the same at all axial stations. Thus there is a dynamical similarity at least of those aspects of the turbulence which control the vorticity balance. It was also seen that in this region: i) the $\frac{\partial u_1}{\partial t}$ is not intermittent; ii) mean strain $\frac{\partial u_1}{\partial \epsilon_2}$ is small and linear; iii) ratios of length and time scales of the flow to the dissipating eddies were high and similar; and, iv) flow was far removed from the wall.

In the wall region, however, vorticity parameters S and G do not follow the isotropic pattern, but the behavior of S is similar to

pipe and the boundary layer flows (measurements of G are not reported for these flows). But the maximum of S does not reach at the point of maximum u_1' fluctuations as in the fully developed pipe and boundary layer flows. It attains its maximum value very close to the wall. This provides a larger region in the diffuser where S is constant as compared to the pipe flow. This also indicates that another layer near the wall analogous to the viscous sublayer in pipe and boundary layer may be developing in the diffuser.

All the experimental results presented here indicate that the flow in the diffuser can be divided in two main distinct regions: i) the core region; and, ii) the wall layer. This division of flow in the radial direction is very much similar to that of the pipe flow except that the expanding geometry of the diffuser makes the wall layer thicker. This wall layer which occupies a very small region in the pipe flow at the diffuser inlet expands considerably in the downstream direction. Since the wall layer is the most important region from the point of view of the structure of the turbulent flow, its expansion allows the measurement of turbulent quantities in this layer without being very close to the wall. This substantially decreases the wall effect on the sensor and thus provides experimental advantages as compared to its study in other wall bounded flows.

RECOMMENDATIONS

It seems apparant following the present investigation that further work should pursue the following course:

- i) Data of the present investigation should be used to investigate the applicability and the required modifications, if any, of the mathematical models for the energy balance used in other flow fields, to the flow in a conical diffuser.
- ii) In order to understand the mechanism of energy transfer between the wall and the core-region of the diffuser, the space-time correlations of the various functions should be studied.
- iii) For the purpose of understanding the structure of turbulence in the diffuser, the wall layer should further be explored. This is of particular importance in the entry region of the diffuser.
- iv) If possible, the pressure-velocity correlations should be measured experimentally. This may help in gaining information about the relative significance of this term in axial and radial directions.
- v) The possibility of the 'extra memory effects' on the structure of turbulence quantities in diffuser should further be examined.

REFERENCES

- Arora, S.C. and Azad, R.S. (1978)
Turbulent kinetic energy balance in a flow with adverse pressure gradient. The University of Manitoba, Canada, Department of Mechanical Engineering, Rep. ER 25.27.
- Azad, R.S. and Hummel, R.H. (1971)
Measurement of the intermittency factor in diffuser-flow. Can. J. Phys., 49, 2917.
- Batchelor, G.K. (1947)
Kolmogoroff's theory of locally isotropic turbulence. Proc. Camb. Phil. Soc. 43, 533.
- Batchelor, G.K. and Townsend, A.A. (1947)
Decay of vorticity in isotropic turbulence. Proc. Roy. Soc. A191, 534.
- Batchelor, G.K. and Townsend, A.A. (1949)
The nature of turbulent motion at large wave-numbers. Proc. Roy. Soc. A199, 238.
- Batchelor, G.K. and Townsend, A.A. (1956)
Turbulent diffusion, surveys in mechanics (G.K. Batchelor and R.M. Davis, eds.), The University Press, Cambridge.
- Betchov, R. (1956)
An equality concerning the production of vorticity in isotropic turbulence. J. Fluid Mech. 1, 497.
- Bradshaw, P. (1971)
An introduction to turbulence and its measurement. Pergamon Press Ltd.
- Bradshaw, P., Ferris, D.H. and Atwell, N.P. (1967)
Calculation of boundary-layer development using the turbulent energy equation. J. Fluid Mech. 28, 593.
- Builtjes, P.J.H. (1977)
Memory effects in turbulent flows. Delft University of Technology, The Netherlands, Department of Mechanical Engineering, WTHD No. 97.
- Chauve, M.P. (1977)
Détermination directe du frottement sur une paroi poreuse a l'aide d'un anémomètre. Institut de Mécanique Statistique de la Turbulence, Marseille. C.N.R.S. No. 130.

- Corino, E.R. and Brodkey, R.S. (1969)
A visual investigation of the wall in turbulent flow. *J. Fluid Mech.* 37, 1.
- Corrsin, S. (1957)
Some current problems in turbulent shear flows. National Academy of Sciences - National Research Council. Naval hydrodynamics, Publication 515, 373.
- Elena, M. (1977)
Etude Experimentale de la Turbulence au voisinage de la paroi d'un tube legerement chauffe. *Int. J. Heat Mass Transfer* 20, 935.
- Grass, A.J. (1971)
Structural features of turbulent flow over smooth and rough boundaries. *J. Fluid Mech.* 50, 233.
- Frenkiel, F.N. and Klebanoff, P.S. (1975)
On the lognormality of the small-scale structure of turbulence. *Boundary-Layer Meteo.* 8, 173.
- Gitton, D.E. (1974)
The effect of high intensity turbulence on the response of a hot-wire. *C.A.S.I. Transactions*, 7, 69.
- Hanjalić, K. and Launder, B.E. (1972 a)
Fully developed asymmetric flow in a plane channel. *J. Fluid Mech.* 51, 301.
- Hanjalić, K. and Launder, B.E. (1972 b)
A Reynolds stress model of turbulence and its application to thin shear flow. *J. Fluid Mech.* 52, 609.
- Hinze, J.O. (1959)
Turbulence, An introduction to its mechanism and theory. McGraw-Hill.
- Huffman, G.D. (1969)
A theoretical analysis of turbulent shear flows. Ph.D. thesis, Ohio State University.
- Hummel, R.H. (1978)
Turbulence structure in a conical diffuser. Ph.D. thesis, The University of Manitoba, Winnipeg, Canada.
- Irwin, H.P.A.H. (1973)
Measurements in a self-preserving plane wall jet in a positive pressure gradient. *J. Fluid Mech.* 61, 33.

- Kim, H.T., Kline, S.J., and Reynolds, W.C. (1971)
The production of turbulence near a smooth wall in a turbulent boundary layer. *J. Fluid Mech.*, 50, 133.
- Klebanoff, P.S. (1955)
Characteristics of turbulence in a boundary layer with zero pressure gradient. N.A.C.A., Rep. No. 1247.
- Kline, S.J. and McClintock, F.A. (1953)
Describing uncertainties in single-sample experiments. *Mech. Eng.* 75, 3.
- Kline, S.J., Reynolds, W.C., Schraub, F.A. and Runstadler, P.W. (1967)
The structure of turbulent boundary layers. *J. Fluid Mech.* 30, 741.
- Kuo, A.Y.S. and Corrsin, S. (1971)
Experiments on the internal intermittency and fine structure distribution functions in fully turbulent fluid. *J. Fluid Mech.* 50, 285.
- Laufer, J. (1951)
Investigation of turbulent flow in a two-dimensional channel. N.A.C.A., Rep. No. 1053.
- Laufer, J. (1954)
The structure of turbulence in fully developed pipe flow. N.A.C.A., Rep. No. 1174.
- Lawn, C.J. (1969)
Turbulence measurements with hot wires at B.N.L. Central Electricity Generating Board. Berkeley Nuclear Laboratories. Rep. RD/B/M 1277.
- Lawn, C.J. (1971)
The determination of the rate of dissipation in turbulent pipe flow. *J. Fluid Mech.* 48, 477.
- Lumley, J.L. (1970)
Toward a turbulent constitutive relation. *J. Fluid Mech.* 41, 413.
- Monin, A.S. and Yaglom, A.M. (1975)
Statistical fluid mechanics, Vol. II. M.I.T., Press, Cambridge.
- Nakagawa, H., Nezu, I. and Ueda, H. (1975)
Turbulence of open channel flow over smooth and rough beds. *Proc. of J.S.C.E.*, 241, 155.

- Nakagawa, H. and Nezu, I. (1977)
Prediction of the contributions to the Reynolds stress from bursting events in open-channel flows. *J. Fluid Mech.*, 80, 99.
- Okwuobi, P.A.C. (1972)
Turbulence in a conical diffuser with fully developed pipe flow at entry. Ph.D. thesis, University of Manitoba.
- Okwuobi, P.A.C. and Azad, R.S. (1972)
Turbulence investigation in a conical diffuser with partly developed flow at entry. The University of Manitoba, Department of Mechanical Engineering, Rep. ER 25.17.
- Okwuobi, P.A.C. and Azad, R.S. (1973)
Turbulence in a conical diffuser with fully developed flow at entry. *J. Fluid Mech.*, 57, 603.
- Okwuobi, P.A.C. and Azad, R.S. and Hawaleshka, O. (1972)
Turbulence structure parameters in an inhomogeneous strain field. *AIAA Journal*, 11, 1414.
- Panchev, S. (1971)
Random functions and turbulence. Pergamon Press, Oxford.
- Pankhurst, R.C. and Holder, D.W. (1952)
Wind tunnel technique. Pitman Press, London.
- Ramaprian, B.R. and Shiva-Prasad, B.G. (1976)
An experimental study of the effect of 'mild' longitudinal curvature on the turbulent boundary layer. Indian Institute of Sciences, Bangalore. Department of Aeronautical Eng., Rep. 76FM2.
- Reichert, J.K. (1977)
A study of developing turbulent pipe flow. Ph.D. thesis, The University of Manitoba, Winnipeg, Canada.
- Reichert, J.K. and Azad, R.S. (1976)
Non-asymptotic behavior of developing turbulent pipe flow. *Can. J. Phys.*, 54, 268.
- Ruetenik, J.R., Corrsin, S. (1955)
Equilibrium turbulent flow in a slightly divergent channel. 50 Jahre Grenzschichtforschung, Friedr. Vieweg & Sohn. Braunschweig, 446.
- Sabot, J. and Comte-Bellot, G. (1976)
Intermittency of coherent structures in the core region of fully developed turbulent pipe flow. *J. Fluid Mech.*, 74-767.

- Saffman, P.G. (1963)
On the fine-scale structure of vector fields convected by a turbulent fluid. *J. Fluid Mech.*, 16, 545.
- Schlichting, H. (1968)
Boundary-layer theory. 6th edn., McGraw-Hill.
- Schraub, F.A. and Kline, S.J. (1965)
A study of the structure of the turbulent boundary layer with and without longitudinal pressure gradient. Stanford University, Department of Mechanical Engineering, Rep. No. MD-12.
- Schubaur, G.B. (1954)
Turbulent processes as observed in boundary layer and pipe. *J. App. Phys.* 25, 188.
- Sovran, G. and Klomp, E.D. (1967)
Experimentally determined optimum geometries for rectilinear diffusers with rectangular, conical or annular cross-section. *Proc. of the Gen. Motors Symp. on Internal Flow.* Elsevier Pub. Co., 270.
- Tennekes, H. and Lumley, J.L. (1972)
A first course in turbulence. The MIT Press, Massachusetts.
- Townsend, A.A. (1956)
The structure of turbulent shear flow. Cambridge University Press.
- Townsend, A.A. (1949)
Momentum and energy diffusion in the turbulent wake of a cylinder. *Proc. Roy. Soc.* A197, 124.
- Thornton-Trump, A.B. (1971)
Error analysis of a hot-wire anemometer and processing circuit. The University of Manitoba, Dept. of Mech. Eng. Publication ER 25.14.
- Trupp, A.C. (1973)
The structure of turbulent flow in triangular array rod bundles. Ph.D. thesis, University of Manitoba.
- Tutu, N.K. and Chevray, R. (1975)
Cross-wire anemometry in high intensity turbulence. *J. Fluid Mech.*, 71, 785.
- Ueda, H. and Hinze, J.O. (1975)
Fine structure turbulence in the wall region of a turbulent boundary layer. *J. Fluid Mech.* 67, 125.

- Ueda, H. and Mizushima, T. (1977)
Turbulence structure in the inner part of the wall region in a fully developed turbulent tube flow. 5th Biennial Symposium on Turbulence, University of Missouri-Rolla.
- Wallace, J.M., Eckelmann, H., and Brodkey, R.S. (1972)
The wall region in turbulent shear flow. J. Fluid Mech., 54, 39.
- Willmarth, W.W. and Lu, S.S. (1972)
Structure of the Reynolds stress near the wall. J. Fluid Mech., 55, 65.
- Wynanski, I. and Fiedler, H. (1969)
Some measurements in the self-preserving jet. J. Fluid Mech., 38, 577.
- Wyngaard, J.C. (1968)
Measurement of small-scale turbulence structure with hot-wires. J. Sci. Instr. (J. Phys), 1, 1105.
- Wyngaard, J.C. (1969)
Spatial resolution of the vorticity meter and other hot-wire arrays. J. Sci. Instr. (J. Phys.), 2, 983.

This was further confirmed by the plot of computed data from other polynomials. Figure A-1 also shows the normalized wall static pressure data obtained from the static pressure holes drilled 6 cm apart in the diffuser wall. There were 4 holes at 90° at each axial station and the indicated readings are average of all 4.

The experimental data obtained in the entry and the exit regions indicated an approximate linear variation with axial distance (figure A-1). Therefore, in order to investigate this possibility and also to improve the accuracy of the curve fitting, pressure data were divided in 3 regions: first from exit to station 20; second from station 22 to 56 and; the third from station 58 to 72, where station 72 is at the diffuser inlet. Polynomials of order one to five were fitted to these regions. It was found that the 4th order polynomial provided the best fit to region one and two; while the 2nd order provided the best fit for region 3. Also the standard errors for regions one and two decreased while that for the region 3 increased as compared to the error of the 4th order polynomial fit to the entire data set (Table A-2). Data points computed from these separate analysis are also shown in figure A-1. This analysis showed that the experimental data did not have linear variation in any region of the diffuser. This, however, cannot be taken as conclusive because the measured data were not corrected for any turbulence and the wall effects. Therefore, it is possible that the true static pressure data may exhibit slightly different variation than indicated here. This aspect of the mean flow evolution is being further investigated and

might be reported later. However, for the present purposes, it was decided that the polynomial curve of the 4th order to the entire data set, sufficiently describes the pressure recovery characteristics of the conical diffuser used. Various coefficients of the 4th order polynomial are given in Table A-3. The pressure gradient curve reported in figure 5 (see 4.2) was obtained from this equation. The axial distance x_1 for the pressure gradient in figure (5) is non-dimensionalized by pipe diameter, whereas the equation given in Table A-3 uses pipe radius for this purpose. Thus a factor of 2 should be used in comparing the figure 5 to that of equation given in Table A-3. Also since axial distance ξ_4 used in equation (given in Table A-3) is measured from the exit of the diffuser, the gradient thus calculated would have negative sign, while the true sign in the direction of the flow would be positive.

APPENDIX B

THE DIFFUSER TURBULENCE DATA

The turbulence data collected for the conical diffuser using a DISA single wire and an x-wire probe are presented in the following Tables B-1 to B-12. The data obtained with an x-wire excluding that of $u_2 u_3$ correlations were collected along the whole diameter of the diffuser to check the symmetrical nature of the functions being measured. A smooth curve was drawn through the data and the reported data are from this curve, only for one side of the diffuser axis. The data presented thus, reflect manual smoothing in radial direction at each axial station. However, no such data smoothing was attempted in axial direction. The data for $u_2 u_3$ correlations and also of ϵ , S and G were not smoothed in radial or axial direction.

The diffuser turbulence data measured in the laboratory at station 67

ξ_2	$\frac{U_1}{U_b}$	$\frac{u_1'}{U_b} \times 10^2$	$\frac{u_2'}{U_b} \times 10^2$	$\frac{u_3'}{U_b} \times 10^2$	$\frac{\overline{u_1 u_2}}{\overline{u_1' u_2'}}$	$\frac{\overline{u_1^3}}{\overline{u_1'^3}}$	$\frac{\overline{u_2^3}}{\overline{u_2'^3}}$	$\frac{\overline{u_1 u_2^2}}{\overline{u_1' u_2'^2}}$	$\frac{\overline{u_1^2 u_2}}{\overline{u_1'^2 u_2'}}$	$\frac{\overline{u_1 u_3^2}}{\overline{u_1' u_3'^2}}$	$\frac{\overline{u_2 u_3^2}}{\overline{u_2' u_3'^2}}$
0.0	1.14	4.10	2.92	3.10	0.0	-.550	0.0	-.303	0.0	-.300	0.016
.02	1.14	4.12	2.92	3.10	.023	-.555	-.020	-.304	-.030	-.296	-.041
.06	1.13	4.20	2.95	3.13	.070	-.560	-.075	-.302	-.075	-.290	-.045
.16	1.12	4.43	3.03	3.28	.170	-.555	-.132	-.294	-.152	-.270	-.099
.26	1.11	4.82	3.15	3.50	.246	-.528	-.185	-.278	-.195	-.244	-.100
.35	1.09	5.28	3.30	3.70	.303	-.488	-.198	-.258	-.200	-.220	-.094
.45	1.06	5.85	3.43	3.97	.342	-.435	-.190	-.235	-.185	-.190	-.124
.55	1.02	6.50	3.62	4.27	.365	-.375	-.180	-.208	-.172	-.155	-.155
.65	.97	7.17	3.75	4.55	.380	-.305	-.160	-.177	-.155	-.115	-.138
.75	.92	7.80	3.95	4.80	.390	-.230	-.130	-.145	-.133	-.065	-.115
.85	.84	8.40	4.17	5.05	.390	-.145	-.130	-.110	-.105	-.015	-.102
.89	.80	8.58	4.40	5.15	.390	-.110	-.145	-.095	-.090	0.0	-.150
.93	.75	8.80	4.70	5.22	.380	-.075	-.230	-.080	-.075	+.030	-.083

TABLE B-1 - Continued

The diffuser turbulence data measured in the laboratory at station 67

ϵ_2	$\frac{\overline{u_1^4}}{\overline{u_1^{14}}}$	$\frac{\overline{u_2^4}}{\overline{u_2^{14}}}$	$\frac{\overline{u_3^4}}{\overline{u_3^{14}}}$	$\frac{\overline{u_1^2 u_2^2}}{\overline{u_1^{12} u_2^{12}}}$	$\frac{\overline{u_1^2 u_3^2}}{\overline{u_1^{12} u_3^{12}}}$	$\frac{\overline{u_2^2 u_3^2}}{\overline{u_2^{12} u_3^{12}}}$	$\frac{\overline{u_1^3 u_2}}{\overline{u_1^{13} u_2^1}}$	$\frac{\overline{u_1 u_2^3}}{\overline{u_1^1 u_2^{13}}}$	ϵ m ² /sec ³	S	G
0.0	3.34	3.38	3.38	1.315	1.38	1.314	0.0	0.0	12.80	.405	41.13
.02	3.34	3.37	3.37	1.317	1.36	1.317	.09	.09	13.08	.406	40.89
.06	3.33	3.36	3.36	1.317	1.34	1.314	.25	.25	13.50	.405	41.67
.16	3.26	3.34	3.31	1.315	1.28	1.314	.56	.56	15.12	.394	45.66
.26	3.14	3.30	3.26	1.310	1.22	1.283	.78	.78	17.94	.416	48.58
.35	3.03	3.27	3.22	1.302	1.18	1.256	.94	.94	21.72	.401	51.04
.45	2.96	3.23	3.19	1.293	1.14	1.263	1.04	1.04	27.39	.400	54.39
.55	2.90	3.21	3.16	1.285	1.11	1.279	1.09	1.09	34.16	.399	56.77
.65	2.82	3.20	3.14	1.272	1.08	1.317	1.12	1.12	45.76	.394	57.56
.75	2.73	3.19	3.14	1.258	1.06	1.325	1.13	1.13	63.11	.377	56.76
.85	2.66	3.19	3.16	1.240	1.05	1.250	1.14	1.14	105.09	.380	52.45
.89	2.66	3.19	3.18	1.235	1.04	1.202	1.14	1.14	144.20	.374	47.61
.93	2.67	3.20	3.16	1.227	1.04	1.129	1.14	1.14	255.58	.395	38.61
.96	2.72	3.25	3.10	1.215	1.04		1.08	1.08	587.72	.465	32.53

The diffuser turbulence data measured in the laboratory at station 65

ξ_2	$\frac{U_1}{U_b}$	$\frac{u'_1}{U_b} \times 10^2$	$\frac{u'_2}{U_b} \times 10^2$	$\frac{u'_3}{U_b} \times 10^2$	$\frac{\overline{u_1 u_2}}{\overline{u_1^2 u_2^2}}$	$\frac{\overline{u_1^3}}{\overline{u_1^2}}$	$\frac{\overline{u_2^3}}{\overline{u_2^2}}$	$\frac{\overline{u_1 u_2^2}}{\overline{u_1^2 u_2^2}}$	$\frac{\overline{u_1^2 u_2}}{\overline{u_1^2 u_2^2}}$	$\frac{\overline{u_1 u_3^2}}{\overline{u_1^2 u_3^2}}$	$\frac{\overline{u_2 u_3^2}}{\overline{u_2^2 u_3^2}}$
0.0	1.10	4.10	2.90	3.17	0.0	-.540	0.0	-.288	0.0	-.300	-.023
.02	1.10	4.12	2.92	3.17	.024	-.545	-.020	-.288	-.023	-.300	0.0
.06	1.10	4.15	2.95	3.20	.068	-.547	-.055	-.285	-.062	-.296	-.045
.16	1.08	4.43	3.03	3.35	.165	-.540	-.148	-.278	-.138	-.280	-.078
.26	1.07	4.82	3.15	3.53	.242	-.512	-.192	-.263	-.193	-.260	-.098
.35	1.05	5.28	3.30	3.73	.302	-.475	-.205	-.244	-.214	-.235	-.107
.45	1.02	5.85	3.43	3.95	.345	-.426	-.205	-.220	-.202	-.210	-.128
.55	.98	6.50	3.62	4.22	.370	-.370	-.190	-.195	-.178	-.180	-.141
.65	.93	7.20	3.75	4.50	.388	-.310	-.167	-.165	-.160	-.142	-.125
.75	.87	7.90	3.95	4.85	.403	-.245	-.150	-.140	-.145	-.100	-.108
.85	.80	8.63	4.17	5.17	.413	-.170	-.150	-.118	-.125	-.045	-.123
.91	.73	9.05	4.40	5.40	.417	-.120	-.170	-.105	-.110	0.0	-.128
.94	.70	9.35	4.70	5.55	.415	-.085	-.195	-.096	-.097	+.030	-.041

The diffuser turbulence data measured in the laboratory at station 65

ξ_2	$\frac{\overline{u_1^4}}{\overline{u_1^4}}$	$\frac{\overline{u_2^4}}{\overline{u_2^4}}$	$\frac{\overline{u_3^4}}{\overline{u_3^4}}$	$\frac{\overline{u_1^2 u_2^2}}{\overline{u_1^2 u_2^2}}$	$\frac{\overline{u_1^2 u_3^2}}{\overline{u_1^2 u_3^2}}$	$\frac{\overline{u_2^2 u_3^2}}{\overline{u_2^2 u_3^2}}$	$\frac{\overline{u_1^3 u_2}}{\overline{u_1^3 u_2}}$	$\frac{\overline{u_1 u_2^3}}{\overline{u_1 u_2^3}}$	ϵ m ² /sec ³	S	G
0.0	3.43	3.39	3.29	1.310	1.45	1.345	0.0	0.0	13.04	.444	42.78
.02	3.42	3.39	3.29	1.310	1.45	1.344	.10	.10	13.27	.451	43.78
.06	3.40	3.38	3.29	1.313	1.44	1.346	.26	.26	13.61	.453	44.20
.16	3.31	3.34	3.28	1.318	1.40	1.348	.58	.58	15.21	.459	47.29
.26	3.20	3.31	3.25	1.320	1.33	1.352	.79	.79	18.03	.436	49.97
.35	3.12	3.29	3.22	1.322	1.26	1.342	.92	.92	22.00	.429	55.09
.45	3.02	3.26	3.17	1.322	1.20	1.324	1.00	1.00	27.42	.431	59.44
.55	2.92	3.23	3.13	1.320	1.15	1.338	1.05	1.05	34.65	.407	61.30
.65	2.84	3.20	3.12	1.318	1.10	1.327	1.10	1.10	44.86	.413	63.23
.75	2.75	3.21	3.13	1.310	1.07	1.257	1.13	1.13	61.23	.405	62.08
.85	2.71	3.20	3.16	1.310	1.05	1.272	1.16	1.16	97.29	.409	59.07
.91	2.72	3.19	3.18	1.292	1.04	1.247	1.16	1.16	161.62	.371	52.02
.94	2.73	3.16	3.18	1.277	1.03	1.254	1.17	1.17	296.21	.401	45.52
.98	2.78	3.15	3.16		1.03		1.15	1.15	571.36	.465	36.36
									777.94	.600	35.37

The diffuser turbulence data measured in the laboratory at station 61

ξ_2	$\frac{U_1}{U_b}$	$\frac{u'_1}{U_b} \times 10^2$	$\frac{u'_2}{U_b} \times 10^2$	$\frac{u'_3}{U_b} \times 10^2$	$\frac{\overline{u'_1 u'_2}}{\overline{u'_1 u'_2}}$	$\frac{\overline{u_1^3}}{\overline{u_1^3}}$	$\frac{\overline{u_2^3}}{\overline{u_2^3}}$	$\frac{\overline{u_1 u_2^2}}{\overline{u_1 u_2^2}}$	$\frac{\overline{u_1^2 u_2}}{\overline{u_1^2 u_2}}$	$\frac{\overline{u_1 u_3^2}}{\overline{u_1 u_3^2}}$	$\frac{\overline{u_2 u_3^2}}{\overline{u_2 u_3^2}}$
0.0	1.05	4.43	2.95	3.35	0.0	-.565	0.0	-.285	0.0	-.280	-.016
.02	1.05	4.45	2.95	3.35	.022	-.565	-.020	-.285	-.027	-.280	-.010
.06	1.04	4.53	2.97	3.38	.063	-.565	-.050	-.283	-.065	-.275	-.015
.16	1.03	4.80	3.05	3.50	.152	-.555	-.136	-.275	-.142	-.260	-.078
.26	1.02	5.28	3.17	3.68	.222	-.530	-.190	-.263	-.192	-.245	-.087
.35	.99	5.88	3.32	3.90	.275	-.495	-.200	-.245	-.210	-.225	-.118
.45	.96	6.48	3.50	4.17	.315	-.450	-.200	-.225	-.203	-.200	-.106
.55	.92	7.13	3.70	4.47	.343	-.400	-.182	-.200	-.183	-.175	-.115
.65	.88	7.82	3.85	4.80	.363	-.358	-.177	-.183	-.167	-.145	-.116
.75	.82	8.60	4.17	5.17	.380	-.320	-.170	-.173	-.158	-.110	-.106
.85	.75	9.50	4.43	5.52	.395	-.290	-.175	-.168	-.152	-.065	-.124
.94	.65	10.72	4.85	5.95	.400	-.250	-.200	-.165	-.142	0.0	-.031
1.02	.55	11.50	5.25	6.20	.390	-.140	-.110	-.082	-.067	+.080	-.086
1.04	.51	11.35	5.22	6.18	.385	-.090	-.06	-.030	-.035	.125	

The diffuser turbulence data measured in the laboratory at station 61

ϵ_2	$\frac{\overline{u_1^4}}{\overline{u_1^4}}$	$\frac{\overline{u_2^4}}{\overline{u_2^4}}$	$\frac{\overline{u_3^4}}{\overline{u_3^4}}$	$\frac{\overline{u_1^2 u_2^2}}{\overline{u_1^2 u_2^2}}$	$\frac{\overline{u_1^2 u_3^2}}{\overline{u_1^2 u_3^2}}$	$\frac{\overline{u_2^2 u_3^2}}{\overline{u_2^2 u_3^2}}$	$\frac{\overline{u_1^3 u_2}}{\overline{u_1^3 u_2}}$	$\frac{\overline{u_1 u_2^3}}{\overline{u_1 u_2^3}}$	ϵ m ² /sec ³	S	G
0.0	3.32	3.38	3.30	1.285	1.42	1.361	0.0	0.0	14.08	.445	45.85
.02	3.32	3.38	3.30	1.287	1.42	1.367	.07	.07	14.22	.437	45.15
.06	3.32	3.37	3.30	1.290	1.42	1.382	.20	.20	14.49	.443	46.92
.16	3.28	3.35	3.29	1.297	1.38	1.395	.48	.48	15.81	.452	49.94
.26	3.23	3.32	3.26	1.305	1.34	1.393	.69	.69	18.40	.457	53.32
.35	3.15	3.29	3.23	1.310	1.28	1.350	.86	.86	21.30	.441	59.66
.45	3.05	3.26	3.21	1.315	1.21	1.318	.94	.94	26.31	.456	61.52
.55	2.96	3.23	3.20	1.315	1.16	1.333	.99	.99	32.53	.457	66.34
.65	2.89	3.23	3.19	1.318	1.11	1.339	1.04	1.04	40.96	.461	68.07
.75	2.83	3.25	3.19	1.327	1.08	1.342	1.10	1.10	55.33	.455	70.80
.85	2.80	3.28	3.19	1.333	1.06	1.312	1.16	1.16	84.28	.440	68.71
.94	2.80	3.28	3.19	1.325	1.04	1.199	1.21	1.21	183.77	.400	63.42
1.02	2.76	3.20	3.19	1.297	1.03	1.124	1.16	1.16	336.00	.400	56.89
1.04	2.74	3.17	3.19	1.230	1.03	1.073	1.10	1.10	460.76	.438	50.05
1.06	2.77	3.16	3.19	1.175	1.03		1.05	1.05	540.65	.654	51.00

TABLE D-4
The diffuser turbulence data measured in the laboratory at station 57

ϵ_2	$\frac{U}{U_b}$	$\frac{u'_1}{U_b} \times 10^2$	$\frac{u'_2}{U_b} \times 10^2$	$\frac{u'_3}{U_b} \times 10^2$	$\frac{\overline{u_1 u_2}}{\overline{u_1^2 u_2^2}}$	$\frac{\overline{u_1^3}}{\overline{u_1^2}}$	$\frac{\overline{u_2^3}}{\overline{u_2^2}}$	$\frac{\overline{u_1 u_2^2}}{\overline{u_1^2 u_2^2}}$	$\frac{\overline{u_1^2 u_2}}{\overline{u_1^2 u_2^2}}$	$\frac{\overline{u_1 u_3^2}}{\overline{u_1^2 u_3^2}}$	$\frac{\overline{u_2 u_3^2}}{\overline{u_2^2 u_3^2}}$
0.0	.99	4.38	2.95	3.43	0.0	-.530	0.0	-.270	0.0	-.260	0.0
.02	.99	4.40	2.95	3.43	.022	-.540	-.02	-.270	-.025	-.260	-.025
.06	.99	4.45	2.98	3.47	.060	-.550	-.08	-.270	-.065	-.260	-.025
.16	.98	4.70	3.07	3.63	.145	-.555	-.140	-.264	-.140	-.260	-.088
.26	.96	5.10	3.20	3.83	.213	-.540	-.180	-.257	-.185	-.245	-.119
.35	.93	5.62	3.35	4.07	.268	-.500	-.210	-.238	-.205	-.225	-.151
.45	.91	6.25	3.53	4.32	.310	-.440	-.215	-.218	-.200	-.210	-.166
.55	.87	6.97	3.72	4.63	.340	-.392	-.210	-.200	-.185	-.180	-.141
.65	.82	7.67	3.93	5.00	.363	-.365	-.200	-.188	-.172	-.150	-.129
.75	.77	8.28	4.15	5.50	.380	-.345	-.200	-.188	-.170	-.120	-.166
.85	.71	9.43	4.20	5.97	.395	-.340	-.210	-.192	-.183	-.090	-.148
.94	.63	10.85	4.88	6.42	.405	-.305	-.220	-.160	-.165	-.040	-.099
1.04	.50	11.72	5.35	6.65	.405	-.145	-.080	-.040	-.060	+.070	+.050
1.08	.44	11.40	5.30	6.57	.398	-.050	+.010	+.035	+.005	.115	-.077

TABLE D-4 - continued
 The diffuser turbulence data measured in the laboratory at station 57

ξ_2	$\frac{\overline{u_1^4}}{\overline{u_1^4}}$	$\frac{\overline{u_2^4}}{\overline{u_2^4}}$	$\frac{\overline{u_3^4}}{\overline{u_3^4}}$	$\frac{\overline{u_1^2 u_2^2}}{\overline{u_1^2 u_2^2}}$	$\frac{\overline{u_1^2 u_3^2}}{\overline{u_1^2 u_3^2}}$	$\frac{\overline{u_2^2 u_3^2}}{\overline{u_2^2 u_3^2}}$	$\frac{\overline{u_1^3 u_2}}{\overline{u_1^3 u_2}}$	$\frac{\overline{u_1 u_2^3}}{\overline{u_1 u_2^3}}$	ϵ m ² /sec ³	S	G
0.0	3.36	3.40	3.30	1.263	1.40	1.272	0.0	0.0	14.59	.478	47.96
.02	3.36	3.40	3.30	1.263	1.40	1.272	.10	.10	14.75	.486	48.43
.06	3.35	3.40	3.29	1.263	1.40	1.281	.26	.26	15.01	.480	50.02
.16	3.30	3.38	3.31	1.275	1.39	1.294	.57	.57	16.32	.483	52.26
.26	3.22	3.37	3.31	1.292	1.35	1.317	.78	.78	18.89	.493	56.80
.35	3.14	3.35	3.29	1.308	1.31	1.318	.91	.91	22.66	.494	63.07
.45	3.06	3.32	3.26	1.320	1.25	1.316	.99	.99	27.40	.483	66.86
.55	3.00	3.28	3.20	1.333	1.20	1.359	1.02	1.02	33.74	.482	72.84
.65	2.95	3.28	3.18	1.347	1.17	1.374	1.08	1.08	43.21	.478	74.01
.75	2.94	3.30	3.25	1.360	1.15	1.353	1.16	1.16	57.75	.448	78.43
.85	2.93	3.36	3.29	1.370	1.13	1.309	1.23	1.23	89.24	.419	78.72
.94	2.84	3.32	3.29	1.335	1.08	1.173	1.23	1.23	172.57	.393	79.18
1.04	2.71	3.14	3.21	1.235	1.03	1.182	1.13	1.13	334.71	.407	68.92
1.08	2.70	3.10	3.19	1.180	1.03	1.303	1.07	1.07	395.83	.439	67.99
1.12	2.74	3.12	3.22	1.140	1.04		1.01	1.01	445.86	.505	66.41

The diffuser turbulence data measured in the laboratory at station 50

ϵ_2	$\frac{U}{U_b}$	$\frac{u'_1}{U_b} \times 10^2$	$\frac{u'_2}{U_b} \times 10^2$	$\frac{u'_3}{U_b} \times 10^2$	$\frac{\overline{u_1 u_2}}{\overline{u'_1 u'_2}}$	$\frac{\overline{u_1^3}}{\overline{u_1'^3}}$	$\frac{\overline{u_2^3}}{\overline{u_2'^3}}$	$\frac{\overline{u_1 u_2^2}}{\overline{u_1' u_2'^2}}$	$\frac{\overline{u_1^2 u_2}}{\overline{u_1'^2 u_2'}}$	$\frac{\overline{u_1 u_3^2}}{\overline{u_1' u_3'^2}}$	$\frac{\overline{u_2 u_3^2}}{\overline{u_2' u_3'^2}}$
0.0	.94	4.55	3.10	3.37	0.0	-.520	0.0	-.263	0.0	-.250	.013
.02	.94	4.57	3.10	3.38	.020	-.525	-.018	-.263	-.030	-.250	-.015
.06	.94	4.62	3.10	3.40	.058	-.532	-.050	-.260	-.072	-.250	-.047
.16	.93	4.97	3.17	3.53	.140	-.540	-.128	-.255	-.140	-.250	-.084
.26	.91	5.40	3.30	3.77	.205	-.530	-.188	-.245	-.178	-.245	-.123
.35	.88	5.95	3.45	4.13	.255	-.520	-.215	-.235	-.195	-.235	-.155
.45	.85	6.57	3.67	4.40	.295	-.505	-.225	-.227	-.198	-.225	-.167
.55	.81	7.25	3.90	4.77	.322	-.486	-.225	-.218	-.190	-.210	-.208
.65	.77	8.12	4.17	5.15	.343	-.462	-.230	-.215	-.185	-.190	-.209
.75	.72	9.10	4.47	5.58	.365	-.430	-.240	-.220	-.197	-.160	-.205
.85	.66	10.10	4.87	6.05	.380	-.380	-.255	-.213	-.180	-.115	-.219
.94	.59	11.60	5.35	6.52	.388	-.275	-.190	-.168	-.130	-.035	-.119
1.04	.49	12.22	5.65	6.65	.390	-.115	-.040	-.055	-.040	+.095	.016
1.14	.37	12.00	5.55	6.40	.390	+.085	+.130	+.140	+.092	.210	.102
1.20	.29	10.80	4.75	5.80	.360	.230	.190	.248	.133	.390	-.118

The diffuser turbulence data measured in the laboratory at station 50

ϵ_2	$\frac{\overline{u_1^4}}{\overline{u_1^4}}$	$\frac{\overline{u_2^4}}{\overline{u_2^4}}$	$\frac{\overline{u_3^4}}{\overline{u_3^4}}$	$\frac{\overline{u_1^2 u_2^2}}{\overline{u_1^2 u_2^2}}$	$\frac{\overline{u_1^2 u_3^2}}{\overline{u_1^2 u_3^2}}$	$\frac{\overline{u_2^2 u_3^2}}{\overline{u_2^2 u_3^2}}$	$\frac{\overline{u_1^3 u_2}}{\overline{u_1^3 u_2}}$	$\frac{\overline{u_1 u_2^3}}{\overline{u_1 u_2^3}}$	ϵ m ² /sec ³	S	G
0.0	3.32	3.40	3.33	1.275	1.39	1.322	0.0	0.0	14.47	.463	53.92
.02	3.32	3.40	3.34	1.275	1.39	1.320	.07	.07	14.41	.463	55.20
.06	3.32	3.41	3.35	1.278	1.38	1.324	.21	.21	14.88	.464	53.95
.16	3.31	3.43	3.35	1.288	1.35	1.328	.49	.49	15.76	.455	56.46
.26	3.29	3.42	3.34	1.300	1.31	1.368	.70	.70	18.04	.479	60.40
.35	3.23	3.39	3.30	1.315	1.26	1.427	.86	.86	21.62	.471	71.55
.45	3.16	3.36	3.28	1.335	1.24	1.518	.96	.96	26.37	.465	75.44
.55	3.08	3.37	3.26	1.358	1.22	1.588	1.03	1.03	33.20	.469	78.25
.65	3.07	3.43	3.32	1.387	1.21	1.527	1.09	1.09	42.29	.459	83.34
.75	3.10	3.46	3.37	1.402	1.20	1.387	1.11	1.11	60.26	.437	89.71
.85	3.00	3.42	3.36	1.358	1.14	1.267	1.10	1.10	89.40	.416	93.59
.94	2.80	3.26	3.28	1.255	1.02	1.165	1.04	1.04	153.20	.387	96.92
1.04	2.64	3.06	3.21	1.170	.98	1.129	.97	.97	246.16	.415	93.88
1.14	2.65	3.11	3.22	1.130	1.02	1.250	.91	.95	333.62	.503	90.90
1.20	2.72	3.30	3.34	1.150	1.09	1.478	.86	.95	341.30	.548	92.26
1.24			3.48		1.15		.80	.95	361.82	.610	94.21

The diffuser turbulence data measured in the laboratory at station 40

ϵ_2	$\frac{U}{U_b}$	$\frac{u'_1}{U_b} \times 10^2$	$\frac{u'_2}{U_b} \times 10^2$	$\frac{u'_3}{U_b} \times 10^2$	$\frac{\overline{u'_1 u'_2}}{\overline{u'_1 u'_2}}$	$\frac{\overline{u_1^3}}{\overline{u_1^3}}$	$\frac{\overline{u_2^3}}{\overline{u_2^3}}$	$\frac{\overline{u_1 u_2^2}}{\overline{u_1 u_2^2}}$	$\frac{\overline{u_1^2 u_2}}{\overline{u_1^2 u_2}}$	$\frac{\overline{u_1 u_3^2}}{\overline{u_1 u_3^2}}$	$\frac{\overline{u_2 u_3^2}}{\overline{u_2 u_3^2}}$
0.0	.89	4.95	3.50	3.60	0.0	-.510	0.0	-.249	0.0	-.255	-.010
.02	.89	4.95	3.50	3.60	.022	-.510	-.020	-.248	-.020	-.255	+.009
.06	.88	5.05	3.52	3.62	.058	-.510	-.055	-.245	-.058	-.255	-.044
.16	.87	5.32	3.60	3.75	.140	-.510	-.135	-.242	-.130	-.250	-.087
.26	.86	5.70	3.77	4.00	.205	-.510	-.200	-.240	-.185	-.250	-.122
.35	.83	6.35	4.00	4.37	.258	-.510	-.250	-.240	-.213	-.250	-.132
.45	.79	7.05	4.33	4.83	.300	-.500	-.275	-.242	-.207	-.245	-.170
.55	.76	7.80	4.70	5.33	.325	-.500	-.295	-.245	-.213	-.235	-.224
.65	.72	9.15	5.15	5.85	.348	-.496	-.310	-.248	-.223	-.215	-.214
.75	.66	10.08	5.60	6.40	.370	-.475	-.300	-.238	-.208	-.170	-.192
.85	.61	11.08	6.10	6.93	.385	-.390	-.220	-.175	-.155	-.095	-.133
.94	.54	11.80	6.45	7.22	.390	-.210	-.110	-.085	-.082	-.005	-.091
1.04	.46	11.88	6.52	7.22	.393	0.00	+.020	+.027	0.0	+.100	+.033
1.14	.38	11.55	6.30	6.90	.378	.173	.165	.162	+.108	.230	.137
1.24	.30	10.50	5.50	6.20	.363	.340	.315	.322	.162	.370	.214
1.34	.22	9.40	4.0	5.28	.322	.495	.385	.525	.185	.520	.048

The diffuser turbulence data measured in the laboratory at station 40

ϵ_2	$\frac{\overline{u_1^4}}{\overline{u_1^4}}$	$\frac{\overline{u_2^4}}{\overline{u_2^4}}$	$\frac{\overline{u_3^4}}{\overline{u_3^4}}$	$\frac{\overline{u_1^2 u_2^2}}{\overline{u_1^2 u_2^2}}$	$\frac{\overline{u_1^2 u_3^2}}{\overline{u_1^2 u_3^2}}$	$\frac{\overline{u_2^2 u_3^2}}{\overline{u_2^2 u_3^2}}$	$\frac{\overline{u_1^3 u_2}}{\overline{u_1^3 u_2}}$	$\frac{\overline{u_1 u_2^3}}{\overline{u_1 u_2^3}}$	ϵ m ² /sec ³	S	G
0.0	3.34	3.42	3.36	1.258	1.36	1.331	0.0	0.0	15.15	.497	60.52
.02	3.33	3.42	3.36	1.258	1.36	1.331	.05	.05	14.74	.498	60.47
.06	3.32	3.42	3.35	1.258	1.37	1.346	.17	.17	14.85	.492	61.19
.16	3.30	3.43	3.33	1.268	1.36	1.382	.43	.43	16.02	.497	62.97
.26	3.28	3.45	3.33	1.300	1.33	1.440	.66	.66	18.18	.492	66.36
.35	3.28	3.49	3.37	1.333	1.31	1.496	.84	.84	21.41	.474	74.43
.45	3.29	3.54	3.42	1.373	1.29	1.556	1.00	1.00	26.95	.490	79.75
.55	3.32	3.61	3.46	1.415	1.28	1.594	1.12	1.12	35.64	.471	86.07
.65	3.29	3.67	3.46	1.445	1.24	1.519	1.16	1.16	46.89	.439	89.39
.75	3.14	3.60	3.38	1.400	1.16	1.370	1.13	1.13	68.16	.444	98.79
.85	2.87	3.42	3.32	1.273	1.06	1.202	1.00	1.00	99.36	.413	98.77
.94	2.66	3.21	3.25	1.170	.99	1.116	.94	.94	146.74	.427	101.37
1.04	2.56	3.02	3.21	1.100	.98	1.076	.93	.95	194.63	.449	109.76
1.14	2.57	3.04	3.24	1.120	1.04	1.108	.94	.99	241.59	.473	114.09
1.24	2.74	3.25	3.38	1.240	1.16	1.279	.95	1.07	256.81	.542	128.31
1.34	2.95	3.86	3.56	1.345	1.35	1.518	.88	1.13	236.91	.623	127.40
1.38	3.05	4.25	3.65	1.382	1.44		.82	1.09	219.66	.738	132.0
1.40			3.70		1.49				207.71	.840	129.79

The diffuser turbulence data measured in the laboratory at station 30

ϵ_2	$\frac{U}{U_b}$	$\frac{u_1'}{U_b} \times 10^2$	$\frac{u_2'}{U_b} \times 10^2$	$\frac{u_3'}{U_b} \times 10^2$	$\frac{\overline{u_1 u_2}}{\overline{u_1' u_2'}}$	$\frac{\overline{u_1^3}}{\overline{u_1'^3}}$	$\frac{\overline{u_2^3}}{\overline{u_2'^3}}$	$\frac{\overline{u_1 u_2^2}}{\overline{u_1' u_2'^2}}$	$\frac{\overline{u_1^2 u_2}}{\overline{u_1'^2 u_2'}}$	$\frac{\overline{u_1 u_3^2}}{\overline{u_1' u_3'^2}}$	$\frac{\overline{u_2 u_3^2}}{\overline{u_2' u_3'^2}}$
0.0	.85	5.20	3.52	3.52	0.0	-.550	0.0	-.270	0.0	-.245	0.0
.02	.85	5.22	3.52	3.53	-.018	-.555	-.025	-.270	-.017	-.245	+.015
.06	.85	5.30	3.55	3.55	.052	-.555	-.065	-.273	-.055	-.250	-.036
.16	.84	5.60	3.65	3.72	.128	-.563	-.155	-.283	-.132	-.255	-.091
.26	.82	6.05	3.85	4.05	.190	-.580	-.240	-.298	-.193	-.260	-.160
.35	.79	6.67	4.15	4.42	.245	-.603	-.315	-.320	-.240	-.265	-.214
.45	.76	7.55	4.47	4.87	.285	-.630	-.365	-.327	-.265	-.260	-.263
.55	.72	8.47	4.85	5.43	.320	-.620	-.375	-.318	-.258	-.240	-.244
.65	.67	9.85	5.35	6.00	.342	-.532	-.320	-.292	-.225	-.195	-.226
.75	.61	10.70	5.85	6.57	.358	-.365	-.250	-.285	-.165	-.130	-.172
.85	.55	11.55	6.13	6.90	.372	-.200	-.150	-.132	-.090	-.050	-.142
.94	.49	11.85	6.25	7.02	.382	-.045	-.040	-.010	-.020	+.050	-.003
1.04	.43	12.05	6.22	6.93	.385	+.090	+.075	+.102	+.055	.160	+.062
1.14	.37	11.75	6.00	6.50	.385	.230	.200	.215	.133	.285	.108
1.24	.31	10.72	5.60	5.83	.370	.365	.320	.330	.205	.415	.177
1.34	.25	9.60	4.82	5.20	.345	.490	.420	.450	.258	.560	.238
1.44	.21	8.00	3.77	4.55	.300	.606	.480	.550	.253	.720	.214
1.50	.15	6.60	2.97	4.15	.245	.672	.430	.598	.218	.830	-.110

The diffuser turbulence data measured in the laboratory at station 30

ϵ_2	$\frac{\overline{u_1^4}}{\overline{u_1^4}}$	$\frac{\overline{u_2^4}}{\overline{u_2^4}}$	$\frac{\overline{u_3^4}}{\overline{u_3^4}}$	$\frac{\overline{u_1^2 u_2^2}}{\overline{u_1^2 u_2^2}}$	$\frac{\overline{u_1^2 u_3^2}}{\overline{u_1^2 u_3^2}}$	$\frac{\overline{u_2^2 u_3^2}}{\overline{u_2^2 u_3^2}}$	$\frac{\overline{u_1^3 u_2}}{\overline{u_1^3 u_2}}$	$\frac{\overline{u_1 u_2^3}}{\overline{u_1 u_2^3}}$	ϵ m ² /sec ³	S	G
0.0	3.26	3.29	3.43	1.258	1.32	1.420	0.0	0.0	16.55	.410	63.53
.02	3.27	3.30	3.44	1.258	1.32	1.417	.07	.07	16.44	.412	62.96
.06	3.29	3.33	3.46	1.260	1.32	1.415	.20	.20	16.97	.416	62.88
.16	3.35	3.39	3.50	1.280	1.33	1.471	.49	.49	18.02	.432	64.47
.26	3.40	3.47	3.55	1.315	1.36	1.563	.73	.73	21.29	.420	74.91
.35	3.45	3.57	3.63	1.390	1.38	1.667	.95	.95	27.22	.422	77.91
.45	3.43	3.66	3.66	1.505	1.34	1.690	1.12	1.12	35.79	.395	84.48
.55	3.32	3.65	3.66	1.410	1.28	1.572	1.15	1.15	48.42	.427	91.35
.65	3.06	3.53	3.56	1.313	1.18	1.387	1.12	1.12	67.64	.420	94.92
.75	2.82	3.33	3.38	1.227	1.06	1.268	1.00	1.00	98.87	.388	103.95
.85	2.64	3.16	3.20	1.152	.96	1.126	.93	.93	132.17	.398	112.83
.94	2.52	3.02	3.11	1.095	.93	1.096	.90	.90	166.59	.406	116.24
1.04	2.53	2.95	3.08	1.090	.95	1.098	.91	.91	200.08	.427	122.49
1.14	2.61	3.02	3.18	1.160	1.03	1.190	.93	.99	227.92	.468	125.83
1.24	2.75	3.21	3.38	1.250	1.16	1.286	.98	1.09	287.00	.514	131.64
1.34	2.88	3.54	3.66	1.345	1.38	1.371	.98	1.20	236.59	.579	142.51
1.44	3.05	4.00	3.96	1.430	1.66	1.571	.86	1.13	225.90	.640	155.42
1.50	3.16	4.34	4.17	1.465	1.78	1.725	.70	1.05	218.00	.674	154.18
1.54					2.0				203.91	.889	168.89

TABLE B-8

The diffuser turbulence data measured in the laboratory at station 24

ϵ_2	$\frac{U_1}{U_b}$	$\frac{u_1'}{U_b} \times 10^2$	$\frac{u_2'}{U_b} \times 10^2$	$\frac{u_3'}{U_b} \times 10^2$	$\frac{\overline{u_1 u_2}}{\overline{u_1^2 u_2^2}}$	$\frac{\overline{u_1^3}}{\overline{u_1^3}}$	$\frac{\overline{u_2^3}}{\overline{u_2^3}}$	$\frac{\overline{u_1 u_2^2}}{\overline{u_1^2 u_2^2}}$	$\frac{\overline{u_1^2 u_2}}{\overline{u_1^2 u_2}}$	$\frac{\overline{u_1 u_3^2}}{\overline{u_1^2 u_3^2}}$	$\frac{\overline{u_2 u_3^2}}{\overline{u_2^2 u_3^2}}$
0.0	.83	5.90	4.27	3.98	0.0	-.715	0.0	-.325	0.0	-.305	-.020
.02	.83	5.92	4.27	4.00	.020	-.715	-.018	-.327	-.032	-.310	+.005
.06	.83	6.00	4.30	4.02	.063	-.720	-.092	-.335	-.082	-.320	-.021
.16	.81	6.43	4.45	4.15	.150	-.745	-.195	-.358	-.192	-.325	-.163
.26	.80	7.15	4.72	4.55	.220	-.795	-.300	-.383	-.275	-.320	-.245
.35	.77	8.22	5.12	5.18	.275	-.845	-.375	-.408	-.315	-.305	-.288
.45	.74	9.50	5.68	5.78	.315	-.828	-.415	-.415	-.312	-.320	-.270
.55	.69	10.60	6.20	6.33	.342	-.725	-.370	-.365	-.290	-.220	-.260
.65	.65	11.75	6.65	6.85	.360	-.570	-.300	-.295	-.232	-.160	-.215
.75	.59	12.77	7.10	7.33	.373	-.386	-.212	-.215	-.160	-.095	-.160
.85	.53	13.33	7.42	7.63	.385	-.220	-.115	-.113	-.088	-.015	-.087
.94	.49	13.35	7.50	7.65	.392	-.065	-.015	-.010	-.013	+.075	-.016
1.04	.43	13.10	7.40	7.50	.397	+.070	+.100	+.095	+.060	.170	+.040
1.14	.37	12.67	7.12	7.07	.397	.205	+.210	.195	.135	.270	.101
1.24	.32	11.98	6.60	6.50	.388	.325	.315	.297	.200	.380	.190
1.34	.26	11.02	5.90	5.82	.365	.435	.420	.393	.250	.505	.233
1.44	.21	9.75	4.97	5.07	.333	.525	.530	.464	.275	.645	.229
1.50	.18	8.95	4.25	4.57	.303	.573	.600	.500	.273	.735	.219
1.54	.16	8.40	3.70	4.22	.275	.605	.590	.522	.263	.805	.206
1.57	.15	7.85	3.10	3.85	.240	.630	.555	.548	.238	.890	.022

TABLE B-8 - Continued

The diffuser turbulence data measured in the laboratory at station 24

ϵ_2	$\frac{\overline{u_1^4}}{\overline{u_1^{14}}}$	$\frac{\overline{u_2^4}}{\overline{u_2^{14}}}$	$\frac{\overline{u_3^4}}{\overline{u_3^{14}}}$	$\frac{\overline{u_1^2 u_2^2}}{\overline{u_1^{12} u_2^{12}}}$	$\frac{\overline{u_1^2 u_3^2}}{\overline{u_1^{12} u_3^{12}}}$	$\frac{\overline{u_2^2 u_3^2}}{\overline{u_2^{12} u_3^{12}}}$	$\frac{\overline{u_1^3 u_2}}{\overline{u_1^{13} u_2^1}}$	$\frac{\overline{u_1 u_2^3}}{\overline{u_1^1 u_2^{13}}}$	ϵ m ² /sec ³	S	G
0.0	3.38	3.42	3.64	1.245	1.57	1.818	0.0	0.0	18.65	.428	68.67
.02	3.39	3.43	3.64	1.250	1.57	1.816	.10	.10	18.44	.437	70.13
.06	3.42	3.47	3.65	1.290	1.57	1.800	.27	.27	18.52	.423	70.48
.16	3.50	3.58	3.70	1.385	1.56	1.759	.66	.66	19.94	.441	71.44
.26	3.61	3.68	3.77	1.465	1.54	1.693	1.00	1.00	24.43	.433	75.12
.35	3.67	3.77	3.80	1.568	1.50	1.598	1.22	1.22	29.98	.438	81.66
.45	3.55	3.76	3.76	1.500	1.43	1.480	1.30	1.30	41.15	.389	87.34
.55	3.30	3.63	3.66	1.380	1.29	1.385	1.25	1.25	56.74	.393	94.19
.65	3.00	3.35	3.40	1.240	1.15	1.308	1.11	1.11	74.40	.382	99.45
.75	2.74	3.15	3.22	1.145	1.04	1.218	1.01	1.01	100.57	.387	109.91
.85	2.58	2.98	3.13	1.095	.94	1.127	.96	.96	128.85	.416	113.46
.94	2.50	2.90	3.06	1.065	.92	1.146	.94	.94	155.53	.423	125.85
1.04	2.51	2.91	3.05	1.070	.95	1.173	.93	.96	185.85	.448	127.67
1.14	2.56	2.97	3.13	1.108	1.02	1.184	.97	1.04	204.94	.509	135.02
1.24	2.67	3.11	3.28	1.198	1.16	1.236	1.04	1.15	217.90	.525	136.28
1.34	2.80	3.39	3.51	1.292	1.36	1.357	1.09	1.28	209.12	.580	155.70
1.44	2.97	3.80	3.80	1.385	1.60	1.507	1.08	1.41	200.95	.617	161.84
1.50	3.08	4.14	4.02	1.420	1.79	1.524	1.04	1.48	184.97	.773	163.36
1.54	3.16	4.42	4.22	1.420	1.92	1.639	.99	1.46	174.21	.786	169.75
1.57	3.26	4.75	4.36	1.415	2.06	1.646	.91	1.37	163.24	.854	188.24
1.61	3.33	5.11	4.55		2.20				152.22	.970	214.54

TABLE B-9

The diffuser turbulence data measured in the laboratory at station 18

ϵ_2	$\frac{U}{U_b}$	$\frac{u'_1}{U_b} \times 10^2$	$\frac{u'_2}{U_b} \times 10^2$	$\frac{u'_3}{U_b} \times 10^2$	$\frac{\overline{u'_1 u'_2}}{u'_1 u'_2}$	$\frac{\overline{u_1^3}}{u_1^3}$	$\frac{\overline{u_2^3}}{u_2^3}$	$\frac{\overline{u_1 u_2^2}}{u_1 u_2^2}$	$\frac{\overline{u_1^2 u_2}}{u_1^2 u_2}$	$\frac{\overline{u_1 u_3^2}}{u_1 u_3^2}$	$\frac{\overline{u_2 u_3^2}}{u_2 u_3^2}$
0.0	.81	6.27	4.60	5.10	0.0	-0.830	0.0	-.392	0.0	-.370	.012
.02	.81	6.28	4.62	5.13	.025	-0.836	-.030	-.397	-.025	-.375	.007
.06	.81	6.35	4.65	5.20	.068	-.850	-.090	-.405	-.080	-.378	-.074
.16	.79	6.83	4.85	5.47	.160	-.880	-.230	-.423	-.195	-.375	-.170
.26	.77	7.75	5.20	6.00	.230	-.890	-.330	-.441	-.285	-.360	-.269
.35	.75	8.87	5.63	6.55	.283	-.865	-.400	-.445	-.313	-.335	-.312
.45	.71	10.0	6.17	7.20	.320	-.770	-.400	-.413	-.295	-.285	-.301
.55	.67	11.15	6.67	7.85	.345	-.640	-.330	-.350	-.248	-.230	-.266
.65	.62	12.28	7.05	8.55	.358	-.460	-.250	-.253	-.185	-.160	-.227
.75	.57	12.75	7.32	9.00	.370	-.286	-.160	-.157	-.120	-.085	-.147
.85	.51	13.0	7.45	9.13	.380	-.130	-.060	-.060	-.055	+.010	-.085
.94	.47	13.03	7.47	9.13	.385	+.012	+.040	+.035	+.010	.100	-.033
1.04	.42	12.85	7.35	8.95	.388	.145	.145	.133	+.078	.200	+.055
1.14	.37	12.35	7.02	8.35	.388	.265	.235	.230	.142	.310	.102
1.24	.32	11.68	6.57	7.60	.380	.370	.340	.335	.200	.420	.151
1.34	.27	10.88	6.00	6.88	.365	.468	.440	.422	.255	.540	.174
1.44	.23	9.98	5.25	6.13	.345	.552	.540	.500	.290	.670	.224
1.54	.19	8.85	4.35	5.40	.315	.622	.625	.565	.292	.800	.274
1.59	.17	8.15	3.65	4.95	.290	.660	.680	.585	.275	.900	.251
1.65	.14	7.53	2.85	4.50	.253	.690	.715	.575	.232	.990	.115

The diffuser turbulence data measured in the laboratory at station 18

ξ_2	$\frac{\overline{u_1^4}}{\overline{u_1^4}}$	$\frac{\overline{u_2^4}}{\overline{u_2^4}}$	$\frac{\overline{u_3^4}}{\overline{u_3^4}}$	$\frac{\overline{u_1^2 u_2^2}}{\overline{u_1^2 u_2^2}}$	$\frac{\overline{u_1^2 u_3^2}}{\overline{u_1^2 u_3^2}}$	$\frac{\overline{u_2^2 u_3^2}}{\overline{u_2^2 u_3^2}}$	$\frac{\overline{u_1^3 u_2}}{\overline{u_1^3 u_2}}$	$\frac{\overline{u_1 u_2^3}}{\overline{u_1 u_2^3}}$	ϵ m ² /sec ³	S	G
0.0	3.90	3.86	4.00	1.470	1.76	1.757	0.0	0.0	22.48	.425	70.85
.02	3.92	3.86	4.00	1.480	1.76	1.757	.12	.12	22.28	.433	72.14
.06	3.98	3.87	4.01	1.503	1.75	1.754	.36	.36	22.35	.433	71.78
.16	4.04	3.86	3.99	1.553	1.70	1.706	.84	.84	24.49	.413	74.90
.26	4.01	3.85	3.92	1.595	1.62	1.635	1.18	1.18	30.15	.418	81.07
.35	3.87	3.82	3.82	1.592	1.50	1.533	1.27	1.27	38.60	.407	89.72
.45	3.51	3.70	3.68	1.515	1.36	1.429	1.26	1.26	51.24	.397	95.60
.55	3.16	3.45	3.49	1.355	1.21	1.353	1.19	1.19	66.62	.380	101.89
.65	2.86	3.25	3.33	1.240	1.08	1.264	1.08	1.08	87.79	.382	107.64
.75	2.65	3.07	3.20	1.145	.099	1.178	1.00	1.00	112.43	.382	109.40
.85	2.55	2.92	3.10	1.088	.092	1.123	0.94	.94	136.37	.394	120.09
.94	2.52	2.88	3.04	1.063	.091	1.149	.92	.92	156.24	.418	121.86
1.04	2.52	2.90	3.05	1.075	.095	1.165	.94	.96	182.20	.442	132.96
1.14	2.58	3.00	3.14	1.117	1.04	1.201	.96	1.03	187.44	.472	144.95
1.24	2.69	3.18	3.29	1.210	1.16	1.281	1.01	1.14	197.76	.521	152.60
1.34	2.82	3.43	3.49	1.320	1.31	1.402	1.07	1.27	202.86	.564	154.74
1.44	2.98	3.74	3.74	1.427	1.49	1.533	1.12	1.43	195.35	.634	164.44
1.54	3.15	4.20	4.05	1.535	1.71	1.683	1.11	1.51	175.24	.746	181.80
1.59	3.25	4.55	4.26	1.560	1.86	1.788	1.05	1.51	160.40	.791	199.21
1.65	3.38	4.96	4.51	1.560	2.01	1.946	.94	1.48	146.20	.920	228.02
1.69	3.47	5.22	4.68		2.12			1.42	137.31	1.050	269.98

The diffuser turbulence data measured in the laboratory at station 12

ξ_2	$\frac{U}{U_b}$	$\frac{u'_1}{U_b} \times 10^2$	$\frac{u'_2}{U_b} \times 10^2$	$\frac{u'_3}{U_b} \times 10^2$	$\frac{\overline{u_1 u_2}}{\overline{u_1^2 u_2^2}}$	$\frac{\overline{u_1^3}}{\overline{u_1^2}}$	$\frac{\overline{u_2^3}}{\overline{u_2^2}}$	$\frac{\overline{u_1 u_2^2}}{\overline{u_1^2 u_2^2}}$	$\frac{\overline{u_1^2 u_2}}{\overline{u_1^2 u_2^2}}$	$\frac{\overline{u_1 u_3^2}}{\overline{u_1^2 u_3^2}}$	$\frac{\overline{u_2 u_3^2}}{\overline{u_2^2 u_3^2}}$
0.0	.79	7.03	5.13	5.63	0.0	-1.000	0.0	-.453	0.0	-.420	.007
.02	.79	7.05	5.15	5.65	.025	-1.005	-.030	-.453	-.055	-.420	-.033
.06	.79	7.17	5.17	5.70	.068	-1.010	-.080	-.454	-.140	-.420	-.088
.16	.78	7.75	5.37	5.95	.170	-1.005	-.200	-.455	-.250	-.410	-.202
.26	.75	8.58	5.72	6.43	.242	-.960	-.300	-.455	-.300	-.390	-.258
.35	.72	9.65	6.15	7.15	.295	-.850	-.362	-.415	-.315	-.350	-.276
.45	.69	10.63	6.55	7.77	.333	-.685	-.357	-.355	-.300	-.290	-.258
.55	.65	11.53	6.87	8.30	.355	-.516	-.290	-.287	-.243	-.230	-.246
.65	.60	12.13	7.15	8.72	.370	-.360	-.212	-.200	-.177	-.160	-.172
.75	.55	12.47	7.35	9.00	.380	-.220	-.122	-.115	-.110	-.080	-.145
.85	.50	12.62	7.45	9.15	.385	-.085	-.020	-.030	-.093	0.0	-.065
.94	.46	12.60	7.45	9.17	.390	+.035	+.065	+.058	+.025	+.085	-.018
1.04	.41	12.38	7.30	9.08	.393	.156	.160	.142	.090	.170	+.020
1.14	.36	11.90	7.05	8.80	.393	.270	.250	.230	.153	.260	.085
1.24	.32	11.35	6.70	8.15	.390	.375	.340	.330	.208	.350	.119
1.34	.27	10.63	6.25	7.40	.383	.472	.427	.420	.250	.450	.143
1.44	.23	9.80	5.72	6.68	.368	.565	.510	.497	.286	.555	.187
1.54	.20	8.95	5.00	5.93	.345	.650	.595	.560	.303	.670	.229
1.63	.17	8.08	4.0	5.20	.310	.730	.680	.610	.293	.785	.232
1.69	.15	7.55	3.25	4.75	.282	.772	.696	.612	.267	.860	.225
1.73	.14	7.20	2.65	4.45	.260	.800	.650	.604	.228	.910	.149

The diffuser turbulence data measured in the laboratory at station 12

$\frac{u_2}{u_1}$	$\frac{\overline{u_1^4}}{\overline{u_1^4}}$	$\frac{\overline{u_2^4}}{\overline{u_2^4}}$	$\frac{\overline{u_3^4}}{\overline{u_3^4}}$	$\frac{\overline{u_1^2 u_2^2}}{\overline{u_1^2 u_2^2}}$	$\frac{\overline{u_1^2 u_3^2}}{\overline{u_1^2 u_3^2}}$	$\frac{\overline{u_2^2 u_3^2}}{\overline{u_2^2 u_3^2}}$	$\frac{\overline{u_1^3 u_2}}{\overline{u_1^3 u_2}}$	$\frac{\overline{u_1 u_2^3}}{\overline{u_1 u_2^3}}$	ϵ m ² /sec ³	S	G
0.0	4.48	4.08	4.10	1.635	1.89	1.733	0.0	0.0	29.57	.407	75.59
.02	4.47	4.07	4.09	1.637	1.88	1.716	.12	.12	29.22	.420	76.14
.06	4.46	4.07	4.07	1.640	1.85	1.693	.36	.36	29.08	.409	78.09
.16	4.38	4.05	3.98	1.650	1.74	1.620	.86	.86	31.15	.386	81.16
.26	4.13	3.98	3.86	1.645	1.62	1.555	1.12	1.12	38.15	.390	84.16
.35	3.69	3.82	3.70	1.530	1.48	1.546	1.18	1.18	48.30	.377	91.81
.45	3.31	3.56	3.51	1.380	1.32	1.404	1.16	1.16	61.49	.383	98.95
.55	3.02	3.33	3.33	1.265	1.17	1.310	1.04	1.04	80.93	.381	105.90
.65	2.81	3.15	3.20	1.170	1.05	1.211	.96	.96	99.74	.382	109.84
.75	2.66	3.00	3.10	1.113	.96	1.156	.92	.92	123.10	.405	119.16
.85	2.55	2.94	3.04	1.083	.92	1.150	.90	.90	144.57	.406	121.93
.94	2.50	2.91	3.01	1.070	.92	1.154	.93	.93	165.47	.424	128.75
1.04	2.50	2.95	3.02	1.085	.95	1.175	.98	.98	172.98	.442	140.72
1.14	2.59	3.06	3.09	1.120	1.02	1.215	1.03	1.05	189.72	.470	143.91
1.24	2.71	3.21	3.23	1.210	1.11	1.294	1.07	1.18	193.56	.528	154.66
1.34	2.86	3.42	3.42	1.308	1.22	1.401	1.10	1.30	180.26	.550	168.54
1.44	3.02	3.70	3.68	1.403	1.36	1.497	1.11	1.42	175.24	.586	171.36
1.54	3.20	4.08	3.96	1.500	1.54	1.601	1.09	1.53	163.24	.632	180.71
1.63	3.39	4.52	4.26	1.595	1.83	1.708	1.02	1.62	149.60	.675	199.12
1.69	3.51	4.88	4.48	1.642	2.04	1.769	.95	1.63	141.28	.690	225.68
1.73	3.60	5.12	4.65	1.658	2.20	1.884	.89	1.60	135.77	.839	238.18
1.77	3.69	5.38	4.82				.81	1.52	130.53	1.060	232.42

TABLE B-11

The diffuser turbulence data measured in the laboratory at station 6

ϵ_2	$\frac{U_1}{U_b}$	$\frac{u_1'}{U_b} \times 10^2$	$\frac{u_2'}{U_b} \times 10^2$	$\frac{u_3'}{U_b} \times 10^2$	$\frac{\overline{u_1 u_2}}{\overline{u_1^2 u_1^2}}$	$\frac{\overline{u_1^3}}{\overline{u_1^3}}$	$\frac{\overline{u_2^3}}{\overline{u_2^3}}$	$\frac{\overline{u_1 u_2^2}}{\overline{u_1^2 u_2^2}}$	$\frac{\overline{u_1^2 u_2}}{\overline{u_1^2 u_2^2}}$	$\frac{\overline{u_1 u_3^2}}{\overline{u_1^2 u_3^2}}$	$\frac{\overline{u_2 u_3^2}}{\overline{u_2^2 u_3^2}}$
0.0	.77	7.40	5.80	5.97	0.0	-1.292	0.0	-.445	0.0	-.442	.049
.02	.77	7.45	5.80	6.00	.020	-1.275	-.020	-.445	-.030	-.442	.012
.06	.77	7.65	5.82	6.05	.060	-1.193	-.095	-.445	-.087	-.440	-.049
.16	.76	8.75	6.0	6.27	.150	-1.035	-.190	-.435	-.193	-.410	-.166
.26	.73	9.60	6.32	6.72	.220	-.865	-.292	-.390	-.268	-.365	-.181
.35	.70	10.45	6.60	7.27	.278	-.705	-.335	-.340	-.280	-.305	-.205
.45	.67	11.20	6.85	7.77	.323	-.545	-.300	-.285	-.255	-.235	-.173
.55	.63	11.95	7.10	8.17	.354	-.387	-.230	-.212	-.193	-.160	-.162
.65	.58	12.65	7.27	8.45	.375	-.245	-.150	-.128	-.130	-.080	-.132
.75	.53	13.10	7.42	8.60	.383	-.125	-.060	-.045	-.068	0.0	-.117
.85	.48	13.30	7.50	8.65	.390	-.018	+.025	+.040	-.005	+.085	-.069
.94	.44	13.35	7.42	8.55	.390	+.077	0.110	.123	+.058	.170	-.011
1.04	.39	13.25	7.20	8.28	.390	.163	0.195	.208	.120	.250	-.008
1.14	.35	12.85	6.87	7.73	.386	.242	0.270	.290	.175	.335	+.025
1.24	.31	12.30	6.42	7.42	.380	.318	.345	.380	.220	.420	.063
1.34	.27	11.50	6.02	6.48	.370	.402	.425	.463	.260	.505	.039
1.44	.24	10.65	5.45	5.80	.357	.482	.505	.533	.288	.585	.046
1.54	.21	9.80	4.83	5.25	.333	.539	.580	.590	.303	.670	.060
1.63	.19	9.10	4.15	4.63	.302	.560	.660	.638	.298	.755	.083
1.73	.16	8.25	3.40	4.00	.263	.593	.660	.670	.255	.840	.004
1.79	.14	7.75	2.85	3.63	.228	.603	.595	.663	.208	.890	-.049
1.83	.13	7.45	2.45	3.38	.193	.597	.500	.648	.175	.920	-.010

The diffuser turbulence data measured in the laboratory at station 6

ξ_2	$\frac{\overline{u_1^4}}{\overline{u_1^2}}$	$\frac{\overline{u_2^4}}{\overline{u_2^2}}$	$\frac{\overline{u_3^4}}{\overline{u_3^2}}$	$\frac{\overline{u_1^2 u_2^2}}{\overline{u_1^2} \overline{u_2^2}}$	$\frac{\overline{u_1^2 u_3^2}}{\overline{u_1^2} \overline{u_3^2}}$	$\frac{\overline{u_2^2 u_3^2}}{\overline{u_2^2} \overline{u_3^2}}$	$\frac{\overline{u_1^3 u_2}}{\overline{u_1^3} \overline{u_2}}$	$\frac{\overline{u_1 u_2^3}}{\overline{u_1} \overline{u_2^3}}$	ϵ m ² /sec ³	S	G
0.0	4.62	4.15	3.99	1.718	1.85	1.685	0.0	0.0	39.68	.374	85.22
.02	4.60	4.15	3.99	1.718	1.81	1.665	.09	.09	40.23	.374	83.88
.06	4.54	4.14	3.97	1.715	1.75	1.638	.23	.23	39.99	.408	84.88
.16	4.28	4.09	3.89	1.700	1.60	1.573	.56	.56	41.80	.423	84.07
.26	3.93	3.93	3.76	1.610	1.45	1.523	.88	.88	47.83	.419	91.72
.35	3.51	3.72	3.60	1.500	1.31	1.412	1.03	1.03	57.88	.416	99.00
.45	3.14	3.45	3.42	1.360	1.18	1.326	1.04	1.04	72.49	.436	106.03
.55	2.90	3.23	3.28	1.240	1.08	1.236	.93	.97	88.70	.424	110.40
.65	2.76	3.10	3.15	1.165	1.01	1.206	.92	.92	107.04	.423	117.27
.75	2.64	3.01	3.05	1.115	.98	1.165	.89	.89	127.56	.428	119.72
.85	2.55	2.94	2.99	1.090	.96	1.153	.89	.89	149.15	.434	129.36
.94	2.54	2.93	2.99	1.004	.96	1.133	.91	.92	161.37	.466	136.10
1.04	2.59	3.00	3.03	1.158	.98	1.136	.93	.96	176.17	.490	140.84
1.14	2.67	3.12	3.12	1.213	1.04	1.148	.98	1.03	187.54	.490	145.52
1.24	2.77	3.30	3.25	1.285	1.16	1.213	1.04	1.12	185.90	.524	159.08
1.34	2.92	3.53	3.42	1.365	1.33	1.285	1.08	1.22	191.03	.533	167.06
1.44	3.08	3.79	3.64	1.455	1.52	1.365	1.11	1.35	181.42	.585	177.38
1.54	3.27	4.14	3.90	1.568	1.75	1.427	1.11	1.44	170.13	.600	183.82
1.63	3.46	4.55	4.20	1.675	2.02	1.488	1.07	1.48	154.88	.607	198.55
1.73	3.66	5.07	4.55	1.752	2.30	1.564	.97	1.46	139.68	.642	217.33
1.79	3.79	5.54	4.78	1.793	2.50	1.558	.87	1.38	124.16	.741	245.90
1.83	3.88	5.59	4.95	1.797	2.64	1.660	.76	1.27	118.14	.848	259.53
1.87	4.0	5.84	5.12	1.795	2.80		.60	1.06	111.87	1.075	284.24

The diffuser turbulence data measured in the laboratory at station 0

ξ_2	$\frac{U}{U_b}$	$\frac{u'_1}{U_b} \times 10^2$	$\frac{u'_2}{U_b} \times 10^2$	$\frac{u'_3}{U_b} \times 10^2$	$\frac{\overline{u'_1 u'_2}}{\overline{u'_1 u'_2}}$	$\frac{\overline{u_1^3}}{\overline{u_1^3}}$	$\frac{\overline{u_2^3}}{\overline{u_2^3}}$	$\frac{\overline{u_1 u_2^2}}{\overline{u_1 u_2^2}}$	$\frac{\overline{u_1^2 u_2}}{\overline{u_1^2 u_2}}$	$\frac{\overline{u_1 u_3^2}}{\overline{u_1 u_3^2}}$	$\frac{\overline{u_2 u_3^2}}{\overline{u_2 u_3^2}}$
0.0	0.76	9.40	6.63	6.58	0.0	-.990	0.0	-.470	0.0	-.410	.021
.02	.76	9.42	6.64	6.60	.022	-.990	-.0240	-.468	-.038	-.410	.005
.06	.76	9.50	6.65	6.63	.068	-.987	-.068	-.463	-.095	-.410	-.006
.16	.74	9.87	6.83	6.81	.168	-.920	-.168	-.440	-.190	-.385	-.058
.26	.72	10.55	7.00	7.10	.247	-.815	-.245	-.400	-.235	-.360	-.117
.35	.69	11.45	7.22	7.50	.308	-.668	-.282	-.345	-.235	-.285	-.197
.45	.66	12.12	7.45	7.93	.350	-.512	-.250	-.275	-.200	-.215	-.105
.55	.61	12.62	7.62	8.30	.373	-.370	-.180	-.190	-.147	-.140	-.090
.65	.56	12.93	7.75	8.72	.385	-.240	-.100	-.108	-.087	-.065	-.070
.75	.51	13.05	7.82	9.00	.395	-.115	-.030	-.025	-.033	+.010	-.044
.85	.46	12.92	7.80	9.15	.402	+.002	+.050	+.058	+.022	.085	-.019
.89	.45	12.88	7.77	9.18	.405	.045	.080	.090	.045	.115	-.008
.94	.43	12.72	7.65	9.17	.407	.110	.125	.140	.077	.160	+.009
1.04	.39	12.38	7.40	9.08	.408	.220	.200	.222	.133	.230	.037
1.14	.35	11.95	7.05	8.80	.404	.320	.278	.308	.183	.305	.064
1.24	.32	11.45	6.70	8.15	.398	.415	.350	.382	.230	.385	.084
1.34	.28	10.87	6.25	7.40	.388	.505	.435	.453	.272	.470	.094
1.44	.25	10.20	5.80	6.67	.378	.594	.510	.520	.312	.560	.097
1.54	.22	9.50	5.25	5.95	.370	.675	.582	.580	.350	.650	.097
1.63	.19	8.75	4.65	5.20	.349	.750	.660	.640	.383	.745	.084
1.73	.17	8.02	4.00	4.45	.328	.820	.740	.693	.390	.840	.053
1.83	.15	7.30	3.20	3.48	.298	.884	.810	.742	.375	.940	-.012
1.87	.13	7.00	2.85	3.22	.283	.910	.835	.743	.345	.985	-.034
1.91	.12	6.72	2.57	3.00	.267	.930	.830	.730	.312	1.030	-.066

The diffuser turbulence data measured in the laboratory at station 0

ϵ_2	$\frac{\overline{u_1^4}}{\overline{u_1^4}}$	$\frac{\overline{u_2^4}}{\overline{u_2^4}}$	$\frac{\overline{u_3^4}}{\overline{u_3^4}}$	$\frac{\overline{u_1^2 u_2^2}}{\overline{u_1^2 u_2^2}}$	$\frac{\overline{u_1^2 u_3^2}}{\overline{u_1^2 u_3^2}}$	$\frac{\overline{u_2^2 u_3^2}}{\overline{u_2^2 u_3^2}}$	$\frac{\overline{u_1^3 u_2}}{\overline{u_1^3 u_2}}$	$\frac{\overline{u_1 u_2^3}}{\overline{u_1 u_2^3}}$	ϵ m ² /sec ³	S	G
0.0	3.99	3.83	3.81	1.550	1.640	1.533	0.0	0.0	53.83	.372	95.08
.02	3.98	3.83	3.80	1.545	1.640	1.535	.08	.08	53.07	.374	95.35
.06	3.94	3.82	3.77	1.528	1.620	1.555	.17	.17	51.40	.388	92.36
.16	3.71	3.74	3.67	1.458	1.540	1.605	.68	.68	53.32	.375	92.99
.26	3.38	3.60	3.57	1.363	1.44	1.552	.89	.89	58.47	.379	97.73
.35	3.11	3.43	3.43	1.270	1.30	1.404	1.0	1.0	68.02	.379	104.82
.45	2.87	3.28	3.27	1.200	1.14	1.323	1.01	1.01	77.46	.380	111.58
.55	2.68	3.14	3.14	1.148	1.01	1.275	.98	.98	94.82	.384	115.53
.65	2.57	3.03	3.07	1.112	.95	1.211	.96	.96	113.34	.403	121.63
.75	2.52	2.95	3.02	1.093	.93	1.158	.95	.95	125.19	.413	128.50
.85	2.51	2.90	2.99	1.088	.95	1.124	.95	.95	140.62	.426	128.52
.89	2.51	2.90	2.98	1.090	.96	1.119	.95	.96	146.10	.435	134.35
.94	2.52	2.93	3.00	1.103	.99	1.098	.96	.99	151.30	.456	140.35
1.04	2.56	3.00	3.06	1.138	1.06	1.103	.98	1.06	164.76	.455	151.85
1.14	2.64	3.10	3.16	1.190	1.15	1.130	1.02	1.12	169.81	.480	153.66
1.24	2.76	3.23	3.18	1.260	1.27	1.207	1.07	1.21	172.60	.538	162.53
1.34	2.89	3.43	3.44	1.348	1.41	1.251	1.13	1.31	167.81	.543	180.13
1.44	3.02	3.69	3.63	1.452	1.57	1.338	1.20	1.43	167.74	.564	178.40
1.54	3.17	4.08	3.83	1.575	1.75	1.407	1.29	1.60	162.76	.646	198.15
1.63	3.34	4.48	4.06	1.732	1.93	1.368	1.33	1.78	147.88	.669	218.41
1.73	3.53	4.91	4.30	1.848	2.14	1.553	1.31	1.92	134.25	.789	247.57
1.83	3.77	5.40	4.58	1.937	2.36	1.619	1.22	2.02	121.43	.802	280.03
1.87	3.89	5.60	4.70	1.970	2.46	1.686	1.17	2.04	115.59	.864	314.01
1.91	3.98	5.66	4.88	1.993	2.56	1.750	1.08	2.07	110.07	1.111	312.08
1.95	4.23	5.96	5.06	2.015	2.66			2.10	104.87	1.250	356.25

APPENDIX C

ERROR CONSIDERATION

Considerable theoretical and experimental work has been directed towards the study of errors involved in flow measurements made with both pressure tube and hot-wire equipment. Discussion of these findings can be found for example, in Pankhurst & Holder (1952), Hinze (1959), Bradshaw (1971), Chauve (1977) and Guitton (1974). The errors involved with the turbulence laboratory measurements with hot-wire can generally be divided in the following categories:

- i) Measurement errors due to the effects of prong interference and of longitudinal cooling;
- ii) Error associated with the non-linearity of the response equation;
- iii) Error associated with large changes of flow direction with respect to the wire;
- iv) Errors due to the effect of high intensity turbulence;
- v) Errors involved in the response of the basic sensor to the flow turbulence;
- vi) Errors associated with the electronic measuring and processing instruments.

The phenomenon related to the first error is associated with blockage of the flow due to the presence of the stem and prongs and can arise when a wire is being used in an orientation other than the one for which it was originally calibrated. However, the modern probe design (DISA types used in present study) has largely eliminated this error. Further, the probe was calibrated in situ in the same orientation as

was used for data collection.

The longitudinal cooling effect is associated with additional heat convection effects when a wire is yawed to the mean flow. This is generally taken into consideration by multiplying the velocity component parallel to the hot-wire by a constant k in the hot-wire response equation. However, the data presented in the present study were not corrected for this effect.

The non-linearity of the response equation can be conveniently removed by linearizing the signal to

$$E \propto U_1$$

and this type of response was assumed throughout this work. This was achieved using a DISA linearizer.

Gitton (1974) states that the large changes of flow direction generally cause greater coolings than the cooling sought; viz., that due to U_1 alone.

The corrections required due to the high intensity turbulence in the conical diffuser were estimated for two axial stations 12 and 6 using Gitton's (1974) equations. These two stations were selected as it was thought that the corrections would be maximum here. The purpose of this exercise was to indicate the maximum possible error that could exist in the data presented due to assumptions made in simplifying the mathematical response equation. According to Gitton (1974), the corrected Reynold's stresses are expressed in terms of coefficients multiplying the measured quantities. Thus

$$\overline{u_{1c}^2} = H_1 \overline{u_{1m}^2}$$

$$\overline{u_{2c}^2} = H_2 \overline{u_{2m}^2}$$

$$\overline{u_1 u_{2c}} = H_3 \overline{u_1 u_{2m}}$$

$$\overline{u_{3c}^2} = H_4 \overline{u_{3m}^2}$$

here c is for corrected values, whereas m indicates measured values.

The coefficients H_1 , H_2 , H_3 and H_4 are defined as:

$$H_1 = 1 + \frac{U_2^2}{U_1^2} - \frac{U_2^2 \overline{u_2^2}}{u_1^2 U_1^2} - \frac{2U_2}{U_1} \frac{\overline{u_1 u_2}}{u_1^2} - \frac{\overline{u_1 u_2^2}}{u_1^2 U_1} + \frac{\overline{u_1^2 u_2^2}}{u_1^2 U_1^2} - \frac{1}{4} \left[\frac{u_2^4 - (u_2^2)^2}{U_1^2 u_1^2} \right] \quad (C-1)$$

$$H_2 = \frac{1}{1 - \frac{2k^2}{\sin^2 \phi}} - \frac{\overline{u_1 u_3^2}}{\cos^2 \phi u_2^2 U_1} (1 + \cot \phi \frac{U_2}{U_1}) - \frac{(H_1 - 1)}{\cot^2 \phi} \frac{\overline{u_1^2}}{u_2^2} + \frac{1}{\sin^2 \phi} \frac{\overline{u_2 u_3^2}}{u_2^2} \frac{U_2}{U_1^2} + \frac{1}{\cos^2 \phi} \frac{\overline{u_1^2 u_3^2}}{u_2^2 U_1^2} + \frac{\overline{u_2^2 u_3^2}}{\sin^2 \phi u_2^2 U_1^2} - \frac{1}{\sin^2 \phi} \left[\frac{u_3^4 - (u_3^2)^2}{u_2^2 U_1^2} \right] \quad (C-2)$$

$$H_3 = \frac{1}{1 - \frac{k^2}{\sin^2 \phi}} - \frac{1}{2 \sin^2 \phi} (1 + \cot \phi \frac{U_2}{U_1}) \frac{\overline{u_2 u_3^2}}{U_1 u_1 u_2} + \frac{1}{2 \sin^2 \phi} \frac{\overline{u_1 u_3^2}}{u_1 u_2} \frac{U_2}{U_1} + \frac{1}{\sin^2 \phi} \frac{\overline{u_1 u_2 u_3^2}}{u_1 u_2 U_1^2} \quad (C-3)$$

$$\begin{aligned}
H_4 = & \frac{1}{1 - \frac{2k^2}{\sin^2 \phi}} + \frac{1}{\sin^2 \phi} \frac{U_2^2}{U_1^2} - \frac{(H_1 - 1) \overline{u_1^2}}{\cot^2 \phi \overline{u_3^2}} + \frac{1}{\cos^2 \phi} \frac{U_2^2}{U_1^2} \frac{\overline{u_1^2}}{\overline{u_3^2}} \\
& - \frac{1}{\sin^2 \phi \cos^2 \phi} \frac{U_2^2}{U_1^2} \frac{\overline{u_2^2}}{\overline{u_3^2}} - \frac{1}{\sin^2 \phi \cos^2 \phi} \frac{U_2}{U_1^2} \frac{\overline{u_2^3}}{\overline{u_3^2}} - \frac{1}{\cos^2 \phi} \frac{\overline{u_1 u_2^2}}{U_1 \overline{u_3^2}} \\
& + \frac{2}{\cos^2 \phi} \frac{U_2}{U_1^2} \frac{\overline{u_1^2 u_2}}{\overline{u_3^2}} - \frac{2}{\sin^2 \phi} \frac{U_2}{U_1^2} \frac{\overline{u_2 u_3^2}}{\overline{u_3^2}} + \frac{1}{\cos^2 \phi} \frac{\overline{u_1^2 u_2^2}}{U_1^2 \overline{u_3^2}} \\
& + \frac{1}{\sin^2 \phi} \frac{\overline{u_2^2 u_3^2}}{U_1^2 \overline{u_3^2}} - \frac{1}{4 \sin^2 \phi \cos^2 \phi} \left[\frac{\overline{u_2^4} - (\overline{u_2^2})^2}{U_1^2 \overline{u_3^2}} \right]
\end{aligned}$$

(C-4)

(ϕ is angle of inclined wire).

In the above correction factors, the constant k was considered to be of the order of turbulence intensity. These correction factors include correlations up to 4th order and in the present work assumptions did not have to be made for the third and fourth order correlations because all the necessary terms except $\overline{u_1 u_2 u_3^2}$ were measured.

Gitton (1974) states that the correlation $\frac{\overline{u_1 u_2 u_3^2}}{\overline{u_1' u_2' u_3'^2}}$ varies between

1 and 3, and he assumed a value equal to the arithmetic mean of the limits of this 4th order tripple velocity correlation. However, the moments measured in the conical diffuser indicated that any correlation involving odd power of u_2 must pass through zero at the diffuser axis (Sec. 6). And since $\overline{u_1 u_2 u_3^2}$ involves the odd power of u_1 and u_2 and thus can be looked as the interaction of $u_1 u_2$ & u_3^2 , and thus should be zero at the axis. Earlier it was shown (Sec. 6.2.1) that

$$\overline{u_2 u_3^2} \approx \overline{u_2^3}.$$

From the above equation, it may be justified to assume that the instantaneous values of these functions would also be equal. Thus

$$u_2 u_3^2 \approx u_2^3.$$

Multiplying the above relation by u_1 and taking its time average yields,

$$\overline{u_1 u_2 u_3^2} \approx \overline{u_1 u_2^3}.$$

The above relationship was used in obtaining the correction factor for $\overline{u_1 u_2}$. The third and fourth order correlations themselves were not, however, corrected for high intensity.

The longitudinal cooling corrections (k) appear only in the first term of the correction factors up to the order of magnitude being considered. Thus these were no longer considered and the correction factors were concerned solely with the high intensity turbulence

effects ($k = 0$ in equations (C-1) to (C-3)). The magnitude of the correction factors thus computed is shown in figures C-1 and C-2 for station 18 and 6. The intensity corrections to u_1^2 are small everywhere and for $\overline{u_2^2}$ and $\overline{u_1 u_2}$ are quite significant in the wall layer of the diffuser. The correction factor H_4 for $\overline{u_3^2}$ is generally same throughout and increases slightly close to the wall.

The errors involved in the electronic measuring and processing instruments are taken into consideration by proper calibration and by keeping a close check on the instrument drifts. Some shift was noticed by Reichert (1977) in the linearization of the hot-wire signals after an extended use of the instruments and because of this the hot-wire was calibrated before and after each test. The D.C. shift in the TM-377 was closely monitored and taken into consideration in data analysis. A detailed discussion of errors due to the hot-wire anemometry is given by Trupp (1973).

The most important part of the turbulence data collecting system is the hot-wire itself. For this study a DISA single wire and the x-wire were used. The x-wire was used for measuring all the moments up to the 4th order while the single wire was used for obtaining the first and second derivative of the u_1 signal. Since the skewness of $\frac{\partial u_1}{\partial t}$ is a very sensitive measurement, it was used to test the high frequency response of the hot-wire. The skewness of $\frac{\partial u_1}{\partial t}$ obtained in the diffuser with a new single wire probe was comparable to the boundary layer (Ueda & Hinze, 1975) and pipe (Ueda & Mizushima, 1977 and Elena, 1977). The value of S at the diffuser axis was of the

while hot-wire anemometry may not give accurate absolute results, it is the ability of the equipment to give reproducible results and indicate proper trends which is most important. This is particularly true since often the measurements are non-dimensionalized by a quantity computed from themselves (e.g., skewness and flatness factors). Therefore, the errors in trends are more significant than absolute errors. Thornton-Trump (1971), who estimated x-probe anemometry (without linearizers) errors using the technique of Kline and McClintock (1953), showed that the trend errors for u_1' , u_2' , u_3' and $\overline{u_1 u_2}$ are only about $\pm 3\%$.

TABLE 1

Mean parameters of flow at the diffuser entry

Pipe Reynolds number, $\frac{U_b R}{\nu}$	58000
Pipe bulk average velocity, U_b (m/sec)	18.32
Pipe radius, R (m)	0.0508
Pipe friction velocity, u_* (m/sec)	0.94
Kinematic viscosity of the air, ν (m ² /sec)	1.59×10^{-5}

TABLE 2

Diffuser radius, pressure gradient and the friction velocity
at various axial stations

Axial station	Local radius cm	$\frac{dP_m}{dx_1/D}$	$\frac{u_*}{U_b}$
69	5.17	0.3818	
67	5.31	0.3432	
65	5.45	0.3077	
61	5.73	0.2453	
57	6.01	0.1938	
50	6.50	0.1261	0.029
40	7.20	0.0702	0.024
30	7.90	0.0470	0.019
24	8.32	0.0419	0.018
18	8.74	0.0390	0.017
12	9.16	0.0348	.015
6	9.58	0.0256	0.013
0	10.0	0.0081	0.017

TABLE 3
(cont'd)

Static pressure data in mm of water with respect to atmospheric pressure (Given pressure data have been multiplied by -1.0)

ξ_2	Axial Stations for Static Pressure Measurements					
	30	24	18	12	6	0 (exit)
1.95						0.10
1.93						0.10
1.87					0.40	
1.83					0.45	0.15
1.79				0.75		
1.73			1.10	0.75	0.50	0.20
1.65		1.6				
1.63			1.20	0.85	0.55	
1.54	2.15	1.65	1.25	0.85	0.55	0.30
1.44	2.20	1.70	1.30	0.90	0.65	
1.34	2.25	1.75	1.30	0.95	0.65	0.40
1.24	2.30	1.80	1.35	1.0	0.70	
1.14	2.30	1.80	1.40	1.0	0.70	0.45
1.04	2.35	1.85	1.40			
.94	2.35	1.85	1.40	1.05	0.75	0.5
.75	2.30	1.80	1.40	1.05	0.75	0.50
.55	2.20	1.75	1.35	1.0	0.70	0.45
.35	2.20	1.70	1.25	0.95	0.65	
.26						0.40
.16	2.20	1.65	1.20	0.90	0.60	
0.0	2.20	1.65	1.20	0.90	0.60	0.40
-.24	2.20	1.65	1.25	0.90	0.60	0.40
-.43	2.20	1.70	1.30	0.95	0.65	
-.53						0.45
-.63	2.25	1.75	1.35	1.0	0.70	
-.83	2.30	1.80	1.40	1.0	0.70	0.45
-1.02	2.30	1.80	1.35	1.0	0.70	0.45
-1.12	2.30		1.35	1.05		
-1.22	2.25	1.75	1.30	1.0	0.70	0.40
-1.32	2.20	1.70	1.25	1.0	0.65	
-1.42		1.60	1.20	0.95	0.60	0.35
-1.44	2.10					
-1.52		1.60	1.15	0.90	0.55	
-1.61				0.80	0.50	0.30
-1.63			1.1			
-1.71				0.75	0.45	0.20
-1.73				0.70		
-1.81					0.40	0.15
-1.91						.05

TABLE 4

Atmospheric conditions for static pressure data
in Table 3

Axial Stations	Air Temp °F	Atmospheric Pressure, mm of mercury	Room air condition	
			Dry Bulb Temp °F	Wet Bulb Temp °F
72	74	735.8	72	63
66	74	735.8	72	63
60	74	735.8	72	63
54	72	734.7	70	61
48	72	734.7	70	61
42	72	734.7	70	61
36	74	741.0	72	62
30	73.5	741.0	72	62
24	73.5	741.0	72	62
18	73.5	741.0	72	62
12	74	743.4	72	62
6	74	743.4	72	62
0	74	743.4	72	62

TABLE 5

Dissipation rate in the diffuser at station 12, $\xi_2 = 0.91$

Probe	Overheat Ratio	$\epsilon_{\text{spectra}}$ m ² /sec ³	$\epsilon_{\partial u_1/\partial t}$ m ² /sec ³	% difference from $\epsilon_{\text{spectra}}$	% difference in two wires at 0.5 overheat ratio with respect to regular probe	
					spectra	$\partial u_1/\partial t$
regular	0.8	145.6	109.2	25.0		
regular	0.5	141.3	107.9	23.7		
special	0.5	174.9	126.8	27.5	23.8	17.6
special	0.4	176.3	128.6	27.0		

TABLE 6

Variations in the ratios of excess production
and dissipation in the diffuser

Station	$\left(\frac{P-\epsilon}{\epsilon}\right) 100$
50	28%
30	8.7%
18	2.8%
12	-.2%
6	-12.0%
0	-3.0%

where P is production and ϵ
is dissipation.

TABLE 7

Various constants associated with figure 80

	u_1	$\partial u_1 / \partial t$	$(\partial u_1 / \partial t)^3$	$\partial^2 u_1 / \partial t^2$
a	gain = 1 1 v/div 5 m sec/div	gain = 5 5 v/div $\tau_1 = .2$ m sec 5 m sec/div	gain = 5 5 v/div $\tau_1 = .2$ m sec 5 m sec/div	gain = 3 5 v/div $\tau_1 = .2$ m sec $\tau_2 = .05$ m sec 5 m sec/div
b	gain = 1 1 v/div 20 m sec/div	gain = 9 2 v/div $\tau_1 = .2$ m sec 20 m sec/div	gain = 9 0.2 v/div $\tau_1 = .2$ m sec 20 m sec/div	gain = 7.5 2 v/div $\tau_1 = .2$ m sec $\tau_2 = .05$ m sec 20 m sec/div

TABLE A-1

The standard error of the static pressure data from
Polynomials of order 1 to 5 fitted to all
data at $Re = 58000$

Order of the Polynomial	Standard Error of Estimation, Se	Comment
1	.0822	Based on this analysis, 4th order polynomial was fitted to normalized pressure data set for its analytical analysis
2	.0324	
3	.0127	
4	.00869	
5	.00884	

TABLE A-2

The least standard error of estimation from polynomials fitted to pressure data in various axial regions of the diffuser. $Re = 58000$

	Axial regions to which Polynomials of varying order were fitted			
Stations	I 0-20	II 22-56	III 58-72	Entire data set 0-72
Order of polynomial with least error	4	4	2	4
Standard error of estimation	.000693	.00175	.0189	.00869

TABLE A-3

Coefficients of the 4th order Polynomial
fit to entire data set. Re = 58000

	a_0	a_1	a_2	a_3	a_4
Coefficients	0.38618E-02	-0.19769E-02	-0.47025E-02	0.67132E-03	-0.41069E-04

$$\frac{\Delta P}{\frac{1}{2} \rho U_b^2} = a_0 + a_1 \xi_4 + a_2 \xi_4^2 + a_3 \xi_4^3 + a_4 \xi_4^4$$

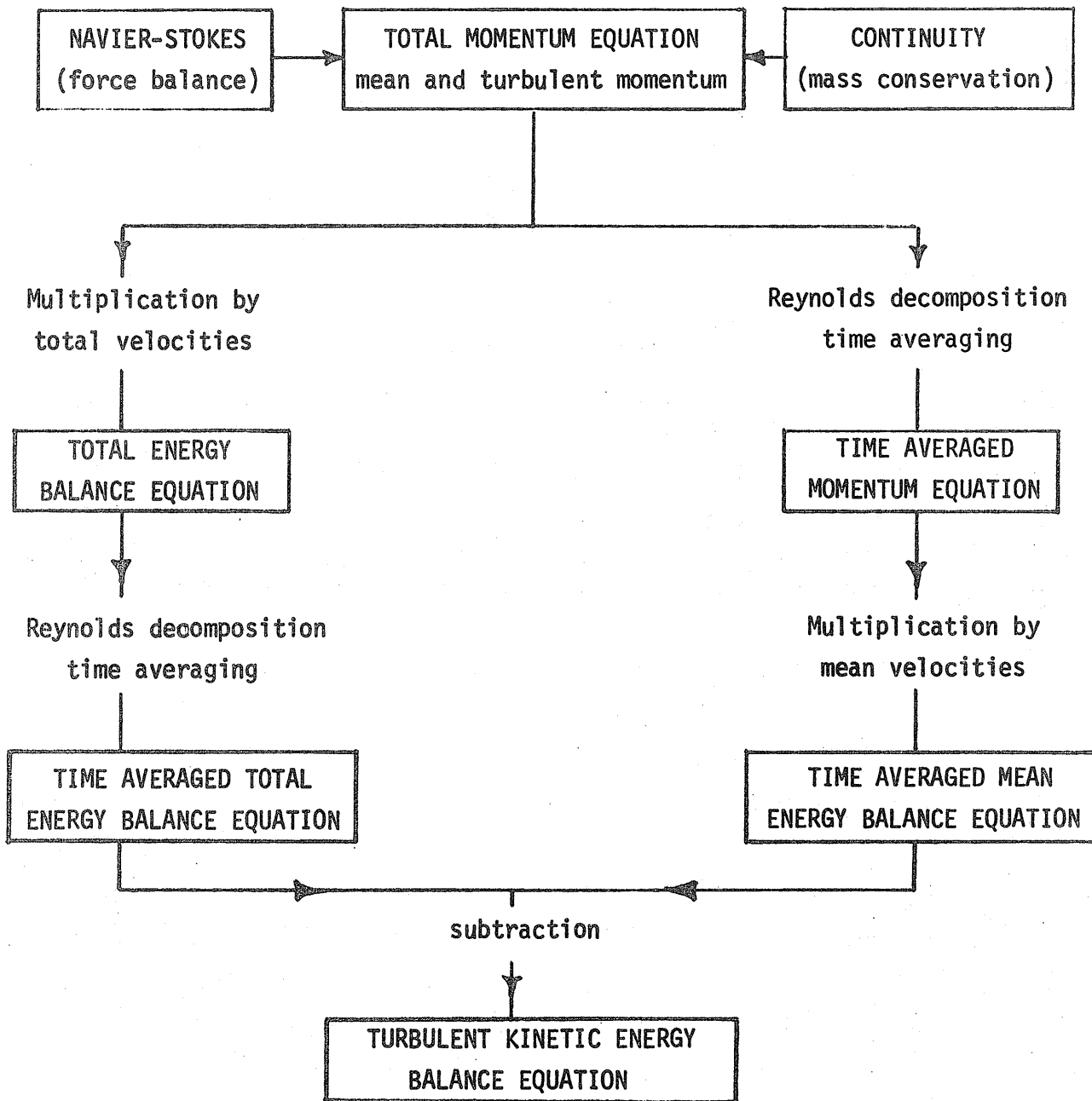


Figure 1 Genealogy of turbulent kinetic energy balance equation (eqn. 1).

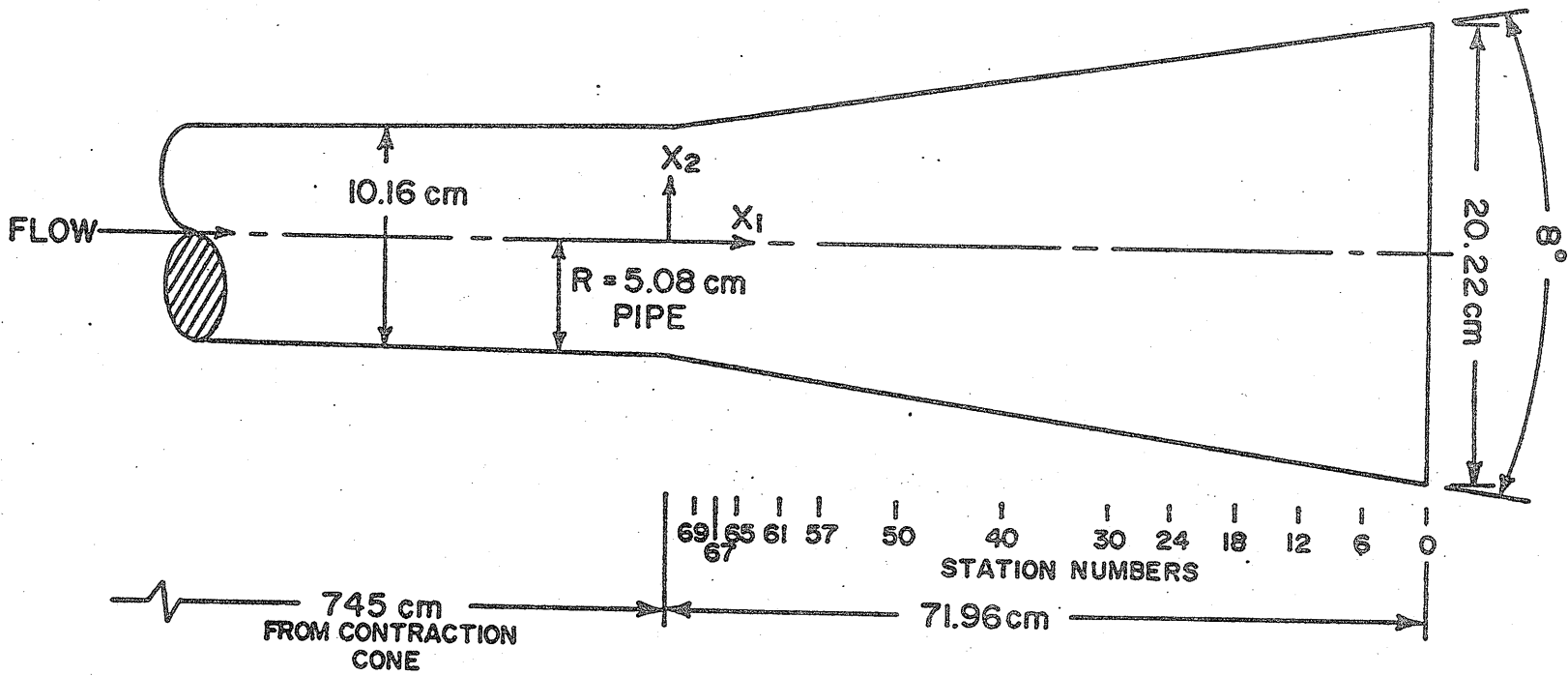


Figure 2 Diffuser geometry.

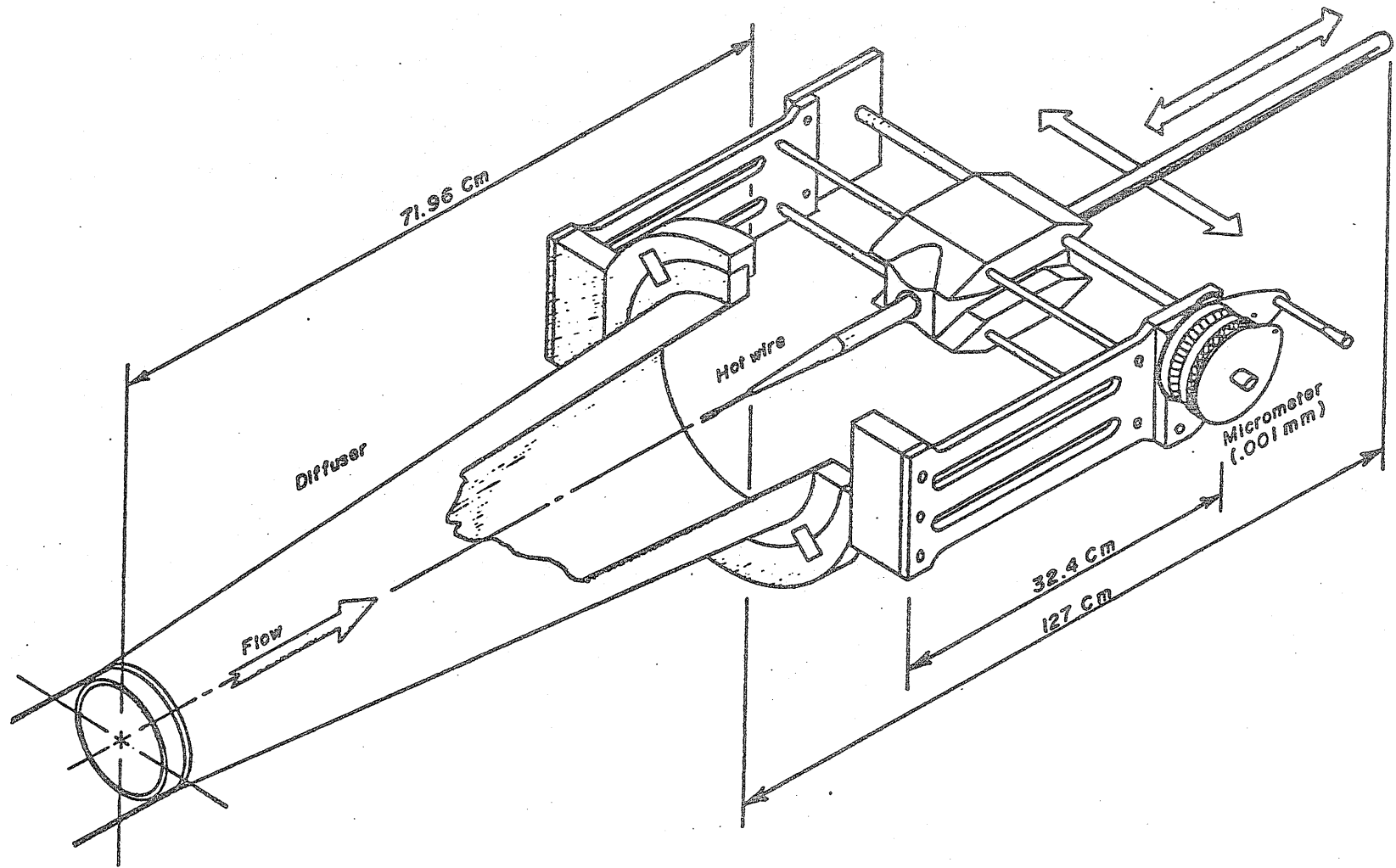


Figure 3 Diffuser traversing mechanism

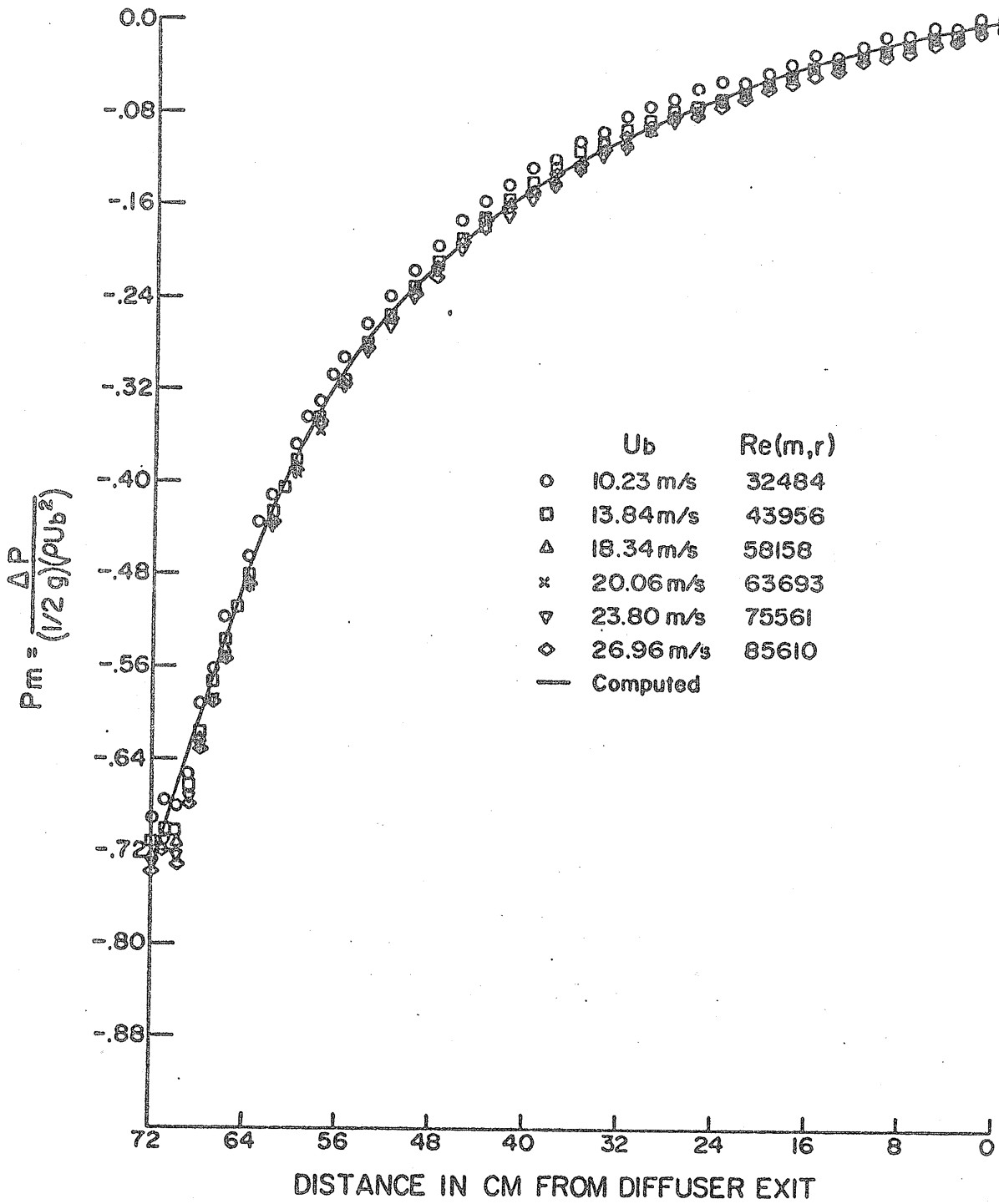


Figure 4 Mean static pressure distribution.

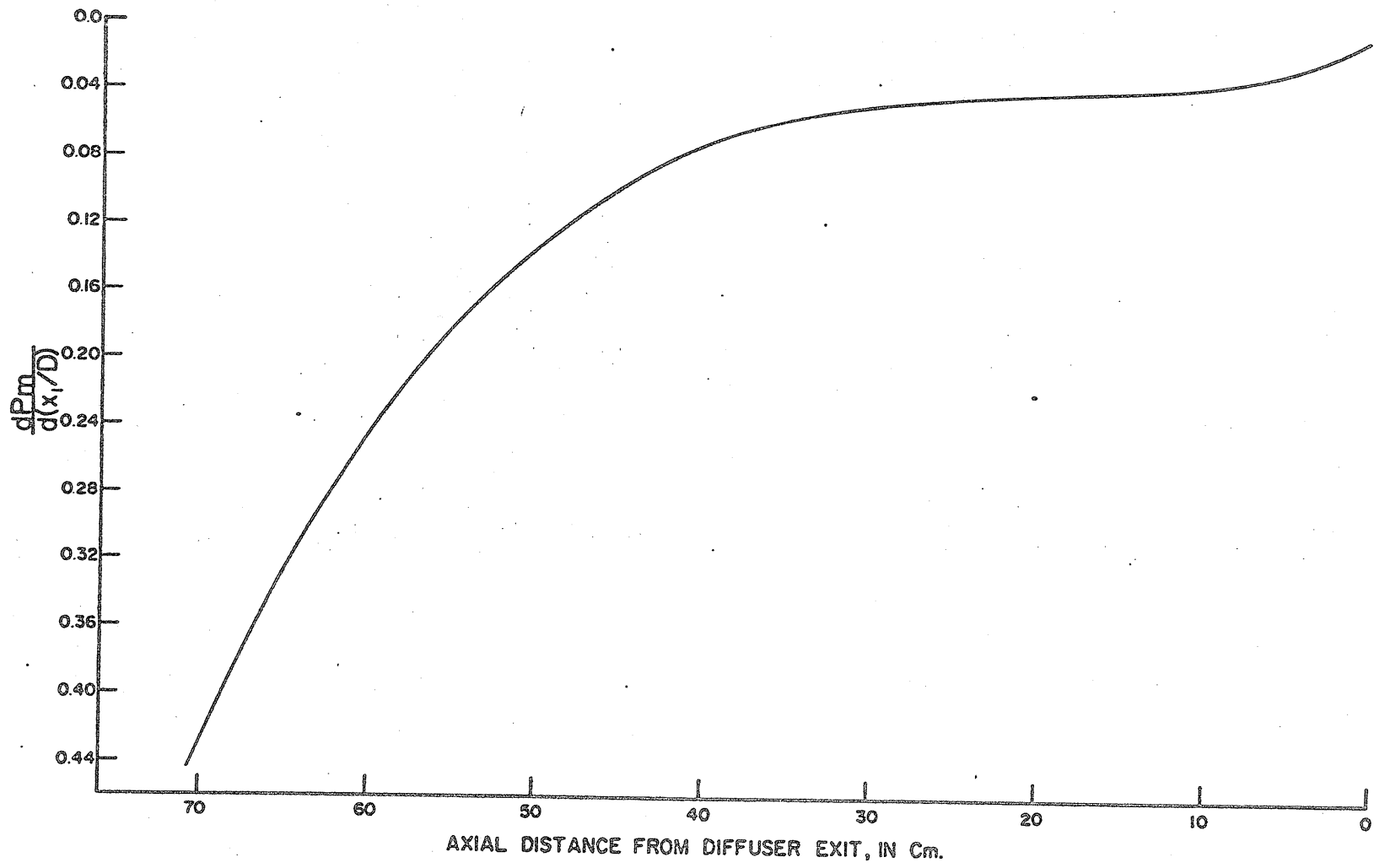


Figure 5 Mean static pressure gradient in the diffuser.

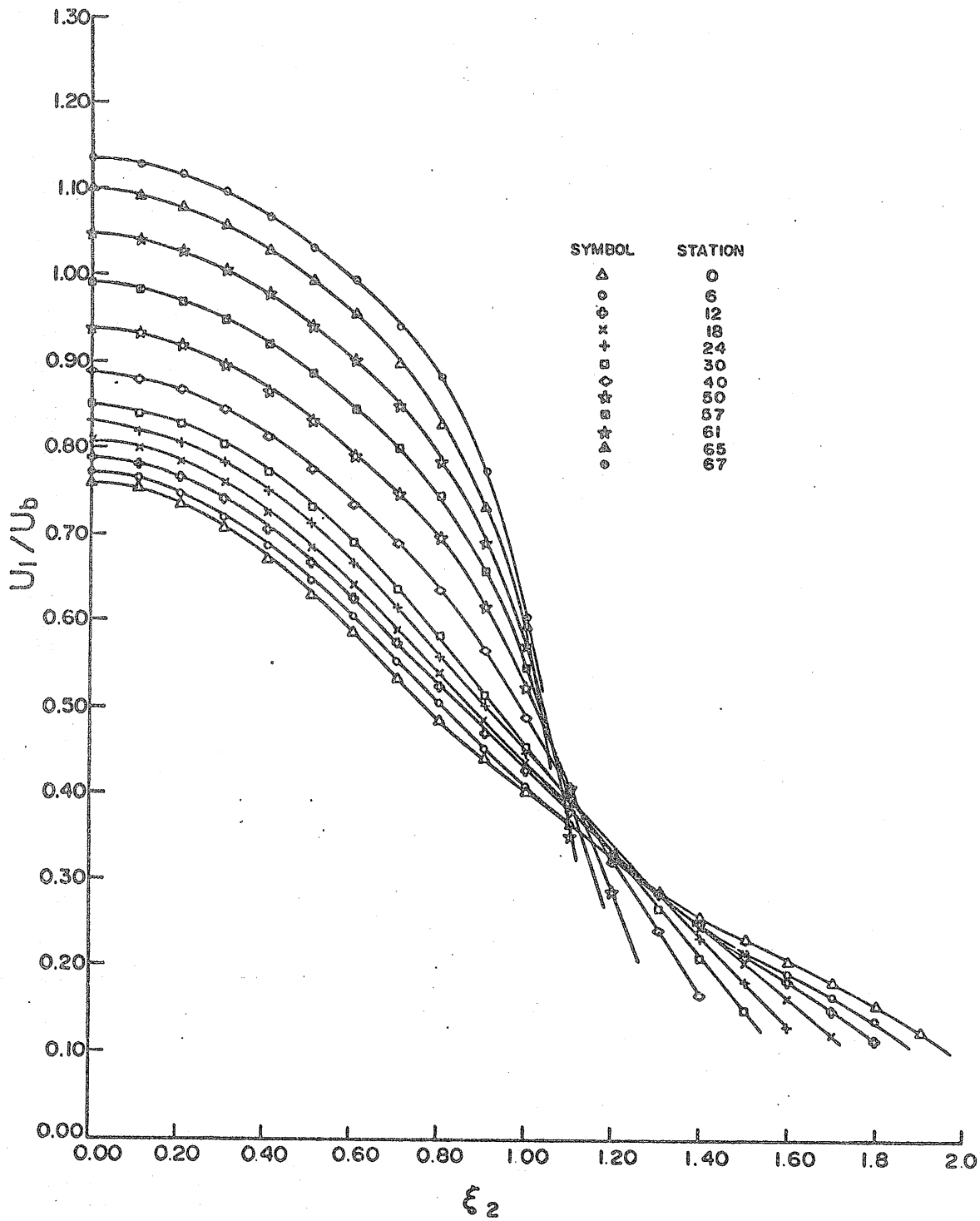


Figure 6 Mean axial velocity profiles.

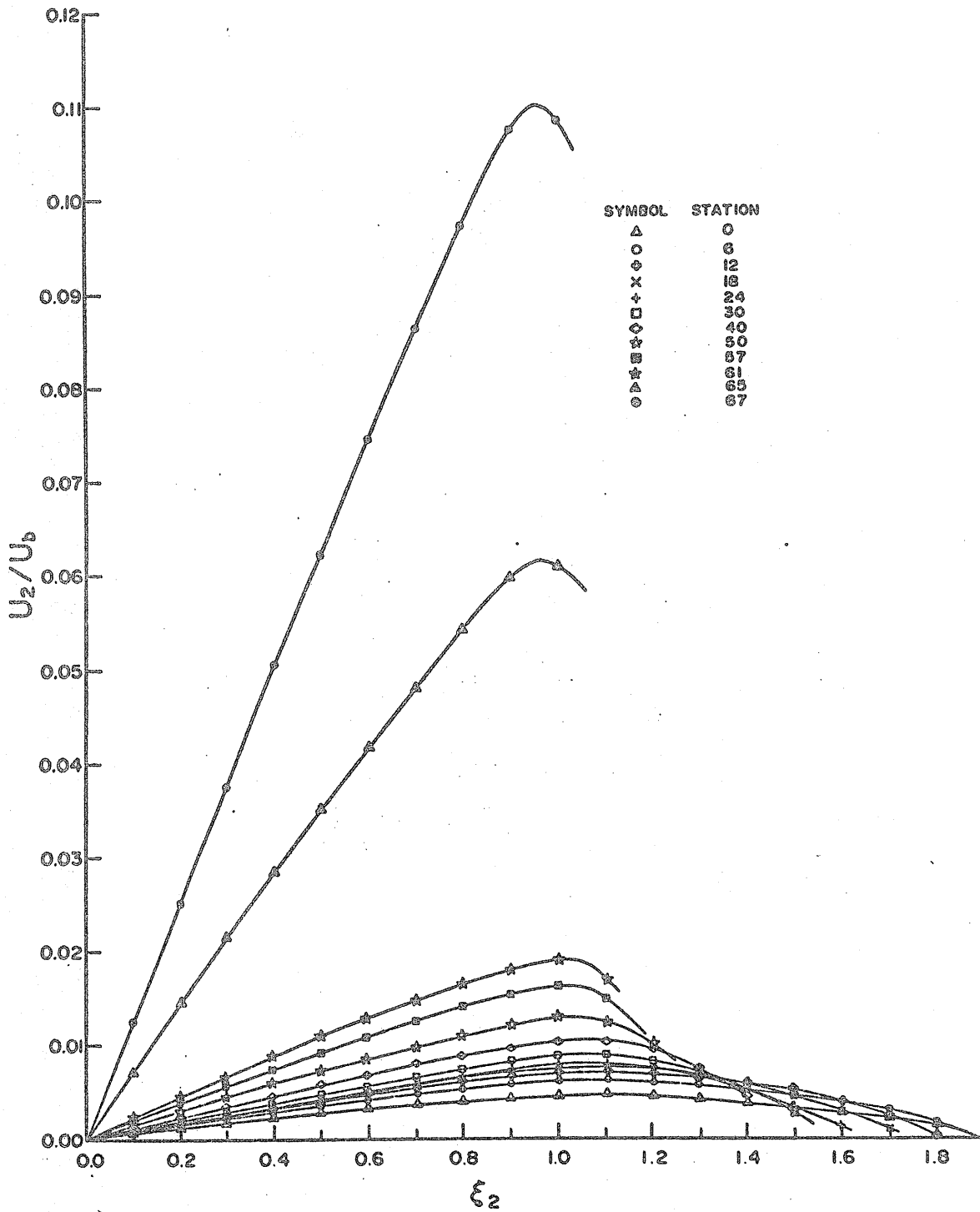


Figure 7 Mean radial velocity profiles.

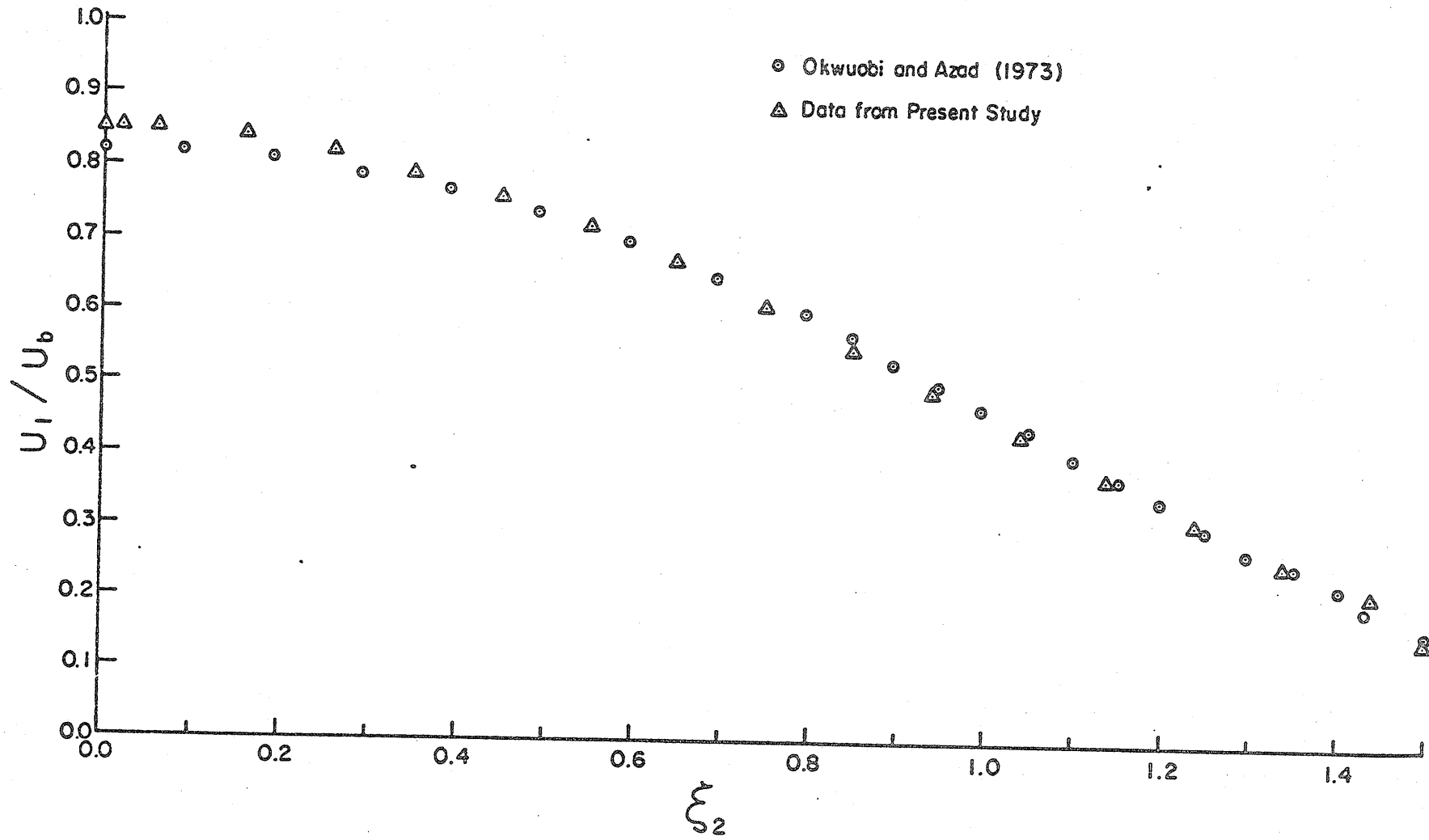


Figure 8 Comparison of mean axial velocity profile at station 30 to that of Okwuobi & Azad.

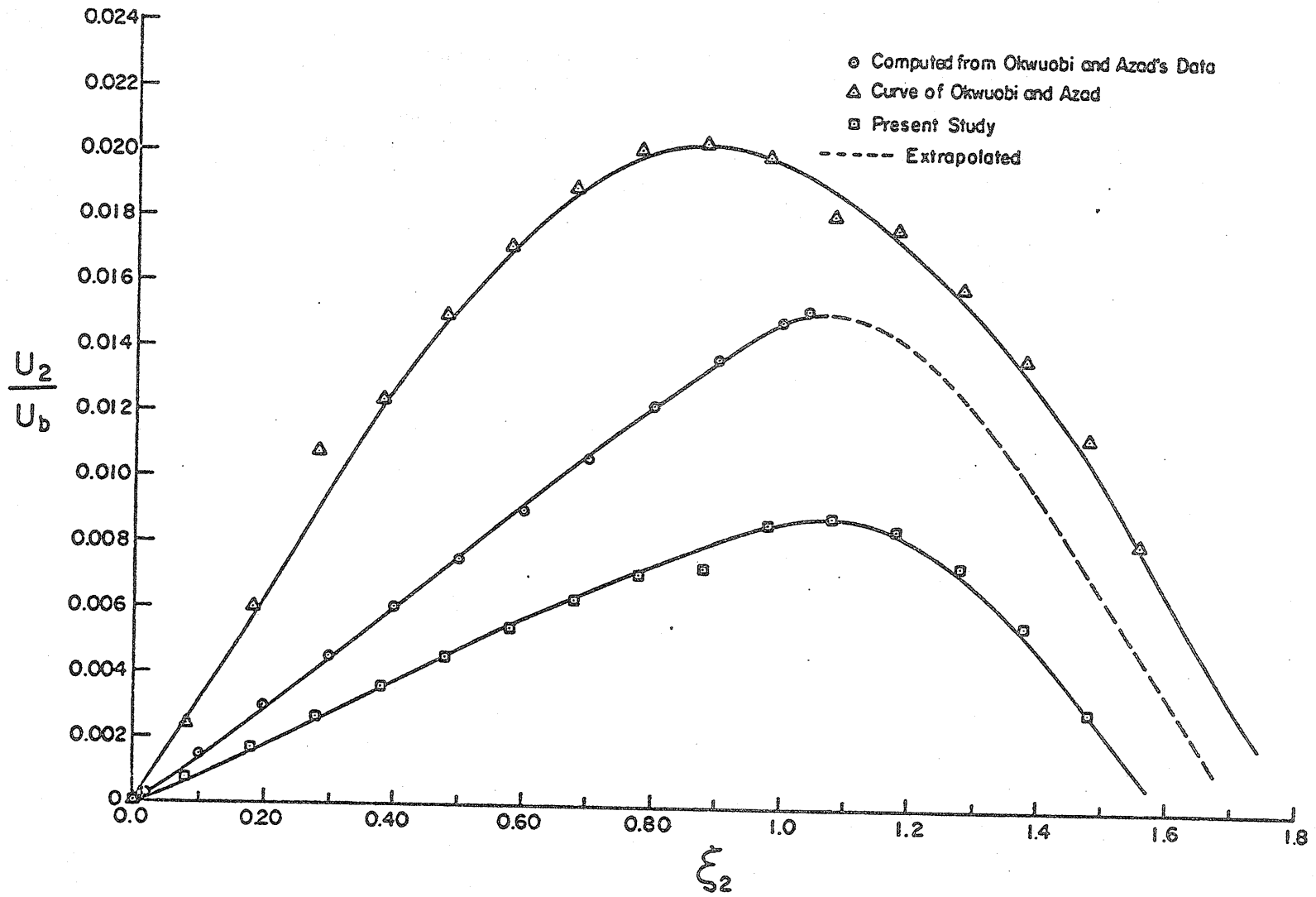


Figure 9 Comparison of mean radial velocity profiles at station 30.

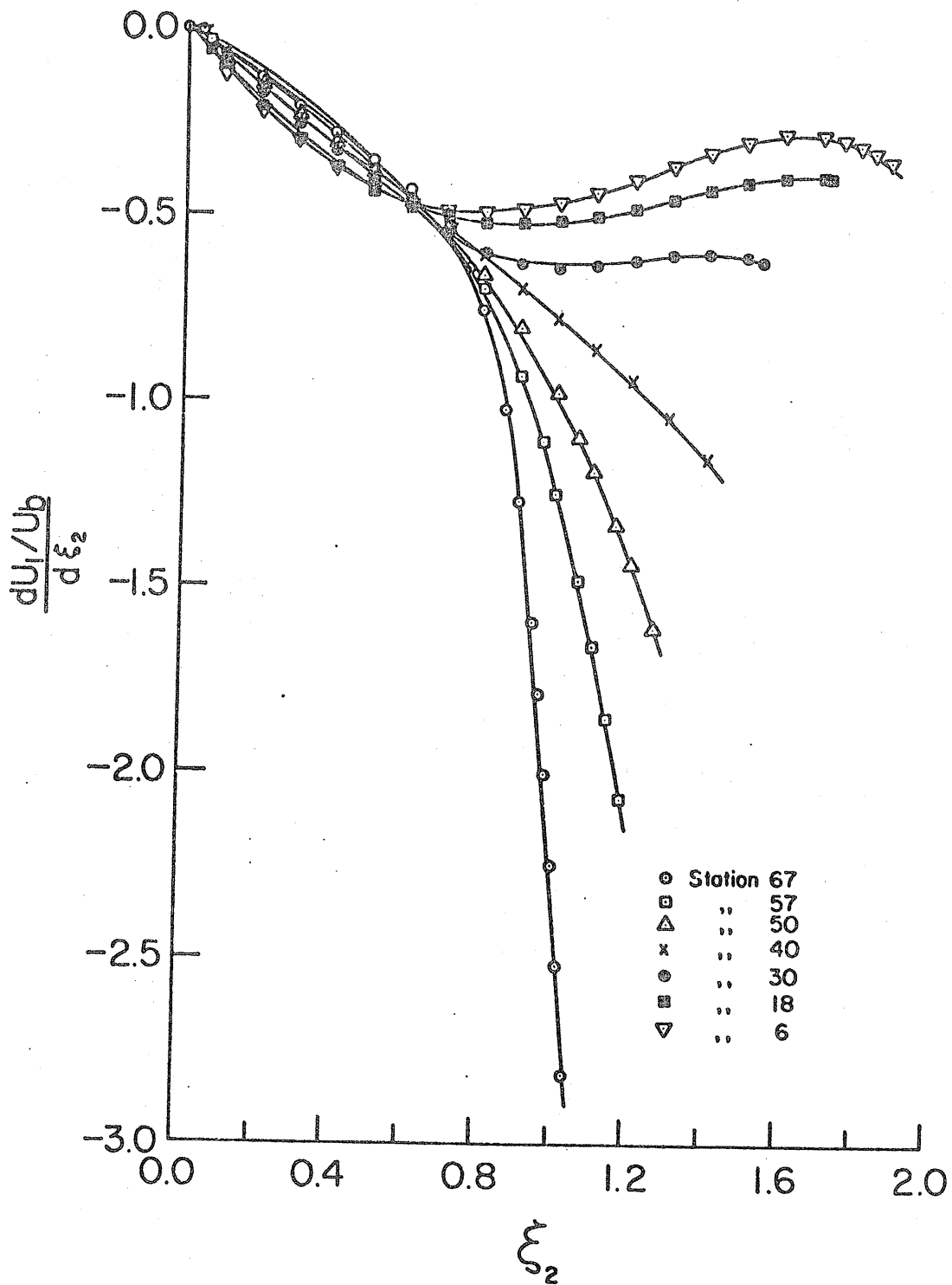


Figure 10 Radial derivative of the mean axial velocity.

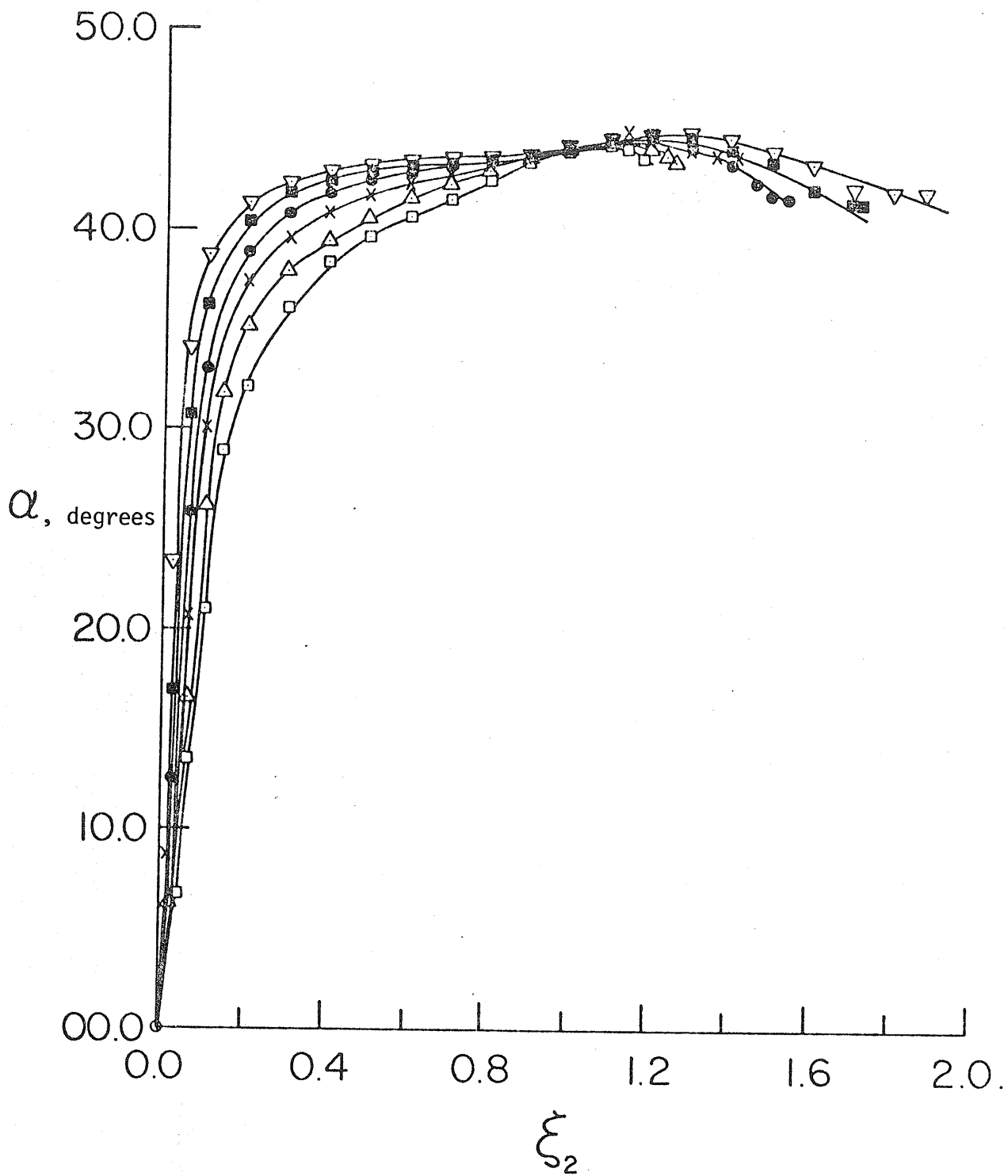


Figure 11 Directions of mean strain rate. Symbols as for figure 10.

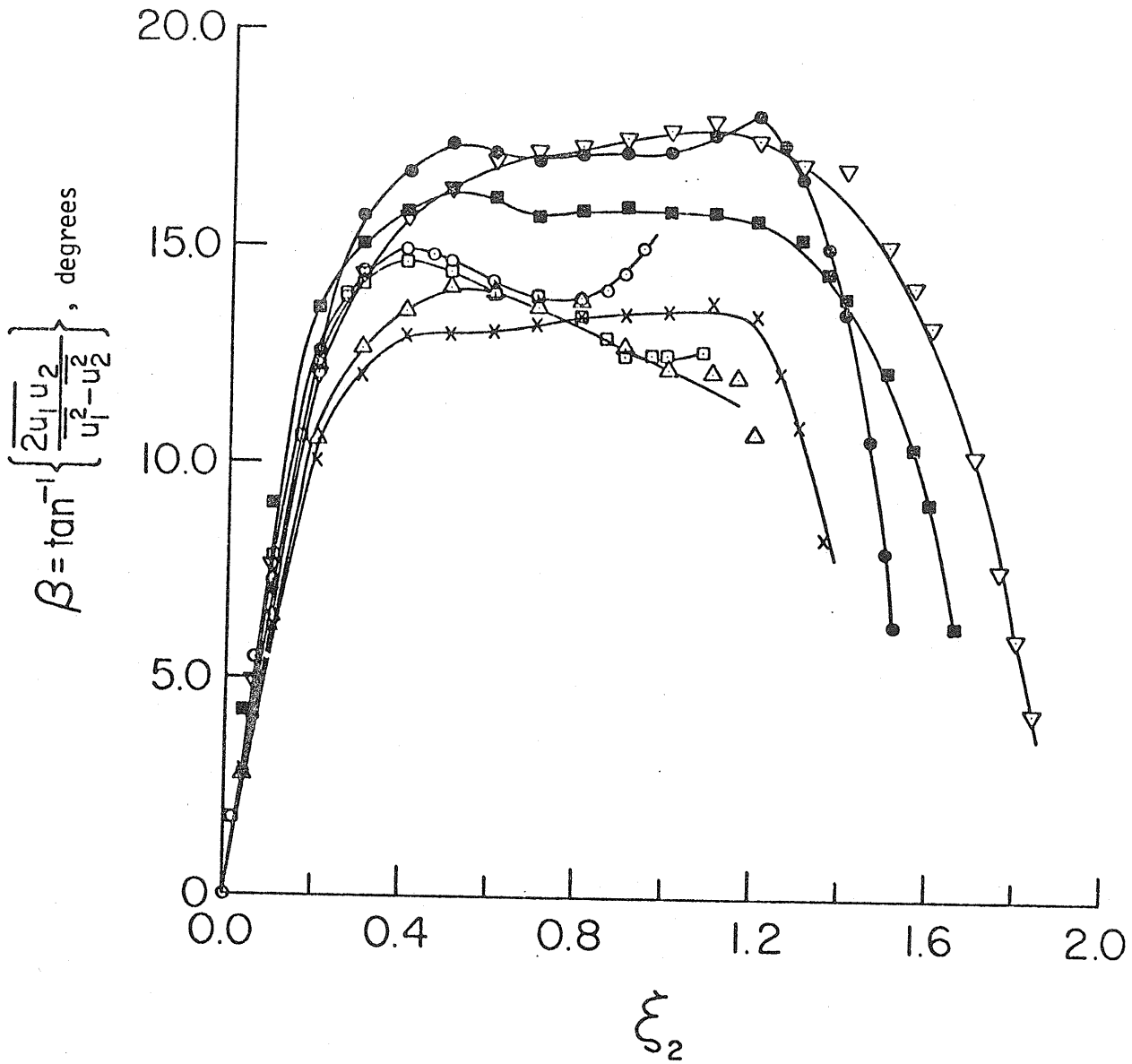


Figure 12 Directions of the mean principal stresses. Symbols as for figure 10.

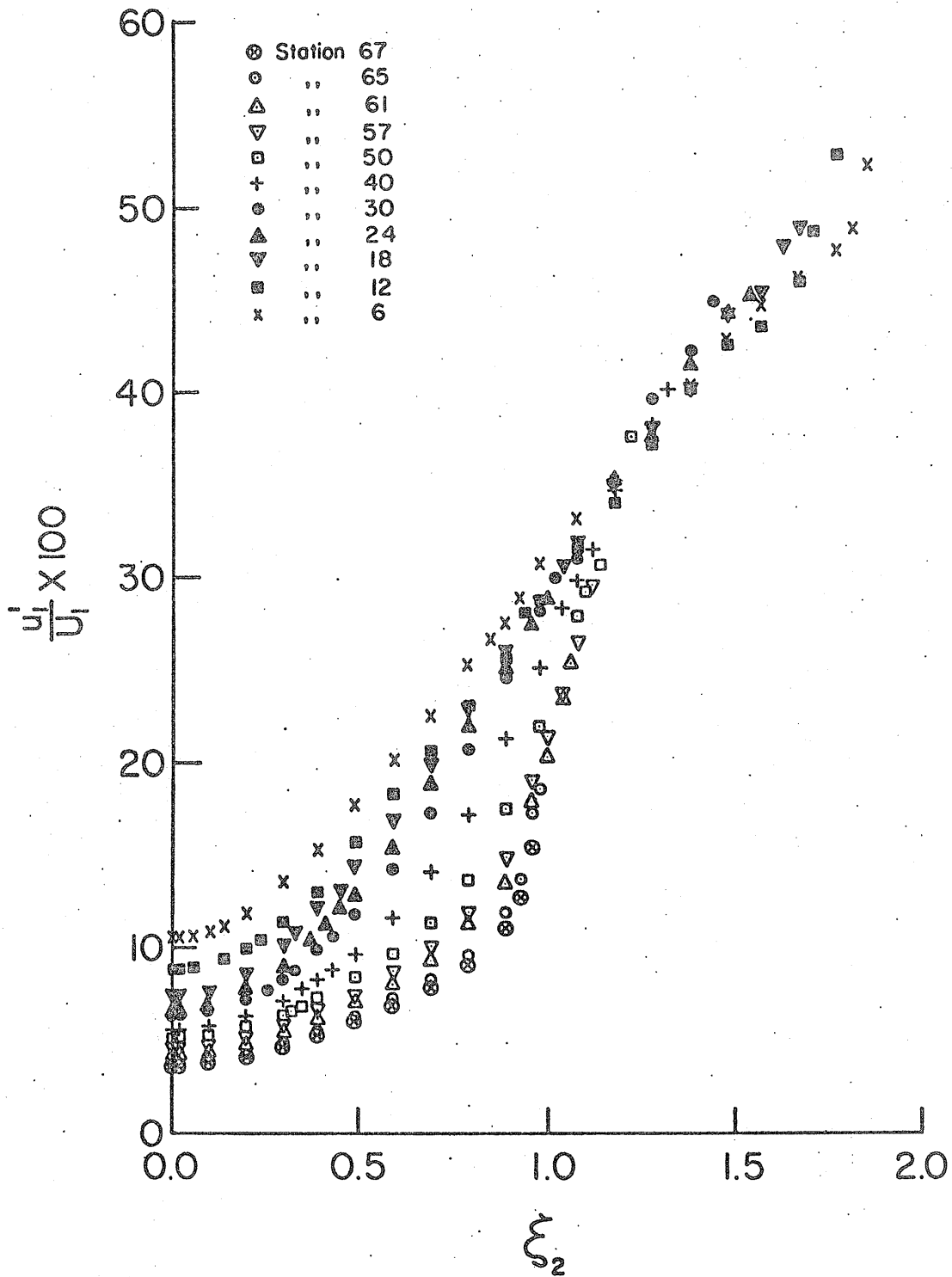


Figure 13a Distribution of relative turbulent intensities, u'_1 .

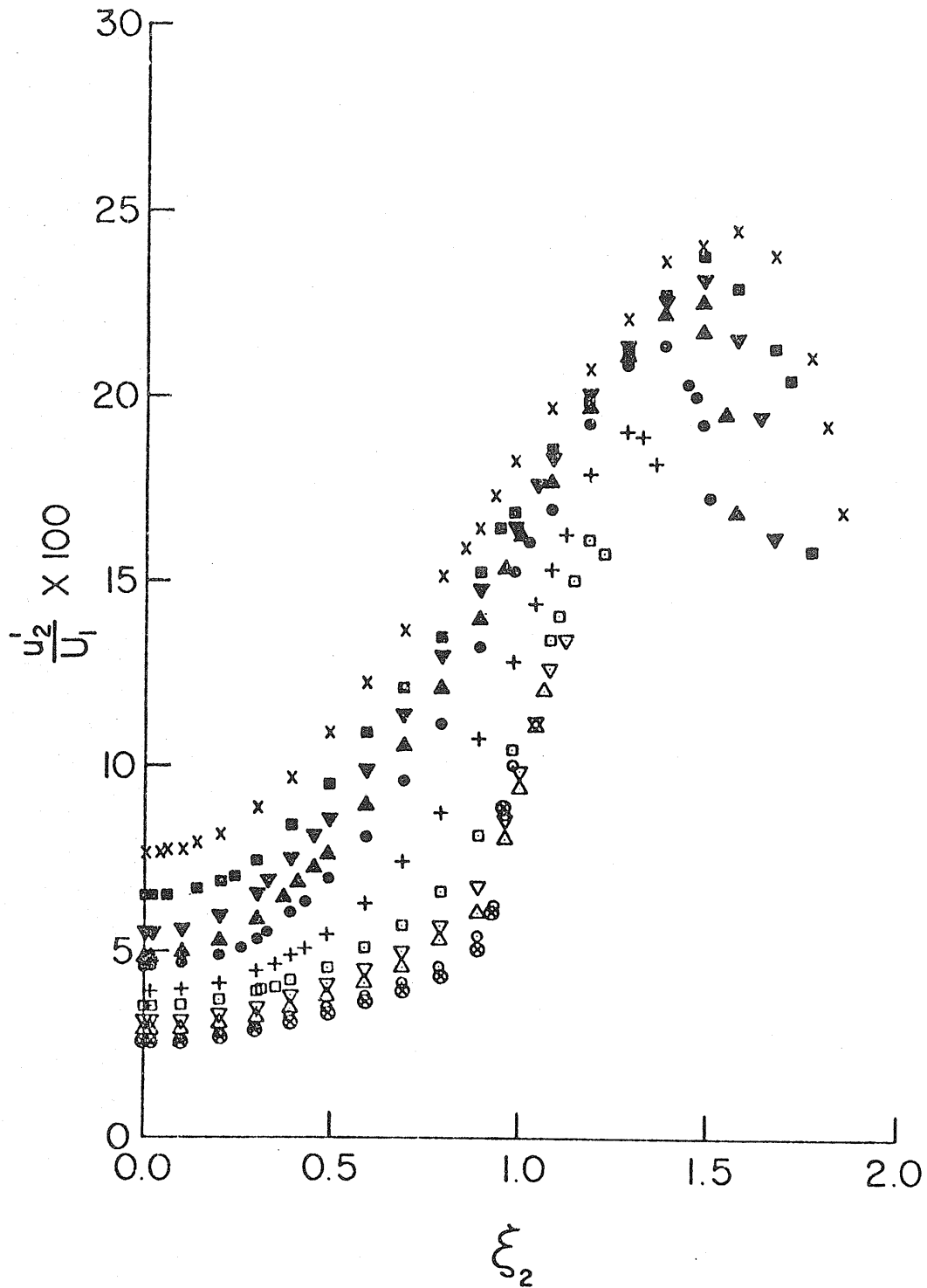


Figure 13b Distribution of relative turbulent intensities, u_2'/U_1 . Symbols as for figure 13a.

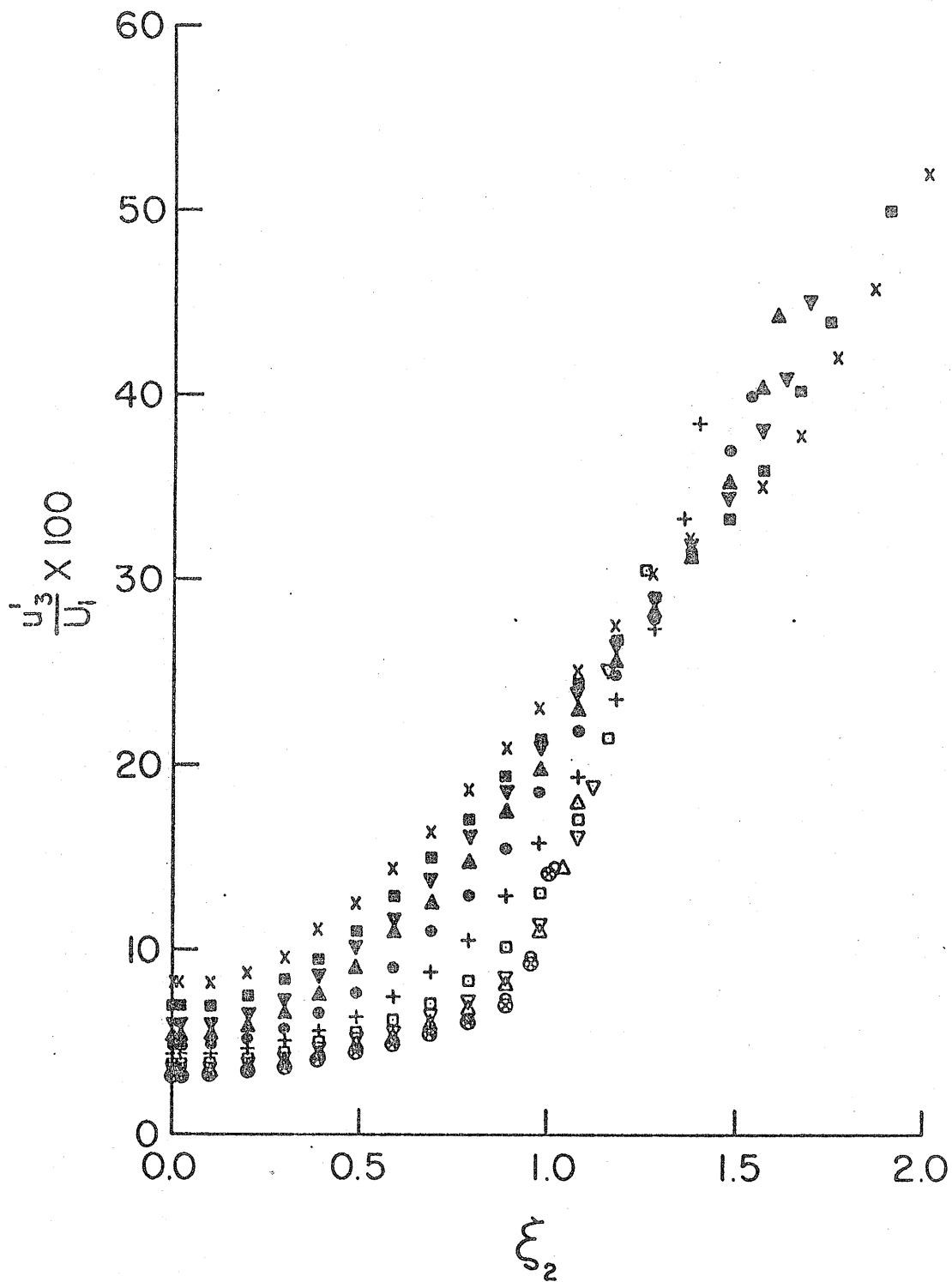


Figure 13c Distribution of relative turbulent intensities, u_3'/U_1 . Symbols as for figure 13a.

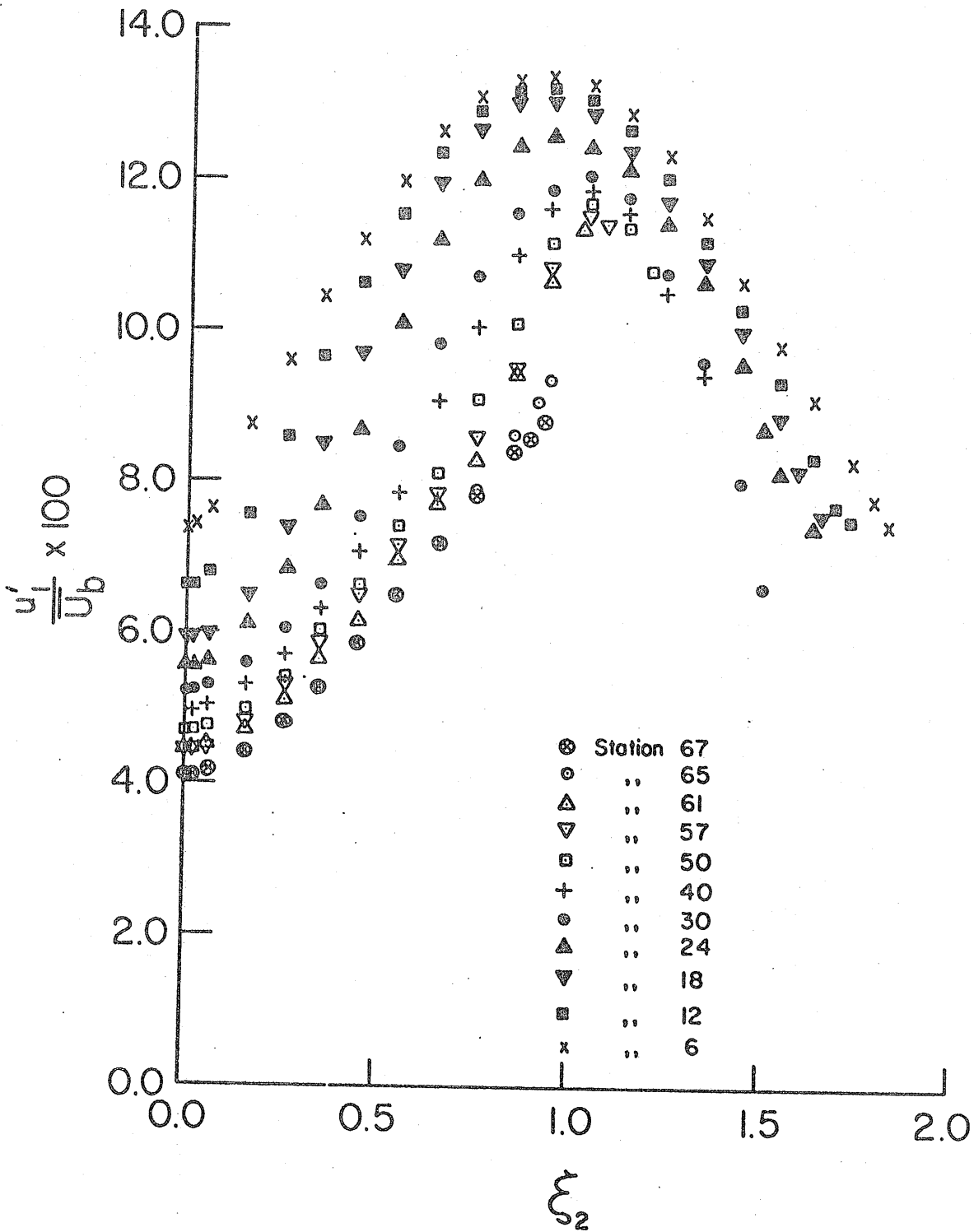


Figure 14 Distribution of the turbulence intensity u'_1/U_b .

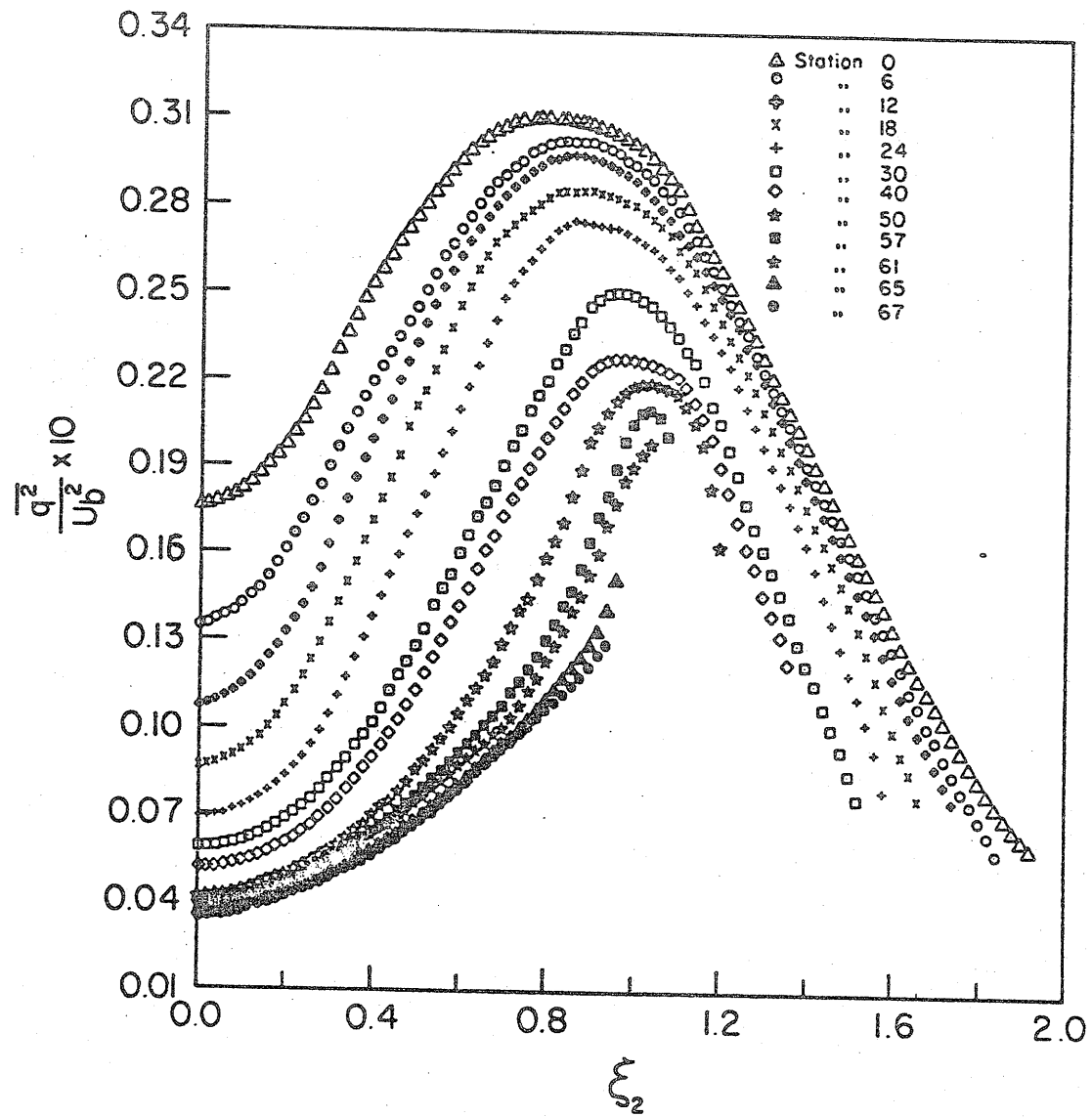


Figure 15 Turbulent stress tensor trace in the diffuser.

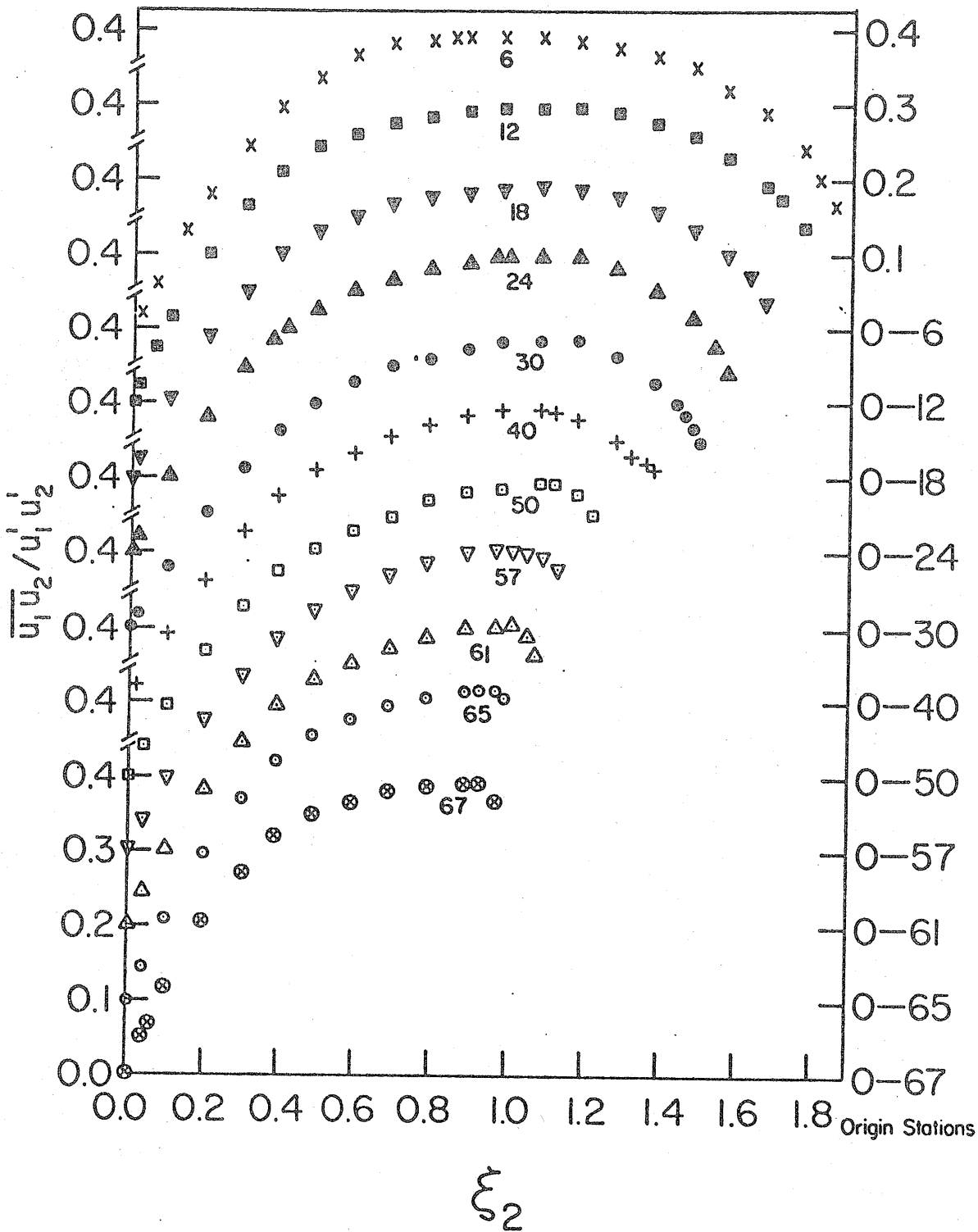


Figure 16 The correlation coefficient in the diffuser.

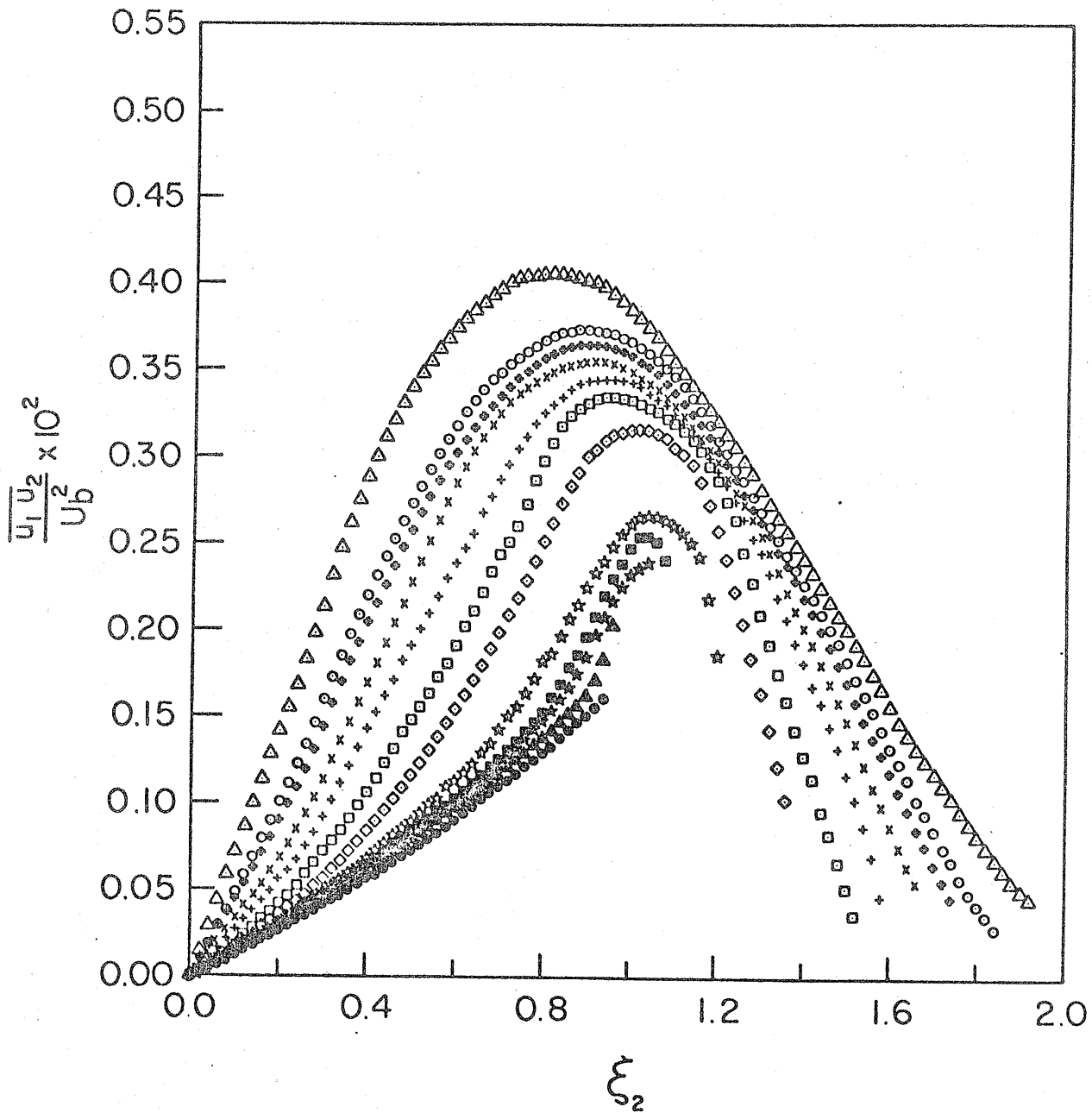


Figure 17 Distribution of the tangential stresses. Symbols as for figure 15.

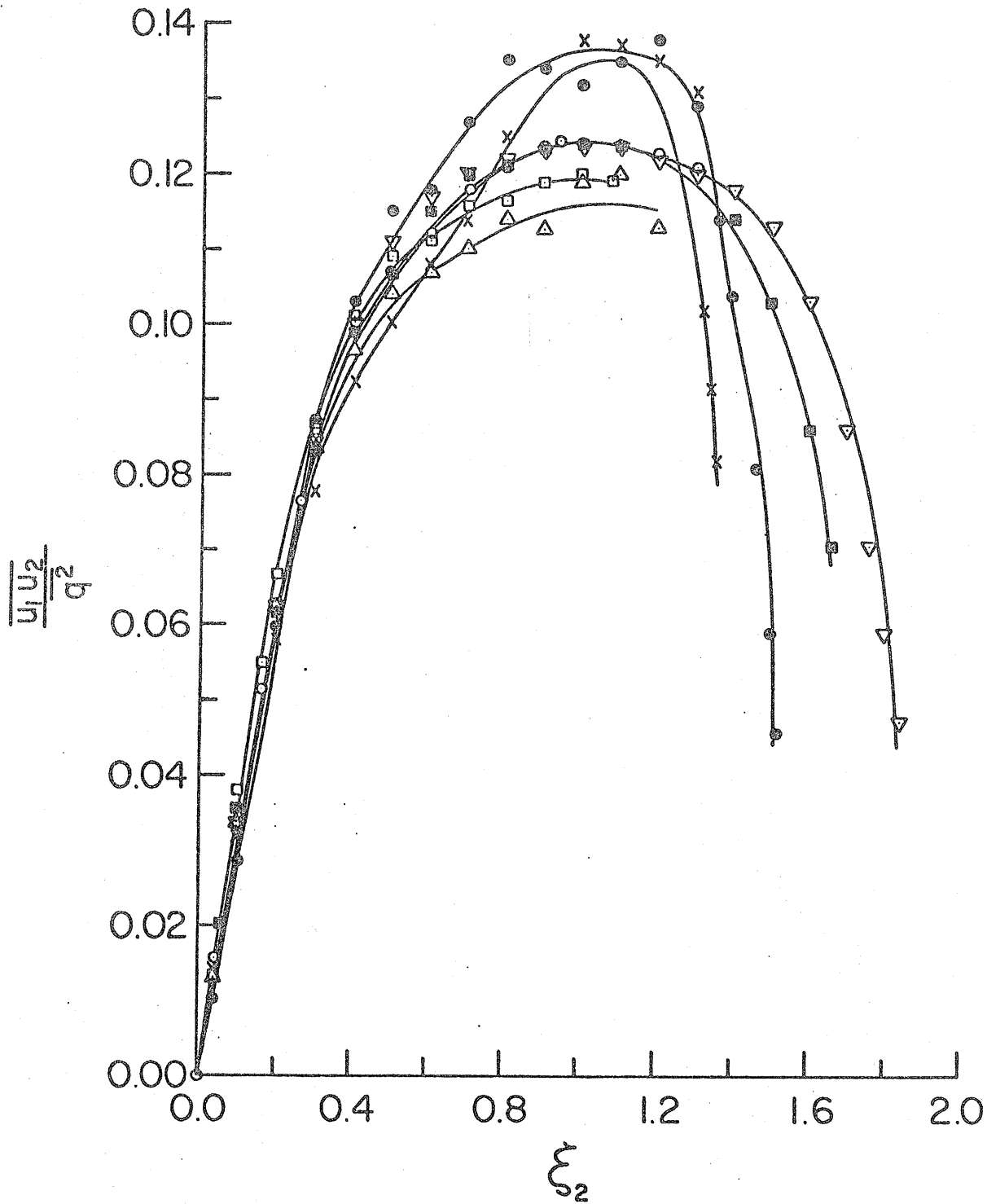


Figure 18 Variation of the ratio of tangential stress to the trace. Symbols as for figure 10.

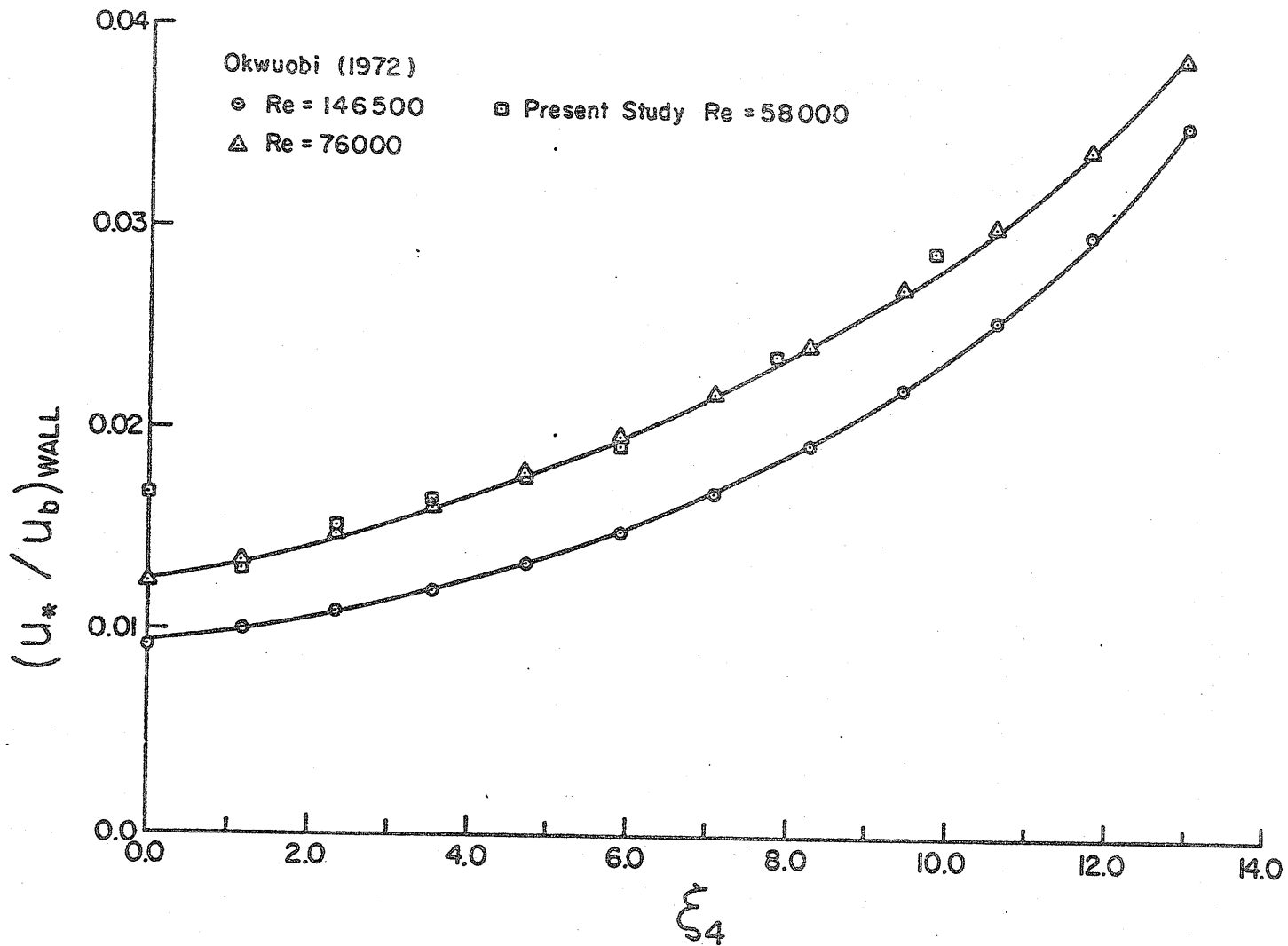


Figure 19 The wall friction velocities (u_*) in the diffuser.

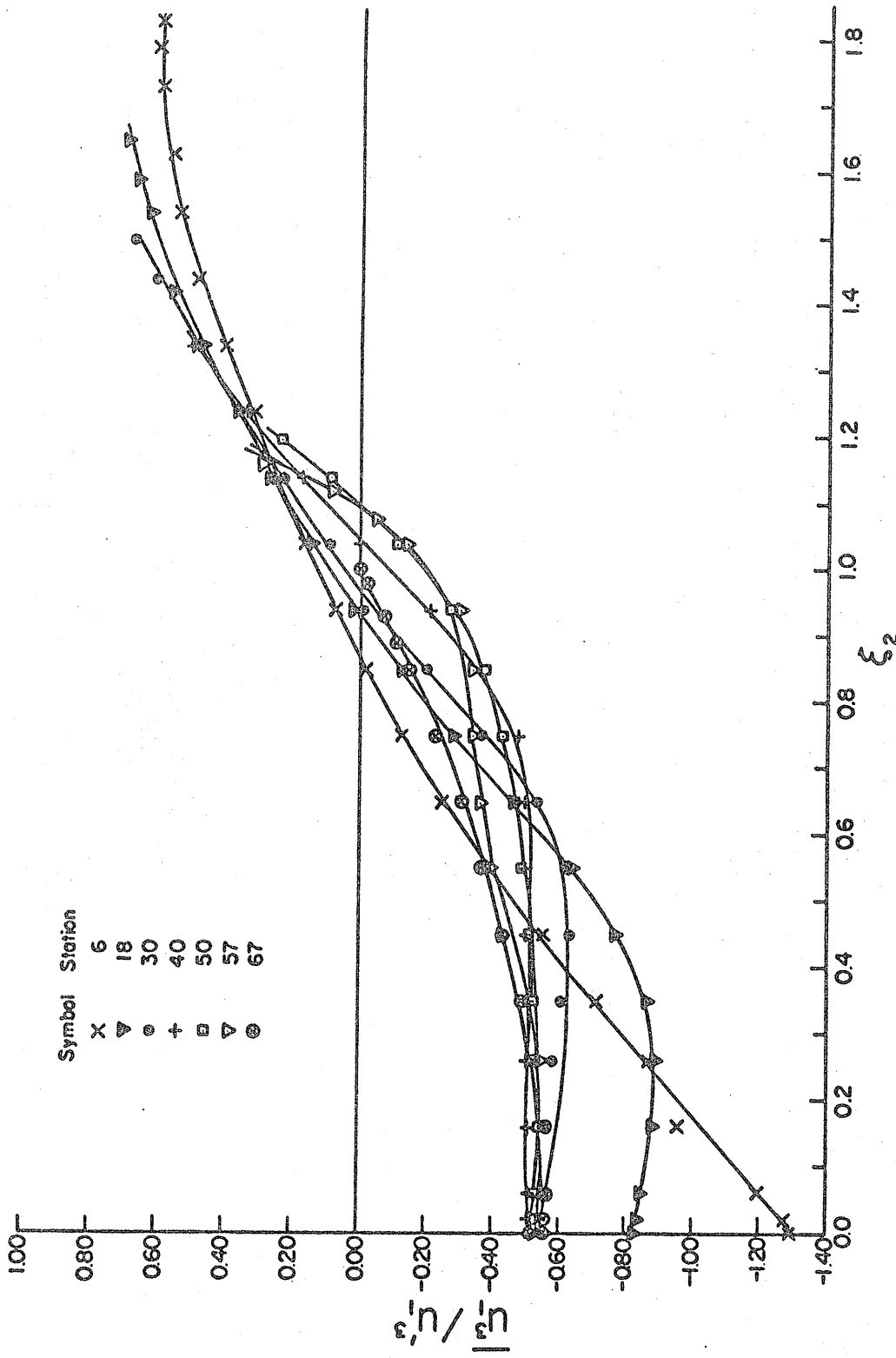


Figure 20 Skewness of u_1 in the diffuser.

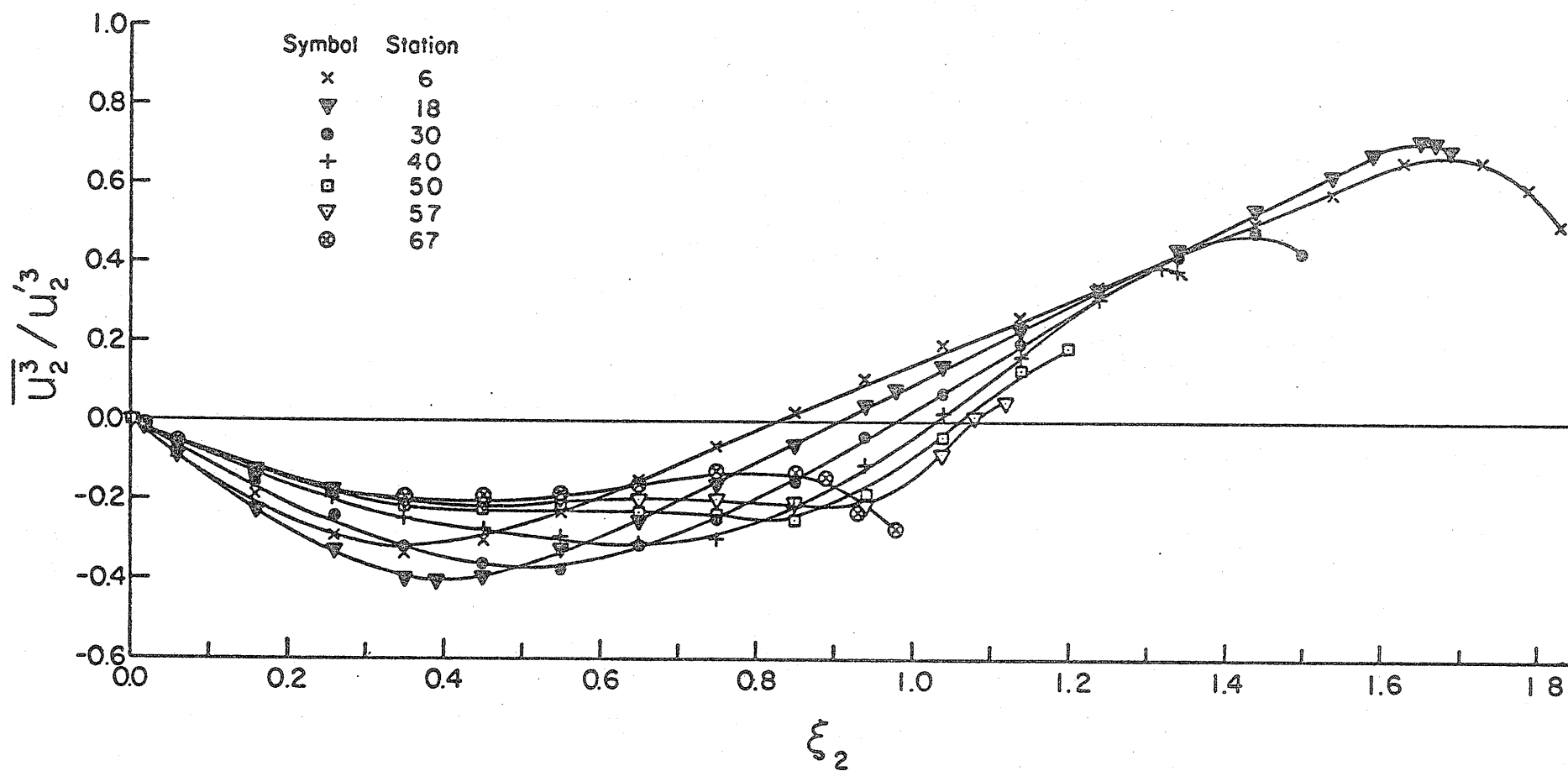


Figure 21 Skewness of u_2 in the diffuser.

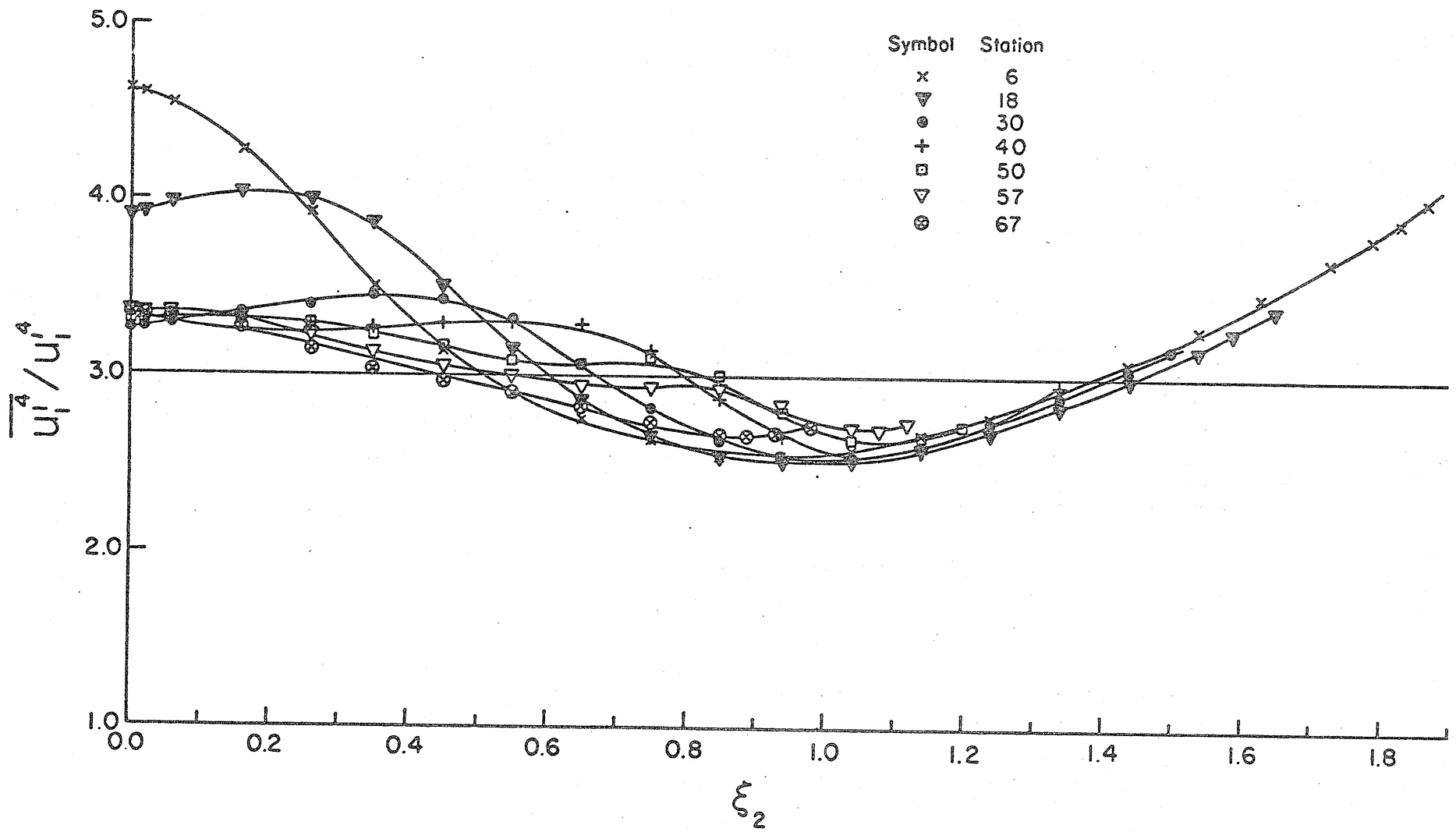


Figure 22 Flatness factor of u_1 in the diffuser.

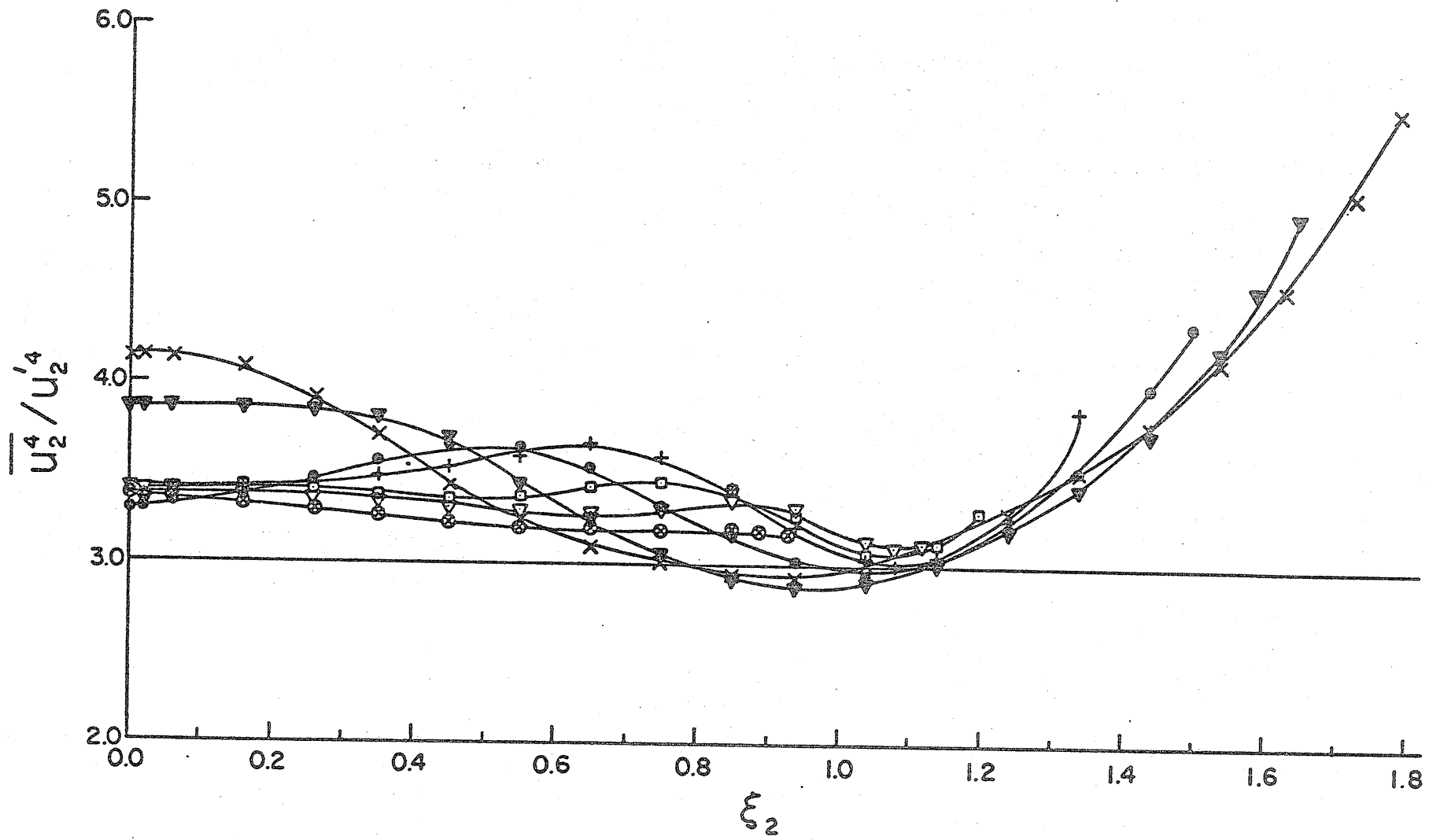


Figure 23 Flatness factor of u_2 in the diffuser. Symbols as for figure 22.

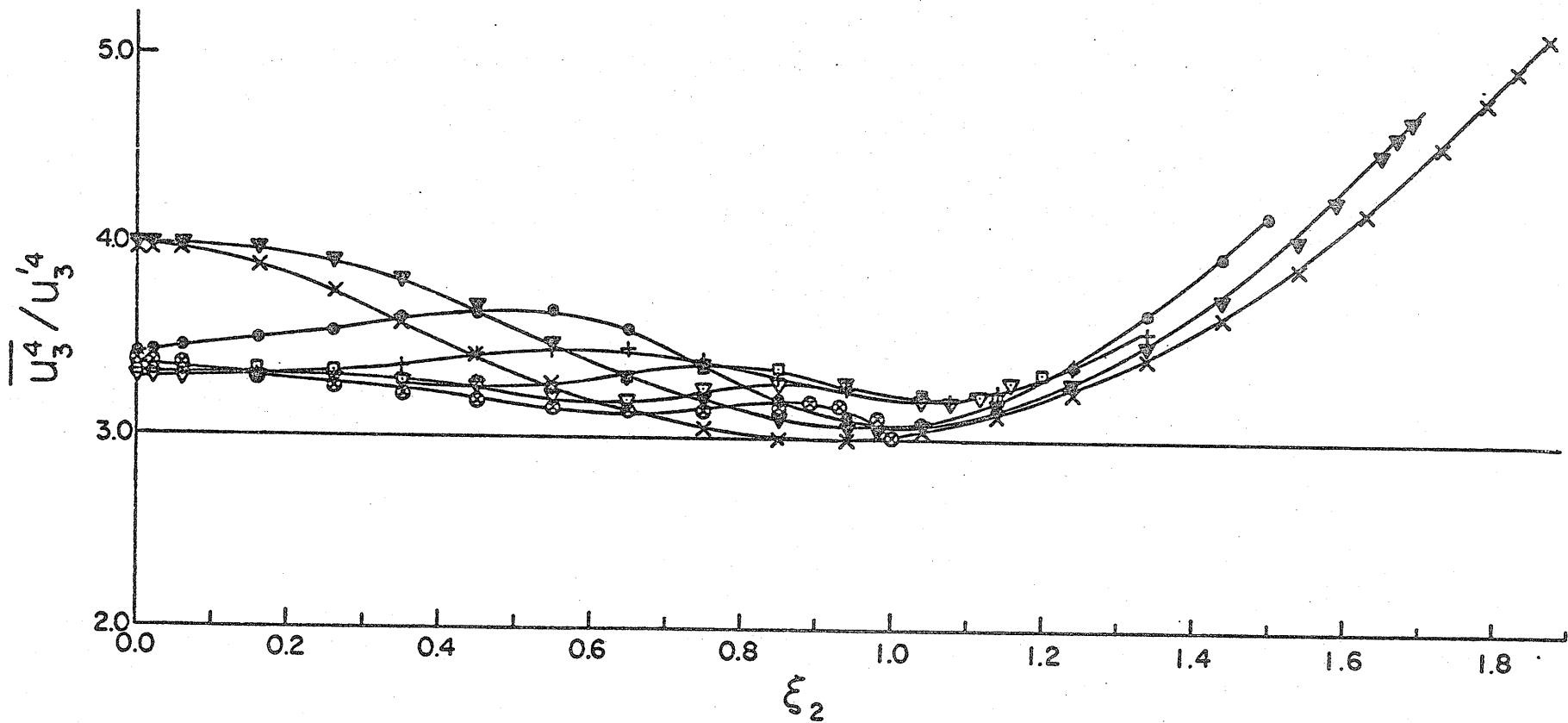


Figure 24 Flatness factor of u_3 in the diffuser. Symbols as for figure 22.

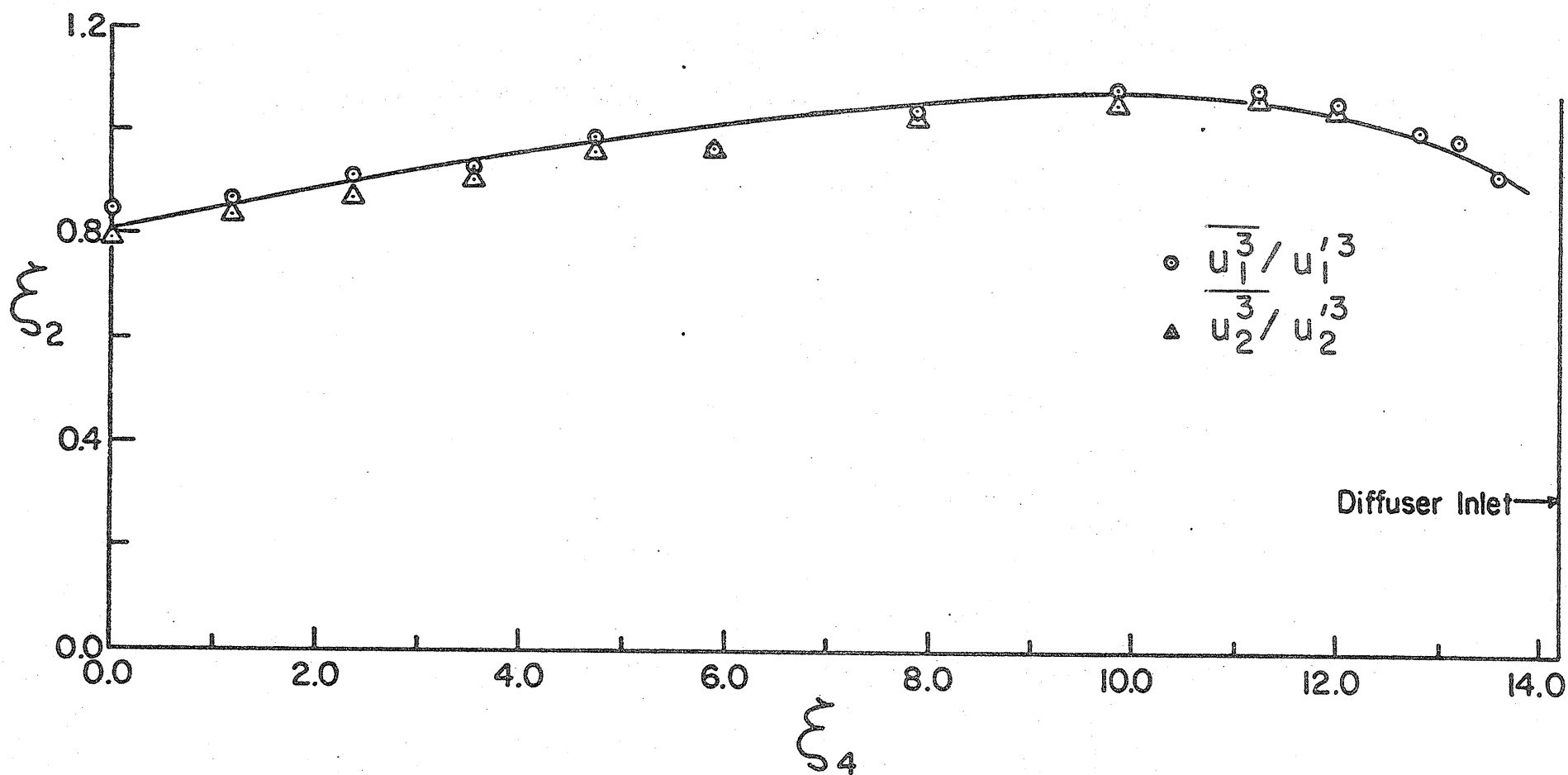


Figure 25 Radial positions where skewness of u_1 & u_2 changes sign.

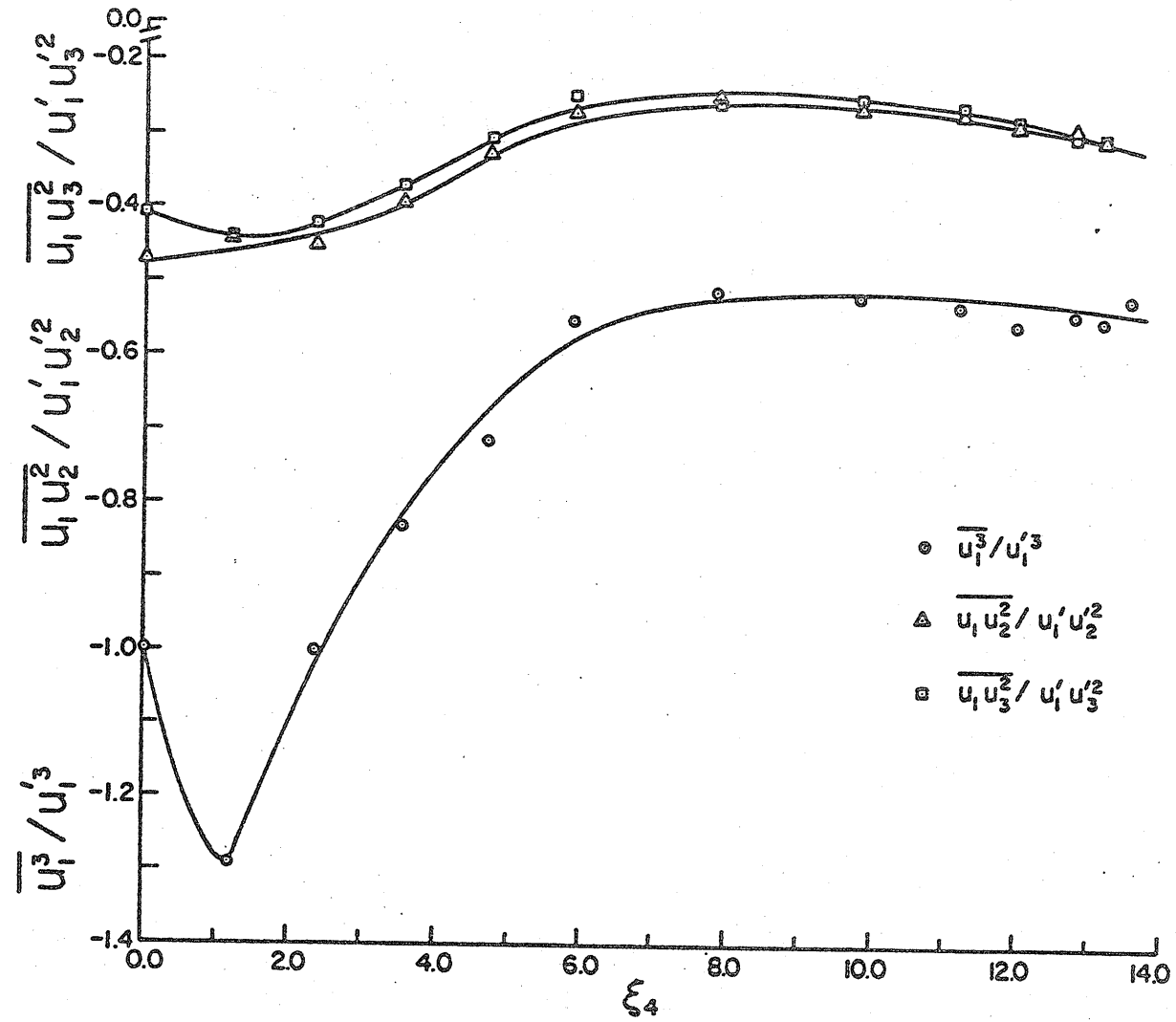


Figure 26 Skewness of u_1 and non zero 3rd order correlations at the diffuser axis.

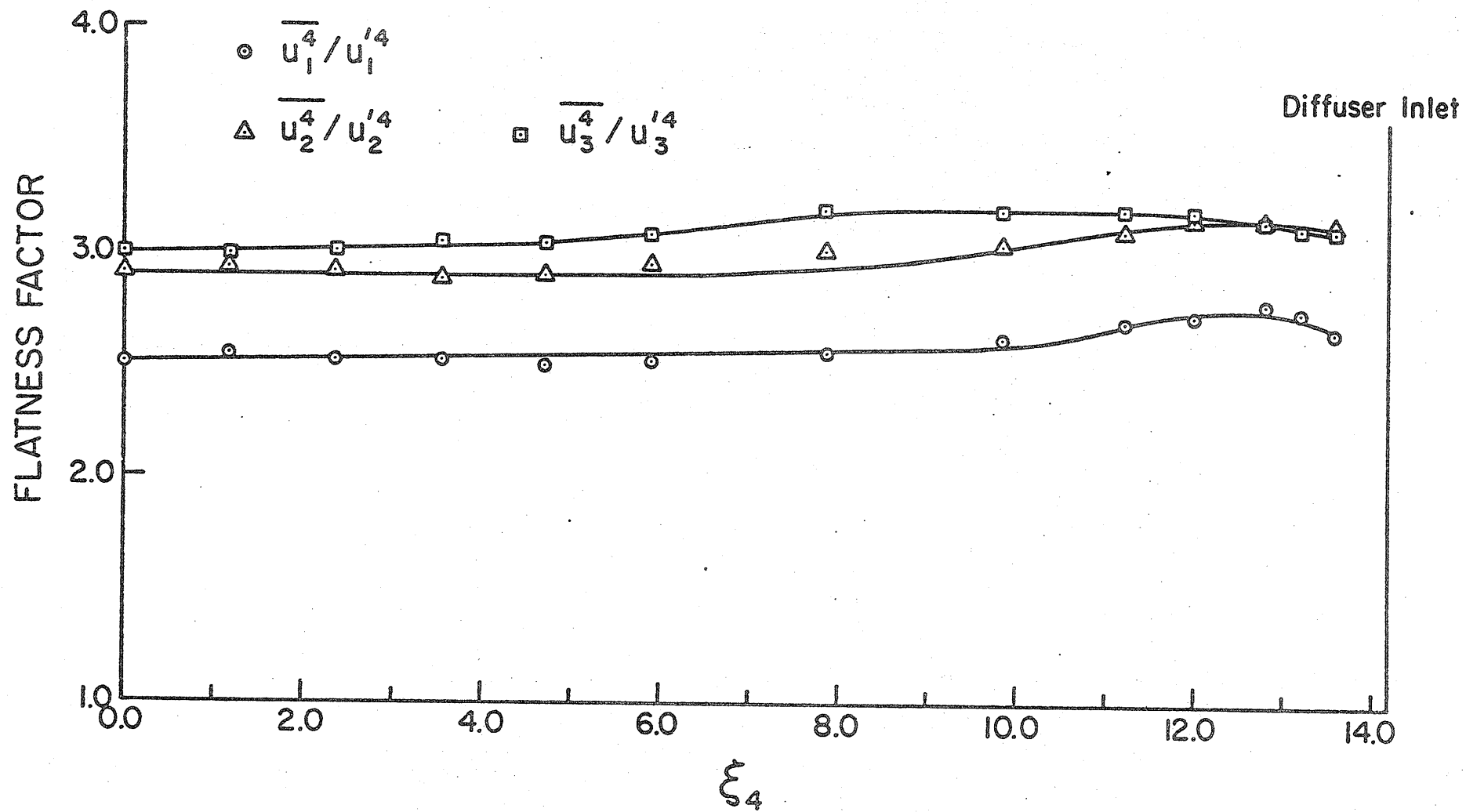


Figure 27 Flatness factors at radial positions where skewness of u_1 is zero.

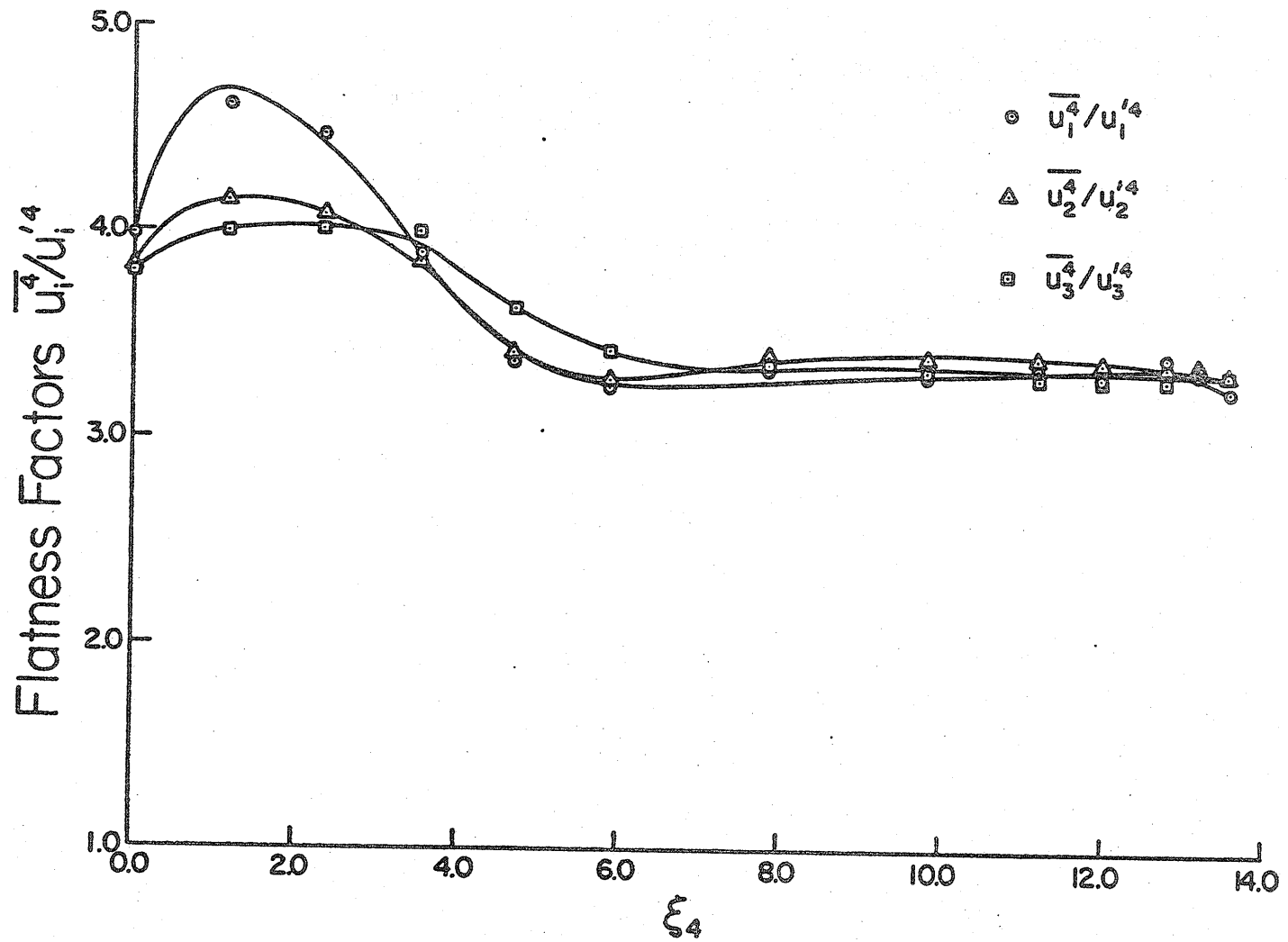


Figure 28 Flatness factors at the diffuser axis.

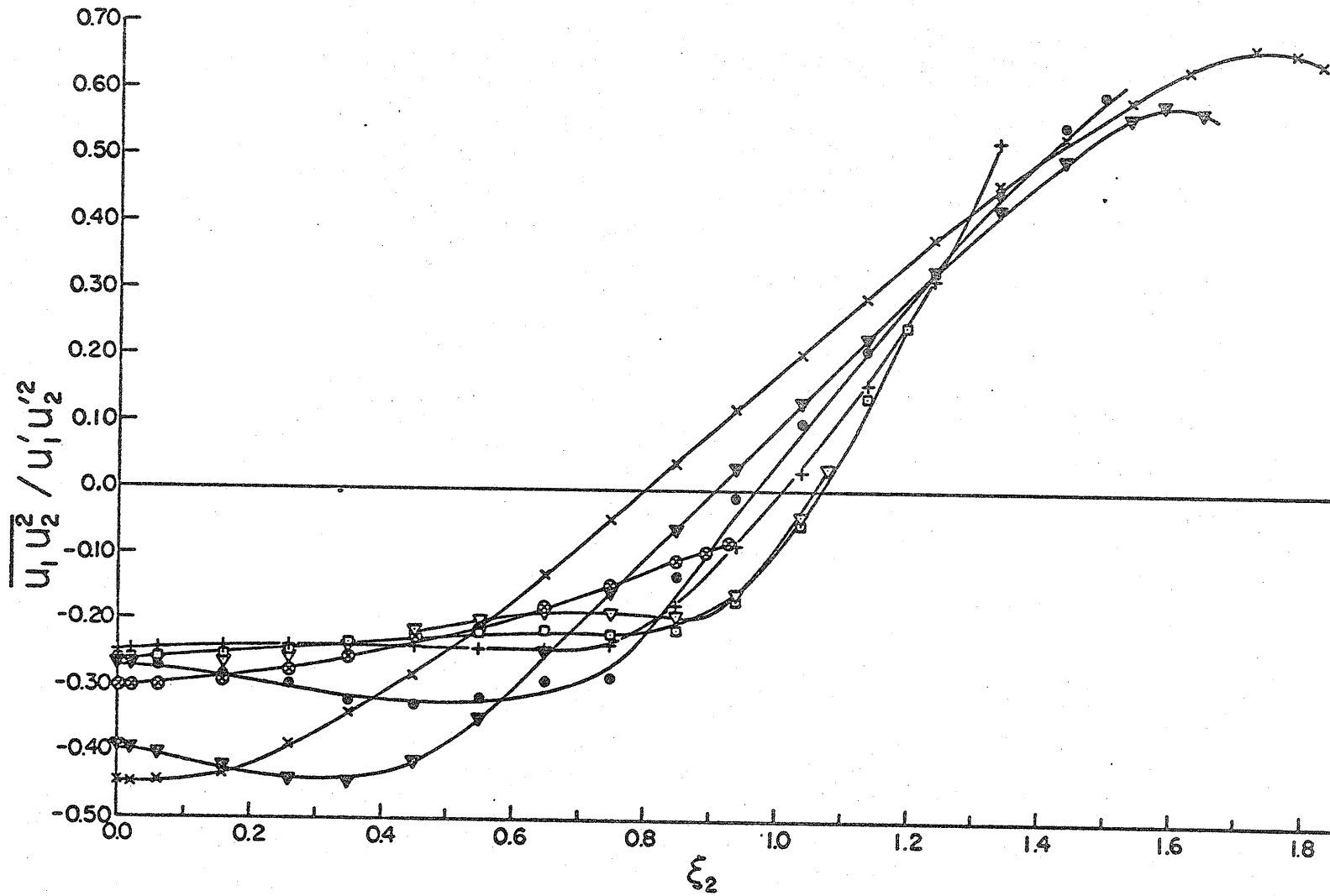


Figure 29 Third order velocity correlations of $u_1 u_2^2$. Symbols as for figure 22.

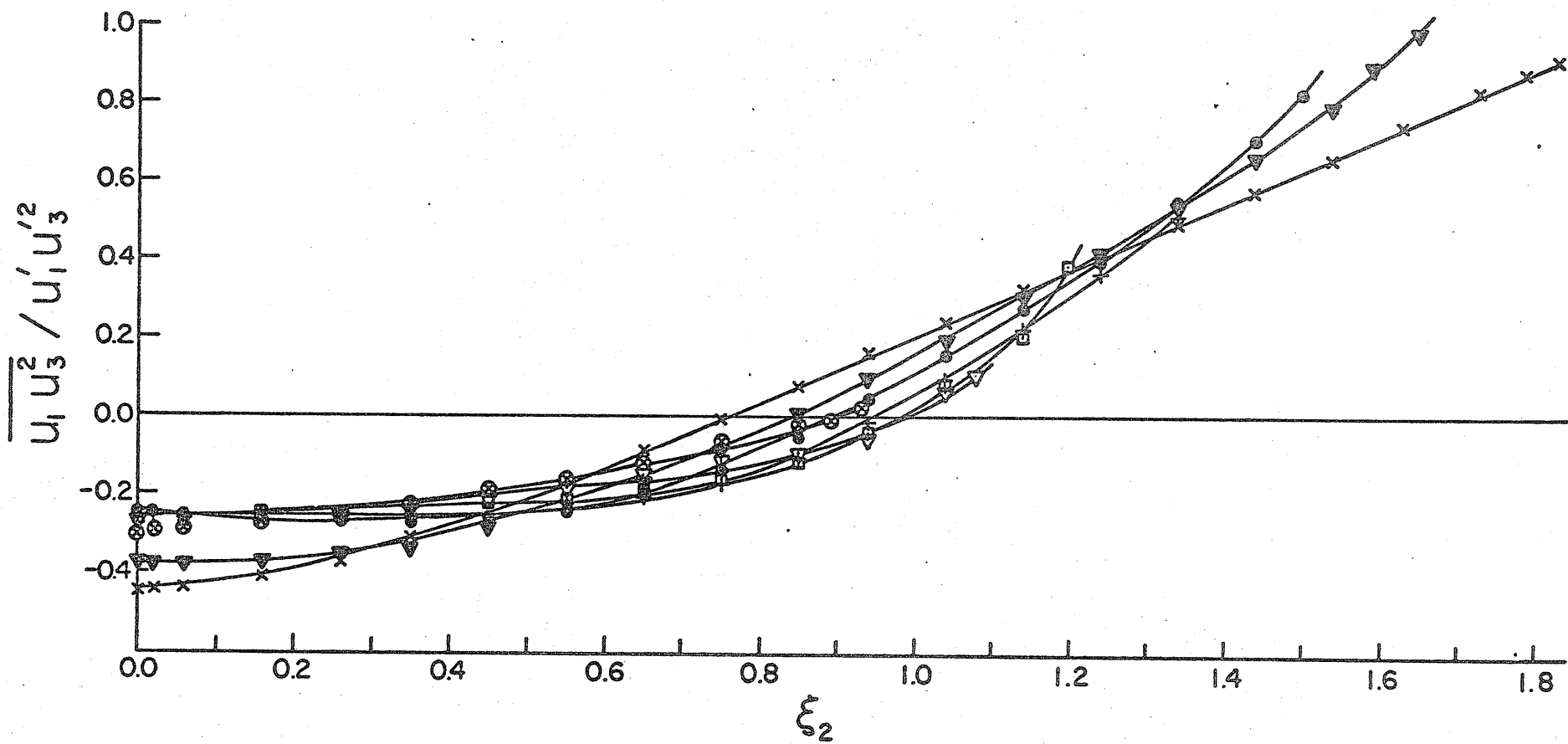


Figure 30 Third order velocity correlations of $u_1 u_3^2$. Symbols as for figure 22.

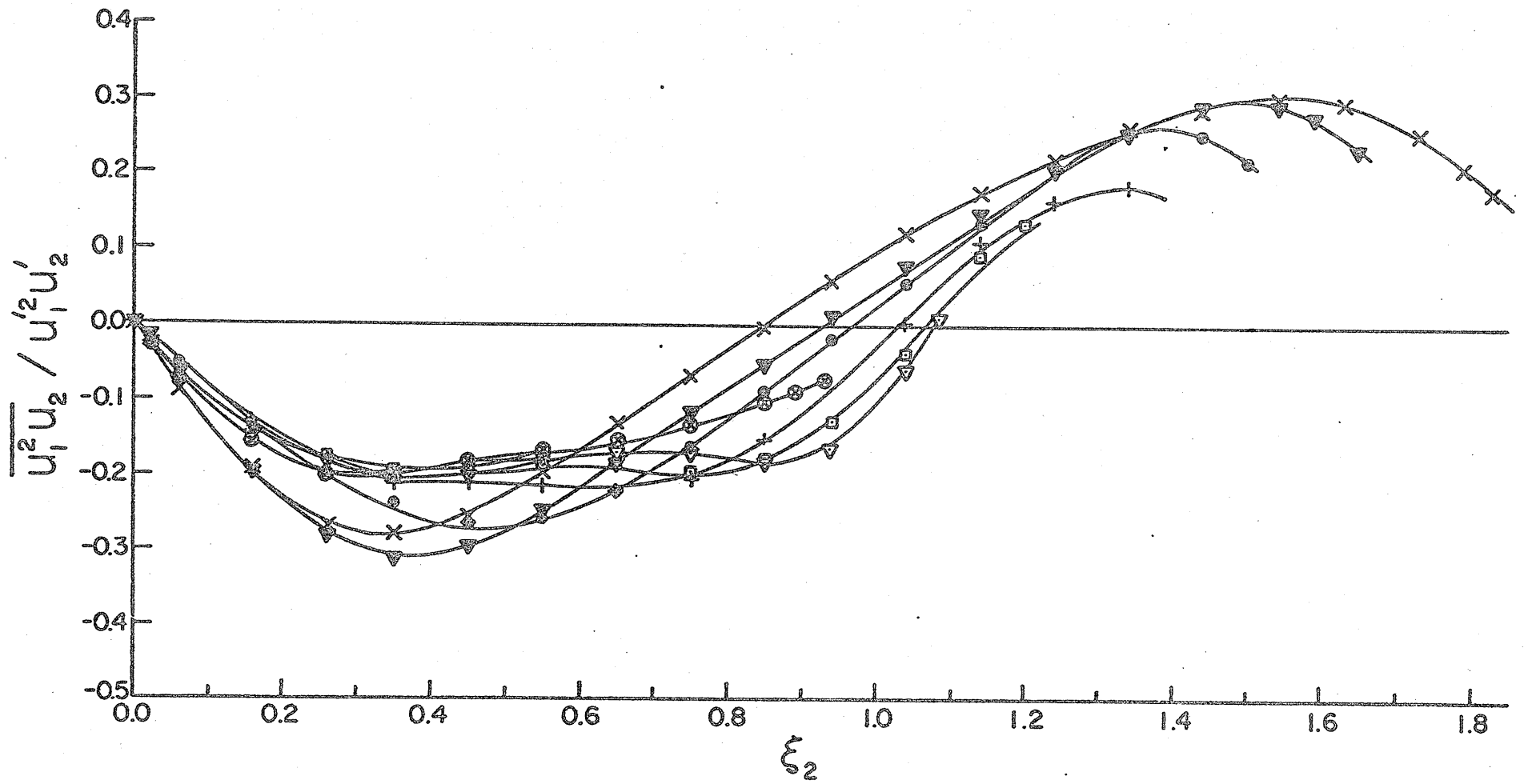


Figure 31 Third order velocity correlations of $u_1^2 u_2$. Symbols as for figure 22.

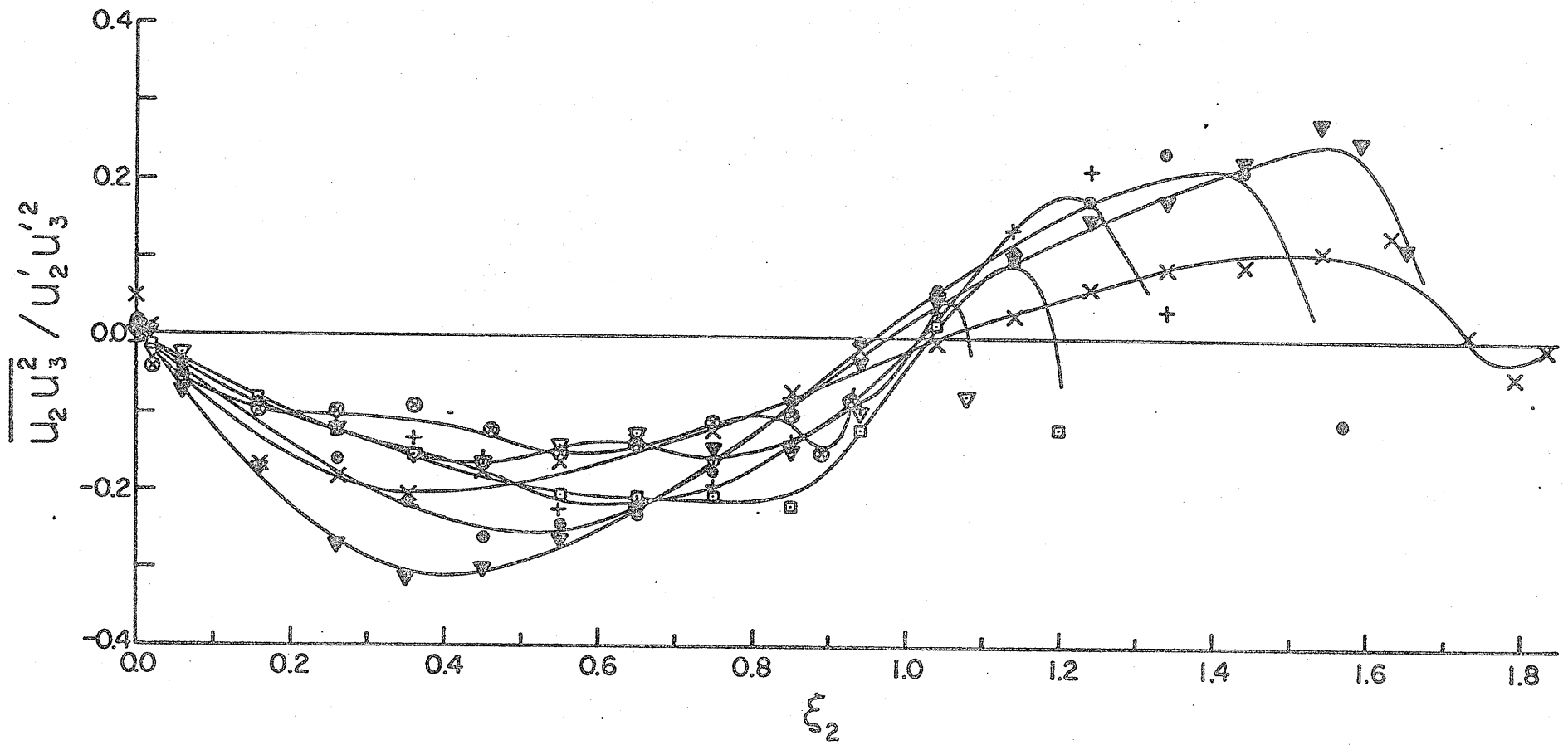


Figure 32 Third order velocity correlations of $u_2 u_3^2$. Symbols as for figure 22.

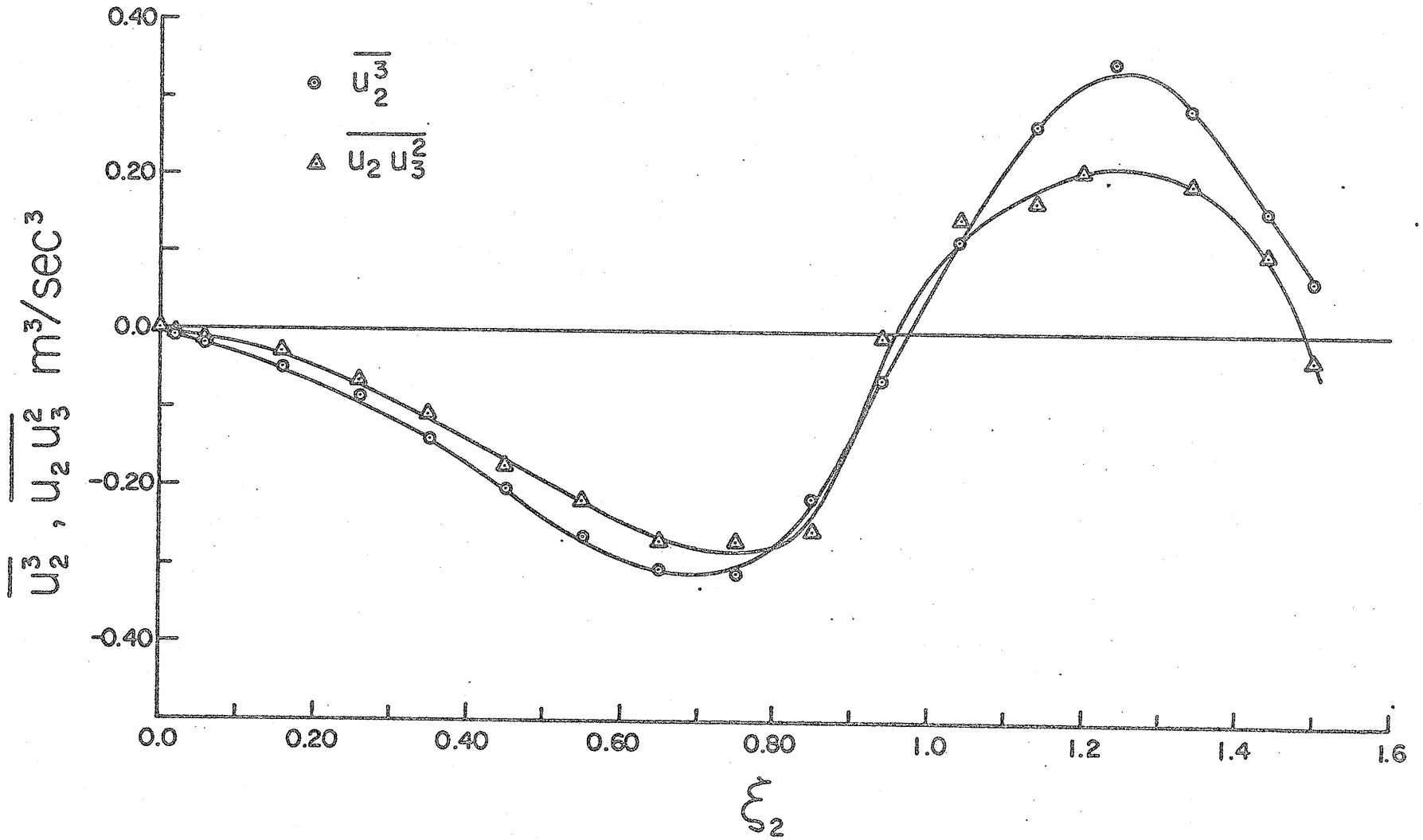


Figure 33 Comparison of $\overline{u_2 u_3^2}$ and $\overline{u_2^3}$ at station 30.

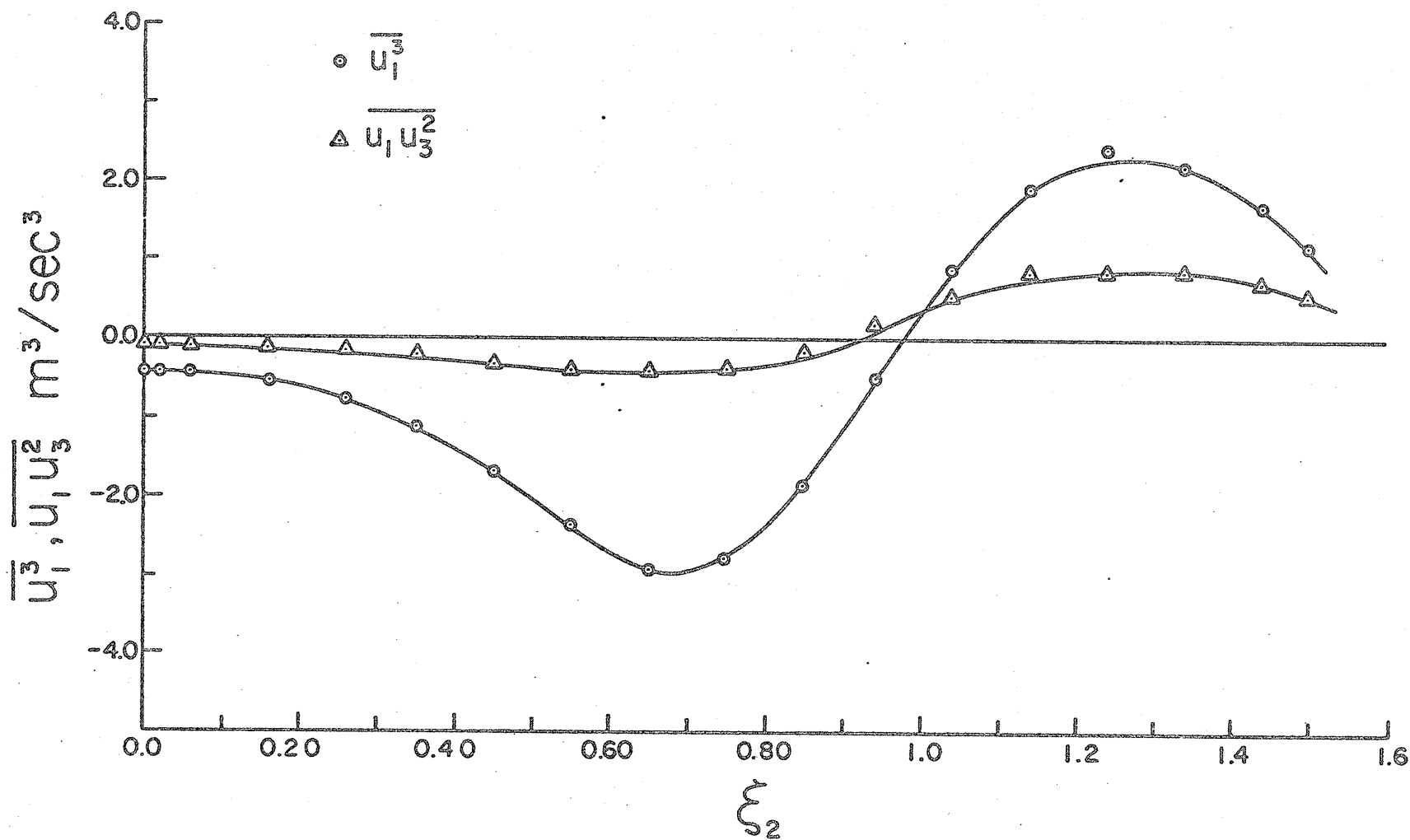


Figure 34 Comparison of $\overline{u_1 u_3^2}$ and $\overline{u_1^3}$ at station 30.

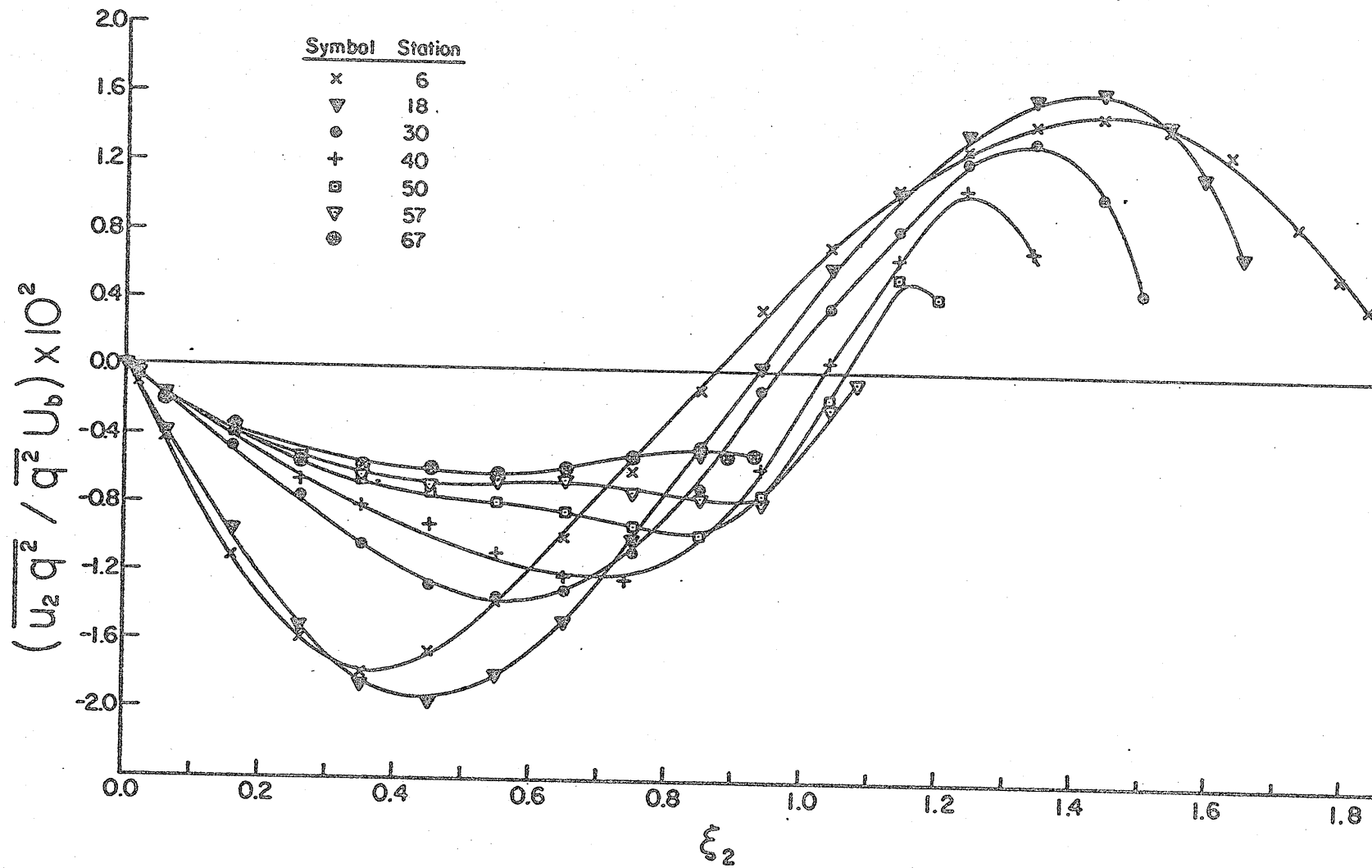


Figure 35 Distribution of the bulk convection velocities in the diffuser.

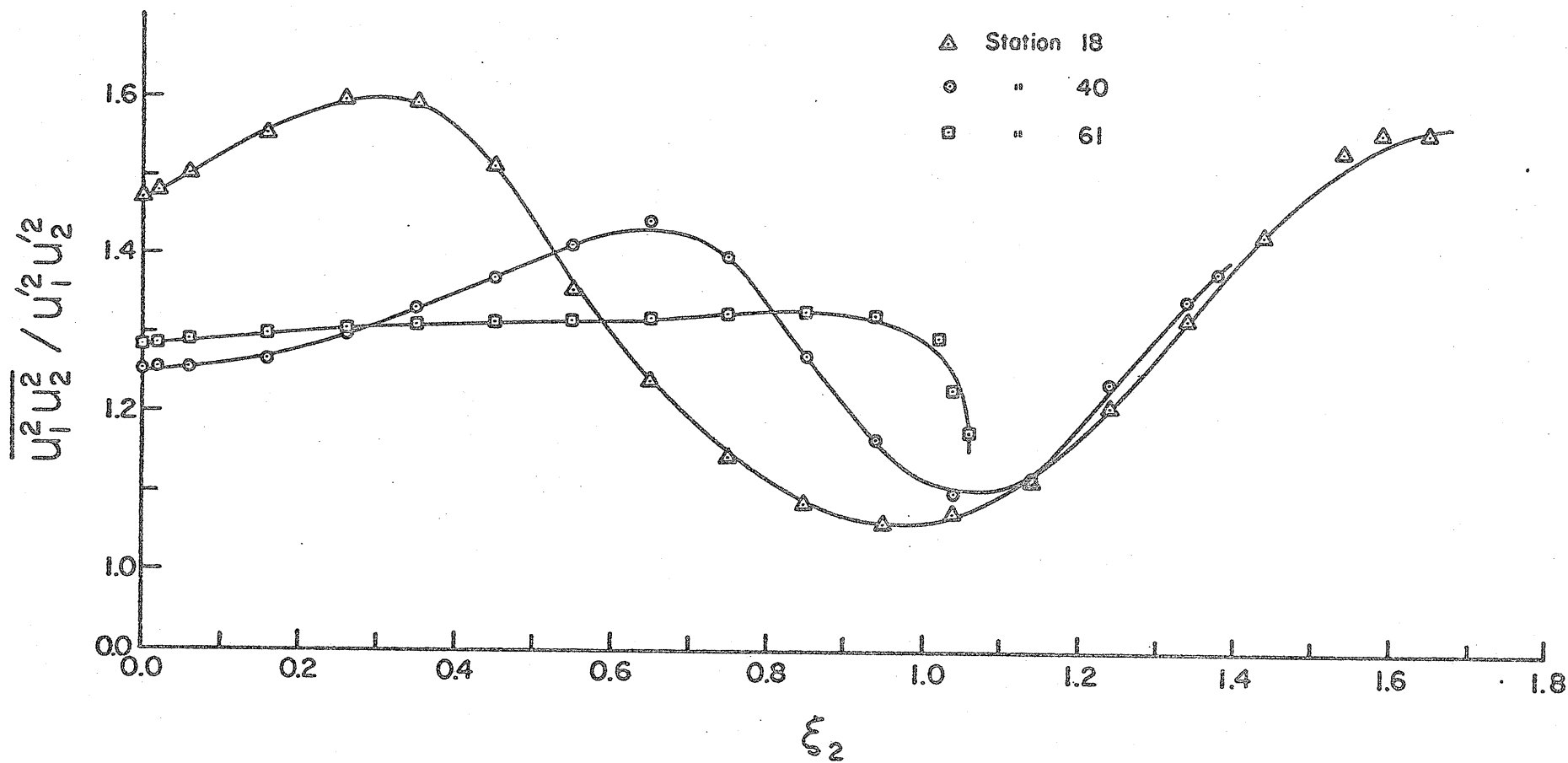


Figure 36 Fourth order correlations of $u_1^2 u_2^2$.

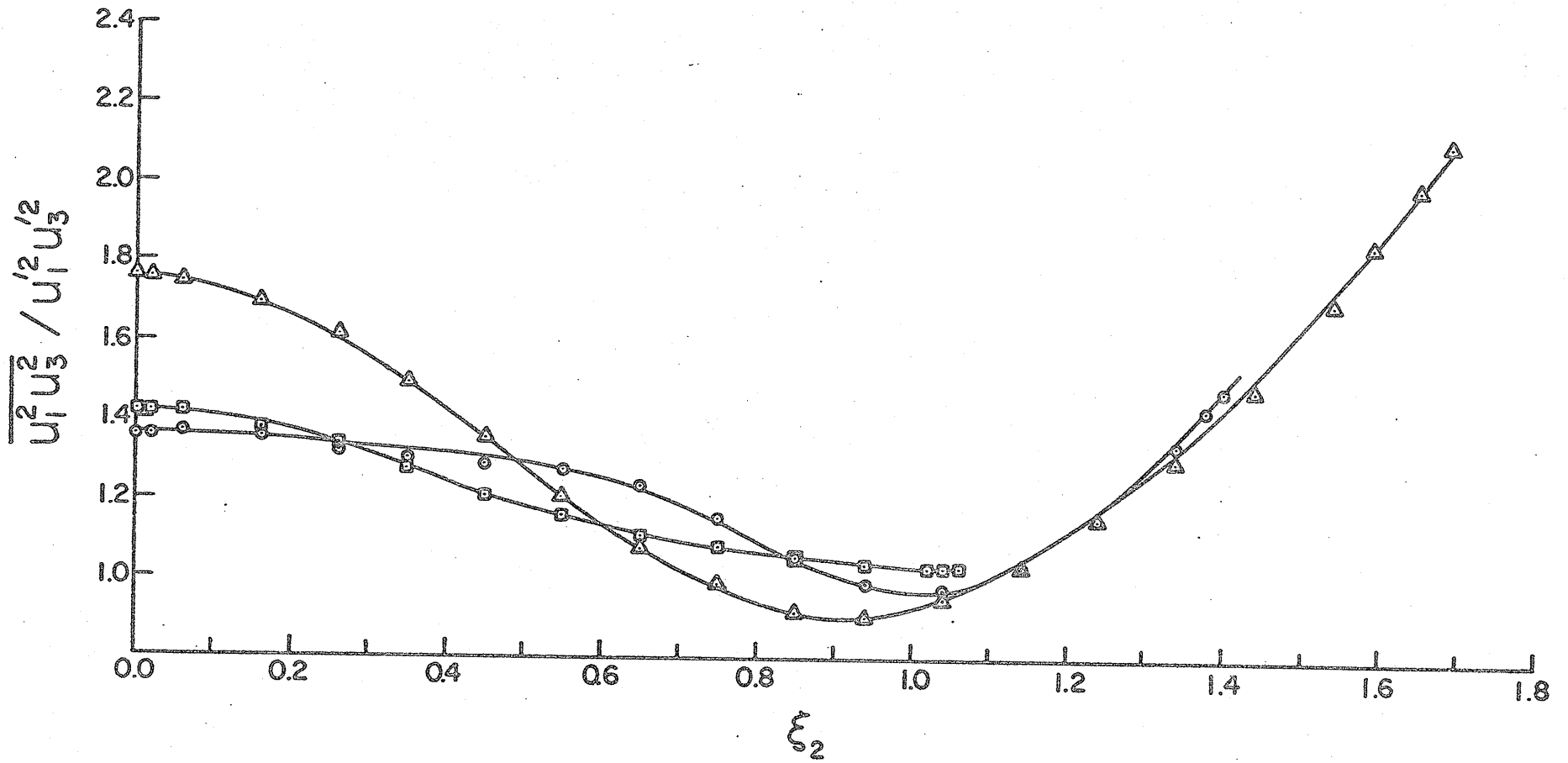


Figure 37 Fourth order correlation of $u_1^2 u_3^2$. Symbols as for figure 36.

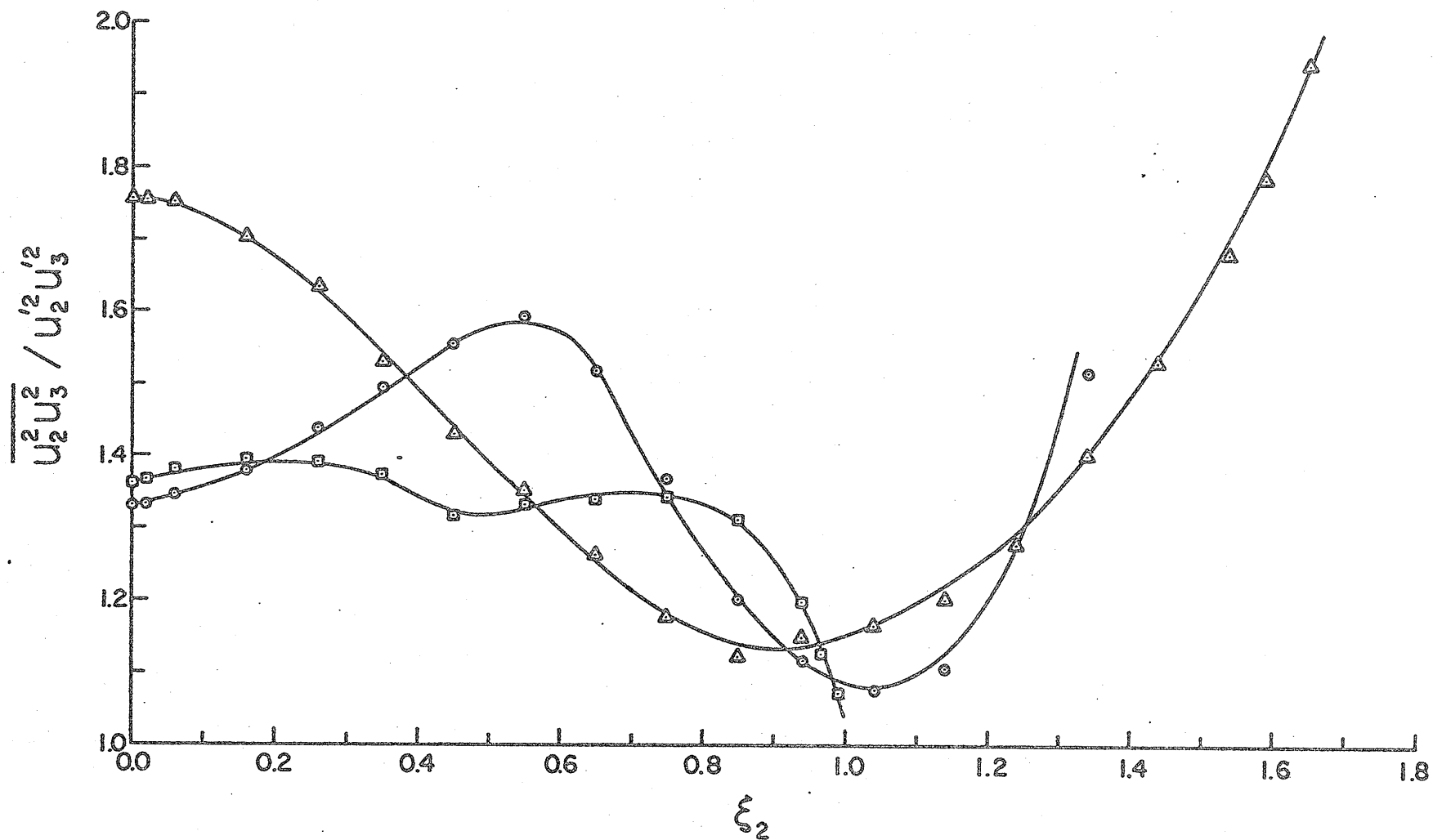


Figure 38 Fourth order correlations of $u_2^2 u_3^2$. Symbols as for figure 36.

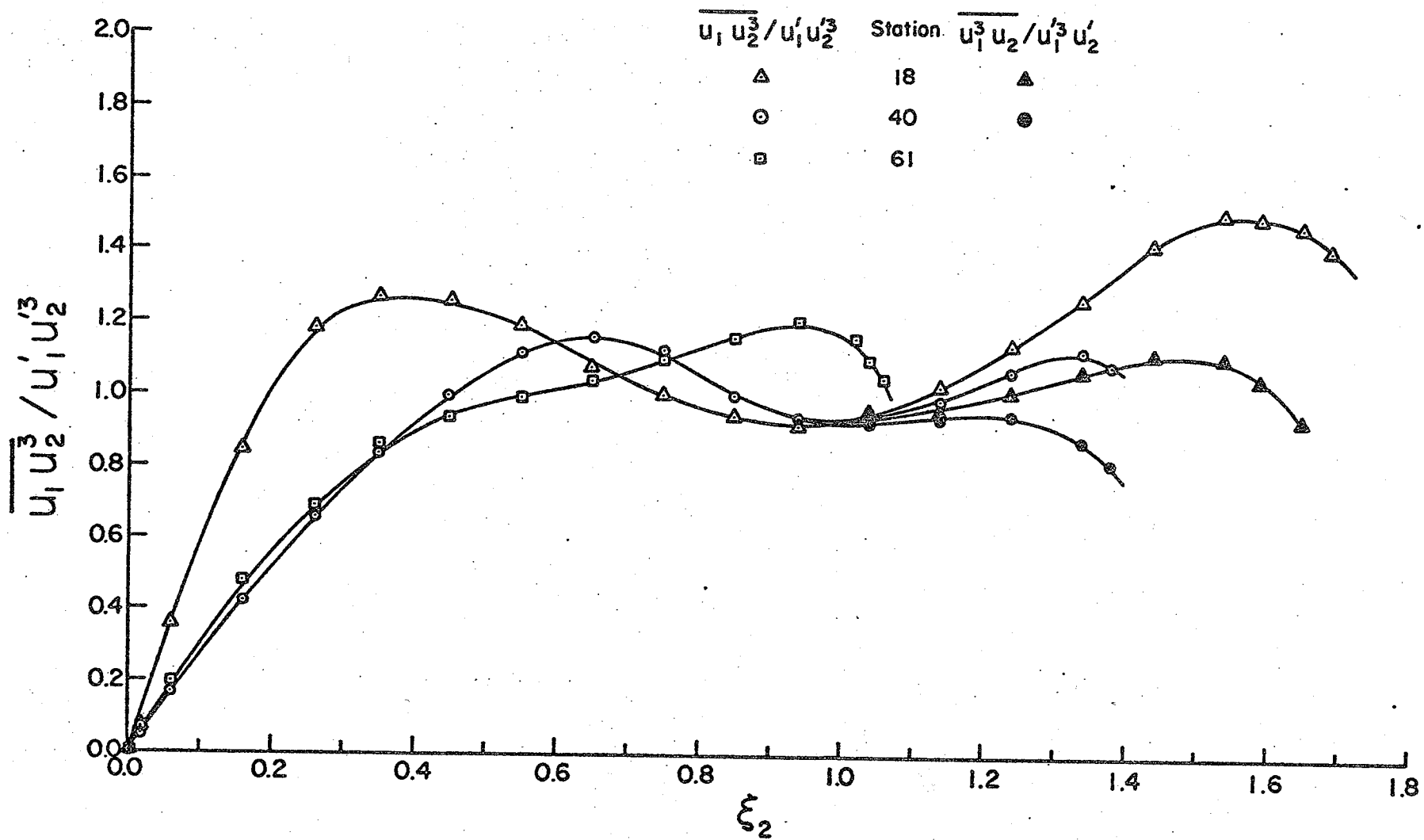


Figure 39 Fourth order correlations of $u_1^3 u_2$ and $u_1 u_2^3$.

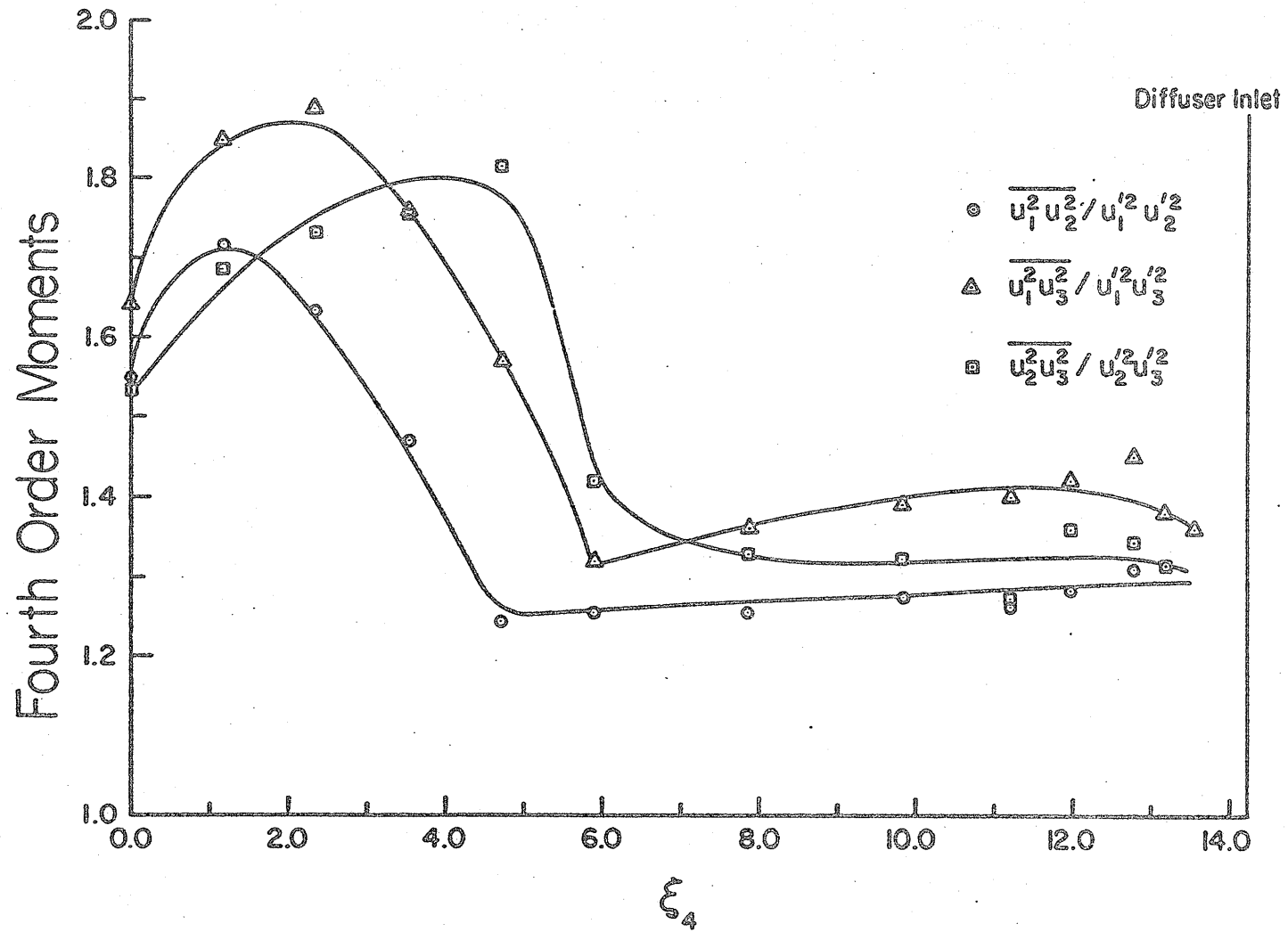


Figure 40 Distribution of fourth order correlations at the diffuser axis.

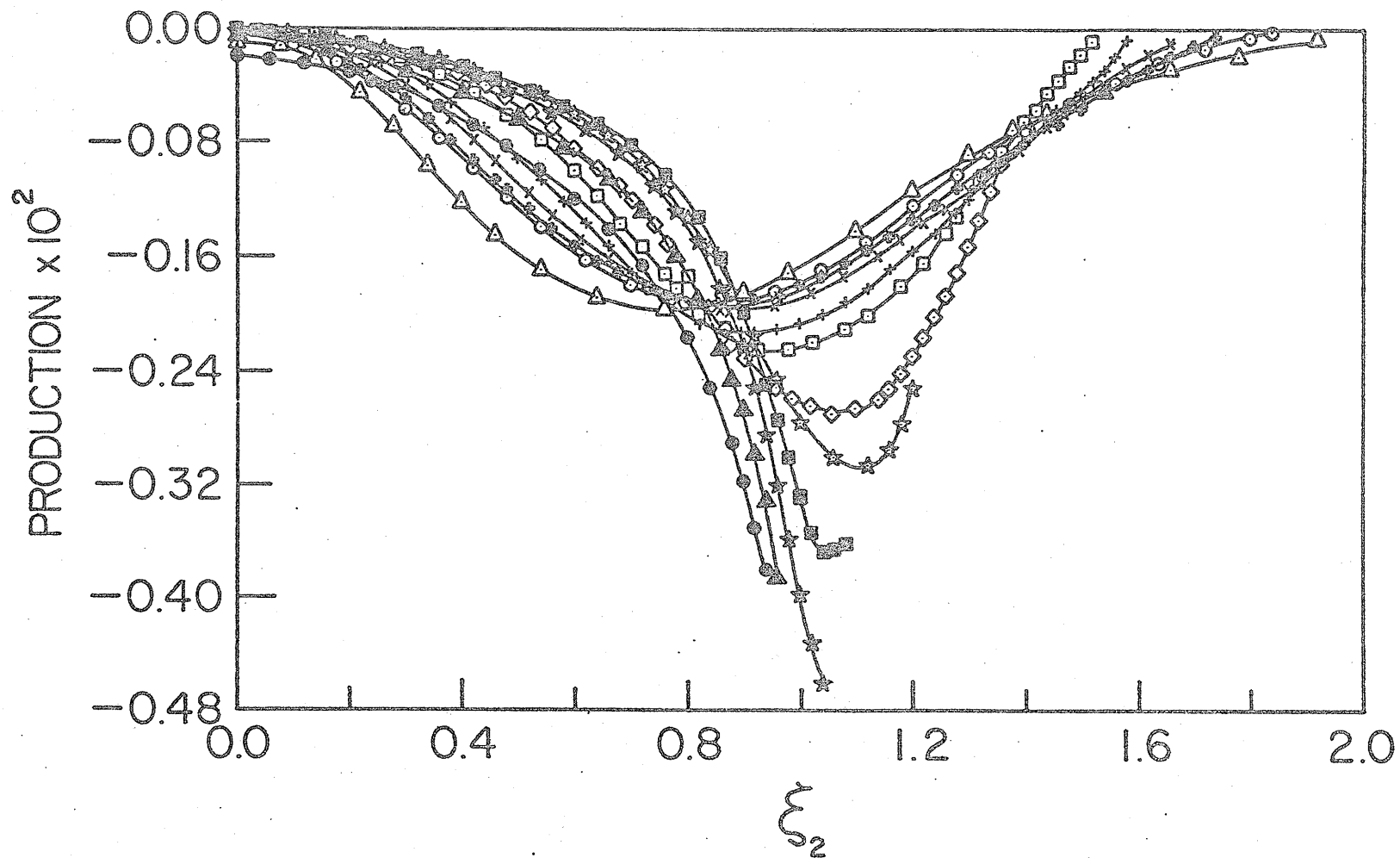


Figure 41 Turbulent kinetic energy production in the diffuser.
 Symbols as for figure 15.

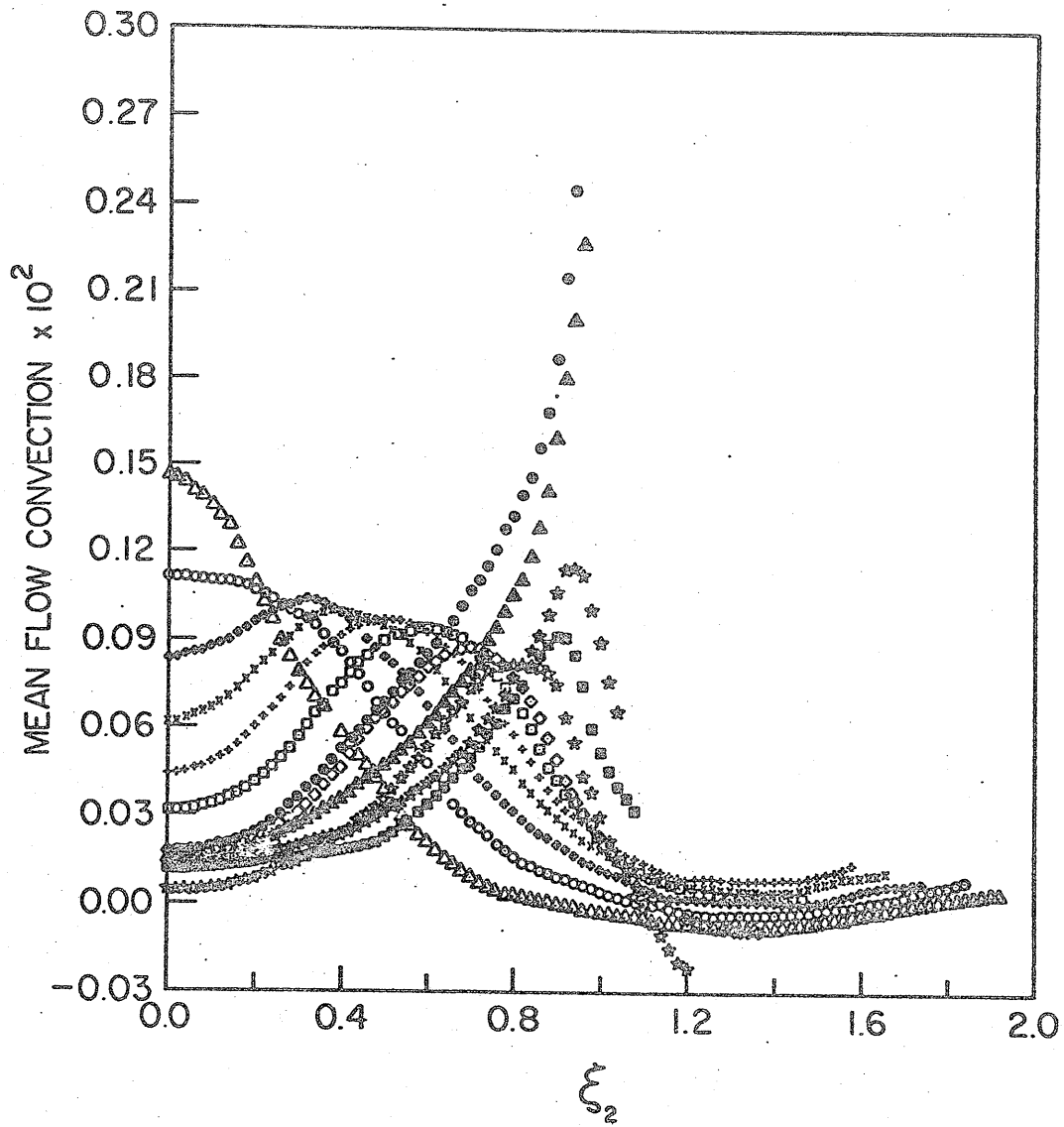


Figure 42 Variation of the mean flow convection term.
 Symbols as for figure 15.

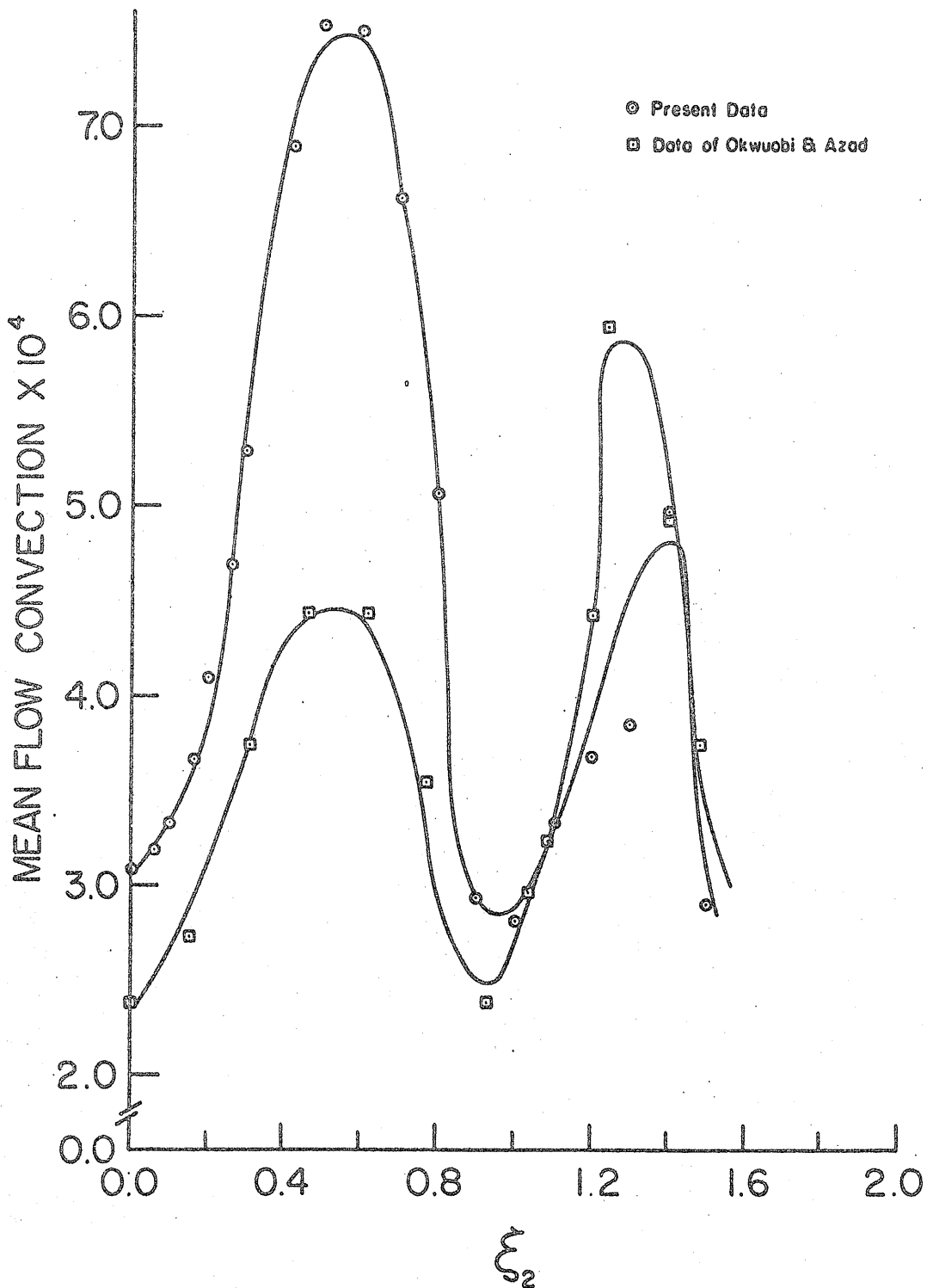


Figure 43 Comparison of the mean flow convection term at station 30 to that of Okwuobi & Azad (1973).

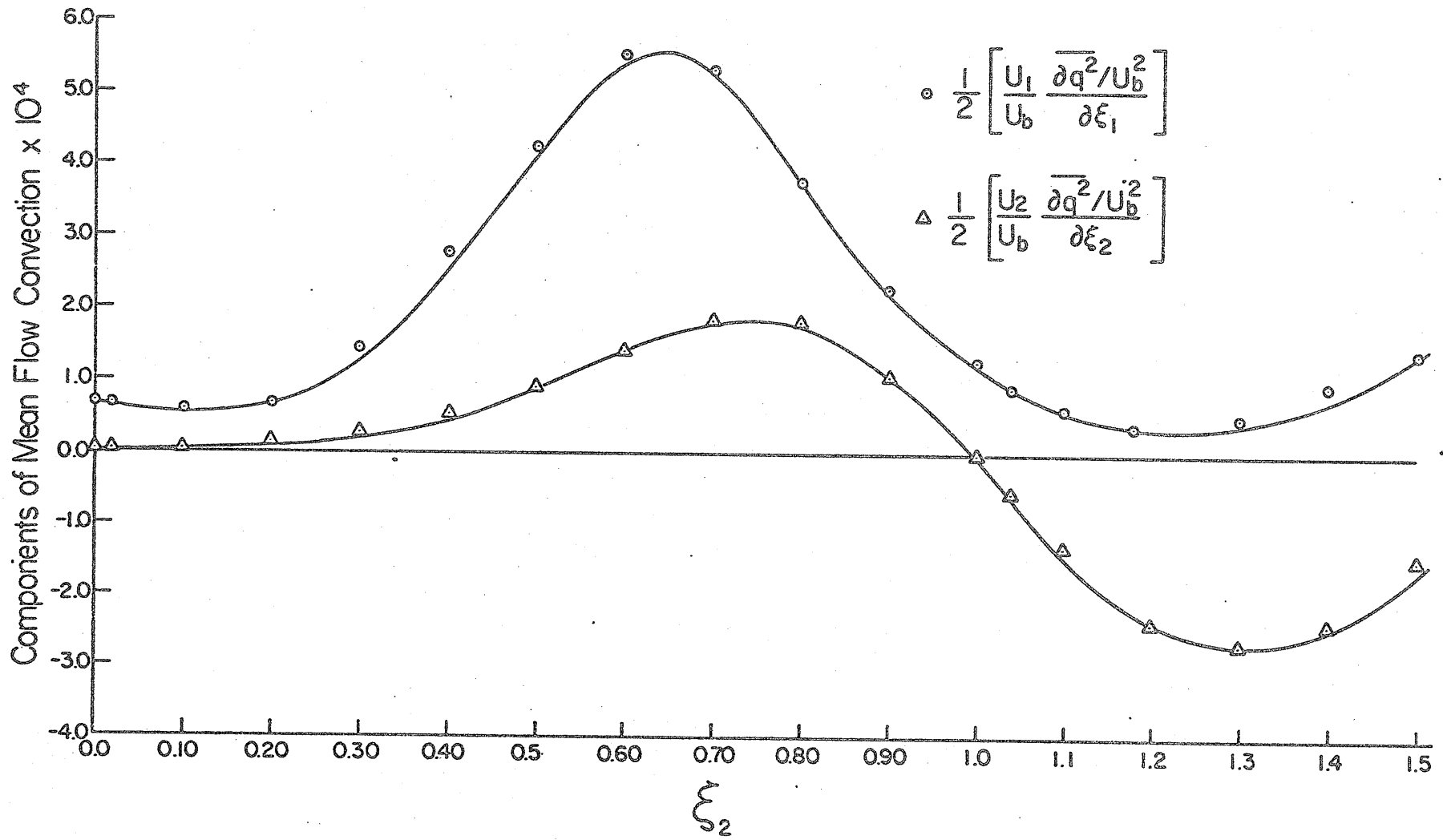


Figure 44 Radial and axial components of mean flow convection term at station 30 evaluated from the data of Okwuobi & Azad (1972).

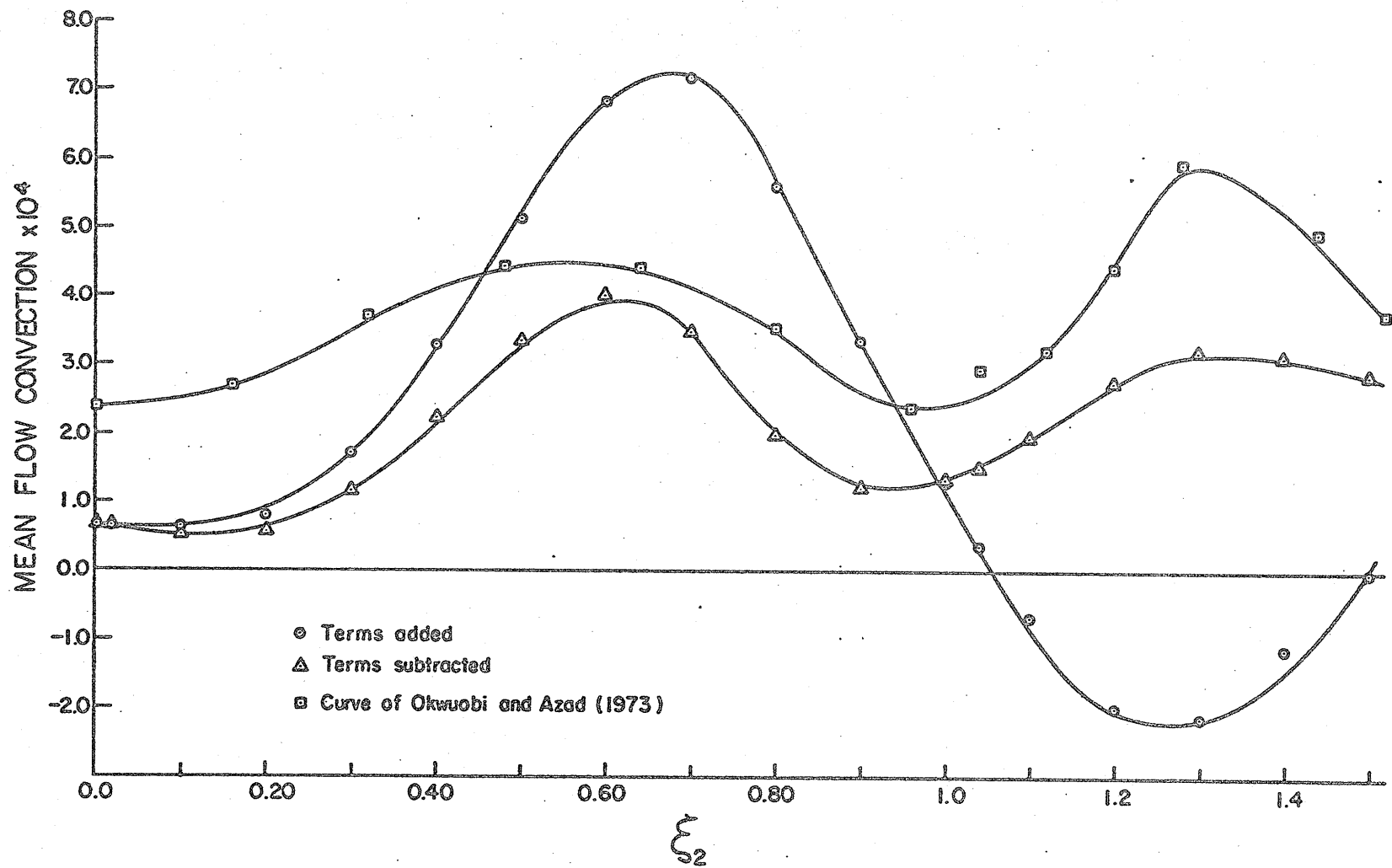


Figure 45 Mean flow convection term at station 30 obtained from figure 44.

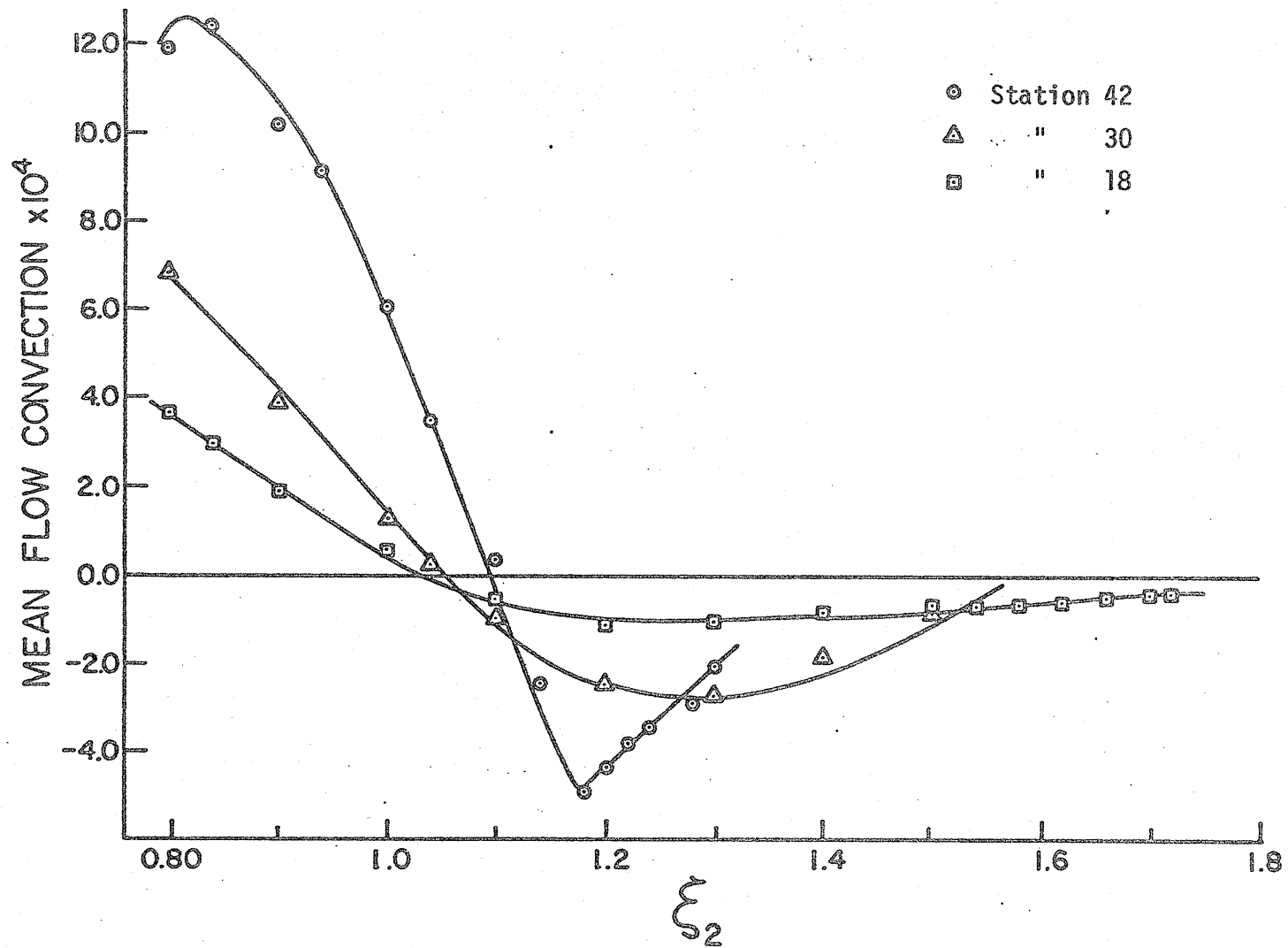


Figure 46 Mean flow convection at 3 axial stations in the wall layer evaluated from the data of Okwuobi & Azad (1972).

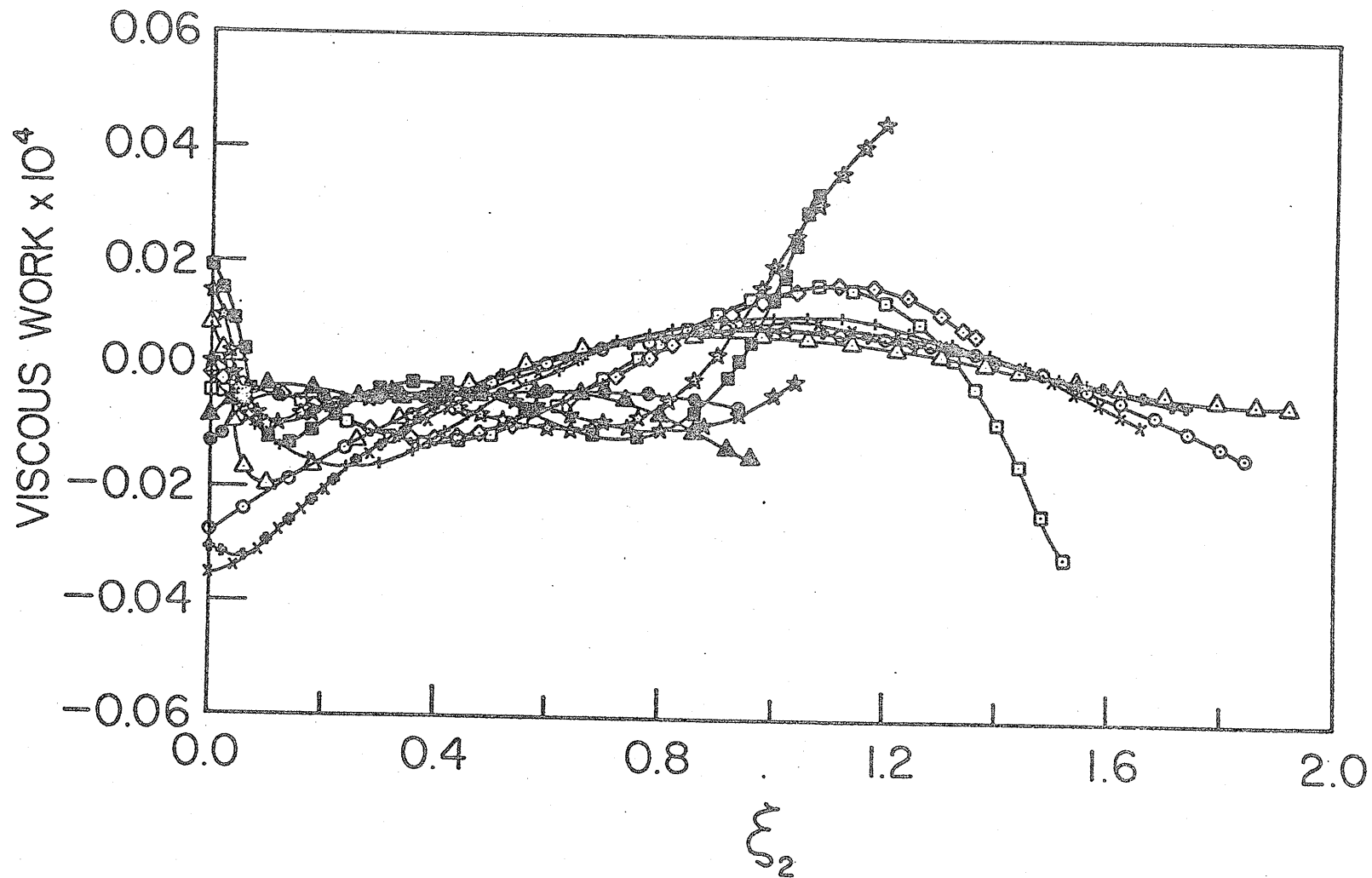


Figure 47 Viscous work term in the diffuser. Symbols as for figure 15.

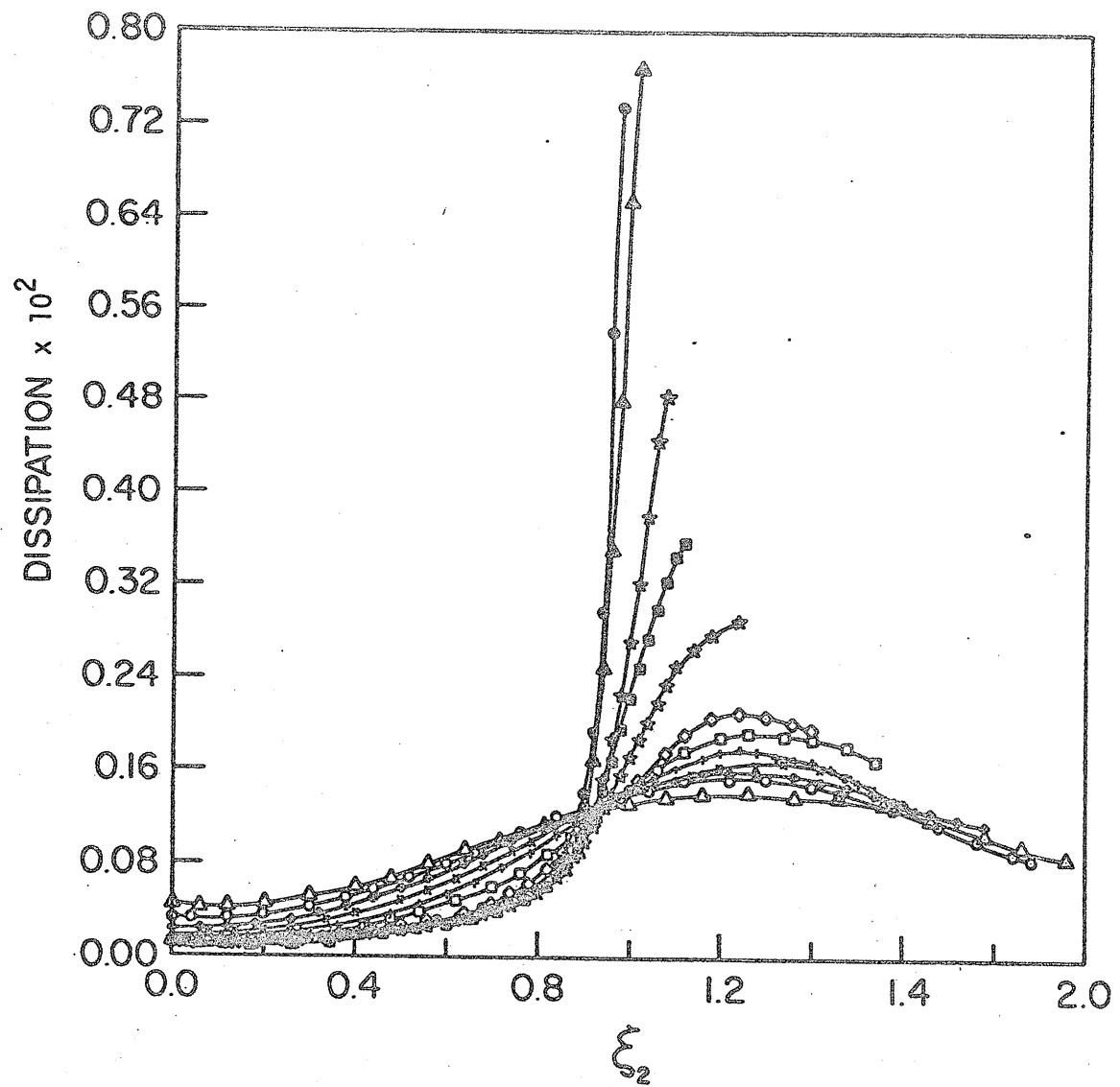


Figure 48. Distribution of the dissipation term. Symbols as for figure 15.

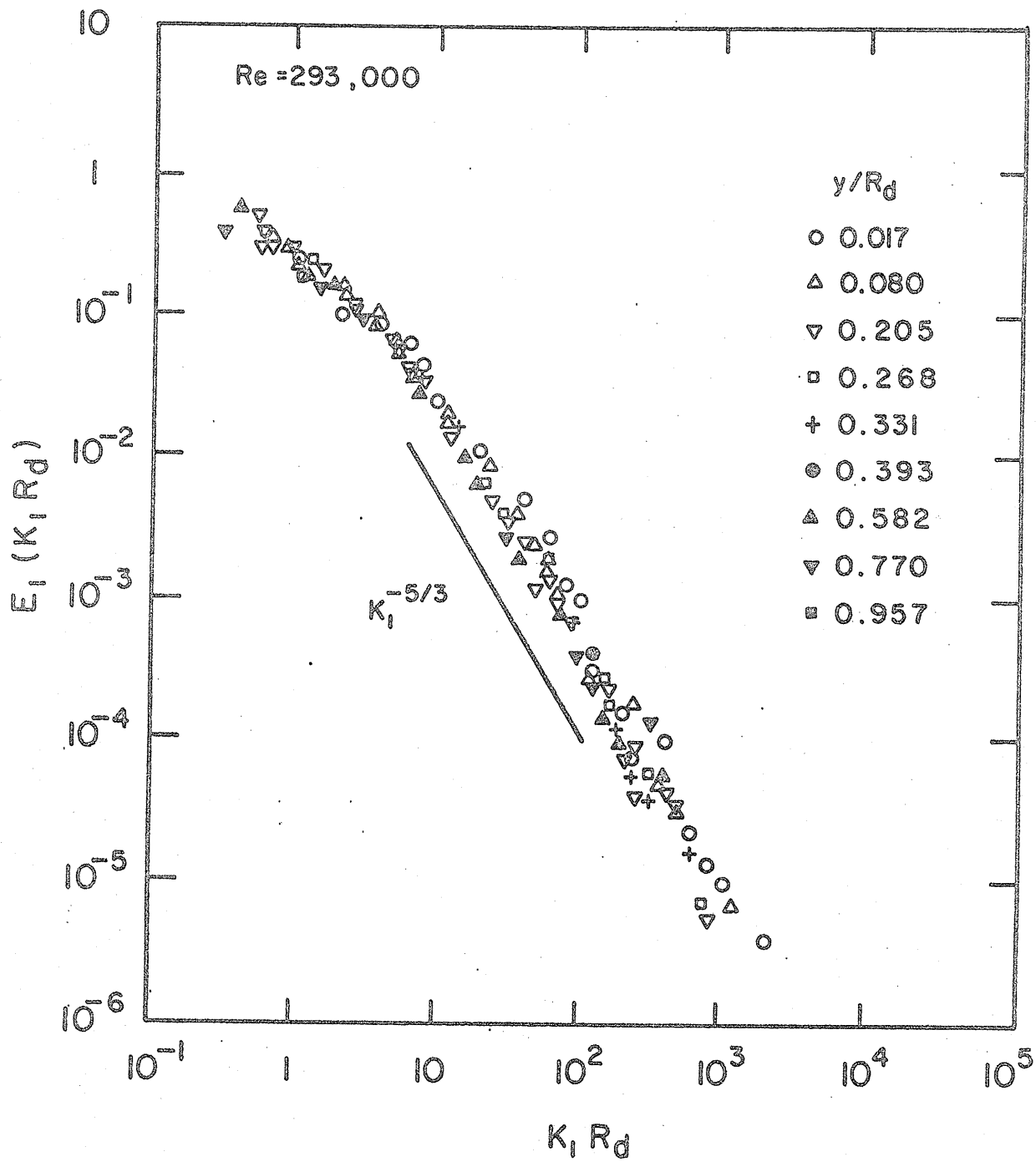


Figure 49 The u_1 spectra at station 30 from Okwuobi & Azad (1973).

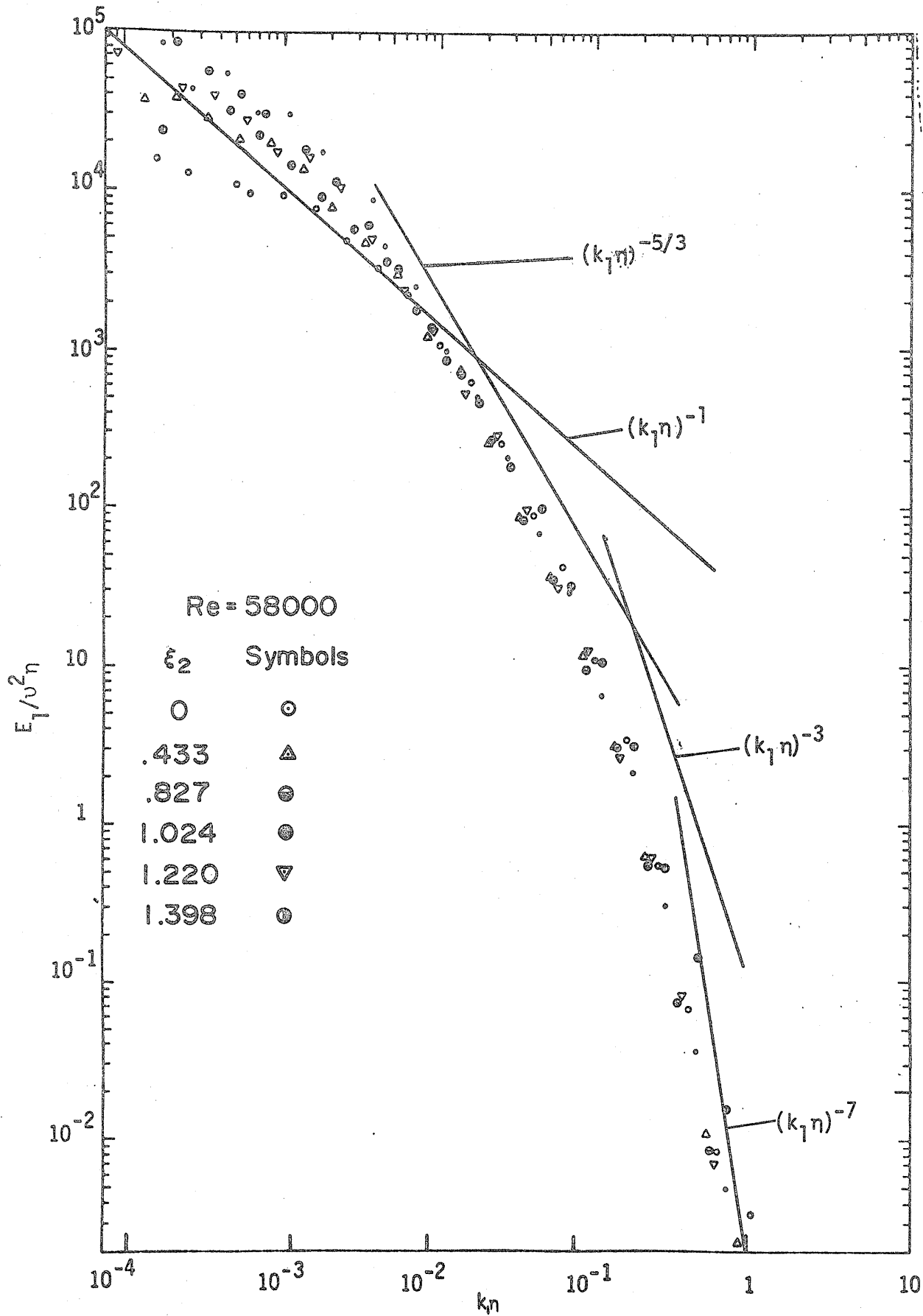


Figure 50 The u_1 spectra at station 30 from Hummel (1978).

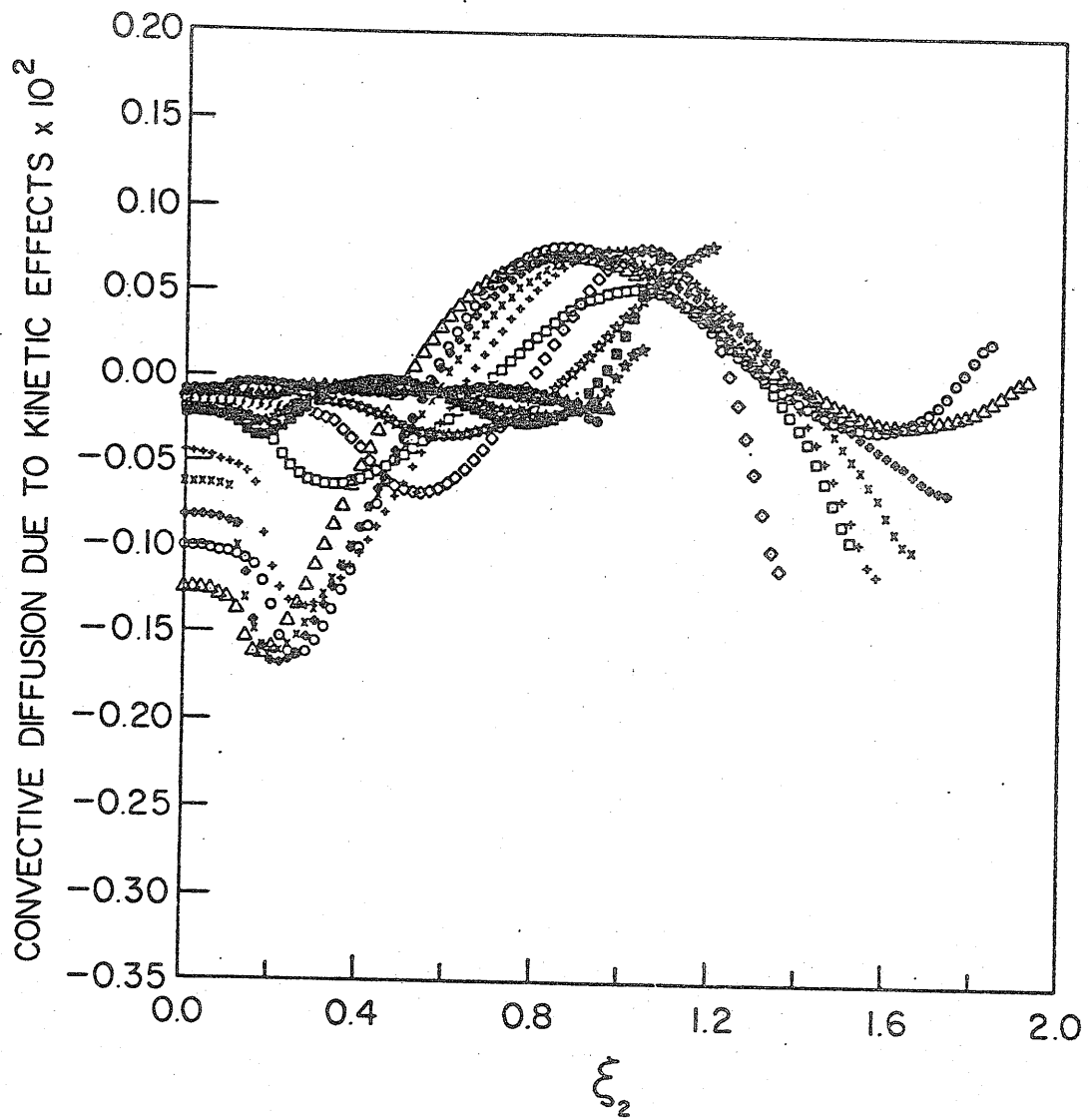


Figure 51 Convective diffusion due to kinetic effects in the diffuser. Symbols as for figure 15.

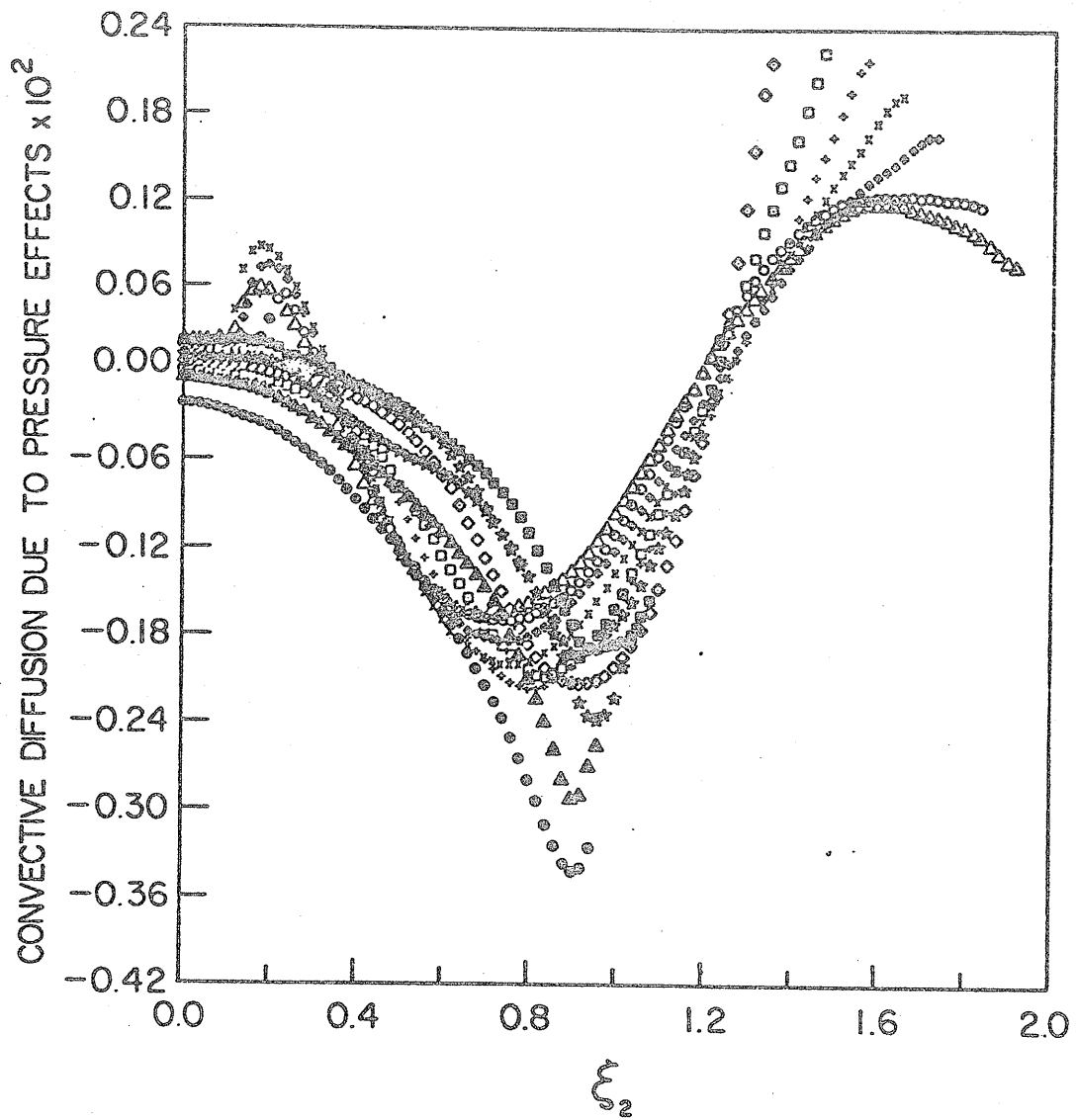


Figure 52 Convective diffusion due to pressure effects in the diffuser. Symbols as for figure 15.

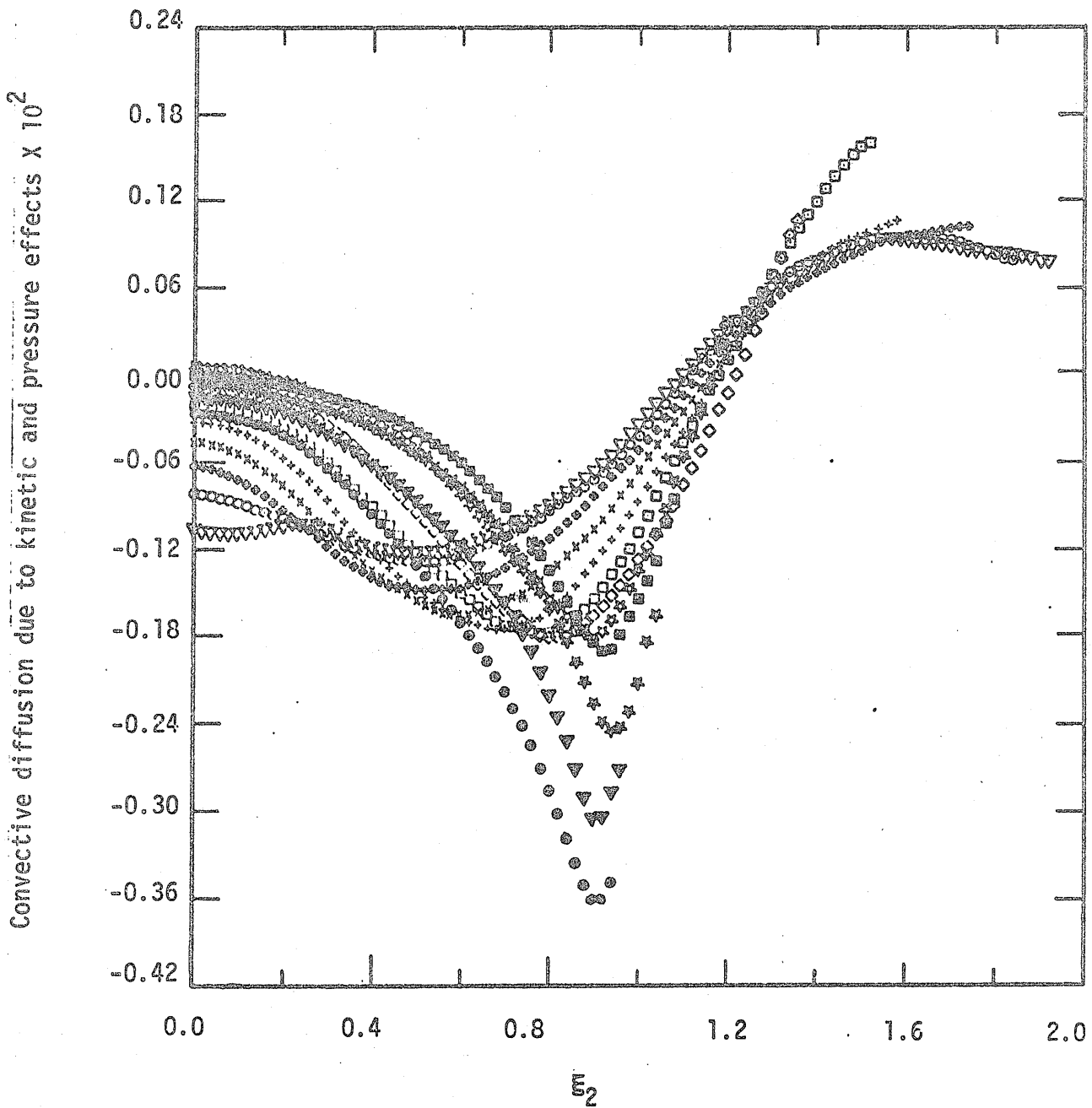


Figure 53 Distribution of the convective diffusion due to kinetic and pressure effects. Symbols as for Figure 53.

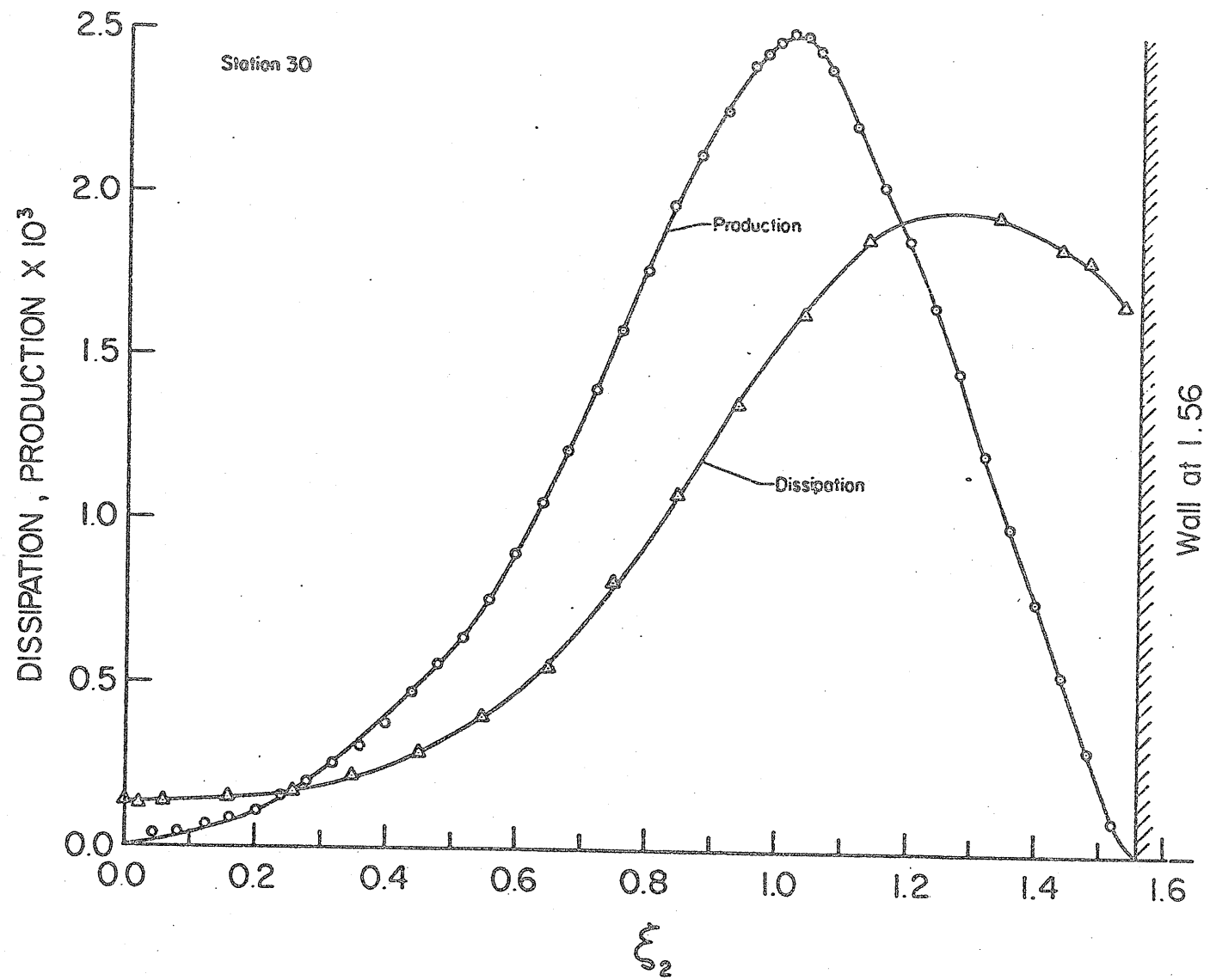


Figure 54 Comparison of the production and dissipation terms at station 30.

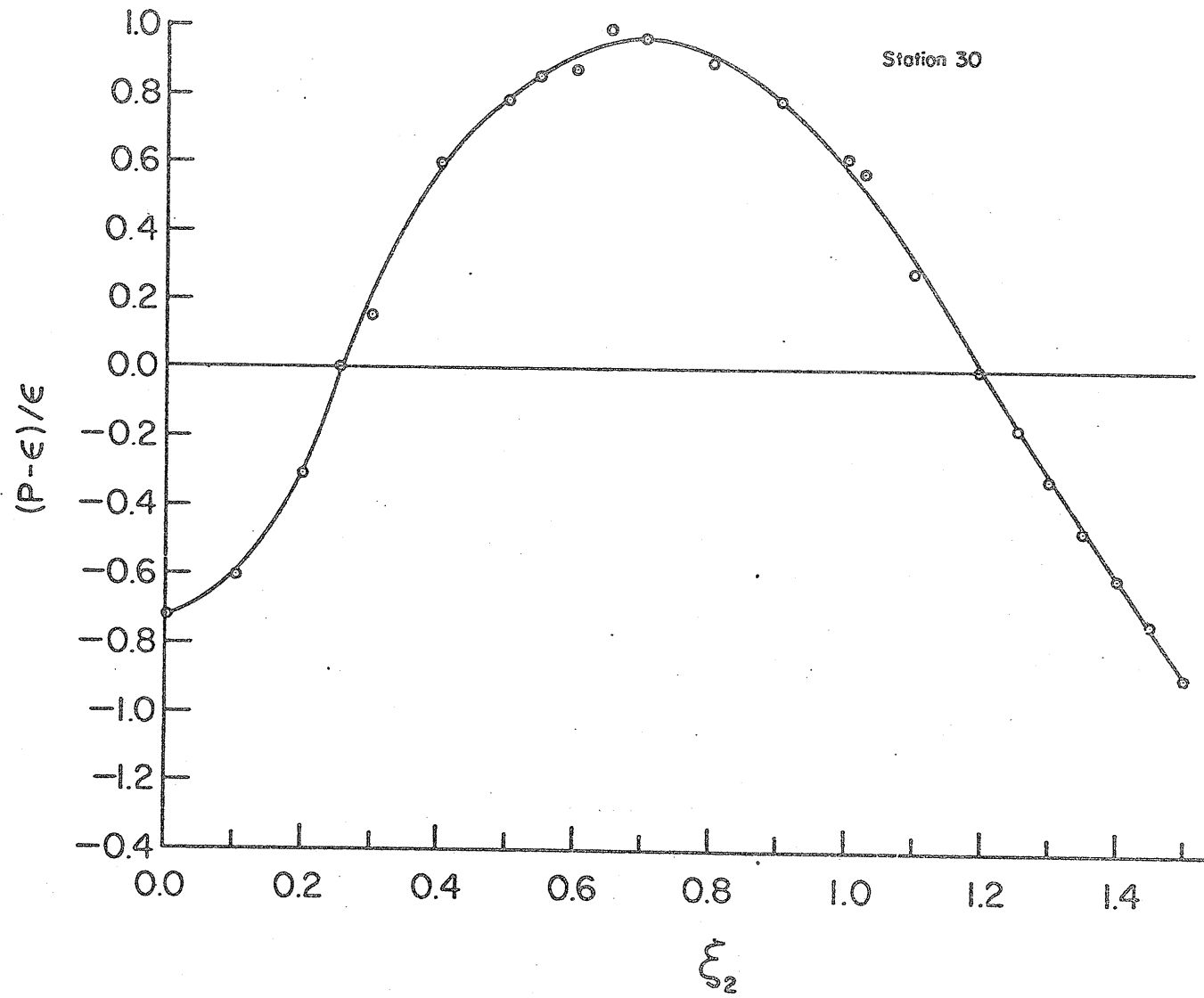


Figure 55 Variation of the ratio of excess production to dissipation at station 30.

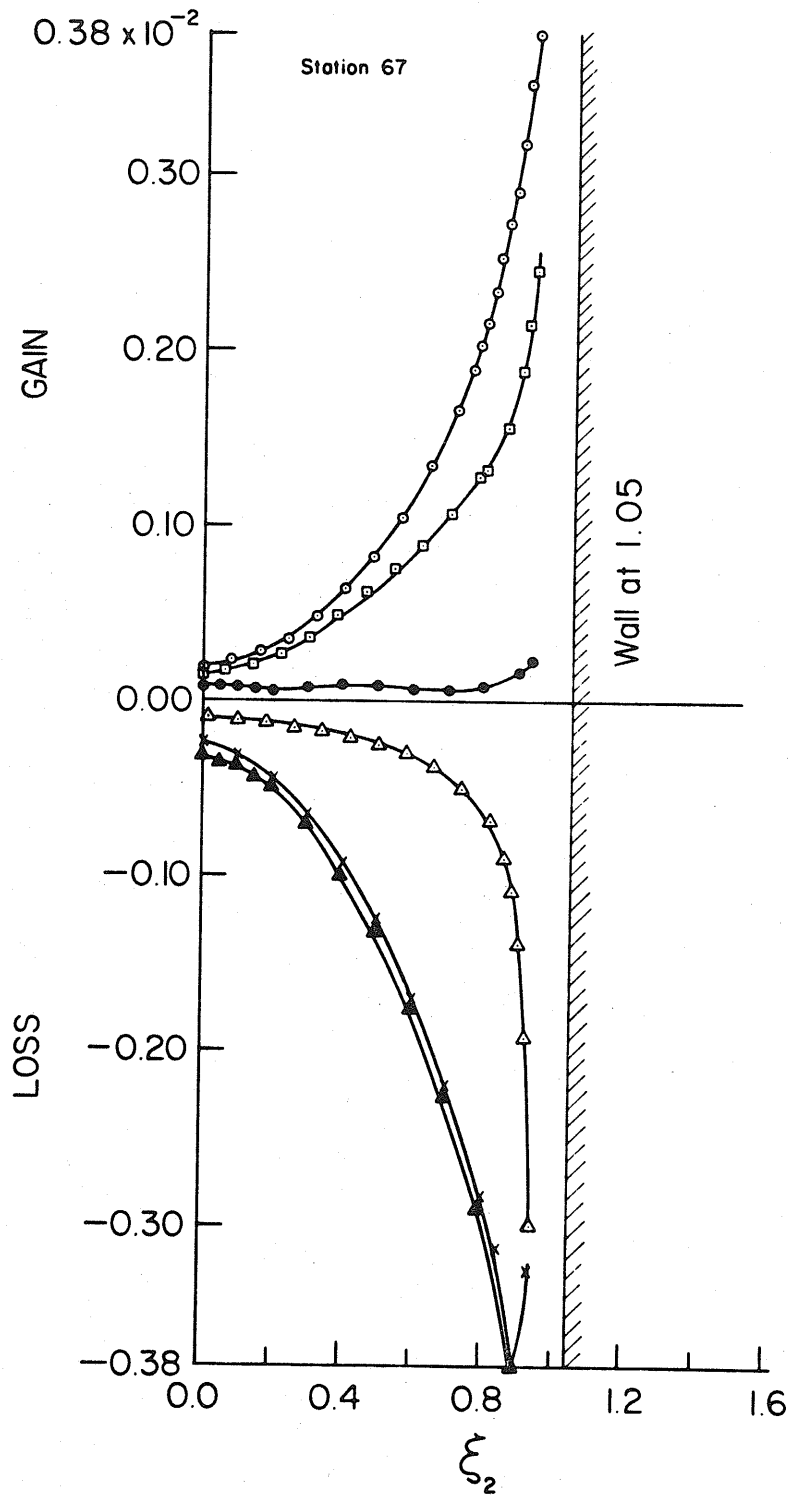


Figure 56 Turbulent kinetic energy balance in the diffuser at station 67. Symbols as for figure 60.

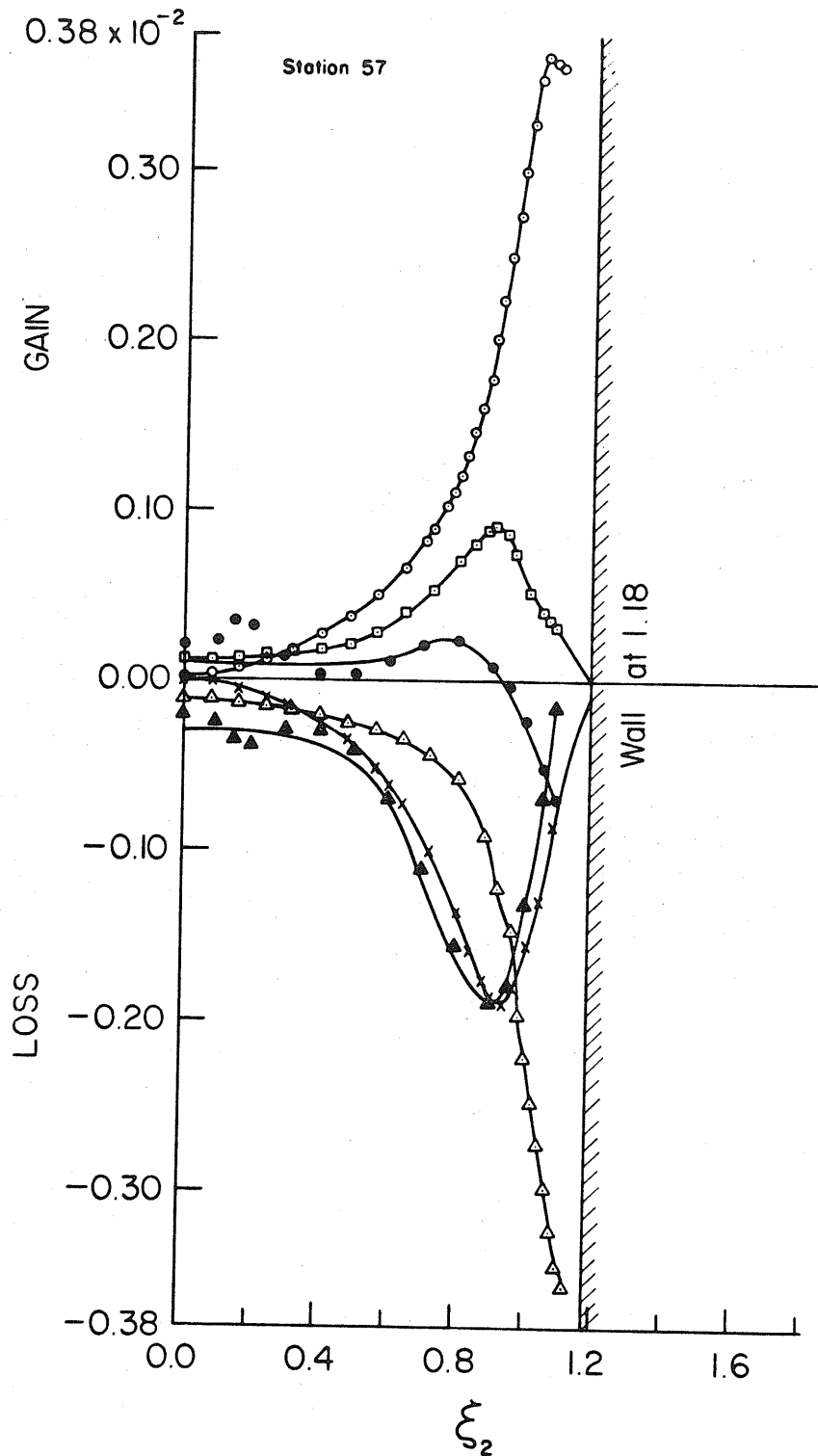


Figure 57 Turbulent kinetic energy balance in the diffuser at station 57. Symbols as for figure 60.

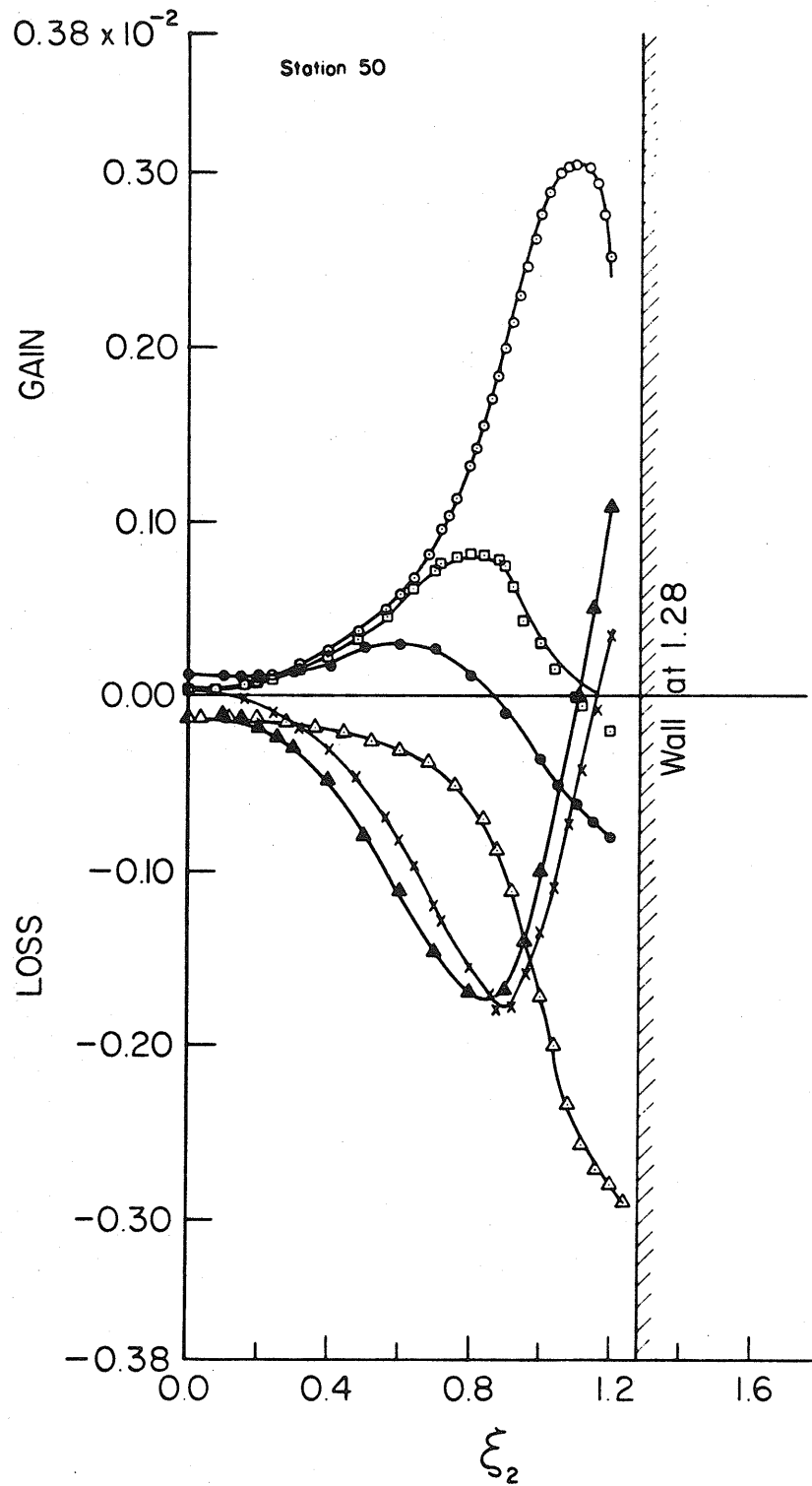


Figure 58 Turbulent kinetic energy balance in the diffuser at station 50. Symbols as for figure 60.

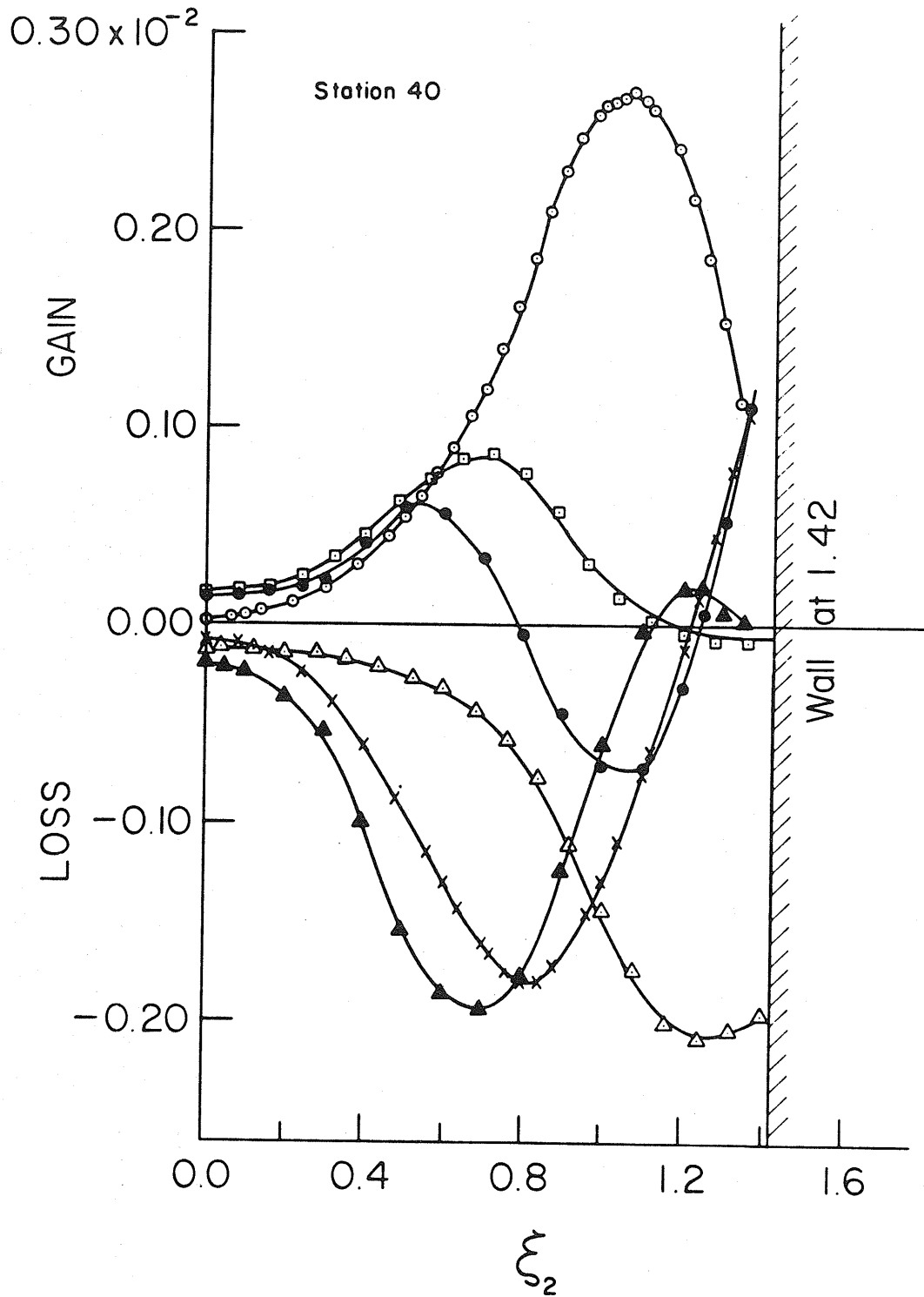


Figure 59 Turbulent kinetic energy balance in the diffuser at station 40. Symbols as for figure 60.

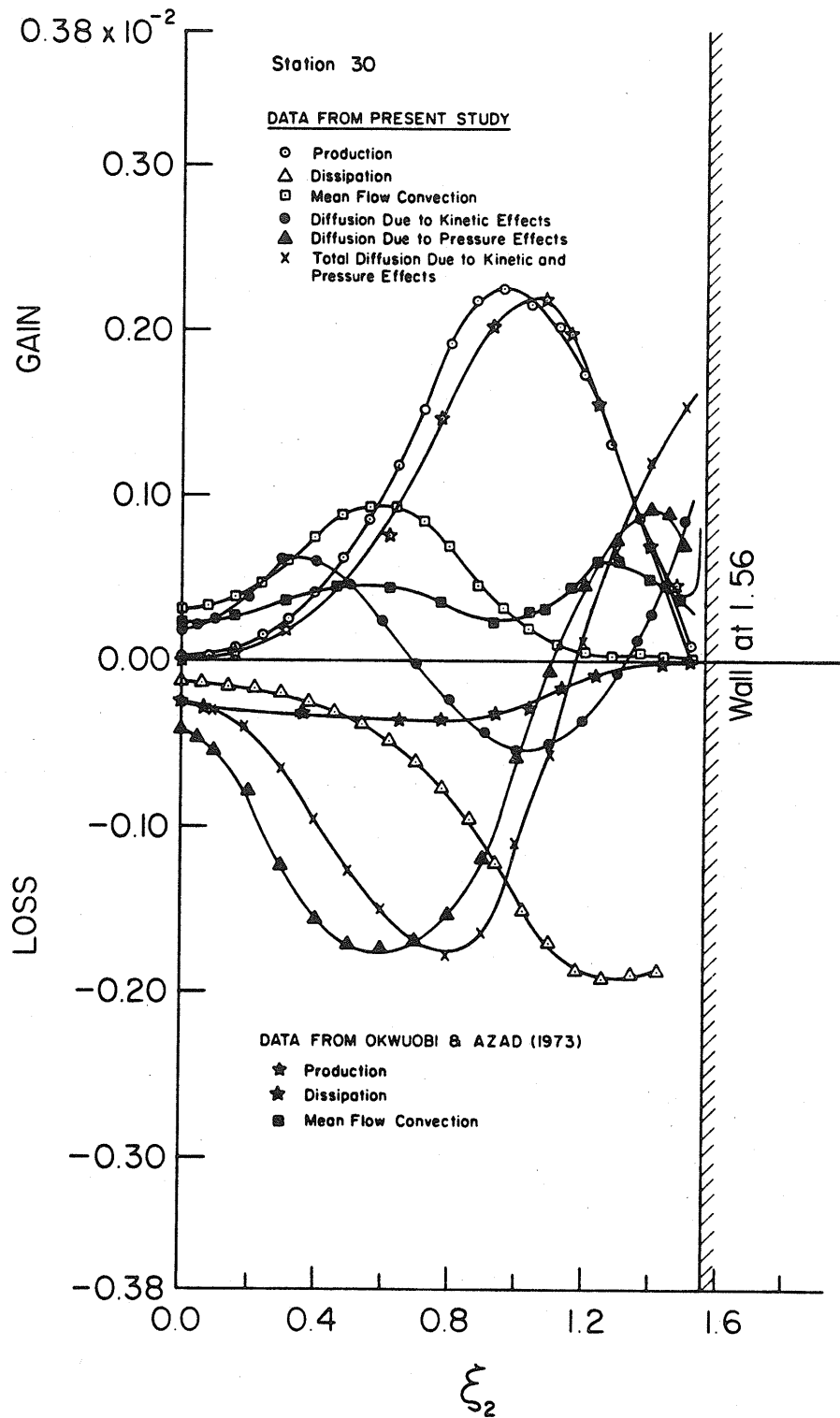


Figure 60 Turbulent kinetic energy balance in the diffuser at station 30.

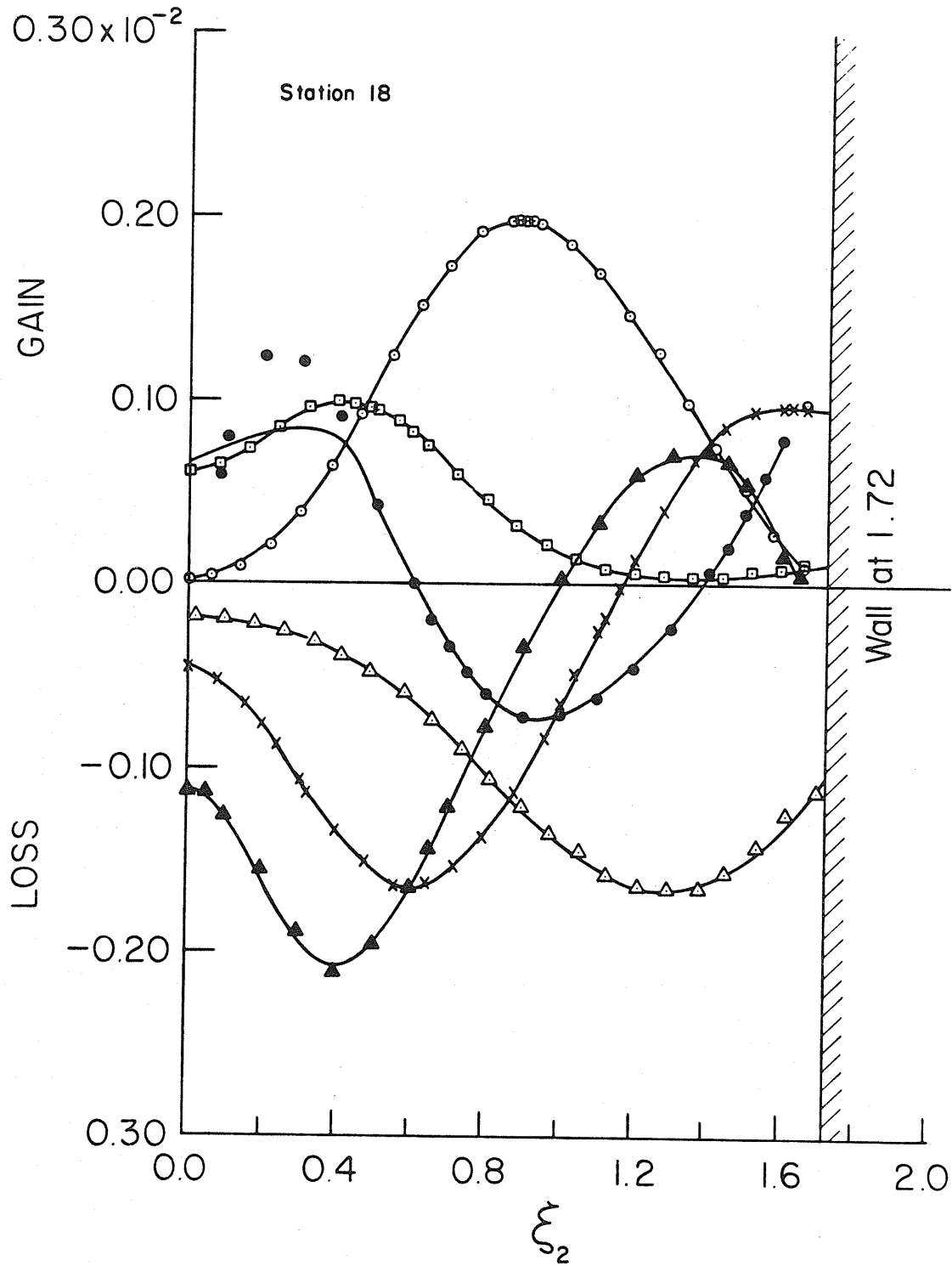


Figure 61 Turbulent kinetic energy balance in the diffuser at station 18. Symbols as for figure 61.

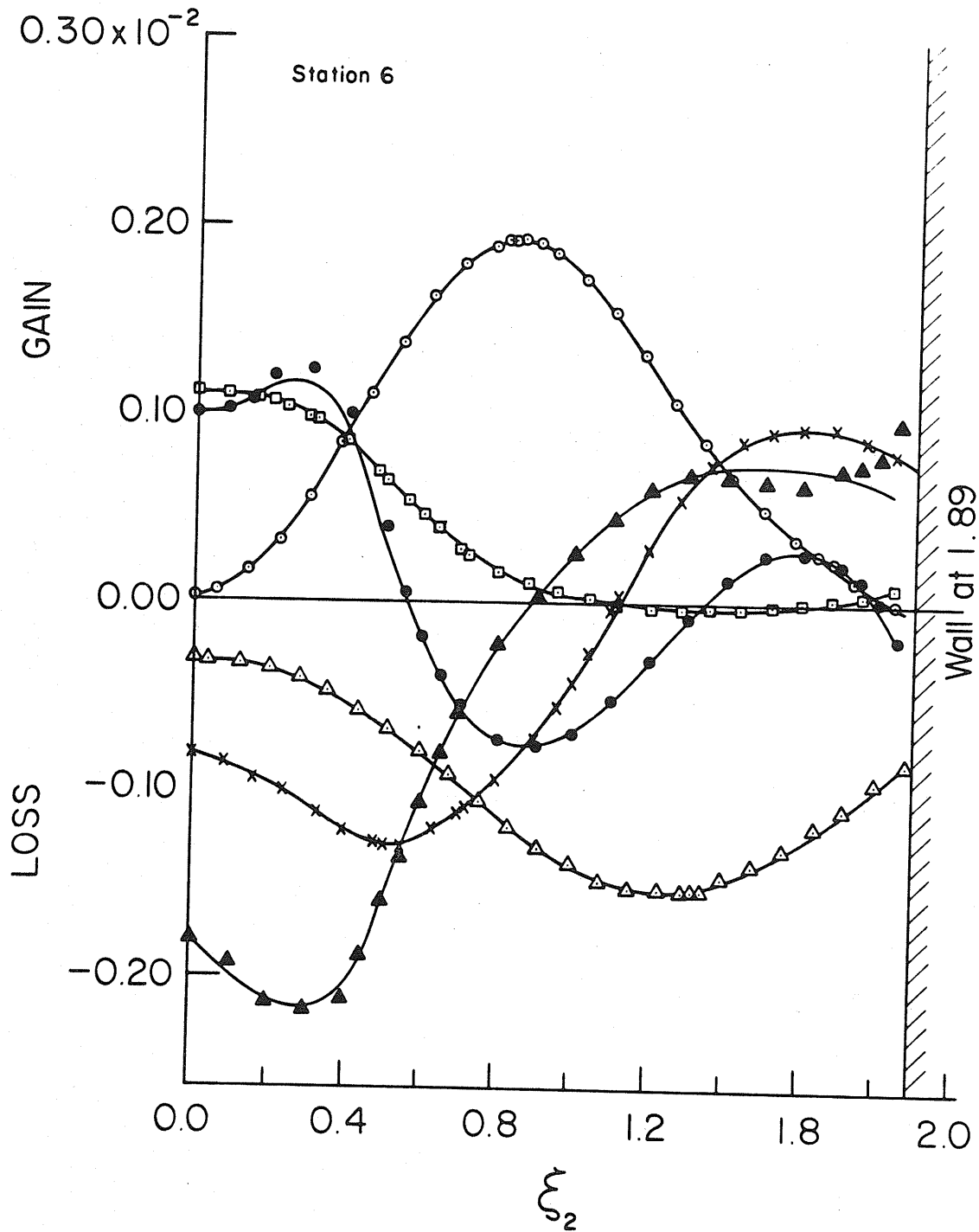


Figure 62 Turbulent kinetic energy balance in the diffuser at station 6. Symbols as for figure 60.

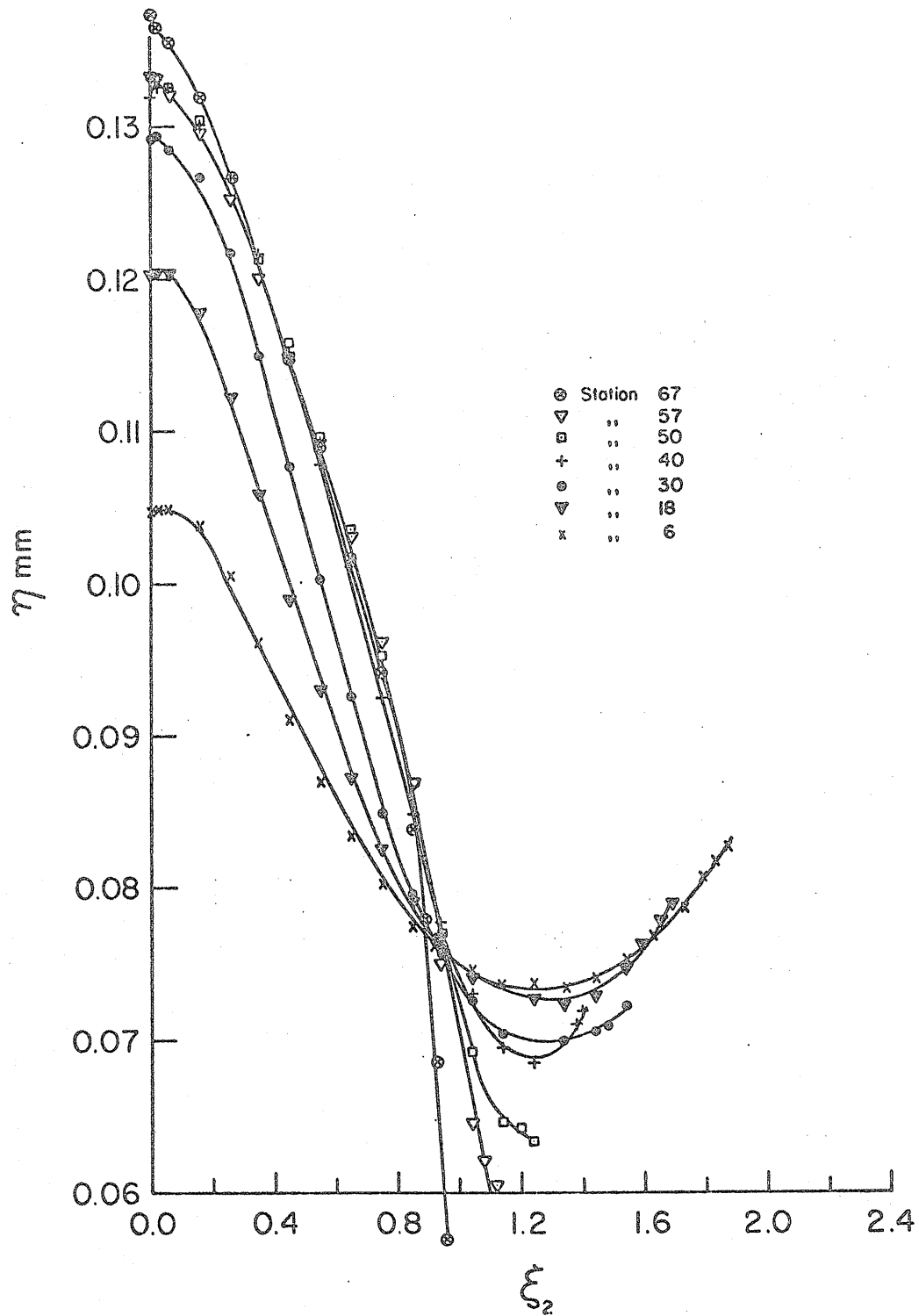


Figure 63 Variation of the Kolmogoroff length scale η .

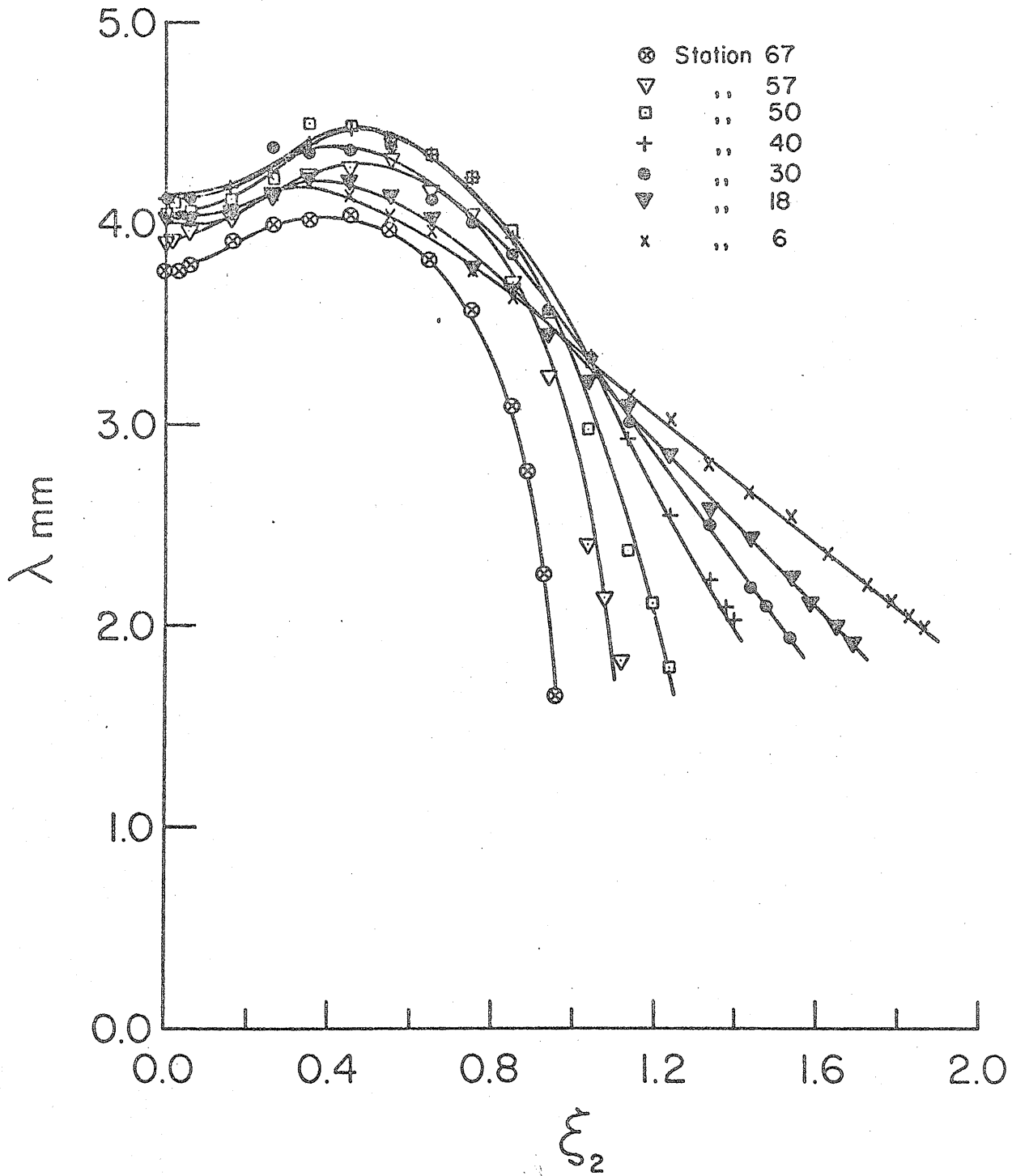


Figure 64 Distribution of the Taylor's microscale λ .

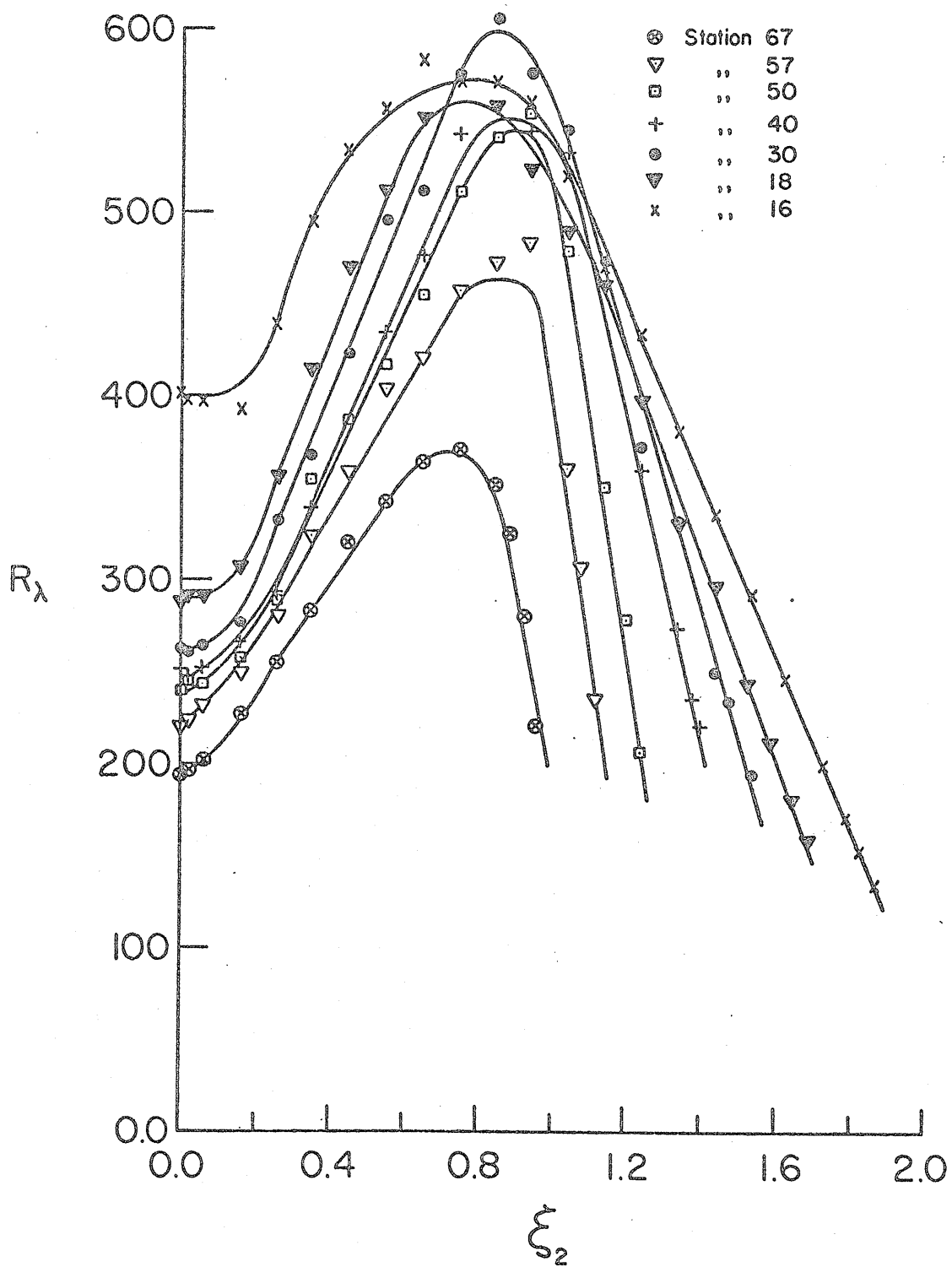


Figure 65 Variation of the turbulence Reynolds number R_λ of the flow.

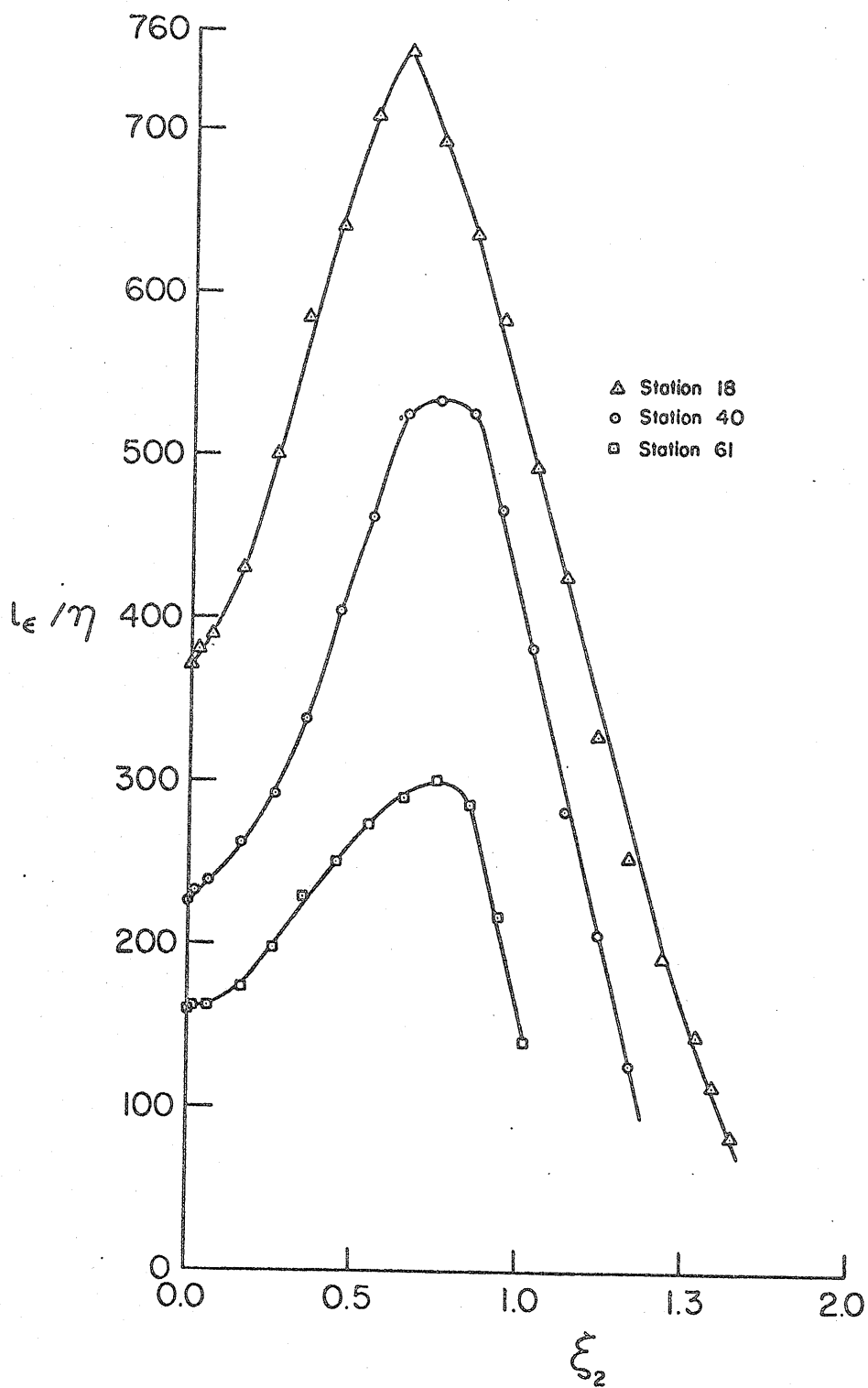


Figure 66 Ratio of the characteristic length scale to that of the Kolmogoroff length scale L_ϵ/η .

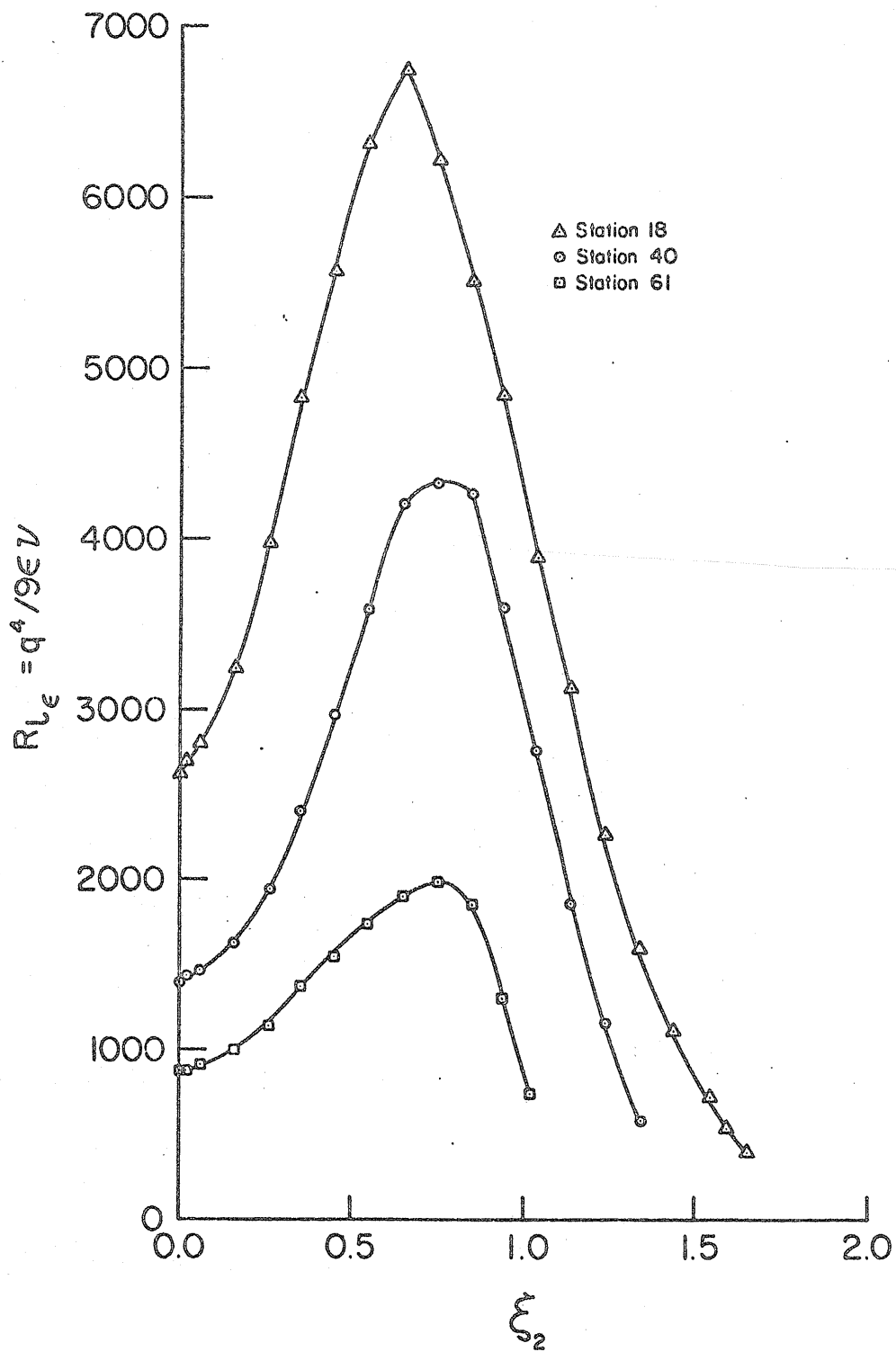


Figure 67 Characteristic Reynolds number ($R_{L\epsilon}$) in the diffuser.

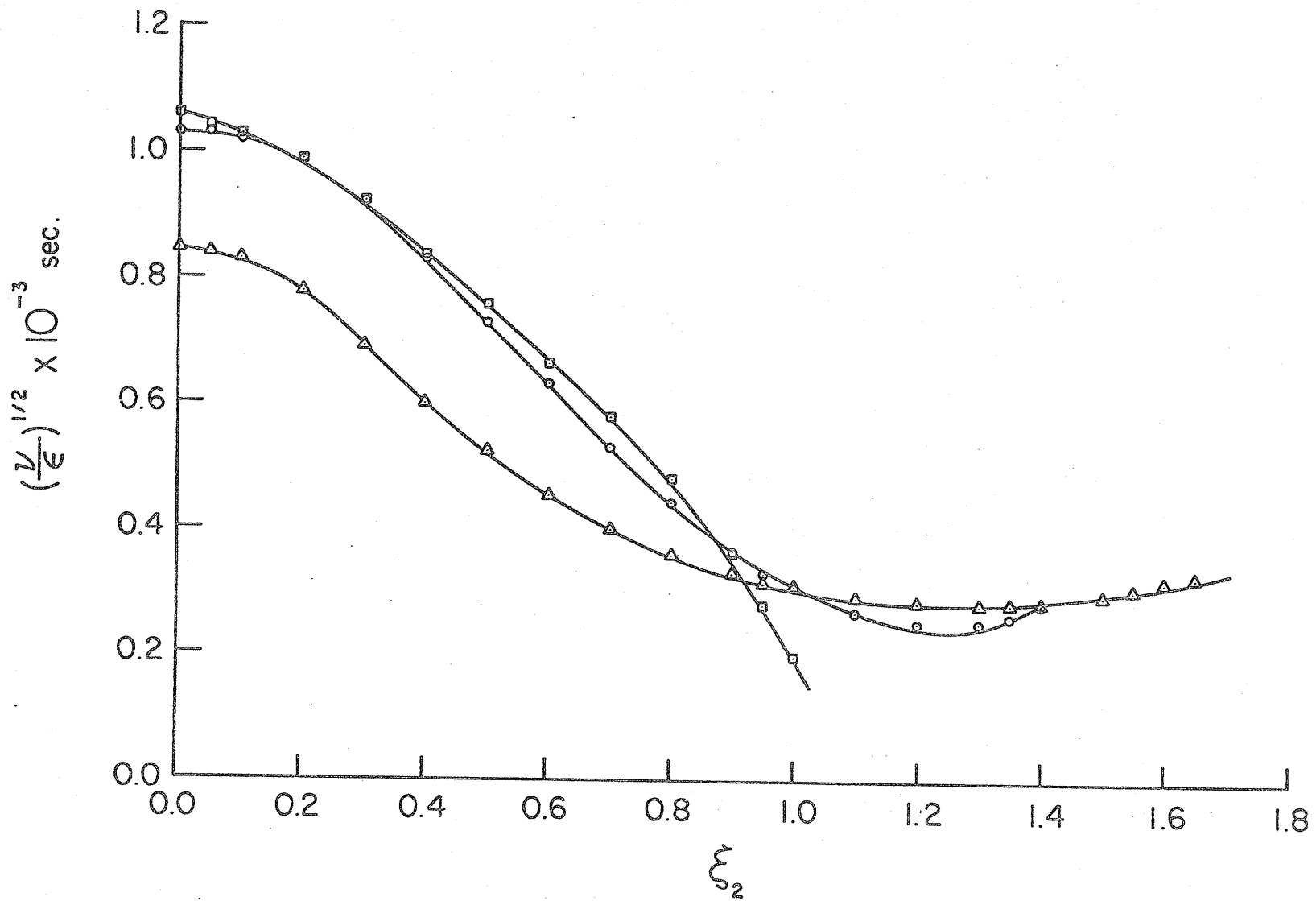


Figure 68 Distribution of the Kolmogoroff time scale.
 Symbols as for figure 67.

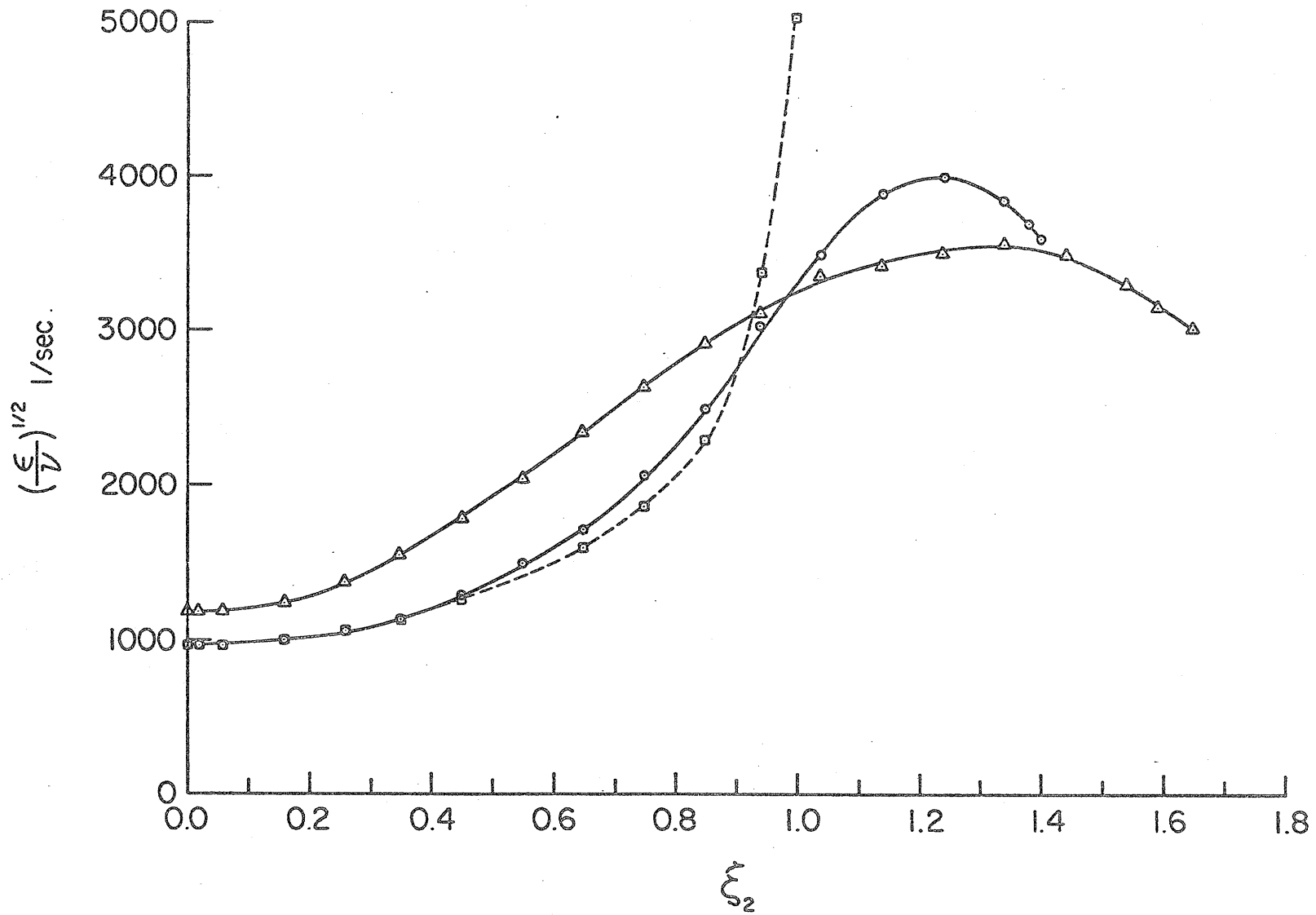


Figure 69 Turbulent vorticity curves for 3 stations. Symbols as for figure 67.

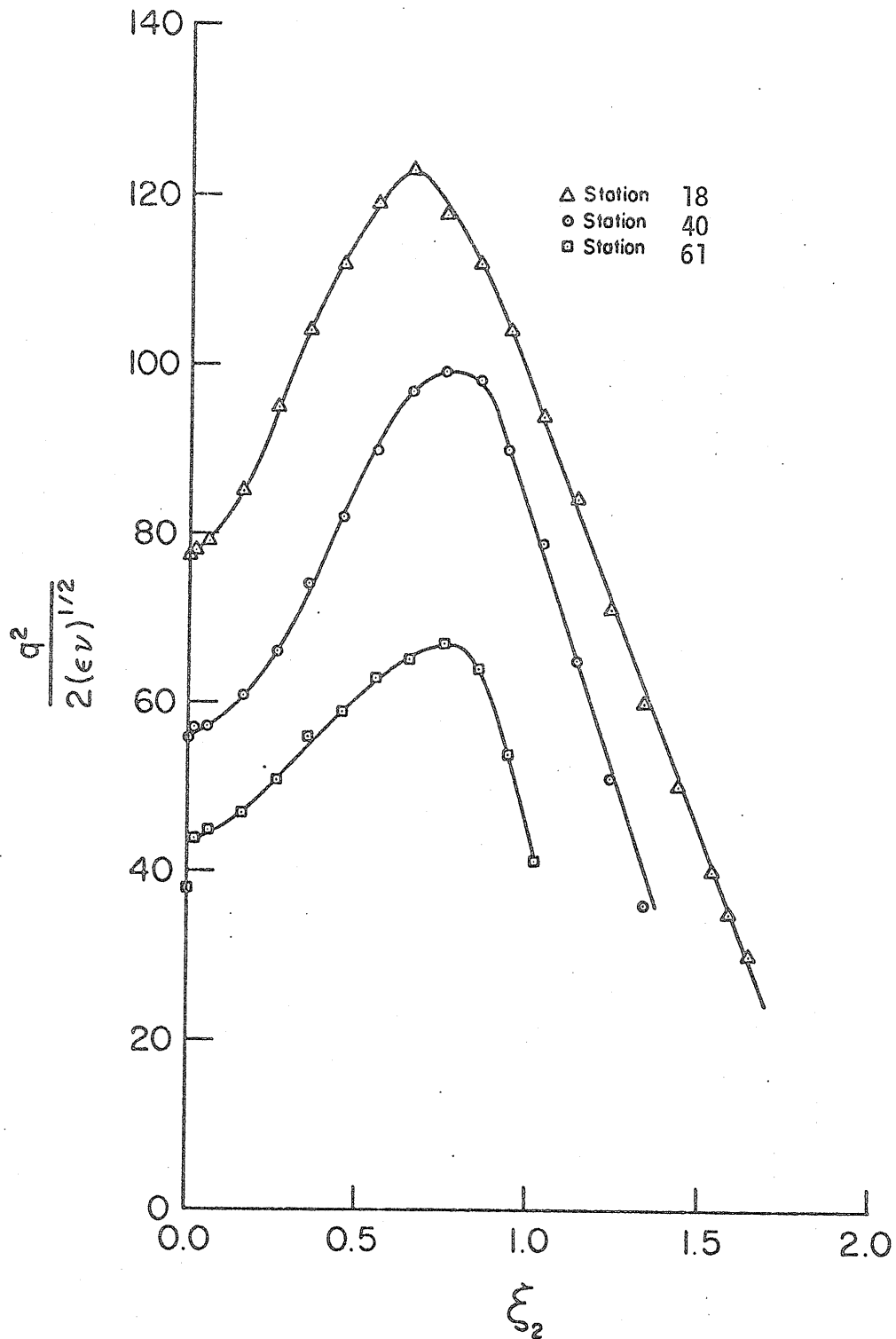


Figure 70 Variation of the ratio of the characteristic time scale of the flow to that of the dissipative time scale, τ/T .

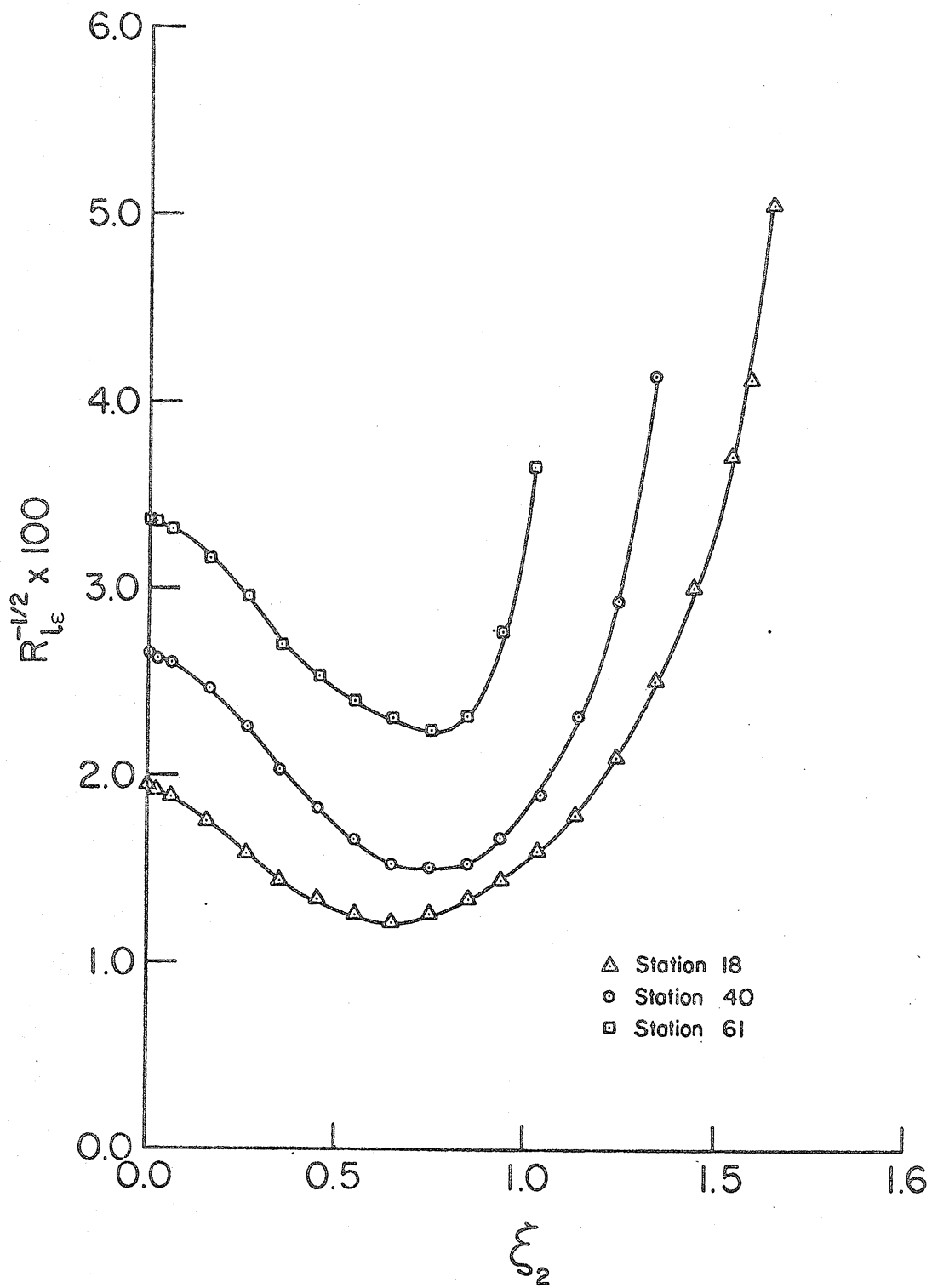


Figure 71 Distribution of the $R_{Le}^{-1/2}$.

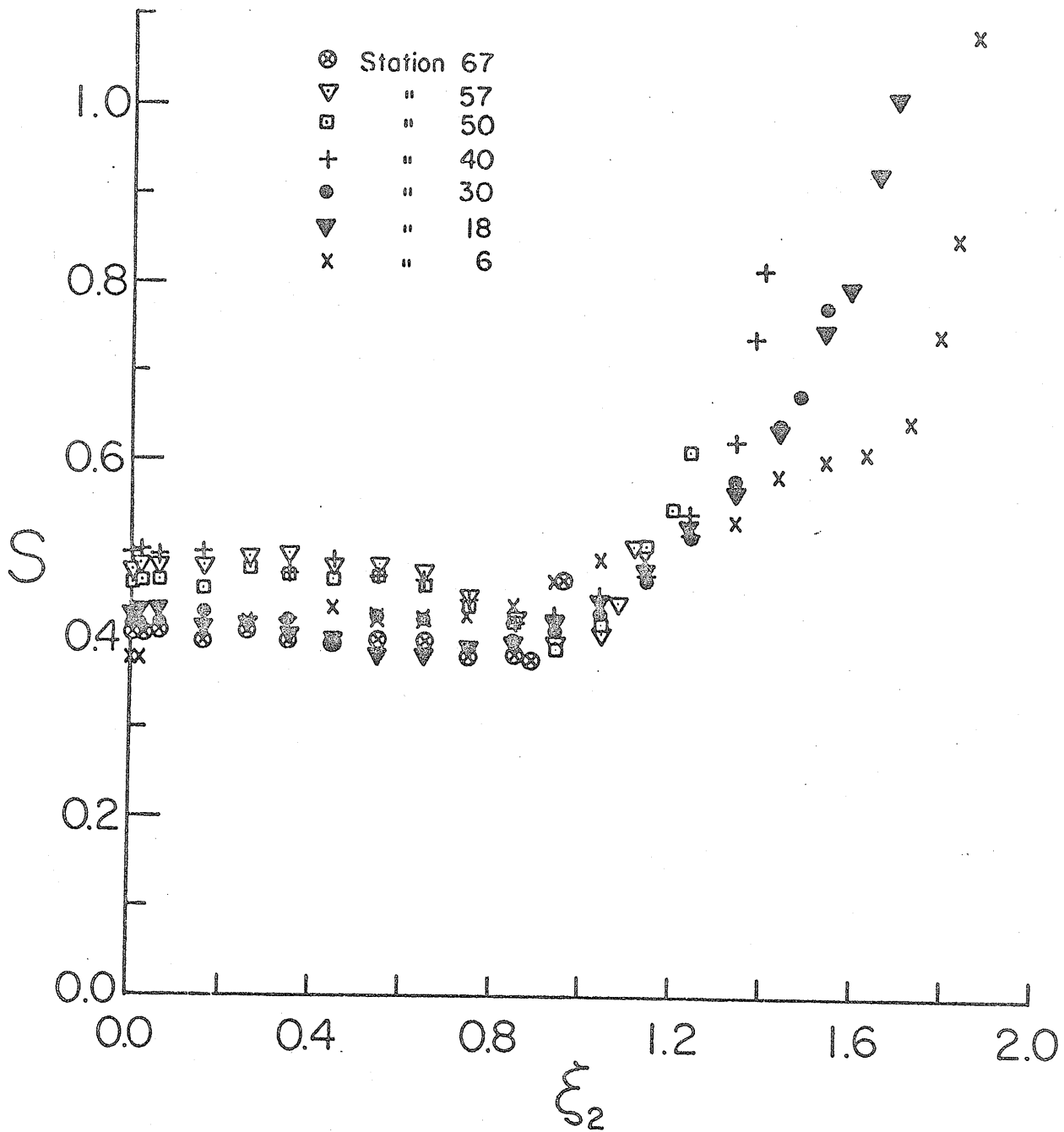


Figure 72 Variation of the skewness of $\frac{\partial u_1}{\partial t}$ at 7 axial stations.

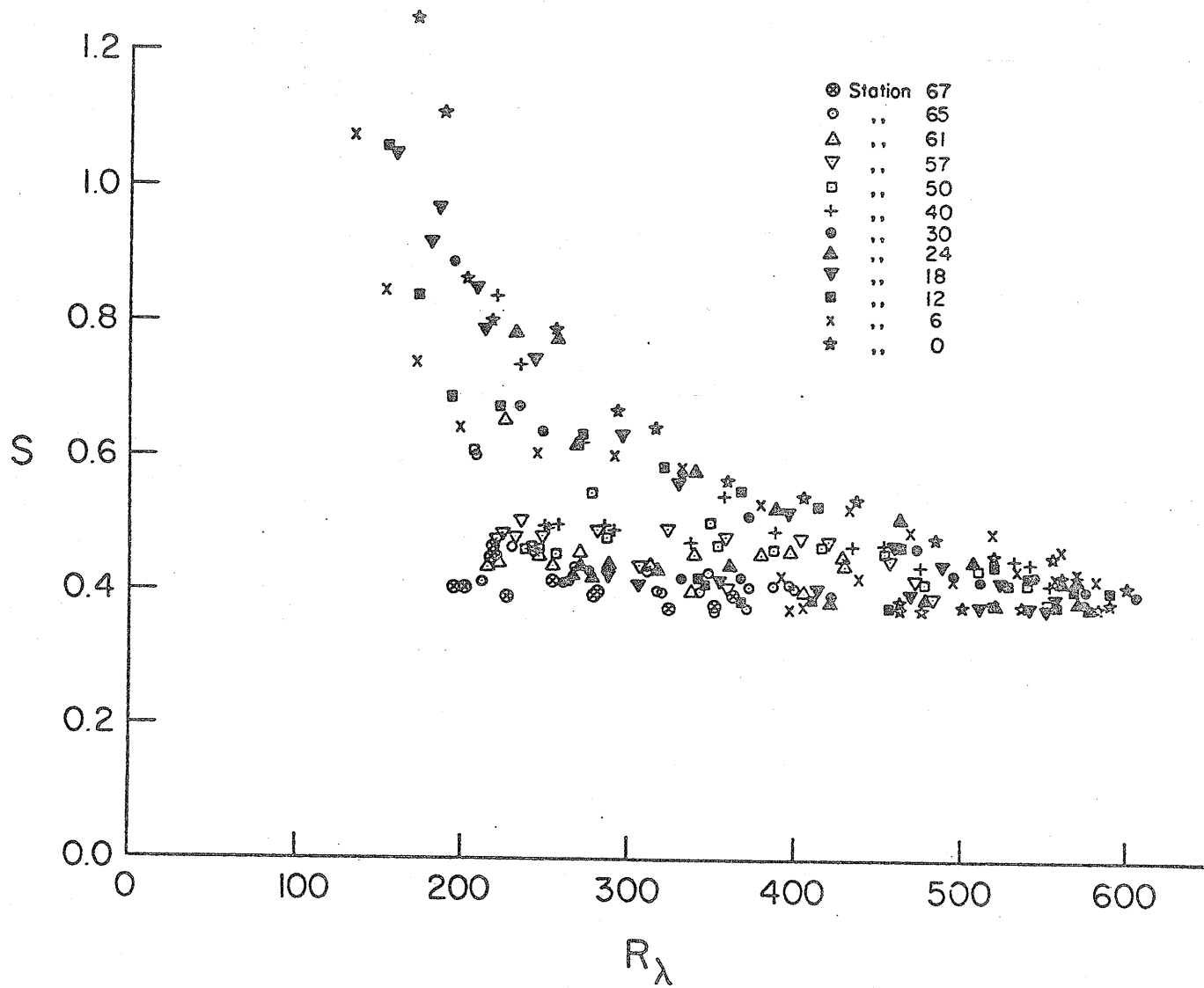


Figure 73 Distribution of S as a function of R_λ .

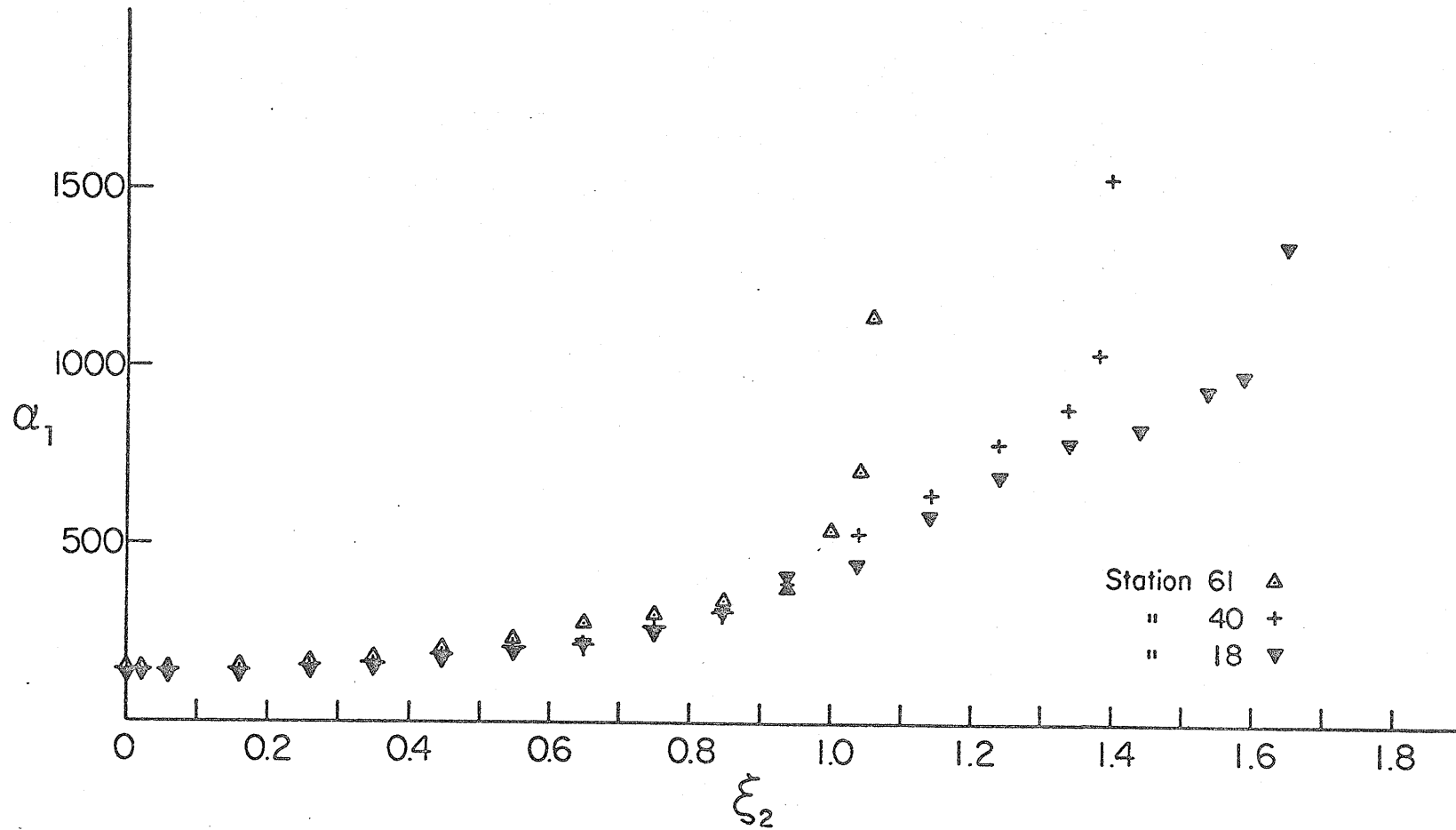


Figure 74 Variation of α_1 in the radial direction for 3 axial stations.

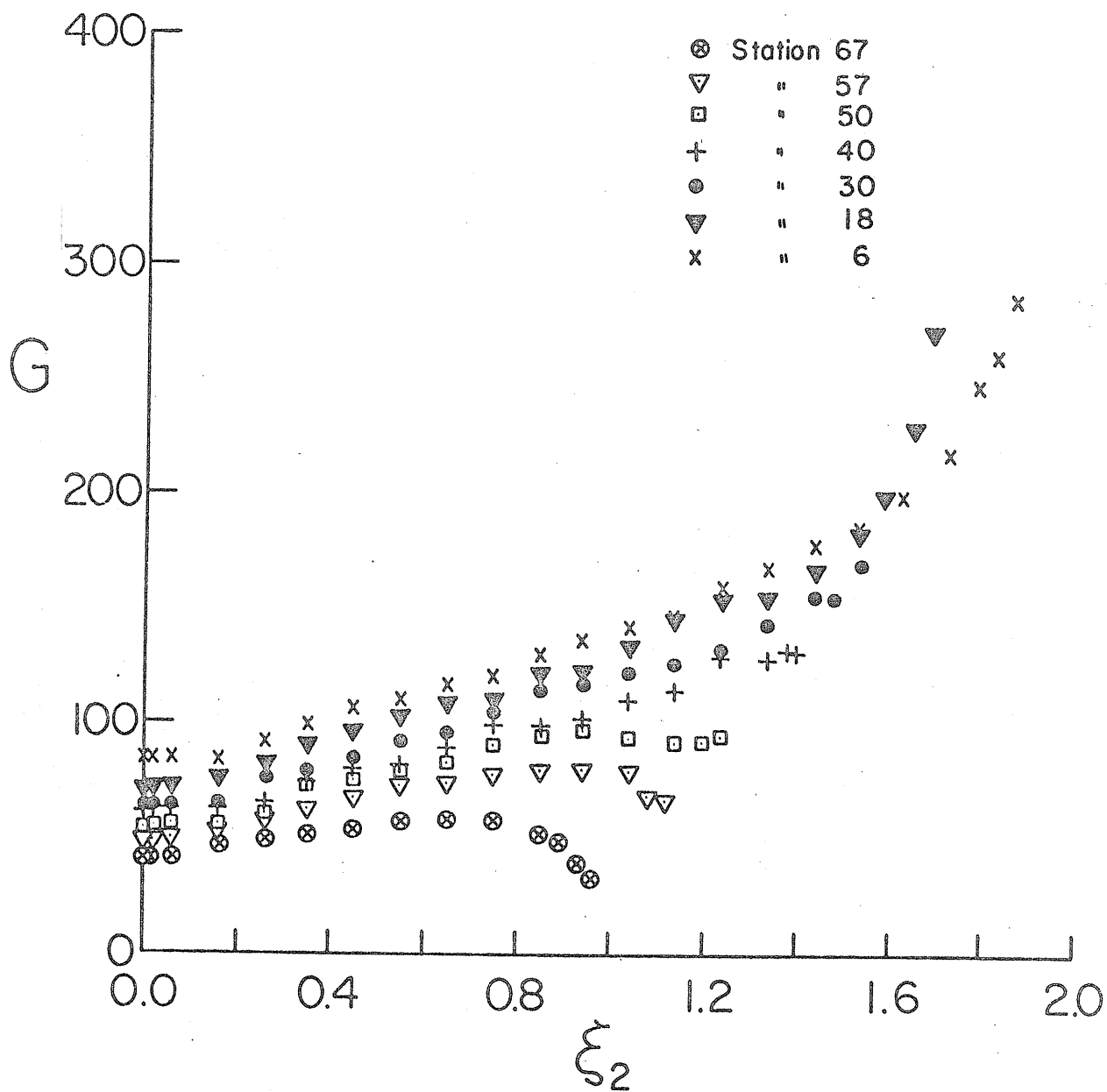


Figure 75 Second derivative of u_1 (G) in the diffuser.

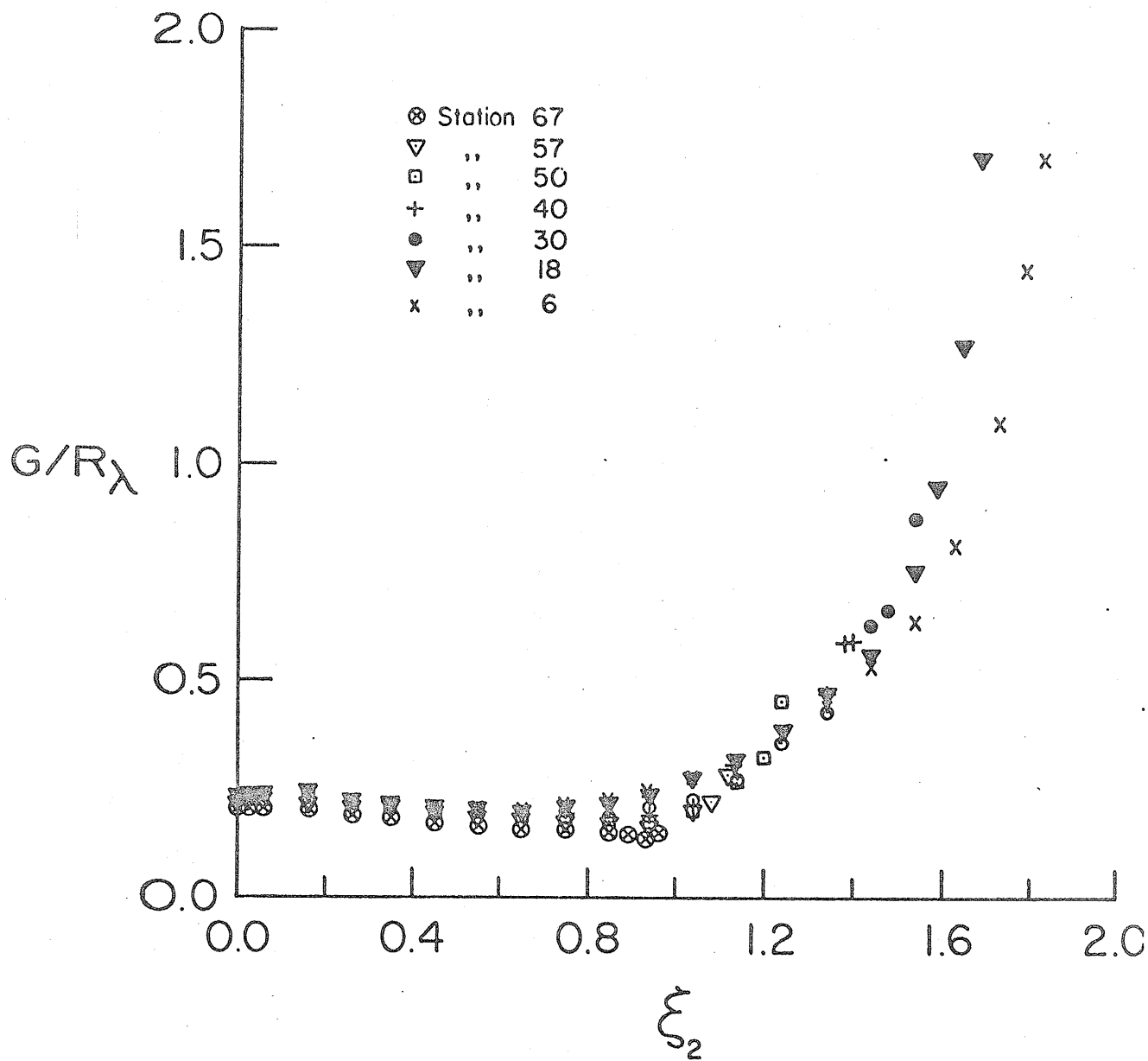


Figure 76 Distribution of G/R_λ in the diffuser.

500

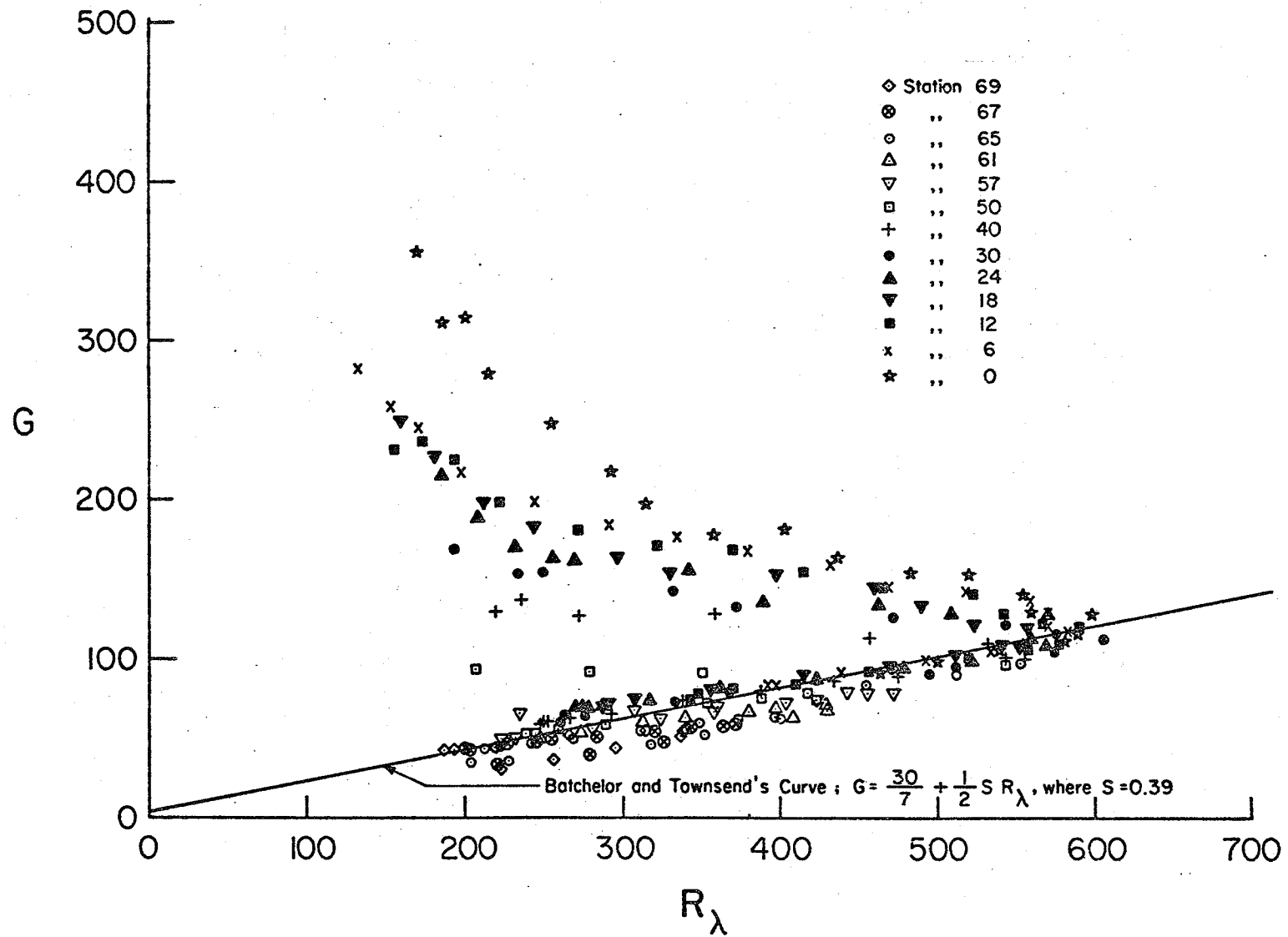


Figure 77 Variation of G as a function of R_λ .

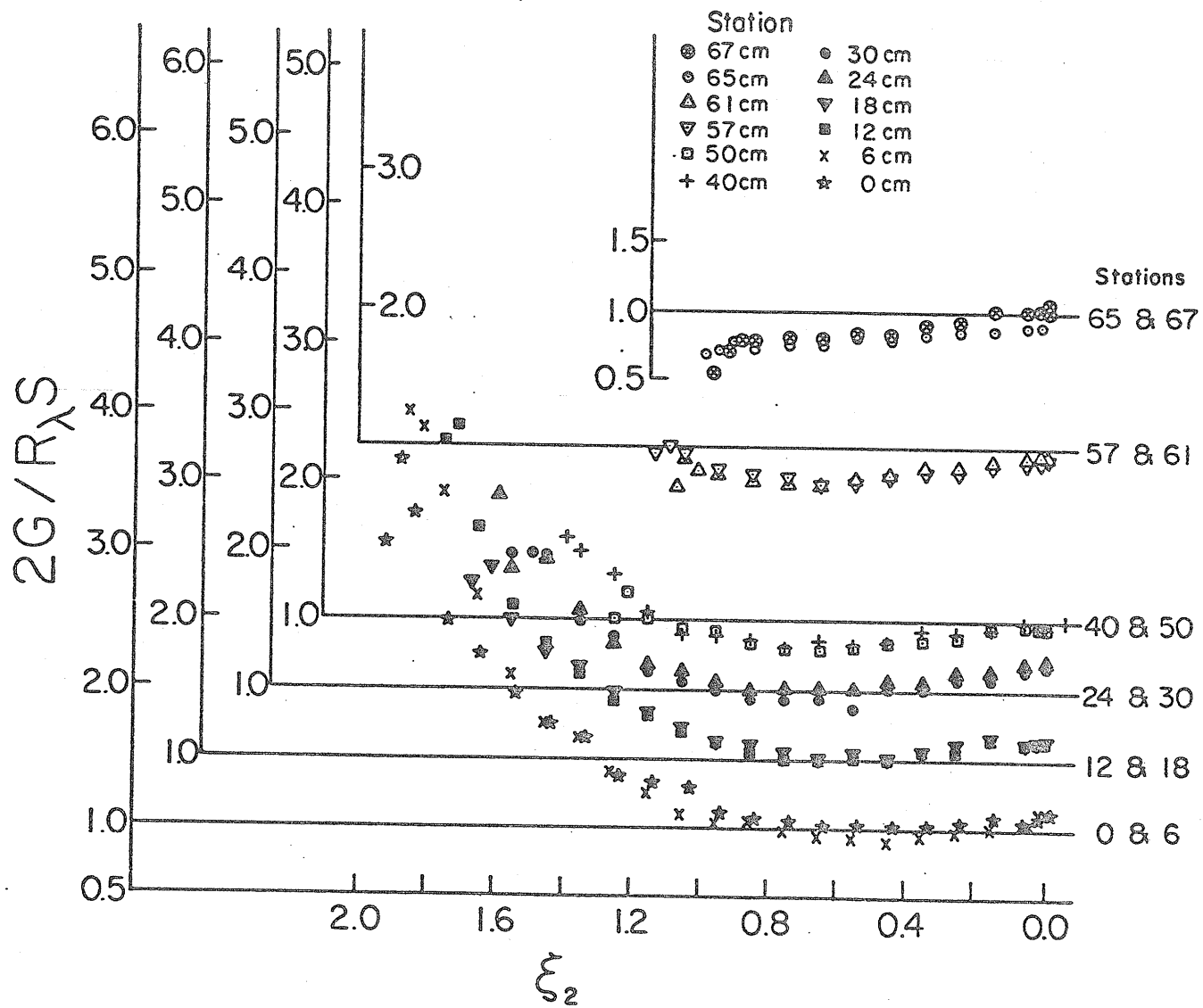


Figure 78 Ratio of the rate of dissipation and the production of vorticity.

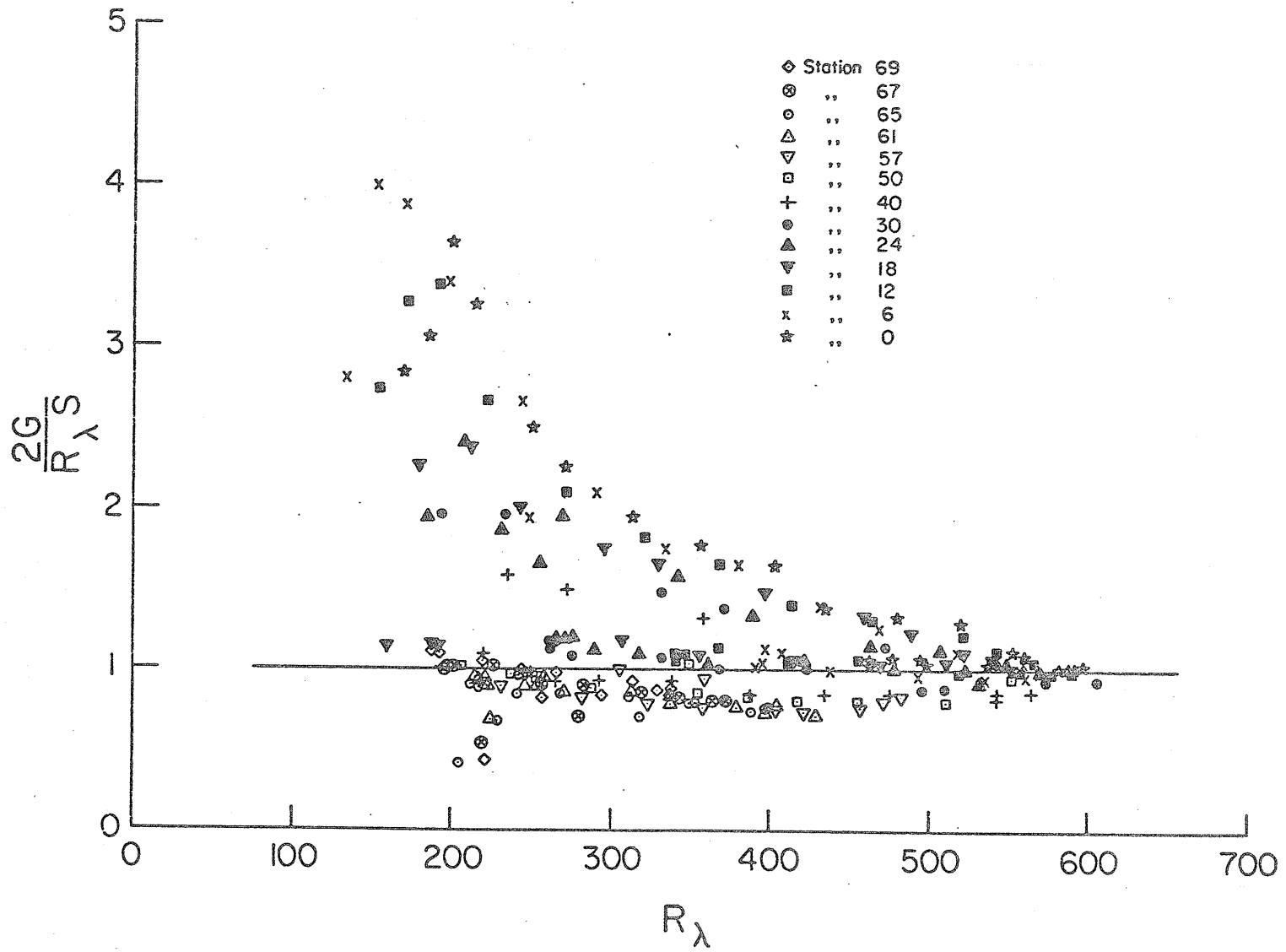


Figure 79 Ratio of the dissipation and production of vorticity as a function of R_λ .

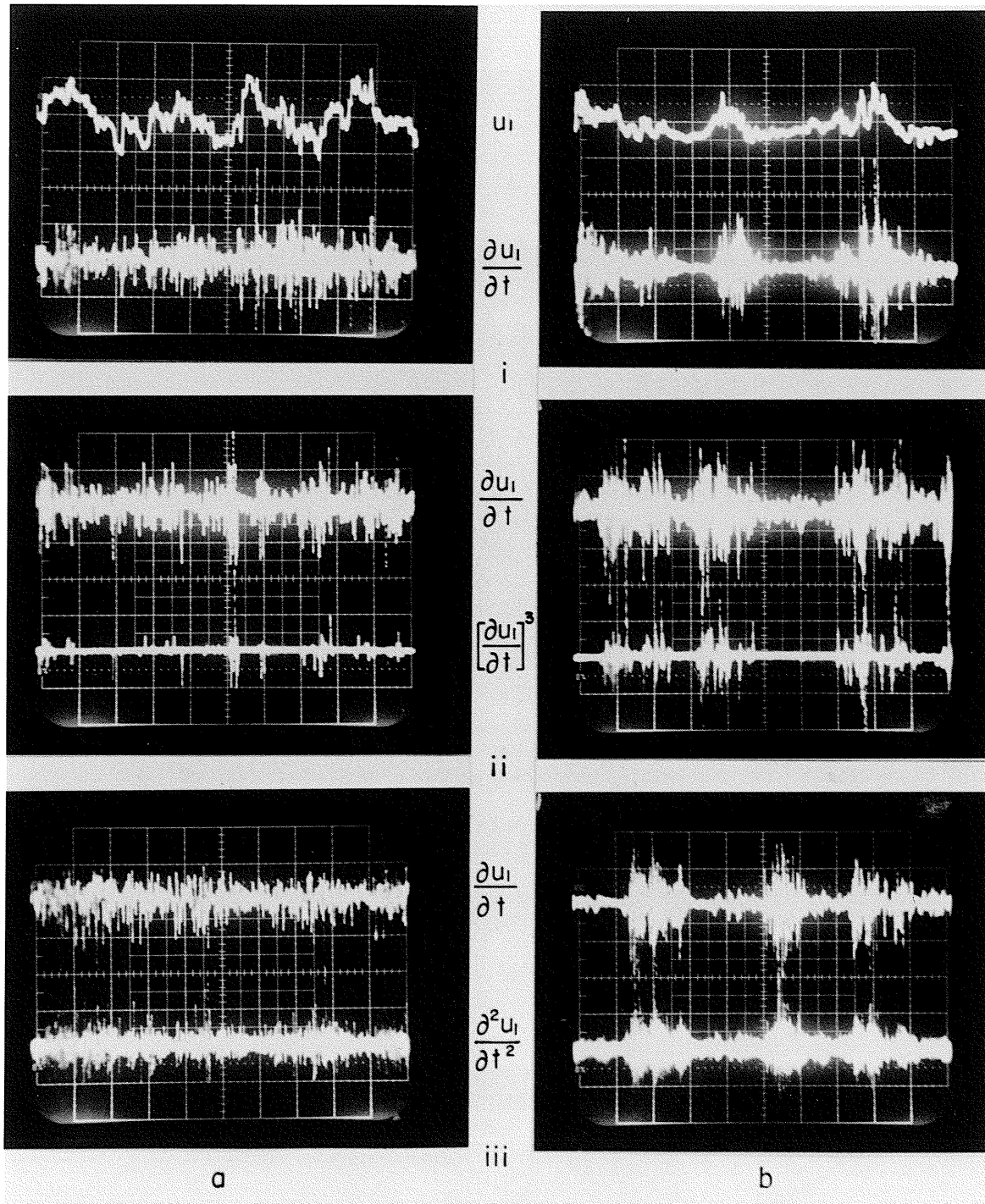


Figure 80 Photographs of oscilloscope traces.
(See Table 7 for scope settings).

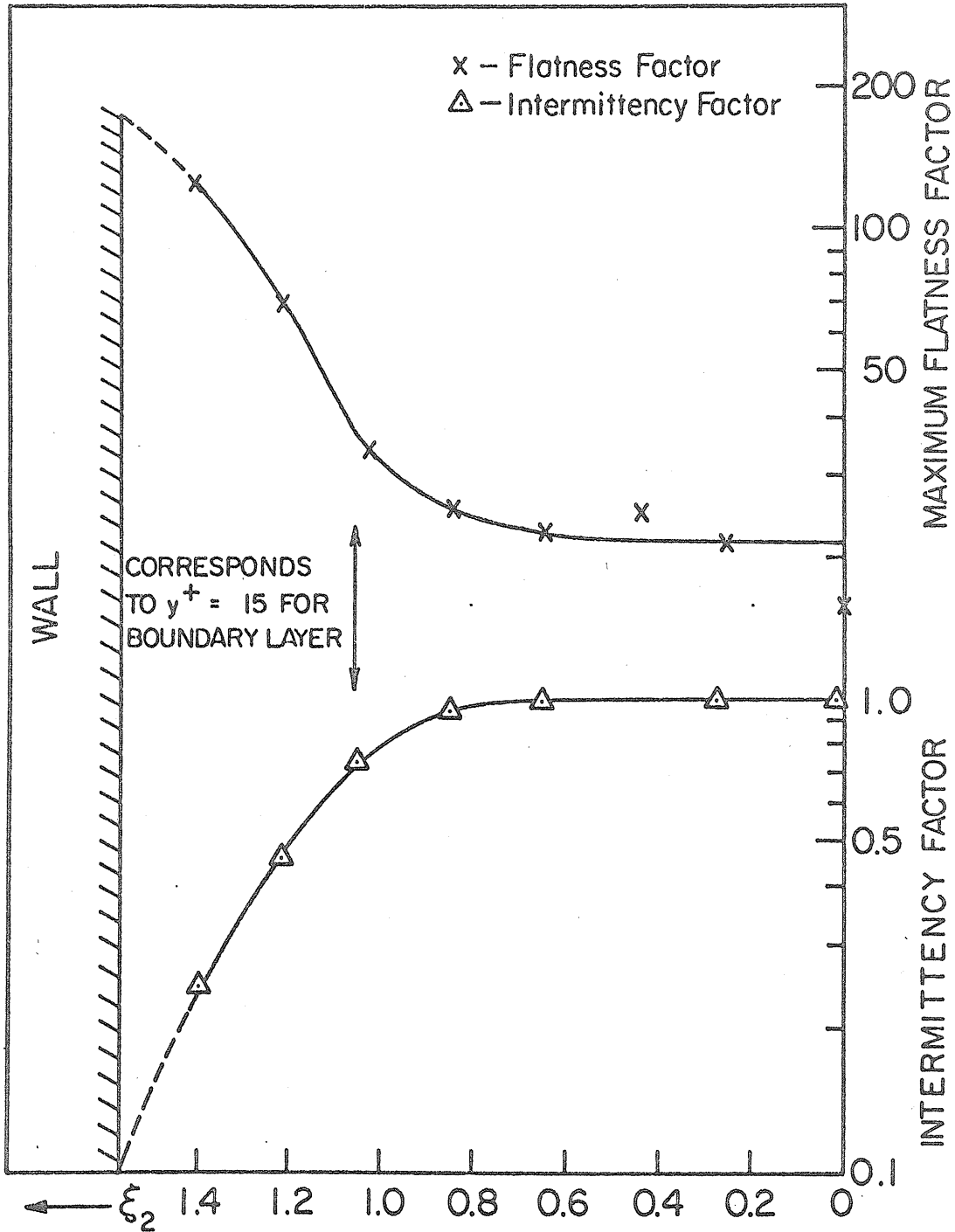


Fig. 81. Maximum FF of Narrow - Band Filtered u and Intermittency Factor of $(\partial u_i / \partial t)$ at Station 30 (Hummel 1978).

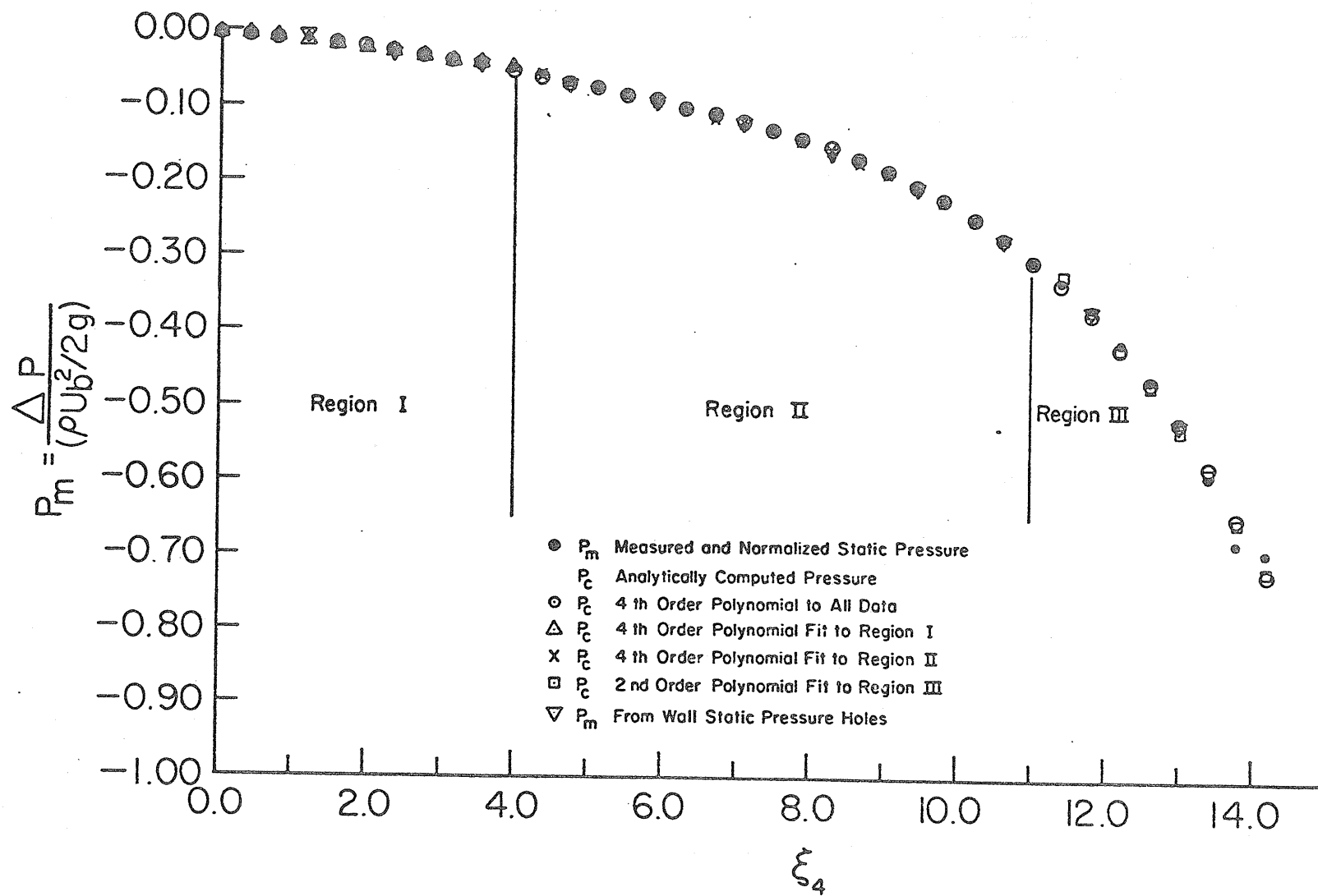


Figure A-1 Mean static pressure distribution for Re = 58000.

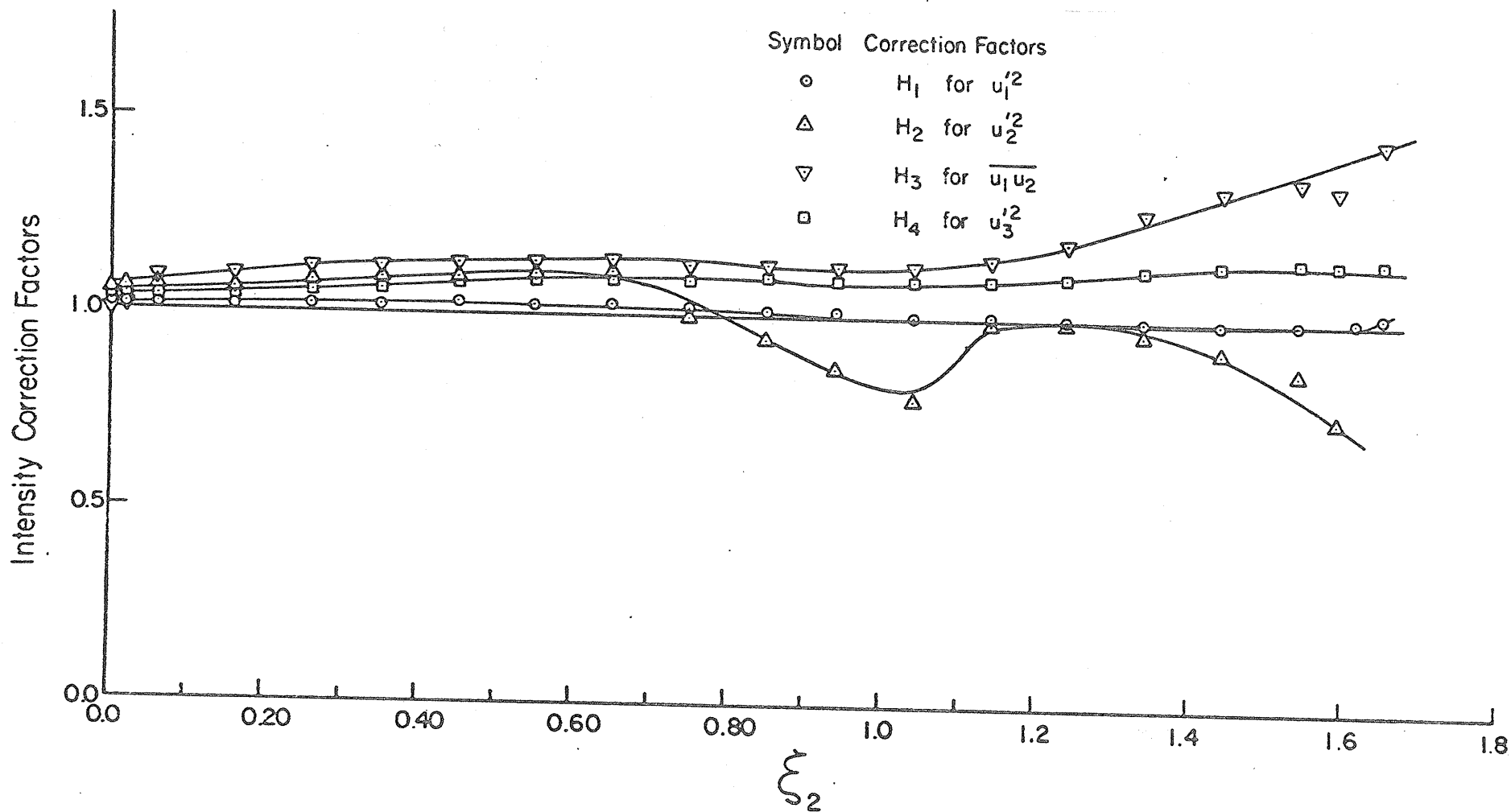


Figure C-1 Various correction factors for station 18.

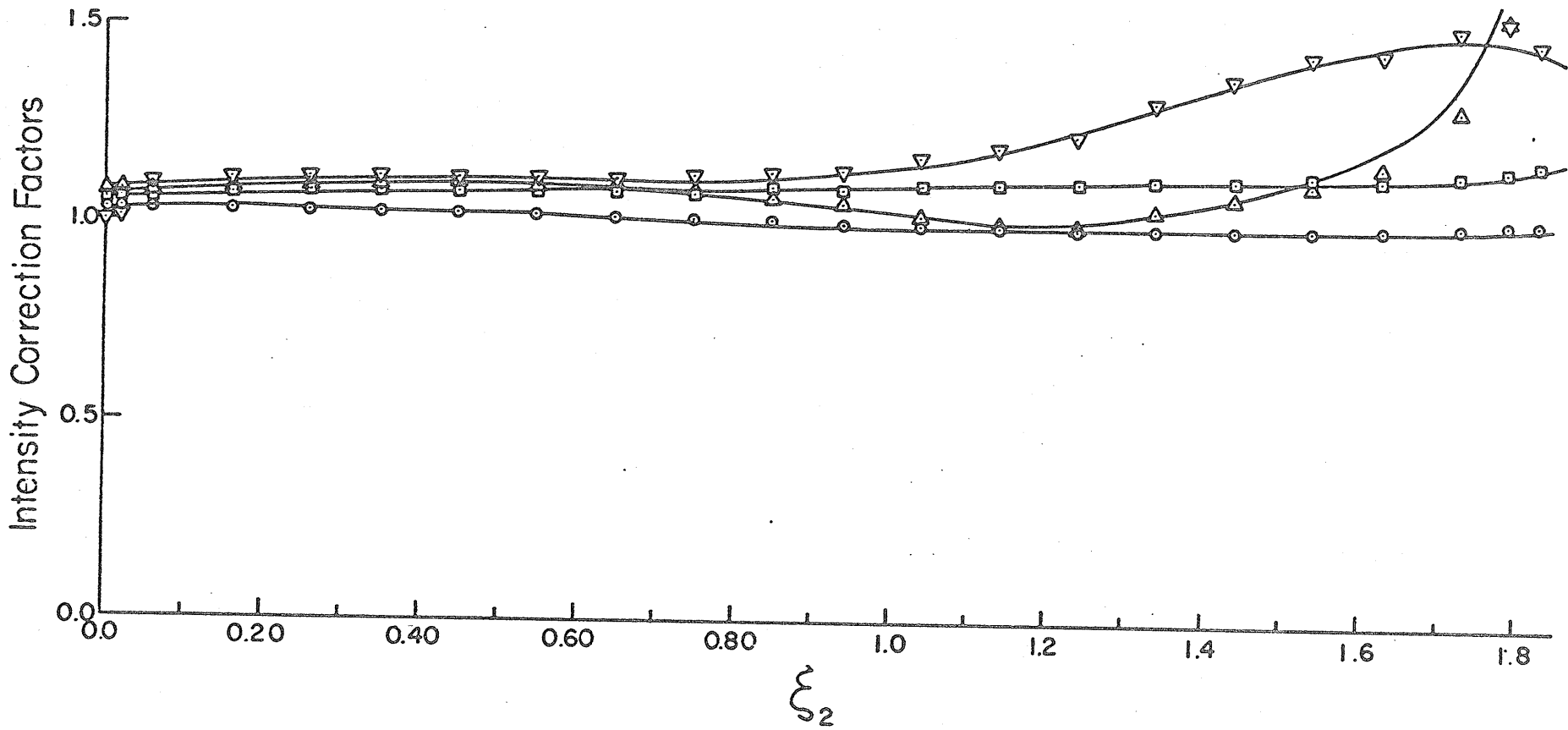
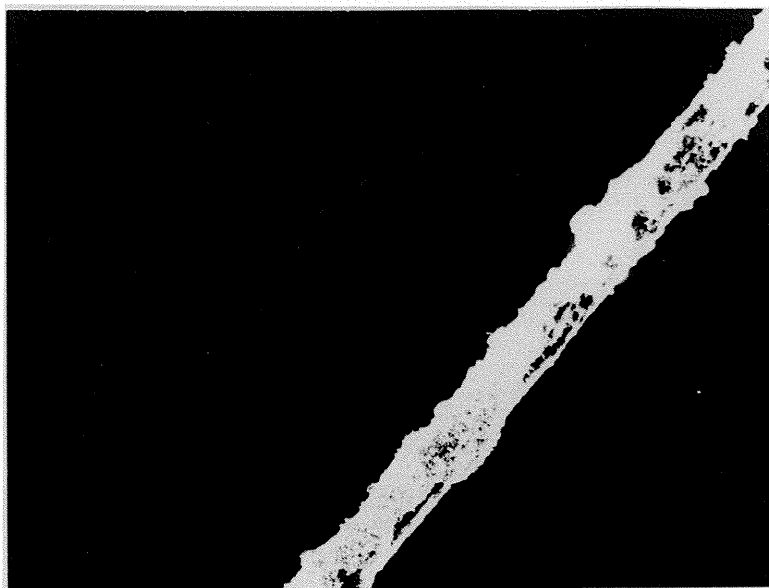
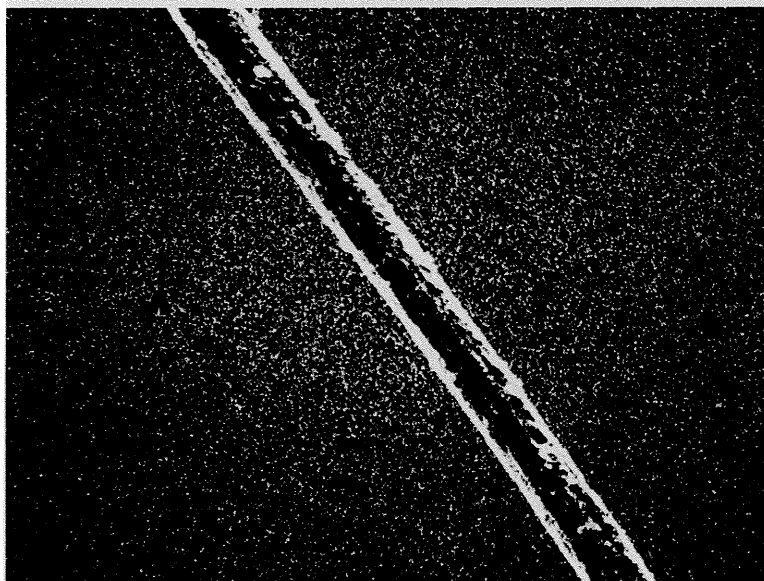


Figure C-2 Various correction factors for station 6.
 Symbols as for figure C-1.



a

(Wire exposed to flow for 80 hours)



b

(Relatively new wire)

Figure C-3 A magnified view of 2 DISA Single hot-wire probes.
Magnification factor = 2,400.

VITA

SUBHASH CHANDRA ARORA

Date of Birth: December 30, 1946

Citizenship: Canadian

(Changed name from Subhash Chandra to Subhash Chandra Arora in Dec., 1976)

EDUCATION:

High School - 1964 A.N. Jha Inter College Rudrapur, Nainital, India.

B.Sc. - 1968 Pant University of Agriculture and Technology,
Pant Nagar, India.

M.Sc. - 1971 University of Manitoba, Winnipeg, Manitoba
Agricultural Engineering.

EMPLOYMENT:

Summer - 1974 Department of Mechanical Engineering, University
of Manitoba, Winnipeg; Heat Transfer in two-phase
flow.

Summer - 1973 Department of Mechanical Engineering, University
of Manitoba; Free-convection heat transfer.

1971 - 1973 Canada Department of Agriculture, Research Station,
Winnipeg; Research on grain storage experiments.

1968 - 1969 Department of Agricultural Engineering, Pant Nagar,
India; Design and development of grain drying
experiments.

PUBLICATIONS

1. R.S. Azad, S.C. Arora and J.K. Reichert (1978)
Spectra of Reynolds stresses in a developing pipe flow.
Proc. of the 26th heat transfer and fluid mechanics institute,
Stanford University Press, p. 281.
2. S.C. Arora and R.S. Azad (1978)
On the applicability of the isotropic vorticity equation in
a conical diffuser. University of Manitoba, Dept. of Mech.
Eng. Rep. ER 25.28.
3. S.C. Arora and R.S. Azad (1978)
Turbulent kinetic energy balance in a flow with adverse
pressure gradient. University of Manitoba, Dept. of Mech.
Eng., Rep. ER 25.27
4. B. Berck and S. Chandra (1974)
Changes in pressure and composition of the institial
atmosphere of stored wheat during and after tempering.
59th Ann. Conf. Amer. Assoc. Cereal Chem. (AACC), Montreal,
Oct. 20 - 24.
5. S. Chandra and B. Berck (1972)
Effect of moisture content and temperature on kernel size
and density of wheat. Proc. Man. Env. Res. Comm. (MERC)
2, 225.
6. B. Berck, S. Chandra, C. Hasselfield and A.W. Bertels (1972)
Thermal conductivity of plastic materials for grain bins.
Proc. Man. Env. Res. Comm. (MERC) 2, 122.
7. B. Berck, A. Kalra, A.W. Bertels and S. Chandra (1971)
Experiments on farm storage of grain, phase one. Proc.
MSCP, Student Employment '71, 110.
8. S. Chandra and W.E. Muir (1971)
Thermal conductivity of spring wheat at low temperatures,
Trans. of the ASAE, 2, 644.